TRINITY COLLEGE DUBLIN

DEPARTMENT OF MECHANICAL & MANUFACTURING ENGINEERING

"COOLING BY HIGH SPEED AIR JET IN ORTHOGONAL MACHINING OPERATIONS"

Thesis submitted to Trinity College Dublin for the degree of doctor of philosophy by

Andrea Bareggi

May 2010

SUPERVISORS:

DR. G.E. O'DONNELL

PROF. A.A. TORRANCE

Declaration

This thesis has not been submitted as an exercise for a degree at any other university. Except where otherwise stated, the work described herein has been carried out by the author alone.

Acknowledgements

I would like to take this opportunity to thanks all those have helped me in this project. First of all I wish to recognise my supervisors, Prof. Andrew A. Torrance and Dr. Garret O'Donnell, for their valuable support and guidance. Other members of the teaching and research staff, Dr. Darina Murray, Darko Babic, Dennis DePellegrin and Tahdg O'Donovan for their advice, and the technical staff, Peter O'Reilly, Gerard Byrne, Paul Normoyle, J.J.Ryan, Sean Doonan and Michael Reilly for their technical support and the patience demonstrated in the experimental phase of the project. Finally I want to thanks my parents, Emilio and Marisa, for their support during all these years spent abroad.

Abstract

Changing environmental awareness has led manufacturing industry to give critical consideration to the use of conventional coolants and traditional cooling techniques in machining processes. Current research shows that impinging gas jets have a much greater potential for reducing the temperature in cutting operations than previously suspected. In this work the mechanical effect produced by a high speed air jet impinging on the cutting area at different directions and pressures was critically investigated. Experimental tests with different pressures and nozzle directions indicate that the mechanical effect of the air jet contribute significantly to the reduction of cutting temperature. The tests show better performance in terms of cooling when the air jet is directed onto the top face of the chip.

The purpose of this work is to provide an explanation for the phenomena observed in the orthogonal cutting tests on AISI 1020 low carbon steel, assisted by an air jet, where the mean chip-tool interface temperature was inferred from measurements made by a thermocouple embedded in the tool.

Finite element simulations show a qualitative relation between the performance of the air jet in terms of reduction of cutting temperature and the amount of effective stress in the shear zone, and also within the insert, next to the chip-tool interface. An analytical model based on energy consideration was developed for explaining the correlation between the altered state of stress in the shear zone shown in the finite elements model and the reduction of the temperature in the cutting zone. The deformation energy induced by the air jet and the thermal energy dissipated by the cooling effect were introduced in the analytical model. The air jet is considered as an external and stationary source of energy. The trends of the results from the analytical model show good agreement with the trends shown by finite element simulations and experimental tests, demonstrating the validity of the theoretical explanation.

Table of Contents

Nomenclature

Symbol	Description	Units
A	chip-tool interface shape coefficient	*[-]*
B	friction slider coefficient	*[-]*
b	depth of cut	*[mm]*
C	friction slider coefficient	*[-]*
c	specific heat	*[J/kg K]*
diam	diameter of the nozzle	*[mm]*
dist	distance between nozzle exit and chip surface	*[mm]*
e	eccentricity (chip)	*[-]*
f	frequency	*[Hz]*
F_p	force normal to rake face	*[N]*
F_q	force tangential to rake face	*[N]*
F_s	shear force (tangential to shear plane)	*[N]*
F_c	friction force (tangential to rake face)	*[N]*
h	convective heat transfer coefficient	*[W/m² K]*
k	thermal conductivity (generic)	*[W/m K]*
L	length of the heat generation zone	*[mm]*
$L_{contact}$	length of chip-tool contact	*[mm]*
L_{stick}	length of chip sticking contact	*[mm]*
$M_{over,\ int}$	moment promoted by the air jet	*[Nm]*
Ma	Mach number	*[-]*
n	strain hardening coefficient	*[-]*
N_c	normal force between tool and chip	*[N]*
N_s	normal force on the shear plane	*[N]*
Nu	Nusselt number	*[-]*
p	pressure of the air jet	*[Pa]*
Pr	Prandtl number	*[-]*
r_t	thickness ratio	*[-]*
r	radial coordinate (chip)	*[mm]*

r_o	external radius of the chip	*[mm]*
r_i	internal radius of the chip	*[mm]*
R_c	chip curvature radius	*[mm]*
R	total cutting force	*[N]*
$R_{1,2,3}$	heat partition coefficient	*[-]*
Re	Reynolds number	*[-]*
St	Strouhal number	*[-]*
t	feed rate	*[mm/rev]*
t_1	chip thickness	*[mm]*
T	temperature (generic)	*[K]*
T_s	temperature of the shear plane	*[K]*
T_t	chip-tool interface temperature	*[K]*
T_{mod}	modified temperature (Oxley)	*[K]*
u	specific cutting energy (generic)	*[MJ/m³]*
u_s	specific cutting energy by shear	*[MJ/m³]*
u_f	specific cutting energy by friction	*[MJ/m³]*
u_H	energy associated to heat transfer	*[MJ/m³]*
u_M	energy associated to elastic deformation	*[MJ/m³]*
V	cutting speed	*[m/s]*
V_{flow}	air jet speed	*[m/s]*

Greek symbols

α	shear plane angle	*[deg]*
β	friction angle	*[deg]*
γ	shear strain	*[-]*
$\dot{\gamma}$	shear strain rate	*[1/s]*
θ	correction for shear plane angle	*[deg]*
ϑ	angular coordinate (chip)	*[rad]*
Φ	shear plane angle	*[deg]*
ε	strain (generic)	*[-]*
μ	friction coefficient	*[-]*
μ_{air}	air viscosity	$[kg\ m^{-1}s^{-1}]$

ρ	density (generic)	*[kg/m³]*
σ	stress (generic)	*[MPa]*
σ_{el}	elastic stress	*[MPa]*
σ_1	stress with unitary strain	*[MPa]*
τ	shear stress	*[MPa]*
χ	thermal diffusivity	*[m²/s]*

1. Introduction

1.1 Context

Since the beginning of the 20th century manufacturing processes have been systematically and scientifically developed and analyzed in order to maximize the efficiency of the processes and to generate a new knowledge and understanding of processes. Byrne et al [1, 2] identified the change drivers in the development in manufacturing process innovation, including: diminishing component size, enhanced surface quality, tighter tolerances and manufacturing accuracies, reduced costs, diminished component weight and reduced batch sizes. These change drivers have a direct influence on the primary inputs to the cutting process namely the cutting tool and tool material, the workpiece material and the cutting fluid.

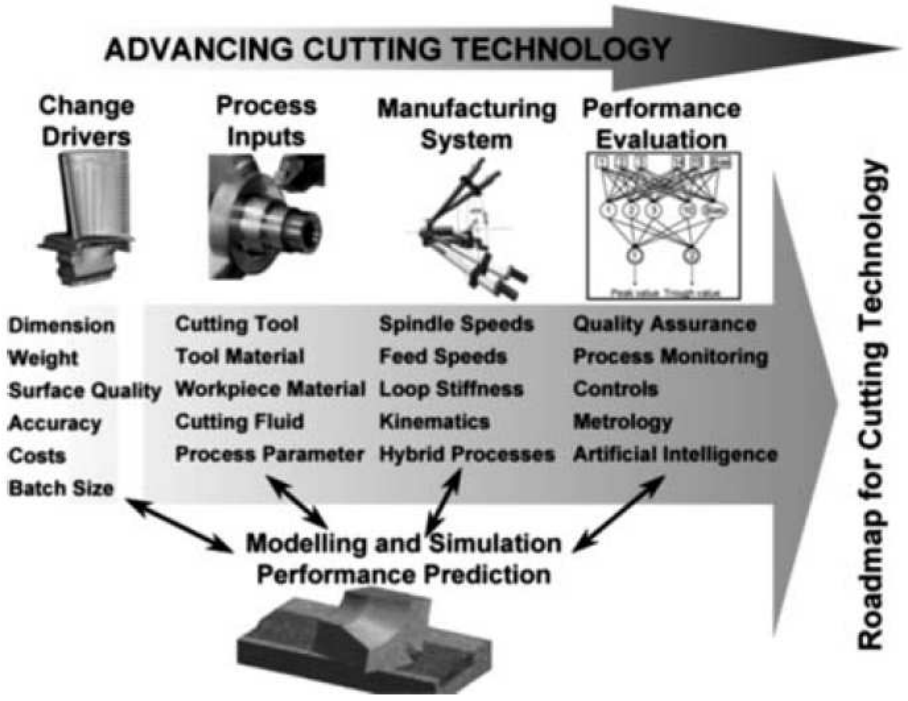

Figure 1.1 – The roadmap for advancing cutting technology [1]

In the past decades within the industrial community there is increasing awareness, that ecological aspects were not considered as a high priority in the development of

manufacturing processes [14]. The challenges associated with environmental protection and energy efficiency in relation to manufacturing is now an area of ongoing and vibrant research activity, as outlined by Byrne et al. [1], Klocke et al. [3] and Weinert [4].

More recently the increasing sensitivity to environmental and health issues is reflected in the increasingly stringent legislation. The restrictions resulting from legislation do not only lead to limitations and difficulties with particular manufacturing processes and an associated undesirable cost factor, but also force scientists and engineers to develop new and alternative technologies. This provides a technological challenge and increases the importance of ecological manufacturing as a competitive factor. This has been the source of a number of initiatives to encourage more research in environmentally efficient manufacturing processes. Klocke et al. [5] reports environmentally efficient machining as one of the main issues stimulating the foundation of the CIRP Working Group on High Performance Cutting. According to Pusavec et al. [6] in the US an initiative on environmentally benign manufacturing has been ongoing since early '90s. This initiative is mostly based on innovative sustainable manufacturing, as shown in Figure 1.2.

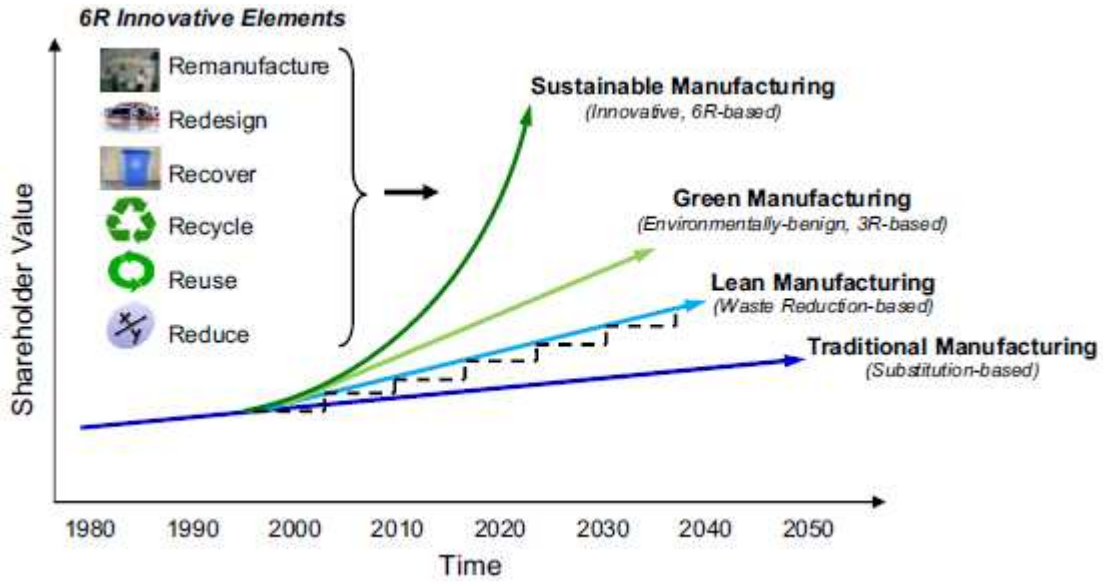

Figure 1.2 – Efficient sustainable machining is based on remanufacturing, redesigning, recovering, recycling, reusing and reducing [6]

When considering the environmental efficiency of a machining processes one of the main challenge faced is the management of temperature at the engagement of the tool and the

workpiece [7]. Temperatures at the chip-tool interface play a major role in tool wear and can also result in modification to the properties of the workpiece and tool materials [8]. As there is a general move towards environmental efficient machining, it is increasingly important to understand how machining temperatures are affected by the process variables involved and by other factor such as tool wear [140, 121]. According to Klocke et al. [5] the increase in power to remove more material in a shorter time increases the heat generation near the cutting edge of the tool. The power consumed in metal cutting is largely converted into heat, for example in the case of low carbon steels approximately 80% of the power input is converted into heat. This heat is dissipated by the five systems processing the material: the cutting tool, the workpiece, the chip formed, the cutting fluid, and the natural convection to air. This means that the cutting tool needs to support higher temperatures at acceptable wear rates [11]. Normally, the temperature achieved by the cutting tool is the factor that limits the rate of machining. This task forced the development of new materials for cutting tools that can resist high temperatures, and methods for managing the temperature rise at the chip-tool interface. The approaches used to manage temperature at the tool chip interface can be broadly classified as management of the temperature by heat transfer (use of cutting fluids, minimum quantity lubrication, and alternative cooling methods) or management of temperature by manipulation of frictional contact [12].

According to Bacci da Silva et al. [58] cooling and lubricating is also a subject of much research activity and it is generally accepted that oil-based cooling/lubrication fluids are one of the most unsustainable elements of machining processes. Cutting fluids have a direct influence on the environment and since early ‘90s are being questioned in the light of economic and ecological manufacture [6]. The exposure of the production operator to cutting fluids can lead to skin and respiratory diseases and there is increased danger of cancer. The cause of this is attributable both to the constituents of the cutting fluids as well as to the reaction products and particles generated during the process [1].

Studies on minimum quantity lubrication and oil mists are relatively well established, as reported by Weinert [4]. However Childs et al [13] reports that the lubricant can gain only a partial access to the chip-tool interface, and so attention should be focused on the sliding region, that can be accessed by the cutting fluid. If a lubricant is applied and it

penetrates only the sliding zone, which makes only a small contribution to the total forces, it will only marginally affect the total force. The sliding zone has the lowest compressive forces and as such can be influenced by small changes in the cutting process. Current strategies for reducing the cutting temperature include the use of multi-layer coatings [14] and self-lubricating coatings in dry machining, and alternative cooling methods (cryogenic technology and manipulation of the frictional contact in the chip-tool interface.

Well established studies on dry cutting, reviewed by Klocke et al. [3], and a strategic approach to high performance cutting in the environmental efficient direction [5] suggest that most of materials (with the exclusion of titanium alloys and nickel based alloys) can be dry machined with multi-layer coatings and self-lubricating coatings (soft coatings) [15]. More recently, cooling systems based on cryogenic technology [16, 17] provided a sustainable alternative to the use of cutting fluids, traditional (flooding) or improved (minimum quantity lubrication or oil mist) [18].

One alternative process for the management of temperature at the tool-chip interface consists of manipulating the frictional contact in the chip-tool interface. According to Friedman and Lenz [19] there is a correlation between maximum interface temperature and chip morphology (curl of the chip and length of the sticking zone). Umbrello et al. [20] estimates the global heat transfer between the chip and the insert as dependent on the stress and temperature in the sticking zone. Studies carried out by Ozel and Altan [21] show that the friction and hence the temperature rise due to friction can be reduced by reducing the stress in the sticking region. The manipulation of the frictional contact can be achieved by using an external source of energy for promoting a deformation in the chip. One of the main purpose of laser and plasma based techniques is the local modification of material properties (such as hardness and stiffness) just before the shear zone, in order to reduce the specific cutting energy required for cutting, hence the stress on the rake face [49, 5, 25].

The approach proposed in this research is based on using high velocity air jets to assist the orthogonal cutting process. The air jet impinging on the surface of the workpiece in the contact zone, on the tool and on the chip introduces both thermal and mechanical effects. Here-to-fore these influences have not been examined.

1.2 Research objectives

The aim of this research is to investigate the use of a high velocity air jets to assist the orthogonal cutting process, both from a thermal and mechanical point of view. A particular focus of this work was the mechanical effect of the air jet impinging on the cutting zone.

- The research set out to develop an analytical model of the orthogonal cutting process assisted by high speed impinging air jet considering the mechanical and thermal effect.
- The research set out to develop a finite element model of the orthogonal cutting process assisted by high speed impinging air jet in order to investigate the effect of the mechanical and thermal effect of the air jet on cutting temperatures including shear plane temperature, and temperature distribution within the insert, effective stress within the insert and the workpiece, and chip morphology including curvature radius, chip thickness, length of the contact with the rake face.
- The research work concluded with experimental investigations in order to validate the analytical and finite element models, and provide a sensitivity analysis to the variation of pressure and position of the nozzle.

1.3 Methodology

Background

The mechanical effect of the high velocity air jet is considered as a pressure applied to the top face of the chip or into the interface between the bottom face of the chip and the tool. The pressure applied by the high velocity air jet promotes the elastic deformation of the chip. This deformation promotes a rotation of the chip that tends to reduce the curvature of the chip. In this work, a hypothesis is presented that the alteration of the curvature of the chip can be associated either with an increment in the energy (reduced

radius of curvature) or with a decrement of energy (increased radius of curvature), as suggested by Baker [10].

In order to develop the argument, the orthogonal cutting process was chosen as the basis for the investigations. The workpiece material was a low carbon steel AISI 1020 and coated tungsten carbide tools TNMG 110302-MF4025 were used. The orthogonal cutting process is well established and well published with significant information available on analytical, finite elements and experimental investigations. Furthermore by primarily considering 2D investigations it was also possible introduce the additional element of the high velocity air jet into the cutting process and to critically consider the sensitivity of the high velocity air jet nozzle position.

Approach

The research project is based on three pillars:

- The development of an analytical model of 2D orthogonal cutting with the integration of the mechanics of the high velocity air jet
- The development of a finite element of 2D orthogonal cutting with the integration of the mechanics of the high velocity air jet. The development of 3D models of the temperature distribution in the cutting tool with the mechanics of high velocity air jet included.
- Experimental investigations with high velocity air jet impinging on the cutting zone under two different impinging conditions

The three pillars of the methodology are graphically illustrated in the Figure below showing the detail involved in each of the approaches.

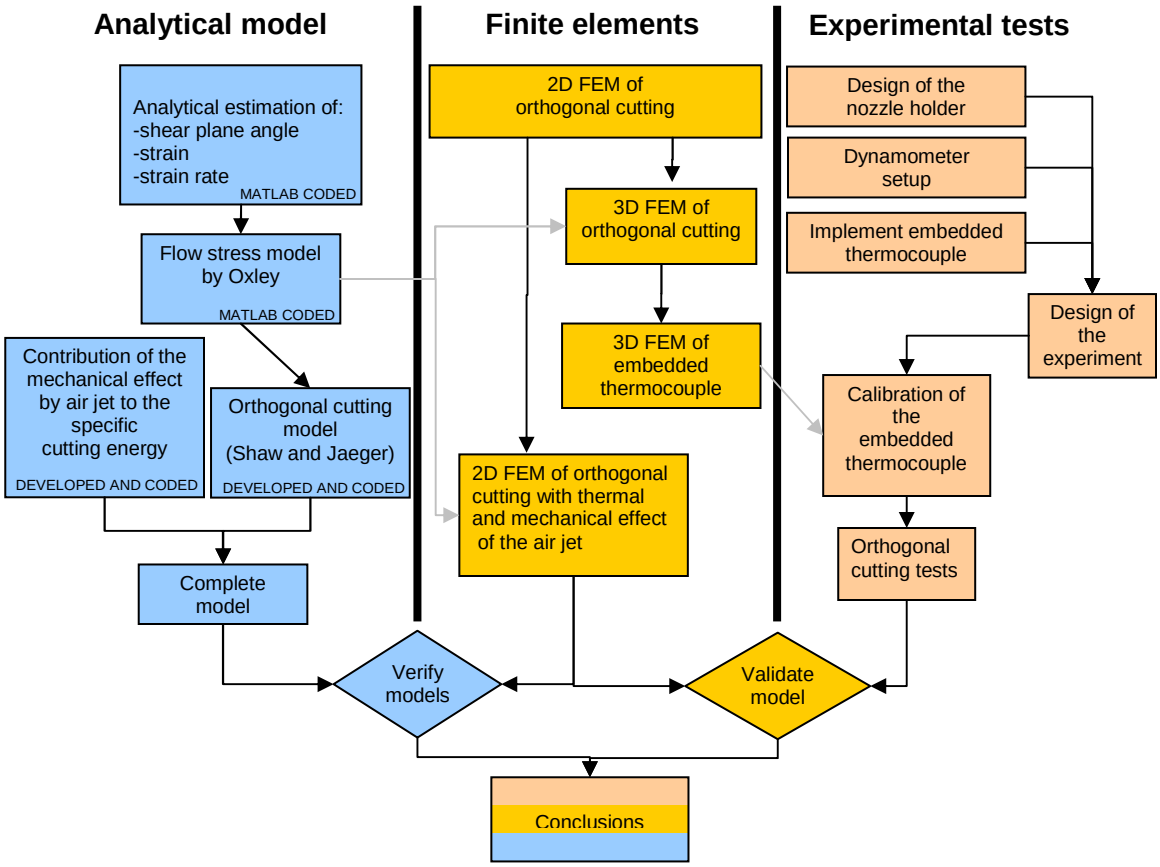

Figure 1.3 – The schematic plan of the research project

Analytical model development

An analytical estimation of the shear plane angle, the strain and the strain rate was coded in MATLAB by using the approach of Merchant [28, 29] and Kececioglu [30]. The shear plane angle, the strain and the strain rate were used to calculate the flow stress as a function of temperature in the workpiece material using the model proposed by Oxley et al [31, 32, 33]. The flow stress was used in the orthogonal cutting model by Merchant [29]. The cutting forces calculated by using the orthogonal cutting model were used for estimating the specific cutting energy in its components U_s (in the shear zone), and U_f (in the friction zone).

The mechanical effect of the air jet on the chip was modeled as a distributed load on a curved elastic beam, and the solution of Saint Venant was used for estimating the deformation energy (U_m) associated with the elastic deformation [34]. The heat transfer by impinging jet was modeled by estimating the Nusselt number for circular jets

impinging on round surfaces, and the heat flux U_h was considered in the energy balance. The two contributions (U_m and U_h) to the energy balance were evaluated for two nozzle positions: the nozzle directed on the top face of the chip known as the overhead position and in the chip-tool interface known as the interface position.

The components of the specific energy were the inputs of the model developed by Shaw [35, 39], that calculates the temperature in the shear zone, and by Jaeger [38], that calculates the temperature rise in the friction zone according to the flash temperature theory [40] and the maximum insert temperature.

Finite element modeling

2D simulations of orthogonal cutting were modeled using DEFORM-2D. The 2D simulations boundary conditions included the heat transfer by impinging jet, modeled as forced convection by using a heat transfer coefficient ($h = 2000\ W/m^2K$), and the mechanical effect of the air jet on the chip, modeled as a pressure applied on the impinged surface. The 2D simulation results include the temperature distribution within the insert and the workpiece, the effective stress distribution within the insert and the workpiece, the 2D chip morphology. The temperature and stress distribution within the insert were particularly influenced by the variations to the direction and pressure of the air jet. The influence of the direction and pressure of the jet was observed also by Diniz et al. [41] in low carbon steel turning tests.

3D simulations of orthogonal cutting without the use of air jet were modeled using DEFORM-3D. The purpose of the 3D simulations was the investigation of 3D morphology of the chip, in particular the contact between the chip and the insert. The 3D morphology of the chip was used as a boundary condition for the 3D thermal simulations on the insert with embedded thermocouple. The 3D thermal simulations of the insert were used for modeling the temperature in the insert with the embedded thermocouple. The thermal simulations of the temperature within the insert provided a relation between the maximum temperature of the chip-tool interface and the temperature read by the thermocouple, improving the method proposed by Ren et al. [42].

Experimental tests

Experimental investigations were carried on AISI 1020 low carbon steel by using a coated insert TNMG 110302-MF4025. A nozzle holder with three degrees of freedom was designed and manufactured. A data acquisition system was commissioned that recorded forces from a three component cutting force dynamometer. The tool temperature was measured by embedding a thermocouple into a cutting tool insert. The tool was calibrated in order to account for the heat transfer through the insert from the cutting tool face. The high velocity jet was directed in four directions, two on the top face of the chip in the overhead position and two in the interface between the chip and the rake face in the interface position in order to provide a sensitivity analysis on the positioning of the nozzle. The main set of tests used two pressures of the air jet (4 and 7 bar), and a set of tests was carried out with small variation of pressure in order to evaluate the sensitivity to the pressure of the air jet. In order to ensure the reliability of the temperature measurement with embedded thermocouple, all the main set of tests was carried out by using two holes for embedding the thermocouple. The results from the orthogonal cutting tests were used for validating the finite element model and the analytical model.

2. Literature review

2.1 Introduction

Metal cutting is one of the most important methods of removing material in the production of mechanical components. The industrial production of useful parts and objects by the removal of material, for the purpose of producing a desired shape, is today almost exclusively carried out by the processes known as machining and grinding [43]. In machining the metal is removed by sharp-edged cutting tools propelled and guided by precise machines termed machine tools. Thus, the technology of the machining is primarily concerned with the characteristics and performance of three main players; namely, the cutting tool, the machine tool and the material being cut [139].

A review of CIRP activities since its foundation [44] shows that metal cutting represents a strong integration of technologies and management using information technologies, integration of the process planning and production planning, simulation of manufacturing systems, agile manufacturing, fast redesign of new products, modeling of manufacturing equipment performance, including the human operator, functional product analysis, virtual machining and inspection algorithms.

The literature review presents the currently used solutions for reducing cutting temperature in machining operations, with particular emphasis on clean production and air jet based cooling technology. Also a literature review on particular finite element applications is presented, since finite element investigations is one of the three pillars on which this research is carried out. A review on the different temperature measurement methods is also presented.

2.2.1 New trends in cleaner production

The global environmental problems caused by the consumption of natural resources and the pollution resulting from the life of technical products have led to increasing political

pressure and stronger regulations being applied to both the manufacturers and users of such products [14]. The idea of sustainable development is well defined and implemented on the production at a macro level, but there is a severe lack of implementation practices on the shop floor dealing with machining technologies [1]. Industry is striving to achieve sustainability through changes in product, material cycles, the recovery of resources, and innovations in production practices in order to fulfill the objectives of sustainable development [45, 46]. With the implementation of sustainability principles in machining technologies, end-users have the potential to save money and improve their environmental performance even if their production stays in the same range or decreases [47]. According to Pusavec et al. [6] in the view of production technologies, the ways to improve the sustainability performance are to:

- reduce machining processes energy consumption
- minimize waste (generate less waste, and increase waste recycling)
- use resources efficiently
- use recyclable materials or reuse machine-tool components
- improve the management of metalworking fluids
- adopt life cycle assessment methods

A key element of sustainability is the prudent use of natural resources. This means using non-renewable resources efficiently and developing alternatives to replace them in the future, while using renewable resources in ways that do not endanger the resource or cause pollution [48]. The main resources of concern in production technologies are: metals used in the machining processes, cooling/lubrication fluids/oils and hydraulic oils, water, and energy. In particular the increasing cost pressure on industrial enterprises has led to a critical consideration of conventional coolants used in most machining processes. Depending on the workpiece, the production structure, and the production location the costs related to the use of coolants range from 7 - 17% of the total costs of the manufactured work piece [3]. By abandoning conventional coolants and using the technologies of dry machining, this cost component can be reduced significantly (Figure 2.2)

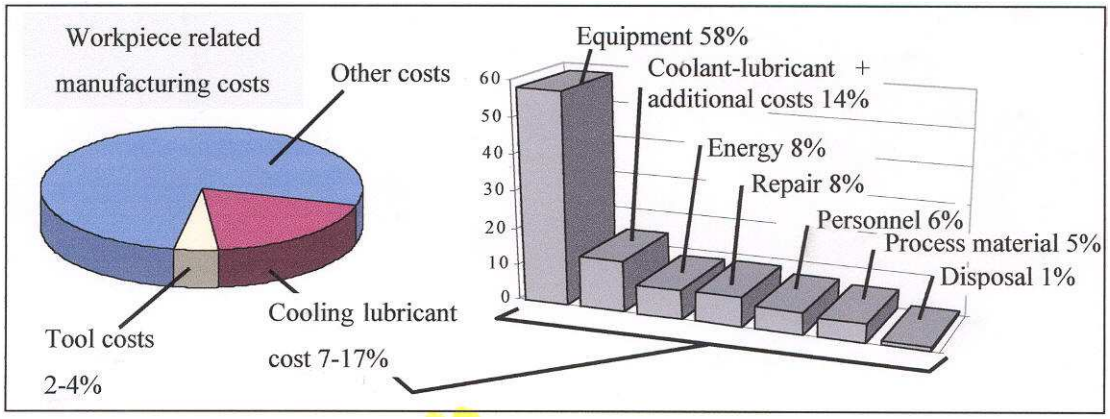

Figure 2.2 – production costs related to a machining process [3]: the cooling lubricant represents the 7-17% of the total production costs

Besides an improvement in the efficiency of the production process, such a technology change makes a contribution to the protection of labour and the environment. The reduction of substantial exposure to coolants in the work place raises job satisfaction and improves the work result at the same time. Furthermore, an enterprise can use economically friendly production processes for advertising purposes, which leads to a better image in the market [4].

2.2.2 Cutting fluids

Early experiences in metal cutting demonstrated the ability of mineral oil in cooling the cutting area, and this has led to the development of fluids specifically designed for metal cutting [18]. The primary functions of cutting fluids are cooling and lubrication. Early observations in metal cutting [50] show that a fluid's cooling and lubrication properties are critical in decreasing tool wear and extending tool life. Cooling and lubrication are also important in achieving the desired size, finish and shape of the workpiece. A secondary function of cutting fluid is to flush away chips from the tool/workpiece. Cooling techniques influences the machining process in various ways. At the contact between the chip and tool, cooling can reduce the chip temperature and, thus, affect directly the friction force between the chip and tool [51]. However, contact pressures are

so high that the cutting fluid has no access to the contact area [52]. The cutting fluid always plays a major role in maintaining the machined material at low temperature, and the demands of high performance cutting require improved cooling ability [53]. Low temperatures were correlated with smaller cutting forces and small chip curl diameters; higher temperatures were associated with high cutting forces, and larger chip curl diameters [54]. According to Sales et al. [56] cutting oils as well as aqueous coolants reduced cutting temperature, the former indirectly by reducing heat generation through improved lubrication, the latter by heat removal. Lubricants reduce friction between surfaces which are in relative motion. At any given rate, the force pressing the parts together controls the intimacy of contact and thus has a direct influence on frictional force. From a tribological point of view, the reduction of the friction between two moving parts depends on the thickness of the layer of fluid, and the thickness depends on the viscosity of the fluid [56]. According to De Chiffre [57], when normal forces are quite low, the viscosity of an intervening layer of fluid can be the major factor in regulating friction. Sales et al. [56] report other properties of the cutting fluid: concentration, fungi and bacteria control, emulsion stability, and pH. However, the most important property considered for this research project is heat transfer ability, and the comparison of the heat transfer coefficient of different cutting fluids and high speed impinging air jet. The most common metalworking fluids used today belong to one of four following categories:

- oil based fluids including straight oils and soluble oils
- chemical fluids including synthetics and semi synthetics
- biological fluids
- foams

According to Hoff [53], the first two categories include fluid that may be hazardous for the operator's health: skin irritation caused by the cutting fluid is well known since early steps of machining technology. However, new trends in using foams and mists lead to critically consider the impact of these new cooling and lubricating techniques on the health of the operator as potential cause of respiratory disease and skin and pulmonary cancer [58, 59]. The knowledge and control of the chip-tool interface temperatures are

essential for the design and accurate selection of a cutting tool for a specific machining application. The maximum temperature generated during machining usually dwells not exactly at the cutting edge, where the compressive and shear stresses are at their highest, but further away on the rake face as shown Davies et al. [60] and Abukhshim et al.[61]. In order to rank cutting fluids according to their cooling ability, cutting temperatures are usually determined experimentally and used as the criterion for comparison. Cutting fluids are also important for lubrication, but in practical conditions it is very difficult to achieve good penetration into the tool-chip interface [13]. Sales categorized the characteristic of various cutting fluids considering their properties and applications. Six different cutting fluids were used:

- Water: Very good cooling quality and poor lubrication quality
- Integral neat oil: Good lubrication and anti-corrosion properties but low specific heat
- Soluble oil has high specific heat with good heat dissipation capability. They possess in their formulation sodium based additives that can reduce superficial stress of the vapour bubbles that occasionally form at elevated temperatures, hindering heat exchange
- Synthetic fluids 1&2 have high specific heat with excellent heat conduction characteristics. Synthetic fluids are polyglycol based, containing water and additives in their formulation. The Synthetic 1 fluid has higher quantities of additives in comparison to the Synthetic 2, therefore it also have a higher viscosity, compared to the Synthetic 2

Sales et al. [56] carried out a series of investigations using AISI 8640 steel and a K10 cemented carbide which quantified the performance of the cutting fluids as shown in Figure 2.1 in terms of temperature of the tool chip interface.

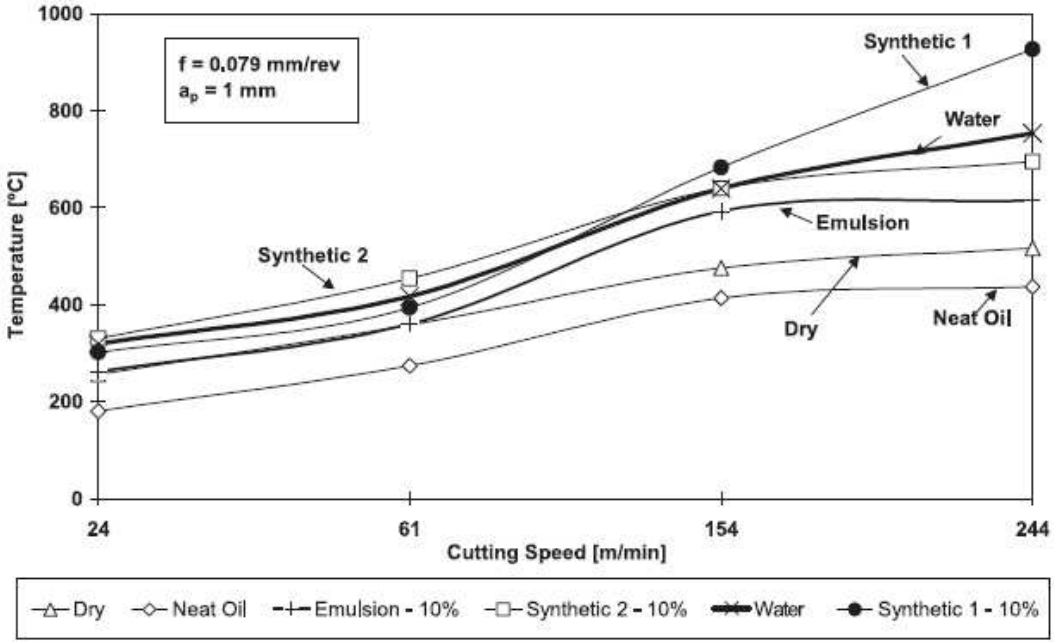

Figure 2.1 – effects of different cutting fluids on cutting temperature (Sales et al.) [56]

The chip-tool interface temperatures encountered in an increasing order are: integral neat oil, dry, emulsion, synthetic fluid 2, water and synthetic fluid 1. The chip-tool interface temperatures were measured using a infrared thermometer. De Chiffre [57] evaluated the performance of integral neat oil, soluble oil and synthetic fluid with sulphur and chlorine additives using the torque of the tool during drilling operations as the controlling parameter to classify the fluids. In two variants of these tests he used pre-drilled holes and tapered holes and concluded that the test is very sensible to the cutting process, the cutting conditions as well as to the established performance criteria. However both De Chiffre and Sales remark that a high heat transfer coefficient of the fluid is not necessarily beneficial, since the cooling ability of the fluid, by reducing the temperature in the shear zone also reduces the softening effect due to the temperature rise in the shear area, consequently increasing the hardness of the workpiece material and causing a local temperature rise. This effect was observed also in the investigation of Liu [62] about the influence of the workpiece hardness on changes in cutting temperature and tool wear. According to Seah et al. [63] the overall effect of applying flood coolant in machining is not always beneficial in terms of wear, since the softening effect that is present with the high temperatures involved in cutting are largely removed by the application of flood

cooling. In the experiments carried out by Seah the low and medium carbon steels AISI 1045 and AISI 4340 were machined on a lathe at a cutting speed of 130 and 190 m/min at a feed rate of 0.15 and 0.20 mm/rev, and a water based coolant was used on the cutting area at a flow rate of 2.5-3.0 l/min (flooding). The findings of Seah are compared with the observation of Shaw [67] on machining of AISI 1020 and AISI 4340. Shaw also report that the use of coolant resulted in a significant shift of the centre of the crater towards the cutting tool tip. Experiments from Seah are consistent with the observations of Shaw. Investigations carried out by Al Huda [64] using a two colour pyrometer for measuring the temperature at the chip-tool interface during AISI 1045 machining at different cutting speeds and feed rates show a minimal reduction of the temperature (less than 3%) when using flood coolants, compared to dry cutting.

2.2.3 Minimum quantity cooling and lubrication

Within the context of dry machining, the term MQCL is generally used to refer to the supply of the coolants in the form of an aerosol. Depending on the type and on the main function of the fluid medium supplied, a distinction can be drawn between minimum quantity lubrication (MQL) and minimum quantity cooling (MQC), according to Figure 2.3. Extensive MQL research has been carried out, including comparison with dry cutting conditions [68, 69, 70, 71, 72]. In contrast to minimum quantity lubrication (MQL), minimum quantity cooling (MQC) has, until now, been a seldom used, and therefore largely unexplored, component of the MQCL technique among industrial users. However, the minimum quantity cooling technique can make a major contribution to the solution of thermal problems affecting the tool and/or the part in dry machining operations [4]. These techniques include high-pressure air jets, water vapour [74] and chilled air [75].

Minimal Quantity Cooling Lubrication (MQCL)
normal consumption per machine hour:
10 – 50 ml MQCL medium

Minimal Quantity Cooling (MQC)	**Minimal Quantity Lubrication (MQL)**
Emulsion (Water+Oil) Water $c_{p,water}$ = 4.18 kJ/kgK Air $c_{p,air}$ = 1.04 kJ/kgK	Oil $c_{p,oil}$ = 1.92 kJ/kgK

Medium	Cooling	Lubrication	Chip removal
Emulsion	excellent	good	excellent
Oil	good	excellent	good
Air pressure	little	no	little

Figure 2.3 – classification of MQC and MQL lubrication and cooling techniques [4]

Diniz et al. [68] has carried out comparative experiments using a CBN tool cutting a hardened steel AISI 52100 workpiece (45–65 HRC) on a lathe, with different cooling methods. Part of the experimental apparatus was a mist coolant device which precisely regulates the oil flow at a constant pressure of 4.5 bar. The nozzle was positioned, 10 mm. away from the tip of the tool, as shown in Figure 2.4. Two phases of experimental investigations were carried out: preliminary experiments and tool life experiments.

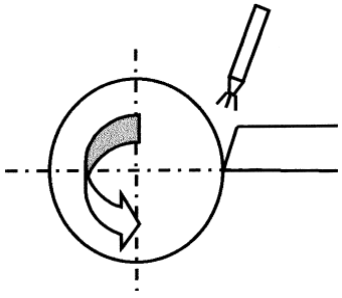

Figure 2.4 – sketch of nozzle's positioning (Diniz et al.) [68]

The preliminary experiments were carried out aiming to establish the best oil flow in the flow of air. The following conditions were used:

- dry cutting;
- compressed air (without any liquid);
- overhead flood (wet cutting with oil/water=1/20);
- MQL with 10 ml/h;
- MQL with 30 ml/h;
- MQL with 60 ml/h.

The cutting conditions used in these experiments were:
cutting speed V =110 m/min; feed rate t =0.08 mm/rev.; depth of cut b =0.3 mm. Tool maximum flank wear and workpiece surface roughness were measured after 553 m of cutting length had elapsed. Each experiment was made with a fresh edge of the insert. Diniz reports that the dry condition and compressed air only presented the smallest flank wear and roughness. This is due to the effect of the high temperature of the cutting zone and to the high hot hardness of CBN. This result confirms the conclusions of Sales et al. [56] about the negative effect on cutting performance of coolants with high heat transfer ability. On the other hand, the softening effect of the workpiece in the shear zone is difficult to control according to Shaw [67]. The reduced heat transfer ability of compressed air allows the control of shear zone temperature without hardening of the workpiece material. For the machining of hardened steel the dry condition seems to be the efficient [75], however dry cutting of soft steels or aluminium alloys produces unacceptable friction. Considering the results obtained in the preliminary experiments by Diniz [68] it can be concluded that the three MQL conditions presented similar results regarding both surface roughness and tool wear. In terms of cutting speed, the maximum value (175 m/min) presented the best surface finishing but rapid flank wear and greater crater wear. The other cutting speeds used did not significantly influence surface roughness and flank wear.
Rahman et al. [70] used energy dispersive x-ray (EDX) and scanning electron microscopy (SEM) in order to investigate the effect of MQL and flood cooling on chips,

In particular that authors focuses on investigating the thermal shock in the cutting are due rapid quenching of the workpiece. Analyses of the cutting force, surface roughness, chip shape and EDX findings reveal that MQL may be considered as an economical and environmentally compatible lubrication technique for conventional machining. Their results with 8.5 ml/h show a considerable reduction in cutting force for the MQL condition when compared to dry cutting and flood cooling. MQL presented the lowest cutting force and lowest flank wear at low speed and low feed. MQL showed an improved tool life compared to flood cooling (insert fracture) and to dry cutting (consistent flank wear due to high friction). SEM images of chips showed evidence of major thermal stress in flood cooling and EDX analysis revealed a better lubricating effect and lower cooling effect for MQL, compared to flooding. Considering the results of Diniz et al. [68] and Rahman et al. [70], it is possible to conclude that MQL is a suitable option for traditional cutting, but it is not always for high performance cutting, and the efficiency of the MQL technique is case specific. Varadarajan et al. [72] and Vikram Kumar et al. [73] made a comparative study on cooling techniques in hard turning, considering dry cutting, flooding and MQL with an extremely low rate of fluid (2 ml/min) with high pressure jet (20 MPa). The performance during minimal cutting fluid application is found to be superior to that during dry turning and conventional wet turning on the basis of cutting force, tool life, surface finish, cutting ratio, cutting temperature and tool–chip contact length. As the minimal rate of application is as low as 2 ml/min a major portion of the fluid is evaporated. These encouraging results could be mostly due by the high pressure applied on the chip, rather than the effective cooling effect of the fluid. This is supported by the work of Çakir et al. [76] who established that the jet pressure in MQL and gas application in machining plays a fundamental role in cooling the cutting area.

The literature presented on MQCL techniques focus on the consequences of the conceptual difference between flood cooling and small flow rate cooling. The MQCL technique avoids the thermal shock that occurs when flood cooling is used, as reported by Rahman [70]. Also the experiences of Diniz [68] suggest that the compressed air has a cooling effect comparable with the cooling effect of MQL techniques. According to Hoff

[53] MQL techniques and oil mists successfully match with high performance cutting operation due to their multiple mechanisms of cooling: the heat transfer due to the contact of the heated surface with the liquid particle and the change of phase of the liquid particle (vaporisation). The multiplicity of mechanism lead to a evenly distributed heat transfer that differs from the use of flood coolants (quenching), and easily leads to thermal shock [5]. Despite the extensive experimental research on MQL, few efforts were made to analytically understand the phenomena. Li and Liang [39] modelled the temperature distributions in the cutting zone under through-the-tool MQL technique, where the coolant was delivered by a hole in the insert. The temperature rise in the chip, the effects of the primary heat source and the secondary heat source were modelled as moving heat sources. For the temperature rise in the tool, the effects of the secondary heat source, the heat loss due to cooling, and the rubbing heat source due to the tool flank wear, were modelled as stationary heat sources. For the temperature rise in the workpiece, the primary heat source, the heat loss due to cooling, and the rubbing heat source due to the tool flank wear were modelled as moving heat sources. The principle used for developing this model is similar to the model proposed by Shaw and co workers [67, 35, 36], also using the Jaeger equations [38] for modelling moving sources of heat and the temperatures of sliding contacts [40]. The model describes the dual effects of air-oil mixture in near dry machining in terms of the reduction of cutting temperature through the cooling effect, as well as the reduction of heat generation through the lubricating effect. Model calibration and validation was achieved by undertaking experimental investigation using an embedded thermocouple in an uncoated tool during the machining of a medium carbon steel. Results show that the tool flank wear has a larger effect on cutting temperature for high cutting speed.

According to Weinert [4] the optimisation of MQL technique leads to further reduction of the amount of coolant in the cutting area, often referred as *near dry machining*. However, near dry machining conceptually differs from MQL technique since the cooling is completely achieved by the vaporization of the fluid particles. Also Klocke [5] affirms the conceptual difference between MQL, near dry machining and dry cutting. Techniques based on dry cutting implicate important advantages from a technological point of view. The thermal shock due to a cooling down of the tools by the cutting fluid is

minimized and therefore the tool life is increased. Moreover the part quality is improved since the rim zone of the machined component cannot be hardened by the rapid quenching due to coolant. However, dry cutting does not represent an improvement in machining materials with a low thermal conductivity, such as titanium alloys and Byrne [1] reports that the introduction of dry cutting requires suitable measures to compensate for the primary functions of the fluid.

2.2.4 Alternative cooling methods

Avoiding the use of cutting fluids in machining operations is one goal of the research in sustainable machining, due to ecological and human health problems caused by the cutting fluid. Usually, cutting fluids still provide a longer tool life for traditional machining operations, but according to Diniz and Micaroni [77] increasing cutting speed and feed rate reduce the difference between wet and dry cutting. Since dry cutting not always represent an optimization of the cutting process (typically with difficult to cut materials), different cooling methods has been experimented, as an alternative to MQL. Han et al. [74] have investigated the use of water vapour.

The tests were carried out by cutting a workpiece of steel 45 with a hard alloy YT15 tool at 86.5 m/min, with a feed of 0.15 mm/rev at four different depth of cut (from 0.5 to 3.5 mm), using the following cooling/lubricant method: dry cutting, compressed air, oil water emulsion, water vapour. Through analysis of the experimental results, water vapour as coolant and lubricant have better lubricating action because of the good penetration performance and the low lubrication layer shearing strength of water vapour. Unfortunately, the use of water accelerates the process of corrosion on the mechanical parts.

Rahman et al. [75] carried out experiments in order to determine the effective zones of the cutting conditions for chilled air in comparison with dry cutting and conventional flood coolant. Chilled air at -30°C at a volume flow rate of 0.4 m^3/min at a pressure of 5 bar was used for cooling the cutting area on a milling machine. Tool damage and chip colour and shape have been observed with SEM and optical photography. Based on the experiments carried out, the following conclusions can be drawn. The tool wear obtained

in chilled air is lower than that for flood coolant at low feed rates and low cutting speeds. However, the tool wear obtained for chilled air is lower than that for conventional flood coolant at low depths of cut except beyond a depth of cut in the 0.2 mm region. This implies that at a lower feed rate, the lubrication ability of conventional flood coolant decreases because of its large oil droplets, which are unable to penetrate effectively into the cutting region. At lower feed rates, the effect of the cooling ability of the chilled air is more evident, thus leading to a lower rate of flank wear. The average surface roughness of the workpiece is lower for chilled air only at higher feed rates. At higher cutting speeds, the average surface roughness of the workpiece in chilled air is comparable to that for flood coolant. The average surface roughness of the workpiece in chilled air is found to be lower than that for conventional flood coolant at a higher depth of cut. However, in the case of machining with chilled air, the chilled air was able to cool the region more effectively than the flood coolant, thus, resulting in a lower average surface roughness of the workpiece. No significant difference in cutting force was observed between the use of flood coolant and chilled air, but the cutting force experienced in dry cutting is higher than that for flood coolant and chilled air because there is little or no lubrication action present and inadequate cooling. A distinct colour difference, due to different degrees of oxidation on the surface of the chips, indicated that the cutting region was cooled more, by a significant amount, in the case of machining with chilled air than with traditional cooling. Despite the low temperature of the air, Rahman remarks that the SEM analysis of the chips do not show any thermal shock due to the temperature difference. The explanation of this behaviour can be addressed to the difference between the chilled air and a flood coolant in terms of convective heat transfer coefficient. Similar observations have been made by Paul et al. [17], using a liquid nitrogen jet and comparing results over dry and wet machining AISI 1060 steel on a lathe.

Specific studies about the effects of the direction of impinging jets, in particular inclination and distance within the hot surface have been carried out by Stevens and Webb [78], Elison and Webb [79] and O'Donovan [80]. However these studies are not related on machining issues. On the other hand an interesting study of heat transfer in machining was carried out by Li [81], paying particular attention to the direction of the jet and jet-flow rate. In this study, the effect of the jet-flow rate of cooling on the

temperature distribution in the cutting region of machining is investigated through numerical simulation using the cooling heat-transfer models previously developed. Two nozzles were placed, one in overhead position, the other along the tool flank, as shown in Figure 2.5. The AISI 1020 was machined at a relatively low speed (61/m/min) but at high feed rate (0.2642 mm/rev) and high width of cut (1.88 mm). The coolant was injected by a nozzle (diameter = 10 mm, distance to shear zone = 40 mm, impingement angle = 60°). Cutting processes with a water coolant applied in overhead-jet cooling and flank-jet cooling at different jet-flow rates were investigated. The flow rates considered in the tests were 10, 15 and 48 l/min for overhead-jet cooling, and 10 and 90 l/min for flank-jet cooling, respectively.

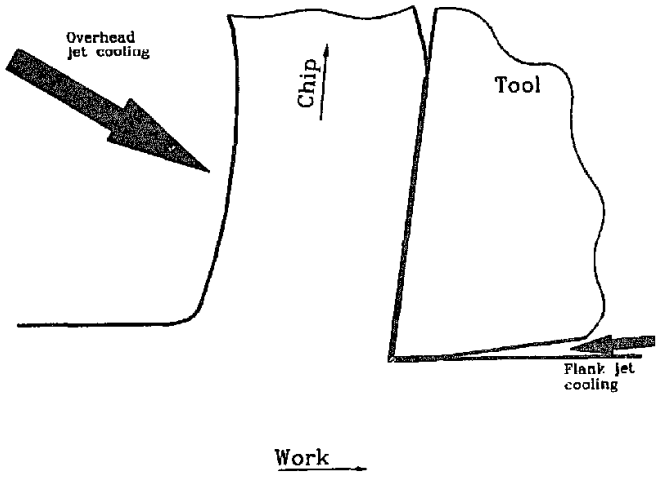

Figure 2.5 – sketch overhead and flank jet positioning in research carried out by Li [81]

In cutting at the testing conditions with overhead jet cooling, when the jet-flow rate was increased by 400%, the temperatures along the tool rake face exposed to coolant and along the flank face were reduced by more than 40% and 26%, respectively, but the temperatures at the tool cutting edge and along the tool-chip interface, including the maximum temperature in the overall cutting region, were little changed. The results show that with the nozzle overhead position it is possible to achieve a good reduction on the rake face and in the cutting area exposed to coolant. The approach of Li is based on low

temperature of gas jet, rather than jet speed and pressurized gas (Diniz [68], Su et al. [82], Li and Seah [83]), and this experience cannot be considered in the group of high speed jet cooling. However, the research carried out by Li establishes a base for further investigations in nozzle positioning.

2.2.5 The mechanical effect of the air jet

The literature on the mechanical effect is poor and case specific. A fundamental study on the mechanical effect of low pressure and high speed air jet in machining process do not exist in the scientific literature. Despite the lack of scientific literature provided the greater motivation in the development of this research work, the need of comparing the results obtained with other works lead to consider the mechanical effect of the air jet in the wider perspective of the machining processes assisted by an external source of energy. The existing works on machining processes assisted by air jets suggest that a mechanical effect exists, but the concept is not critically considered or evaluated as a primary research topic. The motivations in developing an air jet cooling technology are based on ecological and safety issues. Even if MQL is good from an environmental point of view, this is not true for operator's health, since cutting fluid in mist form is easily breathable. Some cooling gases too, despite their efficiency in terms of cooling [76], represent a hazard for the operator's health. If care is not taken, contact of the mist with eyes may cause irritation, and breathing in the mist may cause serious respiratory problems. Mist coolant also causes air pollution. Therefore, a good strategy is to implement air assisted machining as it offers significant benefits. Despite the advantages offered by this cooling technique, technical investigations are still quite rare and strongly dependent on cutting condition and jet direction. Su et al. [82] carried out research on the effects of refrigerated cooling air cutting of difficult-to-cut materials in terms of tool life, surface finishing and chip shape, offering a comparison with different cooling methods (dry cutting, MQL and mist). The results show application of cooing air and mist offer a drastic reduction in tool wear and surface roughness, and significant improvement in chip shape in finish turning of Inconel 718, and also in the high-speed milling of AISI D2, cooling air cutting gave longer tool life and slightly higher surface roughness than dry cutting and MQL. Therefore, it appears that cooling air cutting can provide not only

environmental friendliness but also great improvement in machinability of difficult-to-cut materials, as also reported by Ezugwu [85] for machining aero-engine alloys.

Li and Seah [83] and Davim [84] carried out studies on machining metal matrix composites, which can be classified as difficult-to-cut materials for the high abrasive nature of the hard particles in the relatively soft metallic matrix. Experimental tests for cutting of SiC–aluminum metal matrix composite with different amounts of hardening particles using coated tungsten carbide tools with and without the aid of the pressured air jet were conducted. The results show that tool wear is reduced when using the air jet. Cutting tests were firstly conducted to investigate the effect of pressured air jet directions on the working efficiency of the jet assistance. Best results were observed when the outlet pressure of the air jet used was set at maximum pressure (6.5 bar). The set of tool wear results was obtained from subjecting the cutting area with the air jet directed from overhead position, i.e. on the top face of the chip with no contact with the rake face. The best result has been found when the air jet is directed parallel to the rake face, in interfacial position, even if the beneficial effects of an air jet, compared to dry cutting, are significant in every direction. From the interfacial position the compressed air is able to flush away free SiC particles, loose debris and chips as well as aiding in SiC dislodgment at the cutting surface, thereby reducing abrasion by a significant amount. This effect can be explained by Figure 2.6. Air jet interfacial cooling is particularly efficient with a high amount of particles. The effect is due by the poor adhesion to the rake face of the soft matrix. This allows the air jet to penetrate deeper into the interface. According to the authors, this could be true also for traditional materials, but the interface conditions could be different from dual phase steels and metal matrix composites. Therefore the behaviour at different pressure and different nozzle position could be different, even if there is no doubt of beneficial effect of air jet cooling.

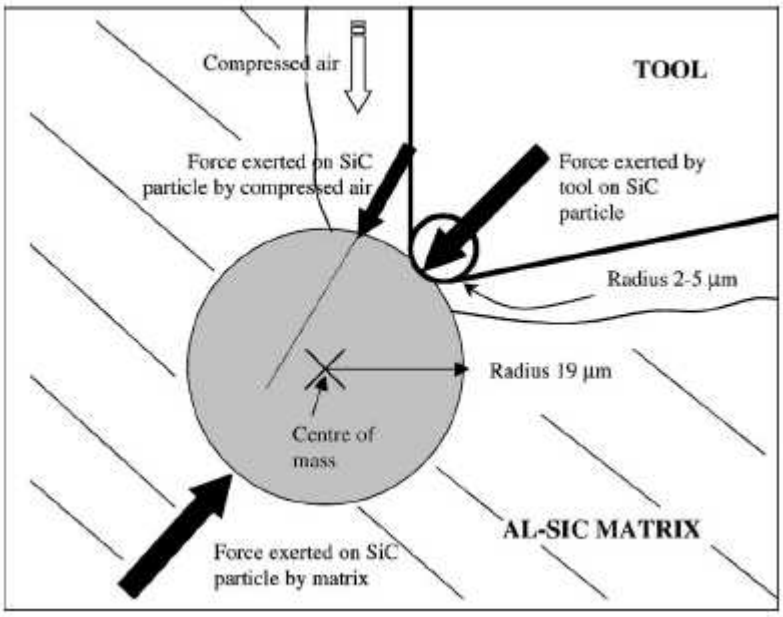

Figure 2.6 – sketch of air jet assisted cutting of Al-SiC metal matrix composite with force applied by air jet on SiC particle (Li and Seah) [83]

The work carried out by Li and Seah is one of the few cases the air jet blowing force is specifically used for its beneficial effects. Since the use of the blowing force to produce a beneficial mechanical effect on the cutting process should be implemented in more general situation in machining processes, a wider perspective is required for understanding the mechanical effect of the air jet, and its role in reducing cutting temperature [65]. Dahlman et al. [66] affirm that a mechanical effect of the jet exists, but they consider it as negligible at conventional pressures. Also Klocke mention the use of high pressure (140 bar) air jet for titanium alloys [5]. In the approach proposed in this thesis the air jet is seen as an external source of mechanical elastic energy applied on the chip. Concluding this part of the review about new cooling methods in machining, different experiments have been carried out on MQL, waer vapour, cooling gases, chilled air and high speed air jet. The purpose of developing all these environmental friendly cooling techniques is to get close to dry machining performances and reducing the tool wear, improving tool life and surface finish. Most jet applications are strongly dependent on jet position and should be discussed for each different situation.

2.3 Machining assisted by external source of energy

The researches carried out on the cooling effect of oil based coolants show that an undesired cooling of the workpiece could represent an obstacle to the optimisation of the cutting process (Paragraph 2.2.2). An area of ongoing research is the attempt of artificially heating the surface of the workpiece just before a cut is taken. This procedure will raise the temperature of the workpiece closer to or slightly above the recrystallization temperature and hence reduce the tendency to strain harden (Shaw [67]). In early research on workpiece heating several methods have been employed, including: furnace, gas torch, induction coil, carbon arc, electrical resistance [1]. Modern methods of locally heat the workpiece include the use of laser and plasma beams. Laser and plasma assisted machining uses a beam focused on the work material just in front of the cutting tool. The beam extends over the entire depth of cut and is positioned and adjusted to soften the material (or to induce a local phase transformation of the workpiece material [22]) on the shear plane without allowing appreciable laser energy to flow into the tool. According to Shaw [67] this constitutes a difficult control problem and requires a relatively expensive high power (15-20 kW for conventional machining) continuous wave or pulsed beam. The high power required is due in part to the fact that the absorptivity of a high-temperature alloy is relatively low. In the past decades a significant effort was carried out in order to study the influence of laser beams in machining, both in conventional materials [23] and hard to machine materials [5]. Pfefferkorn et al. [25] carried out a research on micromachining of AISI 1018 steel workpiece, locally preheated by a laser beam. The energy introduced by the laser (100-175 W) is significantly greater than that generated in the primary and secondary shear zones (less than 10 W) for the operating conditions used in this study. Therefore, energy introduced by the laser is the dominant heat source and controls the level of thermal assistance. The results show that locally preheating a metal workpiece, even a relatively soft metal, can reduce the specific cutting energy enabling a micro end mill to achieve significantly higher feed rates and levels of productivity. The main finding of the research of Pfefferkorn is that, even though micromachining has a higher surface area to cut volume ratio than macro scale machining, the reduction in flow stress of the preheated workpiece is greater than any increase in friction or adhesion. The main consequence of the reduction of the flow stress

is a consistent reduction in the cutting force. Micrographs of the cutting are and chips show a phase transformation on the surface of the workpiece and in the substrate. However, most of the works carried out on the effect of laser preheating of the workpiece, remark that the thermal treatment induced by the laser affect the workpiece only at shallow depth [23]. Dekumbis [86] observes that the shape of the chip is different when the laser is used in machining. In particular the higher curvature radius of the chips suggests that the thermal treatment applied by the laser on the uncut surface promote a stretch of the upper layer of the chip. This effect was observed also when the phase of the material in the upper layer was unchanged. This observation supports the hypothesis that a change in the chip shape is accompanied by a change in the stress distribution on the cutting area. Baker [26] observes that the elastic deformation of the chip produces a local variation of the stress in the cutting area. This observation is fundamental to analytically introduce the mechanical effect of the air jet, which was considered in the analytical model as an external source of energy, able to produce an elastic deformation in the chip.

2.4 Heat transfer by impinging jet

Impinging jets are known as a method of achieving particularly high heat transfer coefficients and are therefore employed in a broad range of engineering applications. Although liquid jet cooling yields higher heat transfer coefficients, air jet cooling can be very effective and clearly has merits in terms of the simplicity of the cooling system. Thus, El Sheikh and Garimella [87] investigated the air impingement cooling of heat sinks for electronics, Roger et al. [88] investigated the jet impingement cooling of a high temperature solar thermal receiver and O'Donovan et al. [89] and Babic et al. [90] used air and mist jet impingement respectively for the cooling of a grinding process. In order to interpret the results from jet impingement cooling, it is necessary to determine the convective heat transfer coefficients. One common technique for determination of convection coefficients from surface temperature measurements involves a step change in temperature of either the fluid or the test specimen; thus the necessity for electrical surface heating, and the associated geometric constraints, is overcome. Most studies based on this technique have involved the instantaneous introduction of a heated flow

field to the specimen [91, 92]. However, in the study of Martinez-Botas et al. [93] the test section is heated and then introduced to an ambient temperature flow. In both cases the rate of heat transfer is found by measuring the surface temperature as a function of time. Although most previous investigations have used liquid crystal thermography for these measurements, Ekkad et al. [92] developed an approach based on IR thermal imaging, which determines both heat transfer coefficient and film effectiveness (non-dimensional adiabatic wall temperature) in a film cooling application. Solution of the transient conduction equation with a semi-infinite solid assumption then yields the convective heat transfer coefficient.

The sensitivity to local heat transfer coefficient in machining operation is low enough to consider only the order of magnitude of local heat transfer coefficient in machining operation [95] and the local heat transfer coefficient in high speed air jet assisted machining is about 100 times greater than free resting air. Recent works carried out by Umbrello et al. [20] demonstrated that the sensitivity of the cutting temperature to the heat is very limited, and Kops [95] confirms the finding of Umbrello. According to Kops, the heat transfer coefficient of free resting air is 20 W/m^2K, and the local heat transfer coefficient of a free air jet impinging estimated by a set of thermocouple embedded in the workpiece is up to 2400 W/m^2K. The Figure 2.7 shows a sketch of the jet regions (free jet region, stagnation region and wall jet region) and distribution of heat transfer coefficient as a function of distance from jet axis. The sketch also show that at 10 mm of nozzle distance from the rake face the circular area in the air cone pattern has a diameter of 3.8 mm. Also the heat transfer coefficient is rapidly falling off with the distance from jet axis [80], demonstrating good area selectivity of air jet, compared to traditional flood coolants. The experience of Kops, supported by the observations of Umbrello and the research carried out on impinging air jet presented in this paragraph, show that air jet cooling in machining is a suitable choice, but its efficiency is strongly dependent by the distance and the position of the nozzle to the surface.

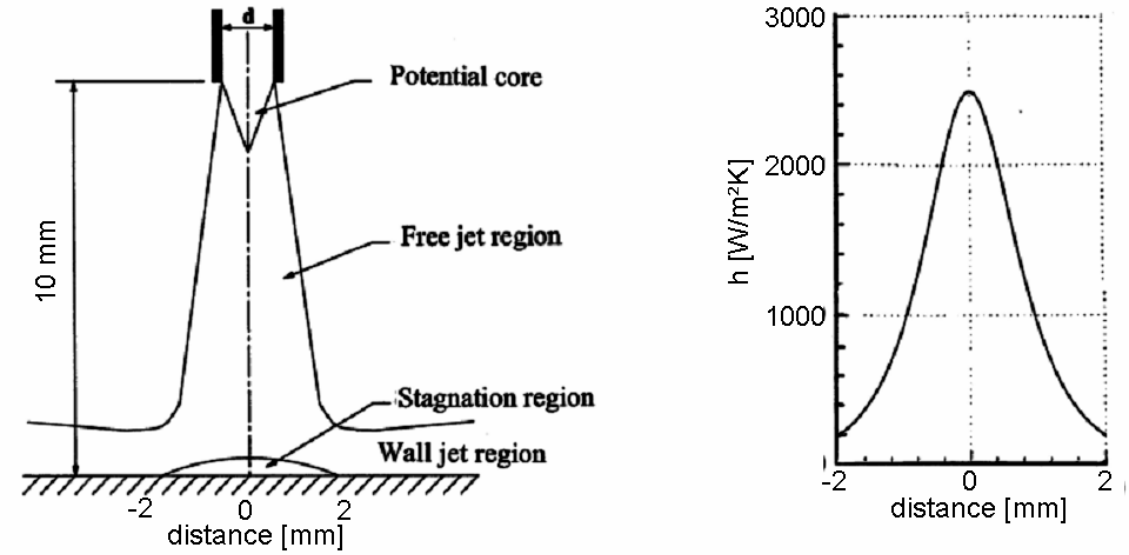

Figure 2.7 – sketch of air jet cone distribution with wall jet region and corresponding qualitative distribution of local heat transfer coefficient as a function of distance [95]

2.5.1 Finite element modelling in metal cutting

Advanced finite element software allows accurate simulations of metal cutting providing all input parameters such as material properties, friction and material separation criteria are known, and allows qualitative and quantitative analysis that are difficult to obtain by experimental methods, as reported by Altan et al. [96]. In metal cutting, deformations take place close to the cutting edge of the tool and high strain-rates and temperatures occur. Workpiece material deformation behaviour is highly sensitive to the cutting conditions, as reported by Potdar et al. [97]. The frictional conditions between the tool and the workpiece are highly complex and also sensitive to the cutting conditions. According to Fisher et al. [98], accurate predictions of the distributions of the process variables such as stresses and temperatures with finite element simulations are useful for identifying optimum cutting conditions, tool material, edge geometry and coating in order to help improve productivity and quality of industrial machining operations.

In finite elements modelling, there are two types of analysis to describe a continuous medium: Eulerian and Lagrangian. In a Lagrangian analysis, the computational grid deforms with the material. In an Eulerian analysis the grid is fixed in space. The

Lagrangian calculation embeds a computational mesh in the material domain and solves for the position of the mesh at discrete points in time. Some of the models used to model orthogonal metal cutting have used Eulerian formulation. The vast majority rely on the Lagrangian formulation, which allows the chip to be modelled from incipient to steady state. However, using a Lagrangian formulation requires a criterion for separation of the undeformed chip from the workpiece. As a result, the development of a realistic separation criterion is an important factor in the FE modelling of cutting. The most common approach is the Arbitrary Lagrangian Eulerian formulation (ALE) that works similarly to an updated Lagrangian formulation but avoids frequent remeshing. In these analyses, two distinct methods, the implicit and explicit time integration techniques can be utilized. The implicit technique is more applicable to solving linear static problems while the explicit method is more suitable for nonlinear dynamic problems. A dynamic explicit FE formulation is very efficient for simulating highly non-linear problems involving large localized deformations and changing contact conditions such as those experienced in machining. With these observations in mind, the choice of the FE software was restrained to the packages that use the ALE formulation.

2.5.2 Flow stress and friction

According to Grzesik et al [100] a review of the technical literature reveals that currently, finite elements modelling of cutting is not fully capable of simulating practical machining operations. The complexity and the diversity of cutting processes are such that a single process model or simulation cannot be applied to all materials and cutting conditions. Since the early ’90s, continuous improvements in the modelling of orthogonal metal cutting have been developed by a number of researchers. Mackerle [102] presented a bibliography which summarises these efforts. Predictions by FE analysis are greatly influenced by two factors; a) the flow stress characteristics of the workpiece in cutting regimes and b) the friction characteristics at the chip-tool interface. The influence of work material flow stress upon FE simulations may be less when there is a constitutive model for the workpiece that is obtained empirically from high-strain rate and temperature deformation tests. Usually this kind of approach is also convenient in terms

of computational time. Özel [101] identifies an empirical flow stress model using the Hopkinson bar (Eq.2.6). Altan et al. [96] summarized the status of finite elements modelling, illustrate a procedure for identifying flow stress empirical law using 2D slot milling tests. Results on low carbon steel seem to confirm the results produced by Özel. According to Özel [101], currently there is not a reliable analytical model for friction conditions at the chip-tool interface, which is the primary heat source for the tool temperatures. This observation is confirmed by the work of Umbrello et al. [20], in which a constant interfacial friction coefficient is used. The friction coefficient used in the finite element simulations in this research work is based on force measurements in preliminary cutting tests.

2.5.3 Finite elements applications in machining

Finite elements analysis is widely used by industry for prediction and optimization of basic manufacturing processes, according to Fischer et al. [98, 99]. However, the use of finite elements for research purposes often requires case specific solutions. An extensive literature review on finite elements modelling for metal cutting goes beyond the purposes of this work. Therefore in this literature review only works particularly related with this research project has been reported. Since the air jet was modelled only by the two controllable variables involved by air jet cooling (the pressure of the jet and the local heat transfer coefficient)

Yen, Altan et al. [103] used DEFORM 2D for estimating tool wear on the tool–chip and tool–workpiece interfaces. Based on temperatures and stresses on the tool face predicted by the finite element analysis simulation, tool wear may be estimated with acceptable accuracy using an empirical wear model. The overall objective of their study is developing a methodology to predict the tool wear evolution and tool life in orthogonal cutting. To approach this goal a tool wear model for the specified tool–workpiece pair is developed via a calibration set of tool wear cutting tests in conjunction with cutting simulations. For the estimation of tool wear rate for a carbide tool in cutting low carbon steel, the wear rate model developed by Usui, has been implemented into the finite elements code. The technique of the moving window-based boundary condition was

widely used by Yen. The same technique was used in the finite element model shown in this thesis, for locally applying the thermal and mechanical boundary conditions.

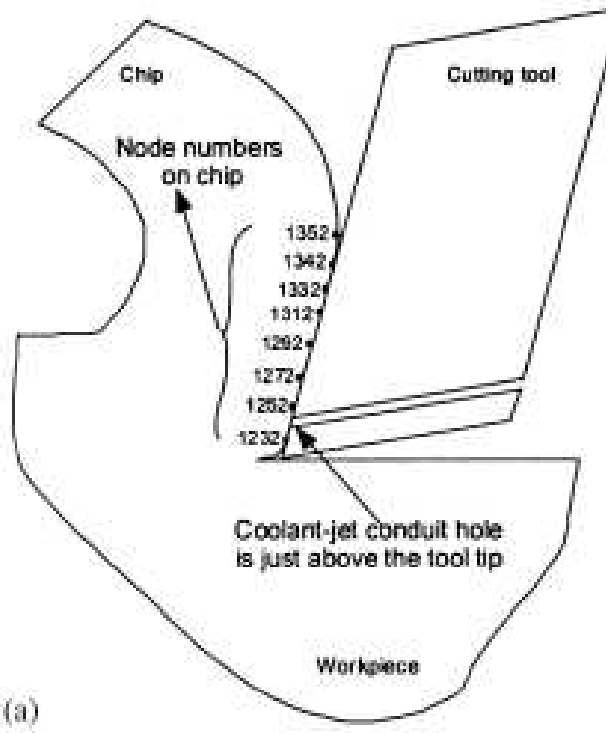

Figure 2.8 – finite elements model concept by Shet et al. [104], showing hole for high pressure coolant in the insert

Shet et al. [104] carried out a work about modelling high pressure water jets in chip-tool interface by finite elements. The model considered a hole through the tool and analysed the reduction of friction in the interface, in relation to the pressure and the position of the hole. The mechanical effect of the high-pressure jet has been approximated as a pressure loading at the tool–chip interface. The frictional interaction along the tool–chip interface is modelled by using a modified Coulomb friction law. Chip separation has been modelled by a nodal release technique and is based on a critical stress criterion. The FE model developed by Shet proposes the idea of a stress distribution modified by the pressure applied by the coolant, which is also used in the finite element model proposed in this thesis.

2.6 Temperature measurement techniques in orthogonal cutting

Most existing methods for measuring temperature have been applied to material removal processes. According to Childs [105], the factors that should be considered when choosing a temperature measurement method for a particular application are:

- temperature range
- sensor robustness
- temperature field disturbance by the sensor
- signal type/sensitivity to noise
- response time
- uncertainty

These should be weighed against the following criteria: ease of calibration, availability, cost, and size. The review on the temperature measurement in metal cutting carried out by Davies et al. [60] provide fundamental guidelines in the choice of the measurement method, and the document largely influenced the choice of the embedded thermocouple for measuring the temperature in this research work. The alternatives to the embedded thermocouple were the tool-workpiece thermocouple assisted by mercury slip ring. In material removal processes, many sources of error associated with the thermocouple cannot be minimized, but instead can be worsened by the removal process itself [106]. For example, thermocouple junctions near a tool edge are subjected to large thermal gradients and/or rapidly changing temperature, introducing the first and second types of uncertainty. According to studies on thermal microscopy of the rake face with a resolution of 5 μm during machining of AISI 1045 steel, carried out by Davies et al. [107], the dynamic or tool-workpiece-type thermocouple is not surprisingly subject to the worst inhomogeneity and gradient errors. The presence of very large thermal gradients in the region of material inhomogeneity actually precludes tool-workpiece thermocouple practice. Nevertheless, researchers have attempted to conduct theoretical and numerical

analyses of the tool-workpiece thermocouple in order to determine the effect of a variable temperature on the tool-work interface [60, 108].

In the work presented in this thesis, the technique of embedding the thermocouple in the cutting tool was used. Shaw [67] reports that the hole in which the thermocouple is placed represents a disturbance and may appreciably change the temperature field being measured unless it is very small. After this qualitative observation, a comprehensive review of the technique was carried out by Attia and Kops [109, 110, 111, 112]. Recently, embedded thermocouples have been used by several authors to establish semi-empirical equations that relate tool temperature to cutting process parameters and tool wear. Such an approach is illustrated in Ay et al. [114, 115], where an experimental study is performed using nine fast response, K-type, fine thermocouples inserted at various locations in a carbide tool in order to monitor temperature variations of the tool and workpiece in orthogonal cutting, by using a thin walled tube. The response time of the thermocouples is less than one second which allows researchers to derive a semi-empirical model of the dynamic temperature changes. Using their measurement setup and a process similar to that used in infrared imaging, the authors are able to provide comprehensive data for temperatures in cutting, with both worn and unworn carbide inserts in a number of materials. Embedded thermocouples have also been used by Kops and Arenson [95] for temperature measurements to determine the convective heat transfer coefficients in turning. This data is necessary for accurate prediction of machining error caused by thermal expansion of the workpiece. The study also revealed that for proper representation of convective cooling of a workpiece in turning, separate values of the heat transfer coefficient (h), are needed for the cylindrical surface, side faces, chuck zone and impinging coolant zone. The single embedded thermocouple measurement method was successfully used by Barlier et al. [116, 117, 118] and the same method was used by Lazard et al. [119] for validating their analytical predictions. In conclusion the literature review on temperature measurements methods shows that the embedded thermocouple is an efficient method for measuring temperature, if appropriate calibration of the sensor is carried out [121].

2.7 Conclusions

The state of the art and the scientific literature reviewed in this chapter focuses on the feasibility of using high velocity impinging air jets for cooling machining processes. A comprehensive review of the cooling methods currently used in machining is presented, with particular emphasis on the environmentally efficient and sustainable machining. With regard to flood cooling, researchers agree that the flood coolant promotes a rapid quenching of the workpiece in the cutting zone. The rapid change of temperature causes, in many cases, hardening of the material, which subsequently promotes a temperature increase. MQCL techniques attempt to provide cooling and lubrication in the chip-tool interface, without promoting the hardening of the workpiece material. From the literature it can be considered that air jet based cooling techniques fit in the group of environmentally efficient cooling techniques, and since the heat transfer coefficient of the air is relatively low, compared to oil based coolants, it avoids the hardening of the workpiece material. Two effects are recognised in air jet cooling: the forced convection and the mechanical effect. From the absence of discussion in the literature on the mechanical effect of the impinging jet, it can therefore be considered as a new concept in the context of its application in machining; A fundamental study of its application in machining does not exist. The air jet can be considered as an external source of energy that promotes an elastic deformation in the chip. A review of alternative techniques for external energy assisted machining such as the techniques based on laser and plasma beam assisted machining was presented. These techniques cause a beneficial alteration of the stress distribution in the cutting area. The mechanical effect of the air jet is believed to have a similar behaviour without promoting the change of phase in the workpiece material at shallow depth. This hypothesis was developed in the analytical work presented in this thesis. Taking into account that temperature during machining is a key metric to evaluate the hypothesis in this research work, a review of the temperature measurement techniques was presented. The scientific literature presented a number of techniques and particular emphasis was placed on the tool embedded thermocouple technique as a pragmatic, robust and reliable method to measure temperature during machining.

3. Finite element modelling of orthogonal cutting

3.1 Finite element method overview

The finite element method was developed towards the end of the 1940s and early 1950s and was first used for solving complex elasticity and structural analysis problems in civil and aeronautical engineering [122]. It gained prominence in the 1960s in parallel with developments in the processing capabilities of computers which made it possible to solve thousands of simultaneous equations in seconds. The finite element method is a computer based numerical technique used to solve complex problems by assuming that the area under investigation can be subdivided into smaller and more manageable elements of finite size. When a solution is obtained for one of these elements, the solution procedure is applied to the remaining sections. The overall solution is based on the assembly of all the partial solutions. For structural or solid mechanics problems, the process uses the relationship between the force applied to a simple spring and the displacement that is caused when this occurs.

$$F = k\,\delta \qquad \text{Eq. 3.1}$$

where F is the force exerted, k is the stiffness of the spring and δ is the displacement. The stiffness of the spring corresponds to the slope of the force versus displacement curve. Knowing this value of stiffness and the force applied, the displacement may be obtained. If a single node in a model is considered, a force on that node deforms the element, giving a displacement value which can be used to calculate strain, and hence stress, using the constitutive equations. However each of the nodal forces may produce a displacement not only of the node on which it is applied, but also to each of the other nodes of the element. The mathematical model representing the force-displacement relationships

requires certain information before it can be solved. These include: co-ordinates of each node, material properties of all materials, loading conditions, boundary conditions, type of analysis to be performed (static, dynamic, thermal). Large numbers of equilibrium conditions are then formulated and these have to be satisfied by solving thousands of equations (depending on size of model) with the aid of finite element software. The resulting nodal displacements are then used to obtain the stress and strain distributions within the entire domain. As the amount of data required for the model to simulate an actual component is large, the computational time is great.

Prior to using any FE models for an engineering application, it is most important that the modelling techniques and the boundary conditions used are defined as accurately as possible. The most assured method of verifying the FE results is by direct comparison with experimental results. Once the predictions from FE results were shown to correlate with the experimental data, the FE technique can be used to its full potential.

Using non-linear stress-strain relationships, FE models can be produced which can optimize a wide range of machining variables which would be difficult to do experimentally. The effective modelling of an orthogonal metal cutting process requires a fully coupled thermo-mechanical simulation to account for the large temperature and strains that occur during machining. A fully adaptive non-linear remeshing algorithm is required to predict the formation of the machined surface and other workpiece factors such as chip curl, thickness and chip/tool contact. The FE method was used in this research project for two purposes. Firstly, to provide a deep insight in the cutting process, by simulating features that can not be experimentally determinate, typically the stress distribution and temperature distribution. Secondly, to provide inputs for the analytical model, such as the stress along the shear plane, the strain rate and the thickness of the shear zone, since this quantities can be calculated only with an analytical model more sophisticated than the model used for this project.

3.2 The choice of FE software

The choice of finite element software for machining analysis is an important factor in determining the quality and scope of analysis that can be performed. Some of the most

popular finite element software packages for metal cutting simulation are DEFORM, ADVANTEDGE and ABAQUS. Gardner et al [123] made a qualitative comparison of a number of finite element software packages that can be used for the modelling of machining processes. Some of the issues are highlighted and discussed below.

ABAQUS

- Manual design of workpiece and tool, mesh refinement and boundary condition have to be set manually
- No material library, but materials can be defined in detail
- Partial support in adaptive remeshing
- Good control of the solver

This is a general purpose finite element package, not specifically designed for metal cutting. The learning curve is steep and the complexity of the package means that there is often a significant time investment before a useful model is realised.

ADVANTEDGE

- Very efficient interface to rapidly configure a model; tool library is provided
- Extensive material library
- Uses adaptive remeshing, but controls cannot be modified
- Not suitable for customising control functions.

This is a package designed specifically for machining, but offers poor control of the solver and poor flexibility in applying unconventional boundary conditions. This software facilitates rapid setup of the model and the libraries are extensive. These features make ADVANTEDGE a powerful tool for industry, but the limited flexibility makes it less suitable for research purposes.

DEFORM

- Built in “wizard” for machining
- Good material library and comprehensive material editor
- Uses adaptive remeshing, good control of meshing parameters
- The user can chose the solver but minimal control is permitted.

This software allows a simulation to be set up in a reasonable amount of time, and the boundary conditions are flexible enough to model the effect of various cutting conditions.
In finite element modelling, there are two types of analysis to describe a continuous medium: Eulerian and Lagrangian. In a Lagrangian analysis, the computational grid deforms with the material. In Eulerian analysis the grid is fixed in space. The Lagrangian calculation embeds a computational mesh in the material domain and solves for the position of the mesh at discrete points in time. Most of the metal cutting modelling software uses a Lagrangian formulation.
In this study, commercial finite element software packages, DEFORM-2D v9.0 and DEFORM-3D v6.1, which have an incremental Lagrangian formulation with an implicit integration method designed for large deformation simulations, are used to simulate the cutting process. The solver used was the sparse matrix with a direct integration method, because the conjugate-gradient offers an improved computational speed but less stability in convergence.
The flow stress material model is critical for a successful incremental simulation. The DEFORM material library provides a wide range of flow stress models in the form of tables and parameters. However the default tables present only a minimal number of points to represent the stress as a function of strain, strain rate and temperature. The comparison between the FE solution and the experimental tests shows that the material model proposed by the material library of DEFORM is more rigid than the material model proposed by Hastings et al. [32] for AISI 1020. Since the simulations carried out with the material model by Hastings better fit the experimental data, the flow stress model by Hastings et al. [32] was coded in Matlab (see Appendix C) and used instead of the default flow stress model for AISI 1020 by DEFORM material library.

3.3 Geometry and mesh

The 2D geometry of orthogonal cutting is limited to the region where the variables of state considered (temperature and stress) presented a gradient. Figure 3.1 shows an overview of the 2D geometry, composed by the workpiece (yellow) and the insert (blue).

The tables in the Figure 3.1 show the thermal properties of the materials used for modelling the workpiece and the insert. The geometry of the insert represents a slice of the 3D sketch realized for the 3D analysis. Figure 3.2 shows the 3D sketch of the insert that represents the geometry, complete with the holes for the thermocouple. The 3D sketch was sliced in the plane shown in the sketch.

Workpiece	
Material	AISI 1020
k (W/mK)	51.9
c (J/KgK)	486

Insert TNMG 11 03 02-MF 4025			
Material	WC	TiC	TiN
k (W/mK)	84	54.1	35.6
c (J/kgK)	180.7	192.7	144.6

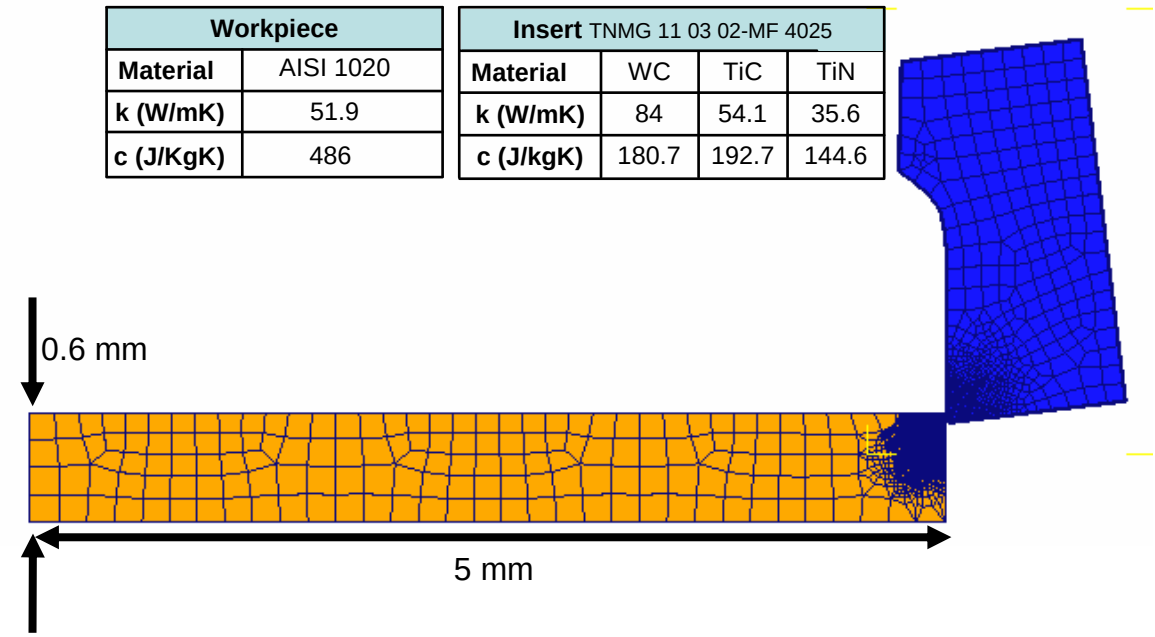

Figure 3.1 – The geometry used in the 2D finite element model. The workpiece is shown in yellow, the insert is in blue

In the 2D geometry the hole for the thermocouple was omitted so as not to compromise results in the 2D tool stress analysis. The presence of the hole in the 2D plane added concentrated stress at the edge of the hole for the thermocouple, represented as a rectangle in the 2D geometry, which is not realistic in a 3D geometry, and may lead to misinterpretation of results. The insert used in this work has three layers of coating for a total thickness of 5.5 µm. According to the Coromant technical guide [124] the edge radius is at least twice the total thickness of the coatings; therefore an edge radius of 12 µm was used in the geometry used for FE modelling. Figure 3.2 also shows the height from the rake face and the distance of the chipbreaker from the cutting edge, and the clearance angle of 7°. DEFORM uses an automatic remeshing algorithm. Remeshing is triggered by the penetration of the insert into a generic element of the workpiece. For a

fine mesh the typical value of the interference depth between the master object (the insert) and the slave object (the workpiece) is roughly half of the length of the slave element. Window meshing and relative element size were used for providing optimal mesh control at a relatively low computational cost. Figure 3.3 shows the meshing of the workpiece and the meshing of the insert.

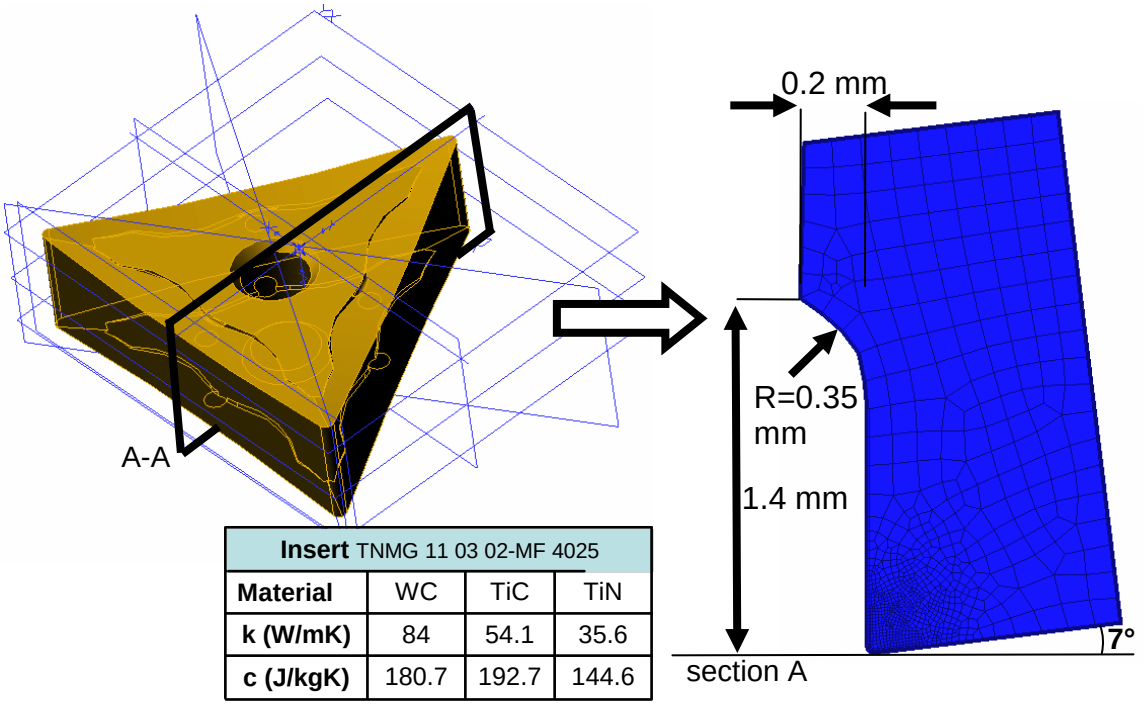

Insert TNMG 11 03 02-MF 4025			
Material	WC	TiC	TiN
k (W/mK)	84	54.1	35.6
c (J/kgK)	180.7	192.7	144.6

Figure 3.2 – The 2D geometry has been obtained by the section A-A of the 3D geometry. The 2D geometry reports the main geometrical features of the insert

Most of the workpiece was meshed by using a ratio of 0.15 between the smallest and the largest element, shown in the figure as coarse mesh. The cutting area shows a finer mesh with a ratio of 0.001 between the smallest and the largest element, so that the elements in the cutting area have a size of 8.75 μm, and the interference depth for triggering the remeshing is 4.54 μm. According to the user manual of DEFORM [125] the interference depth should be approximately half of the minimum element size. Since the insert is considered as a rigid object, it does not require remeshing. The mesh of the insert is refined close to the cutting edge. The insert is modelled as a multiphase object, since four materials are used: the substrate of WC, and the three layers of coating (Ti(C,N), Al_3O_2

and TiN). Special meshing is required for coating, and three bands of elements, with different material properties, distributed along the edge of the geometry. Each band has a thickness of 1.8 μm, so that the total thickness of the three bands represents the thickness of the coating (5.5 μm).

Workpiece	
Material	AISI 1020
k (W/mK)	51.9
c (J/KgK)	486

Insert TNMG 11 03 02-MF 4025			
Material	WC	TiC	TiN
k (W/mK)	84	54.1	35.6
c (J/kgK)	180.7	192.7	144.6

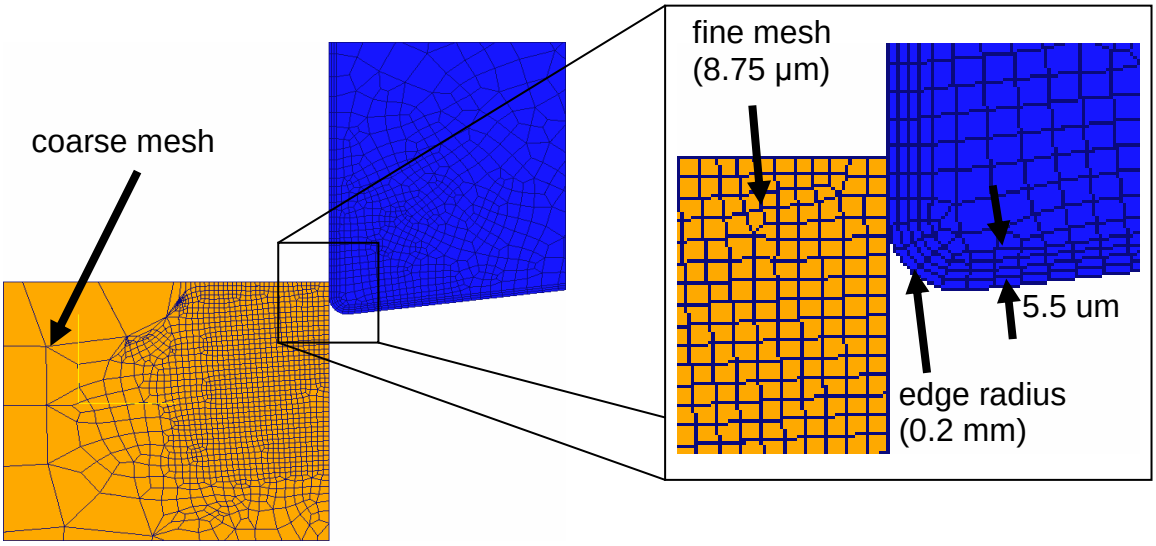

Figure 3.3 – Workpiece and insert meshing. The mesh in the cutting area is finer than the mesh not in the vicinity of the insert. The presence of multilayer coating influences the mesh of the insert and the cutting edge radius

A mesh sensitivity analysis was performed in order to identify the best compromise between error in cutting temperature and computational time. Figure 3.4 shows the error in cutting temperature when the same simulation is run with different mesh sizes. Since the error is supposed to be related to the mesh size, a simulation with an extremely fine mesh was chosen for defining the error. The reference mesh size is 2.13 μm. The error shown in Figure 3.4 is determined by comparing the simulation results with the

simulation with a mesh size of 2.13 μm. The length of each incremental simulation was 100 steps. The results of each simulation were compared at the same step number and the error shown in the table is the mean error over 100 steps. It can be observed that for mesh finer than 0.01 the error became scattered. Therefore, there is no need in choosing the finest mesh size. For the simulations carried out for this research project a mesh size of 8.75 μm was chosen.

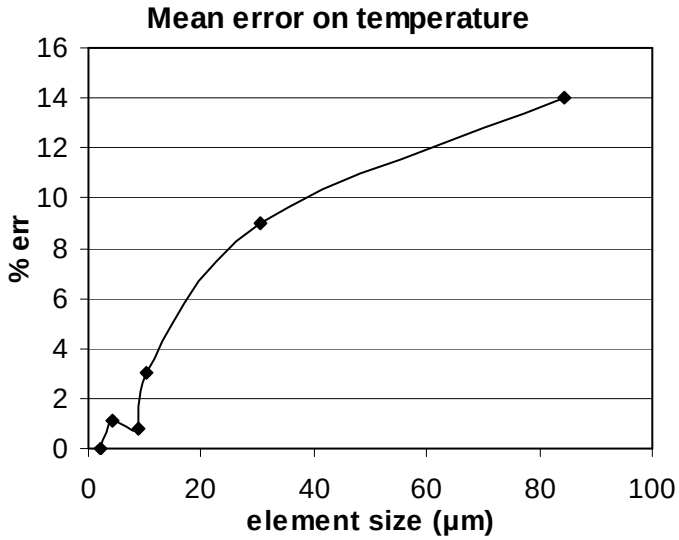

Figure 3.4 – Sensitivity of the solution to mesh size, based on an arbitrarily small element size (2.13 μm).

3.4 The finite element simulations

Table 3.1 shows the plan of the simulations carried out and the result achieved. Three groups of simulations are shown. The 2D incremental simulations model the orthogonal cutting process and consider the thermal and the mechanical effect of the air jet and they reproduce the experimental tests presented in Chapter 6. They provide information on the cutting forces, the temperature and stress distribution within the insert and the workpiece, and the 2D chip morphology. The boundary conditions for this first set of simulations include the convective heat transfer coefficient due to the air jet. The literature [57, 63, 78, 79] suggests a heat transfer coefficient of 2000 W/m²K, and this was used. A

sensitivity analysis on the heat transfer coefficient was carried out with a set of purely thermal 3D simulations of the insert, shown on the right side of Table 3.1.

METHODOLOGY			
MODEL	2D – incremental and tool stress: orthogonal cutting (thermal and mechanical effect of air jet)	3D – incremental: orthogonal cutting	3D – stationary: thermal simulation of the insert
FEATURE	• two cutting speeds • two feed rates • dry cutting and air jet assisted cut • two pressures	• two cutting speeds • two feed rates • dry cutting	• two contact lengths • two contact widths • four heat transfer coeff. • thermocouple heat flux
GOAL	• cutting force • temperature within the insert • stress within the insert • chip morphology and chip-tool contact	3D chip morphology: • contact width • contact length • chip curvature radius	sensitivity analysis for thermocouple calibration design

Table 3.1 – List of the simulations in the upper part of the figure, and simulations objectives in the lower part

This set of simulations reproduces the process of the calibration of the temperature sensor with the highest degree of reality allowed by FE simulation with DEFORM-3D. These simulations model the temperature rise within the insert, due to a thermal load distributed on the nodes of the insert in contact with the chip. The contact between the chip and the insert was investigated both by 2D and 3D incremental simulations. These gave results on the contact between the chip and the insert which were used as boundary condition for the thermal load distribution in the 3D stationary simulation of the insert only.

It is commonly assumed [96, 101, 102] that the elastic component of the total strain in the workpiece can be neglected, as the plastic strain component is the more dominant during machining. The workpiece material was modelled as plastic, while the insert was modelled as a rigid material. Only in the tool stress analysis is the tool was modelled as elastic material. The results provided by one kind of analysis have often been used for providing fundamental boundary condition for other simulations. The material model for the workpiece was developed by Oxley et al. [31, 32] and was coded in Matlab (see Appendix C), and it is based on the calculation of a modified temperature as a function of

the strain rate and a strain hardening coefficient. The 2D incremental simulations of orthogonal cutting provide information on the cutting force and temperature rise in the area surrounding the shear plane and in the chip with the broadest range of cooling conditions (dry cutting, air jet in overhead and interface position with two pressures). On the basis of the temperature rise and distribution in the workpiece, a steady state simulation for each cutting condition was carried out in order to obtain the temperature distribution within the insert. The cutting force over a representative number of steps in the incremental simulation was interpolated to give the boundary condition for the stress analysis of the tool. The incremental analysis also provided information on chip curl and the contact between chip and tool. A more complete insight into the contact between chip and tool is provided by the 3D incremental simulations. Since, in the experimental investigation, the temperature at the chip-tool interface was directly measured using a complex device based on a thermocouple embedded in the insert, the complete calibration process was modelled by a set of 3D finite element stationary thermal simulation. The following section provides details of the 3D incremental thermo-mechanical simulations and the 3D stationary thermal simulation.

3.5 Incremental 3D thermo-mechanical simulations of orthogonal cutting

Reliable incremental 3D simulations require a particularly high number of tetrahedral elements and a huge amount of simulation time. The Figure 3.4 shows the thermal boundary conditions on the workpiece and on the insert. The convective heat transfer coefficient of 20 W/m^2K (natural convection, no air jet used) was applied in the areas highlighted in green and the ambient temperature of 20°C was applied on the nodes of the mesh marked in red. In order to save computational time, the remeshing of 3D simulation was triggered by the strain and strain rate in the workpiece. This meshing method creates a fine mesh only where a large number of elements is needed. The main purpose of this simulation is to provide information on the contact nodes and 3D chip geometry. This information is compared with images of the rake face taken in an optical microscope and was used for designing the calibration of the sensor composed by the insert and the

embedded thermocouple. Due to the extremely high computational time, the dry cutting condition only was modelled. Two cutting speeds (83 and 129 m/min) and two feed rates (0.06 and 0.12 mm/rev) were used.

A constant shear friction coefficient ($\mu = 0.55$) and a constant global heat transfer coefficient for the contact nodes ($h = 45$ W/m²K) were used. These values are consistent with the investigation of Umbrello et al. [20], Fischer et al. [98] and Özel [101]. The solution was obtained by using the methods of conjugate gradient on direct iteration, with a time step of 5e-5 seconds. The maximum convergence errors were 0.005 m/s for the velocity error and 0.05 N for the force.

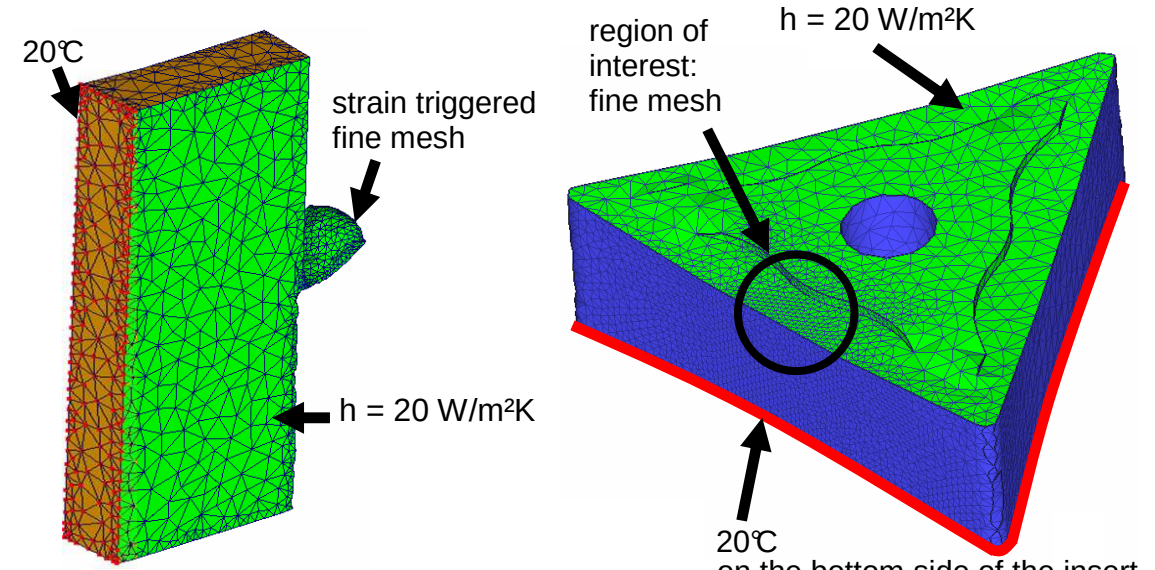

Workpiece	
Material	AISI 1020
k (W/mK)	51.9
c (J/KgK)	486
ρ (kg/m³)	8000

Insert TNMG 11 03 02-MF 4025			
Material	WC	TiC	TiN
k (W/mK)	84	54.1	35.6
c (J/kgK)	180.7	192.7	144.6

Figure 3.4 – The thermal boundary conditions on the workpiece in the 3D incremental simulation. A fine mesh is triggered by strain and strain rate in order to save computational resources

The results of the four simulations are summarised in the Table 3.2. The table shows the most relevant quantities in chip morphology: chip thickness, chip width and chip curl radius.

cutting speed (m/min)	feed rate (mm/rev)	chip thickness (mm)	chip width (mm)	chip curvature radius (mm)	chip-tool contact length (mm)
83	0.06	0.14	1.04	0.72	0.13
83	0.12	0.14	1.35	1.83	0.28
129	0.06	0.28	1.09	0.71	0.13
129	0.12	0.28	1.42	1.81	0.28

Table 3.2 – results of 3D incremental simulations: chip morphology

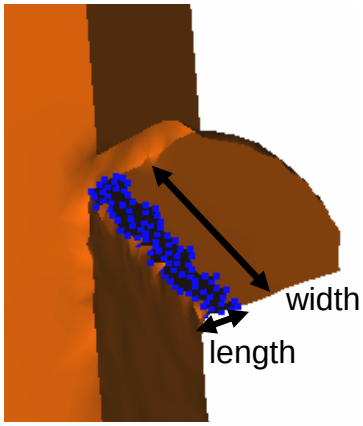

Workpiece	
Material	AISI 1020
k (W/mK)	51.9
c (J/KgK)	486

Feed rate (mm/rev)	Chip width (mm)
0.06	0.13
0.12	0.28

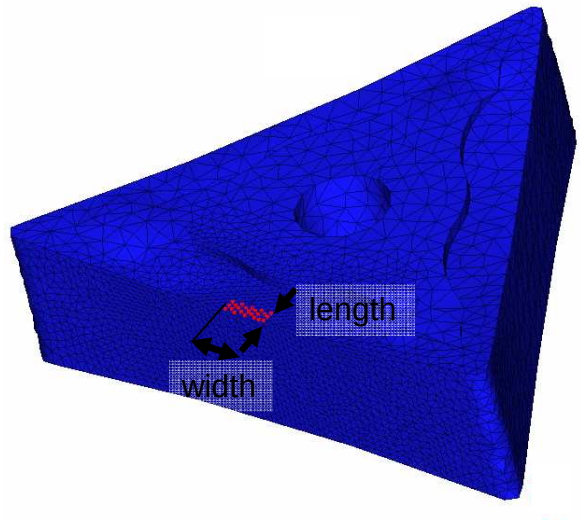

Insert TNMG 11 03 02-MF 4025			
Material	WC	TiC	TiN
k (W/mK)	84	54.1	35.6
c (J/kgK)	180.7	192.7	144.6

Figure 3.5 – The results by the 3D incremental orthogonal cutting simulations (dimension of the chip-tool contact) was used as an input for the 3D stationary thermal simulation on the insert

In orthogonal cutting the chip is assumed to flow orthogonally to the cutting edge. This is an approximation which is not true in all the regions of interest: the chip width is not constant and not equal to 1 mm. At small feed rates, chip flow in the lateral direction can be neglected, but at high feed rates the difference in chip width is not negligible.
Only by 3D incremental simulations of orthogonal cutting was possible to have a deeper insight into the dimensions of the contact between the chip and the insert. The results of the 3D incremental simulations (width and length of the contact) were used as input for the 3D thermal simulation of the insert, and identifying on the insert the nodes of contact, as shown by Figure 3.5. It was observed that the cutting speed does not influence the contact between the chip and the insert.

3.6 Stationary 3D thermal simulations of the insert

Since the temperature sensor used for the experimental investigation is not a standard sensor, the purpose of this set of simulations is to provide a consistent insight into the parameters that affect the calibration of the temperature sensor. The sensor is composed of the insert and the k-type thermocouple embedded in the insert. The calibration of the sensor consists in applying a constant temperature to that part of rake face in contact with the chip and reading the output measured by the thermocouple.

The finite element model provides essential information on the shape of the thermal load on the rake face, the effect of convection by the air jet and the thermal flux due to the thermocouple and how they influence the calibration process. The insert was considered alone for the stationary 3D thermal simulation and the mesh was refined in the area where the thermal load was applied. The shape of the contact between the chip and the rake face, deduced from the incremental 3D thermo-mechanical simulations was used for the temperature boundary condition of the stationary 3D simulations. The heat transfer

boundary conditions used for the 3D stationary thermal simulation are the same used for the 3D incremental simulations (convection to ambient temperature on the rake face, 20°C imposed on the nodes in contact with the tool holder), but several different values of the convective heat transfer coefficient on he rake face were used, to determine the sensitivity of the measurements to this parameter. Four parameters (the width and the length of the contact between the chip and the rake face, the power absorption due to the thermocouple and the convective heat transfer coefficient) were also varied in order to estimate the sensitivity of the results to these parameters.

The power absorption due to the thermocouple was modeled as a negative heat flux of 8 W/m² flowing away from the hole where the thermocouple is embedded in the insert. The Table 3.3 shows the four parameters that were changed in the simulation and the last column indicates the purpose for changing the parameters, referred to in the sensitivity analysis. Sixteen different temperatures were imposed as boundary condition for testing the response of the modified insert to the temperature in the range of the cutting temperatures (20-820°C).

ID	width (mm)	length (mm)	Heat flux TC (W/m²)	h (W/m²K)	purpose (sensitivity)
Sim 1	1	0.13	8	20	Length
Sim 2	1	0.28	8	20	Length
Sim 3	1.4	0.28	8	20	Width
Sim 4	1.4	0.28	0	20	heat flux TC
Sim 5	1.4	0.28	8	1000	h
Sim 6	1.4	0.28	8	2000	h
Sim 7	1.4	0.28	8	3000	h

Table 3.3 – The different simulations carried out for the sensitivity analysis on the four parameters involved in the stationary 3D thermal simulation on the insert

The Figure 3.6 shows the temperature distribution on the surface of the insert when the heat transfer coefficient is changed, while all the other parameters are constant (contact length, contact width, heat flux by the thermocouple). A temperature of 700°C was imposed on the contact nodes.

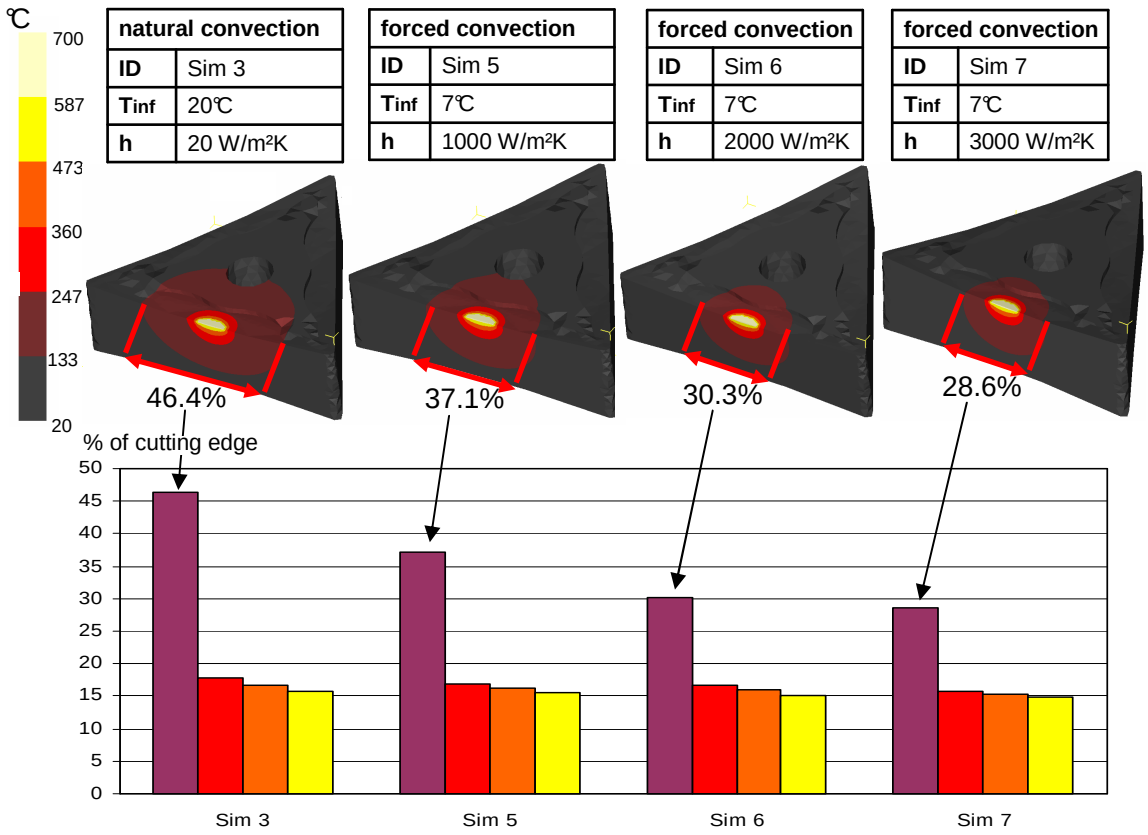

Figure 3.6 – The 3D stationary thermal simulation of the insert. The simulations reproduce four different cooling conditions: natural convection and forced convection with three different heat transfer coefficients.

The results show the influence of the convective heat transfer coefficient on the temperature distribution. However it could be observed that the variation of the heat transfer coefficient affects the temperature field on the rake face, and only minimally on the flank face.

The quantitative results in Figure 3.6 show the percentage of the cutting edge intercepted by temperature isosurfaces: four areas at different temperature are highlighted. The zones at high temperature are minimally influenced by the variation of the heat transfer coefficient. This results is consistent with the analysis of Umbrello [20], and show that the heat transfer between the rake face and the thermocouple is purely conductive, and only minimally influenced by variation of the local heat transfer coefficient. Only a

variation of two orders of magnitude (from 20 to 2000 W/m²K) produced an appreciable difference in the temperature distribution. The 3D stationary thermal simulations of the insert were used for predicting the temperature read by the thermocouple. The Figure 3.10 shows the mean temperature of the nodes in contact with the thermocouple as a function of the temperature of the nodes in contact with the chip.

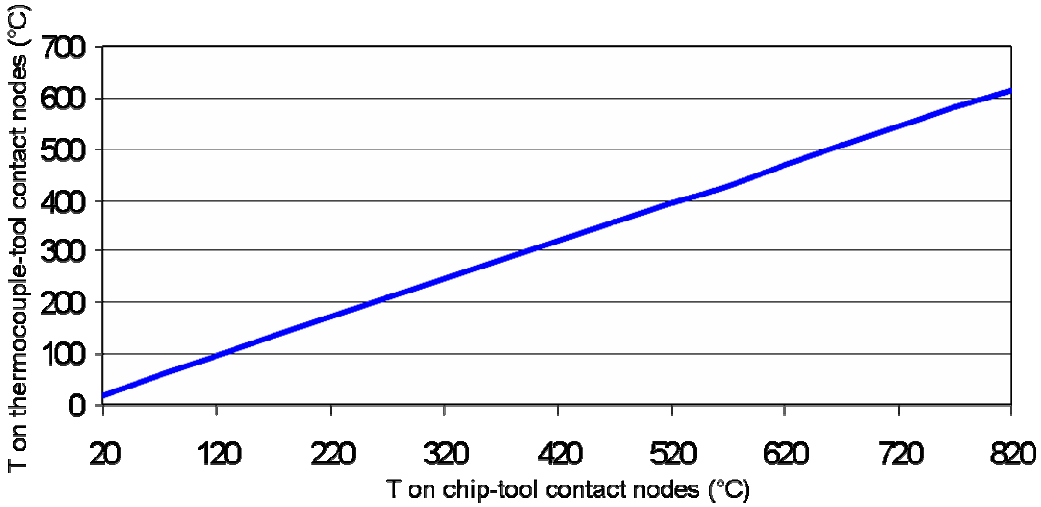

Figure 3.7 – Results of the 3D stationary thermal simulation of the insert, with a width of contact of 1.4 mm, a length of contact of 0.28 mm, heat flux due to the thermocouple and natural convection (Sim3, see Table 3.3): the temperature at the tip of the thermocouple as a function of the temperature on the contact nodes between the chip and the rake face

The temperature read by the thermocouple is the mean value of the temperature of the 23 nodes of the top face of the cylinder that represents the hole for the thermocouple. The Table 3.4 shows a comparison between two simulations: in the first case the heat flux due to the thermocouple has not been considered. From the comparison it is possible to assume that heat flux produced by the thermocouple can be neglected, since the difference of temperature introduced by not considering the heat flux due to the thermocouple is less than 0.4%. The results from the 3D stationary thermal simulations on the insert show that the calibration of the system composed by the insert and the embedded thermocouple can be achieved by heating the zone of the rake face corresponding to the contact between the chip and the tool to a known temperature. The

3D stationary thermal simulations on the insert show that the sensitivity to the heat flux due to the thermocouple is very limited, and the interaction between the temperature of the chip-tool interface and the temperature read by the thermocouple is based on conduction, with a minimal influence of the heat transfer coefficient by convection.

temperature on the contact nodes (℃): Input	**temp. simulated TC with heat flux (℃): Sim 3**	**temp. simulated TC without heat flux (℃): Sim4**
20	20	20
70	59	60
120	96	97
170	133	134
220	170	171
270	207	209
320	244	246
370	282	283
420	319	320
470	356	357
520	393	395
570	430	432
620	468	469
670	505	506
720	542	543
770	579	580
820	616	618

Table 3.4 – Comparison between the simulations Sim3 (with heat flux) and Sim4 (without heat flux). The column on the left represents the temperature of the nodes of contact between the chip and the tool, used in the simulation as an input

The main limitation of the calibration method is the shape of the heated zone, since the temperature in the contact zone is not evenly distributed and the shape of the contact zone is not constant in time. However the simulations show that the shape of the contact has a limited influence on the temperature detected by the thermocouple, if the thermocouple is not placed in the proximity of the rake face. The thermal gradient generated by two different distribution of temperature on the rake face can be detected only in proximity of the rake face, but at the depth were the thermocouple is placed (0.25 mm from the rake

face) the local effects of the two different distribution of temperature can be neglected. A similar technique was used by Ren et al. [42], that calculated by using the finite elements the maximum interface temperature and using the data from a distant embedded k-type thermocouple as an input. The use of this technique at the calibration process allow to obtain a linear relation between the maximum temperature at the chip-tool interface and the temperature read by the thermocouple, as shown in Figure 3.7.

3.7 2D thermo-mechanical simulations with air jet

The core of the finite element simulations for this research project is the incremental 2D thermo-mechanical simulation. 2D simulations have the capability of reproducing orthogonal machining and the 2D domain allows the geometries to be represented with a high number of elements, as described in paragraph 3.3. The boundary conditions for incremental 2D simulations include the effect of the air jet from a thermo-mechanical point of view.

The blowing force is represented by a pressure on the elements exposed to the air jet and the thermal effect was modelled by setting the heat transfer coefficient to 2000 W/m^2K, as in the literature [78, 79], with a fluid temperature of 7°C (measured by a thermocouple placed at the exit of the nozzle). The Figure 3.8 shows the thermo-mechanical boundary condition when the air jet is in the overhead or in the interface position. In the figure the blowing force was represented by a red arrow, pointing towards the element where the pressure is applied.

The main limitation of the model represented in Figure 3.8 is the assumption that the blowing force of the air jet generates an evenly distributed pressure on the chip, in both overhead and interface positions. Since the fluid-dynamic field in the 2D domain cannot represent the 3D situation, and a complete fluid-dynamic investigation should include 3D domain features, and the solution of compressible Navier-Stokes equation in a time variable domain, the simplification made represents a reasonable approach to the problem in term of feasibility. Results from the incremental 2D simulations include the cutting forces, temperature distribution within the workpiece, and stress distribution within the workpiece.

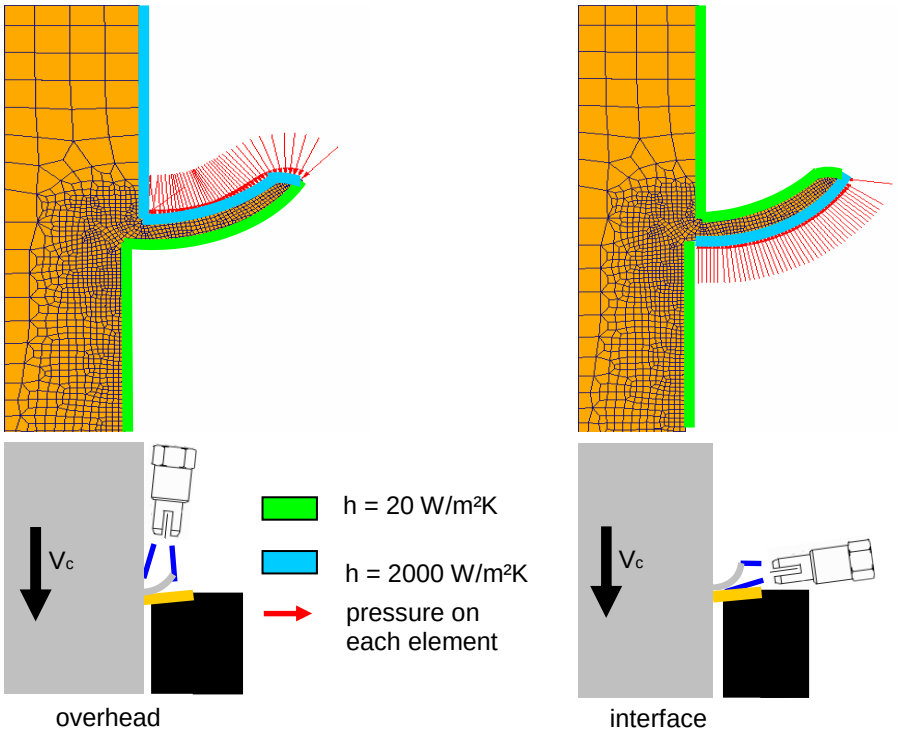

Figure 3.8 – Thermo-mechanical boundary condition on the workpiece. When the jet is positioned, a pressure is supposed to generate a pressure on the upper side of the chip (overhead position) or on the lower side of the chip (interface position)

The results from 2D incremental simulations are used as a boundary condition for simulating the temperature distribution within the insert by steady state thermal simulation. The cutting force from the incremental simulation is used as a boundary condition for the stress analysis on the insert modelled as an elastic body for this kind of simulation only. With the three different kinds of 2D simulation, incremental thermo-mechanical, steady state thermal and steady state insert stress analysis, it was possible to get a deep insight into the thermo-mechanical effect of the air jet in machining.

3.8 2D simulation results

The results obtained from incremental 2D simulations, steady state 2D thermal simulations and steady state 2D insert stress analysis include maximum insert temperature, maximum stress within the insert, maximum stress within the workpiece,

and the following results along the shear plane: shear plane angle, shear strain, shear strain rate. The results in terms of shear plane angle, strain and strain rate for the four different dry cutting conditions (two cutting speeds, 83 and 129 m/min, and two feed rates, 0.06 and 0.12 mm/rev) were used for verifying the analytical input of the flow stress model developed by Oxley et al. [31, 32], coded in Matlab in the Appendix C. The flow stress material model developed by Oxley was more similar, in terms of cutting forces, to the material behaviour during the orthogonal cutting test, compared to the model presented in the DEFORM material library. The shear zone was considered to start when a consistent difference in the strain rate is observed (1/10 of the maximum strain rate, since the gradient of the strain rate is steep in the shear zone). The Figure 3.9 shows the strain, the strain rate and the effective stress for the following cutting condition: 83 m/min of cutting speed and 0.12 mm/rev of feed rate.

The thickness of the shear zone resulted to be relatively constant, with a mean value of 0.025 mm and a standard deviation of 0.002 mm over the four cutting condition considered. Since the thickness of the shear zone can be considered as constant, the strain rate was verified to be proportional to the cutting speed by using the finite elements. It was also observed that on the line identified as the shear plane the effective strain is unitary. On this line the effective stress of the material should be maximal, according to the cutting theory of Merchant [28, 29], however boundary effects have been observed by FE simulations, due to the penetration of the insert in the material (maximum effective stress) and to the free surface of the chip (minimum effective stress). Excluding the boundary effects, the effective stress shown is constant on the line identified as the shear plane, and the standard deviation (3 MPa) is mainly due to misalignment of the nodes on the shear plane. The Table in the Figure 3.9 shows the quantitative results for strain, strain rate, effective stress, and shear plane angle. It was observed that the mechanical effect of the air jet do not affect the shear plane angle, the strain and the strain rate. The results of the 2D finite element simulations of orthogonal cutting with thermal and mechanical effect of the air jet include the temperature distribution within the insert, and the stress distribution within the insert and the workpiece.

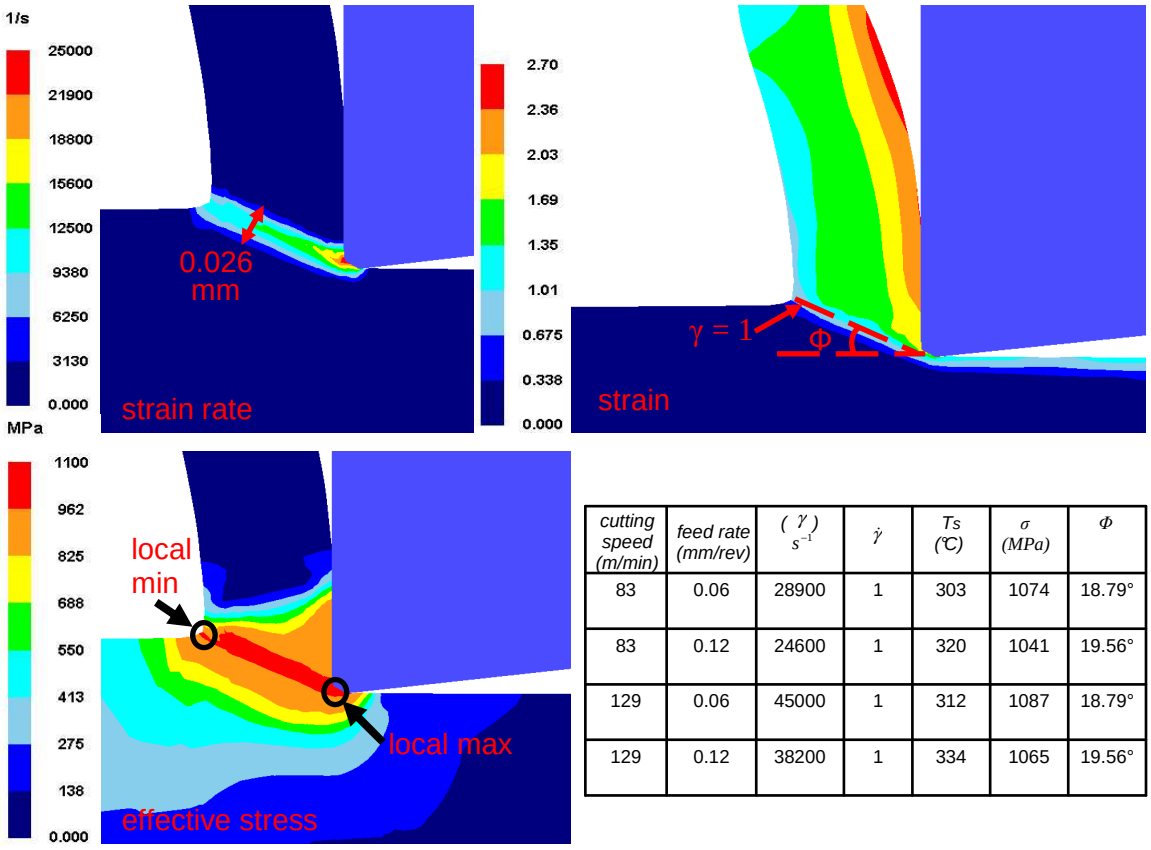

cutting speed (m/min)	feed rate (mm/rev)	(γ) s^{-1}	$\dot{\gamma}$	Ts (℃)	σ (MPa)	Φ
83	0.06	28900	1	303	1074	18.79°
83	0.12	24600	1	320	1041	19.56°
129	0.06	45000	1	312	1087	18.79°
129	0.12	38200	1	334	1065	19.56°

Figure 3.9 – The strain, strain rate and effective stress in the 2D incremental simulation of orthogonal cutting. The simulation with 83 m/min of cutting speed and 0.12 mm/rev is shown in the figure.

The temperature distributions are shown in the Figures 3.10a, b, c, d. Five different cooling conditions identified by colour code, are compared: dry cutting and air jet in overhead and interface position with air jet pressures of 4 and 7 bar. Qualitative results show the temperature distribution within the insert, while the quantitative results show the temperature distribution along the rake face, starting from the cutting edge. For all the combinations of cutting speeds and feed rates the best cooling condition was achieved with the air jet in overhead position with 7 bar of pressure. It can also be observed that the increment of pressure when the nozzle is in the interface position produces an increment of the temperature, while the same variation of pressure when the nozzle is in the overhead position produces a decrement of temperature.

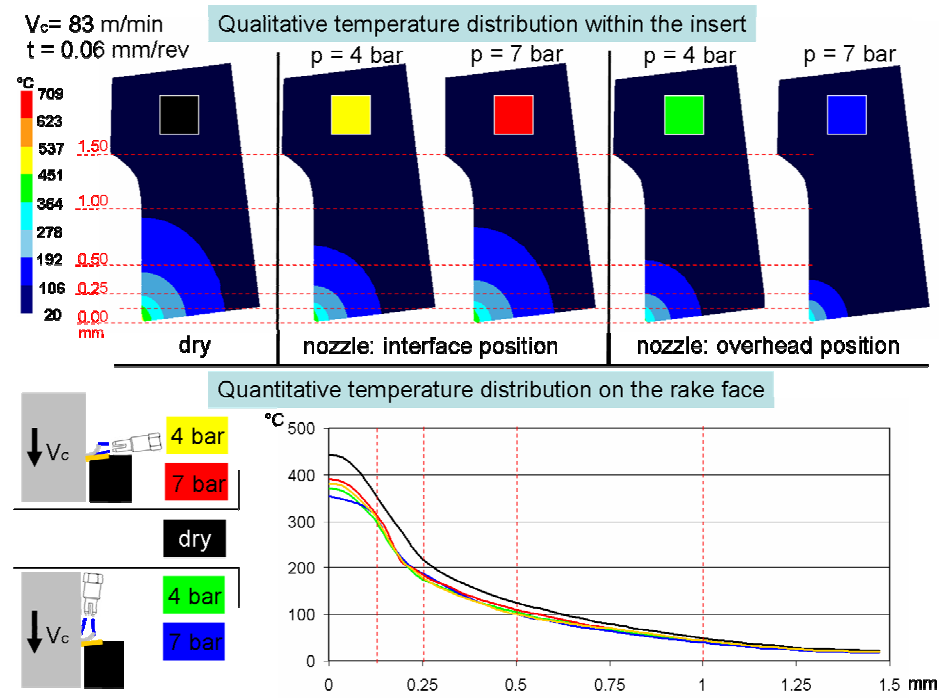

Figure 3.10a – The temperature distribution within the insert and along the rake face. The cutting speed is 83 m/min and the feed rate is 0.06 mm/rev.

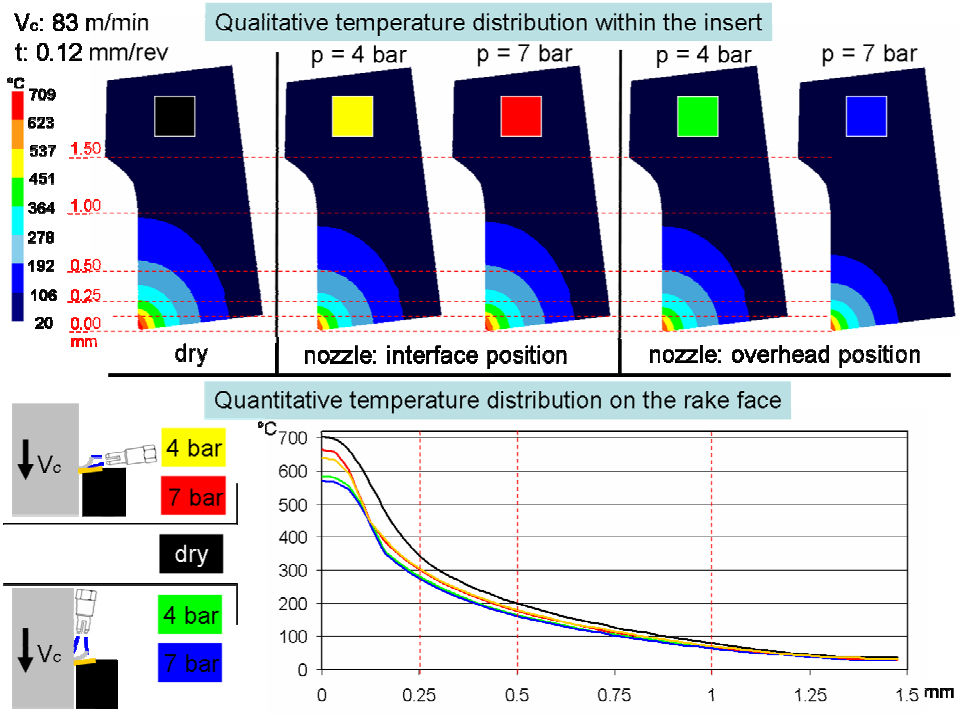

Figure 3.10b – The temperature distribution within the insert and along the rake face. The cutting speed is 83 m/min and the feed rate is 0.12 mm/rev.

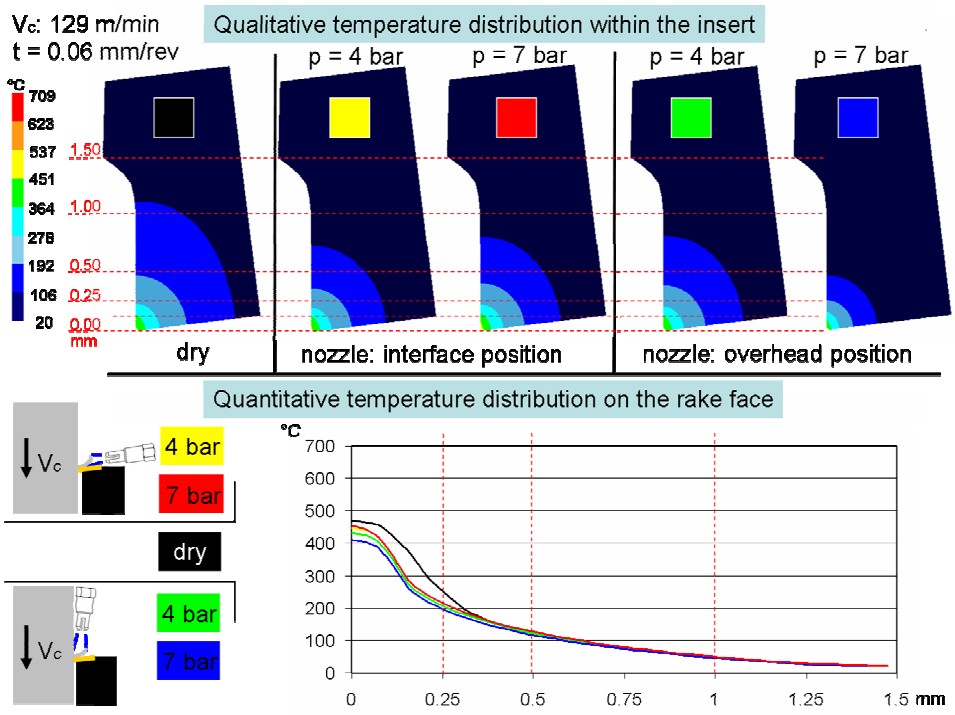

Figure 3.10c – The temperature distribution within the insert and along the rake face. The cutting speed is 129 m/min and the feed rate is 0.06 mm/rev.

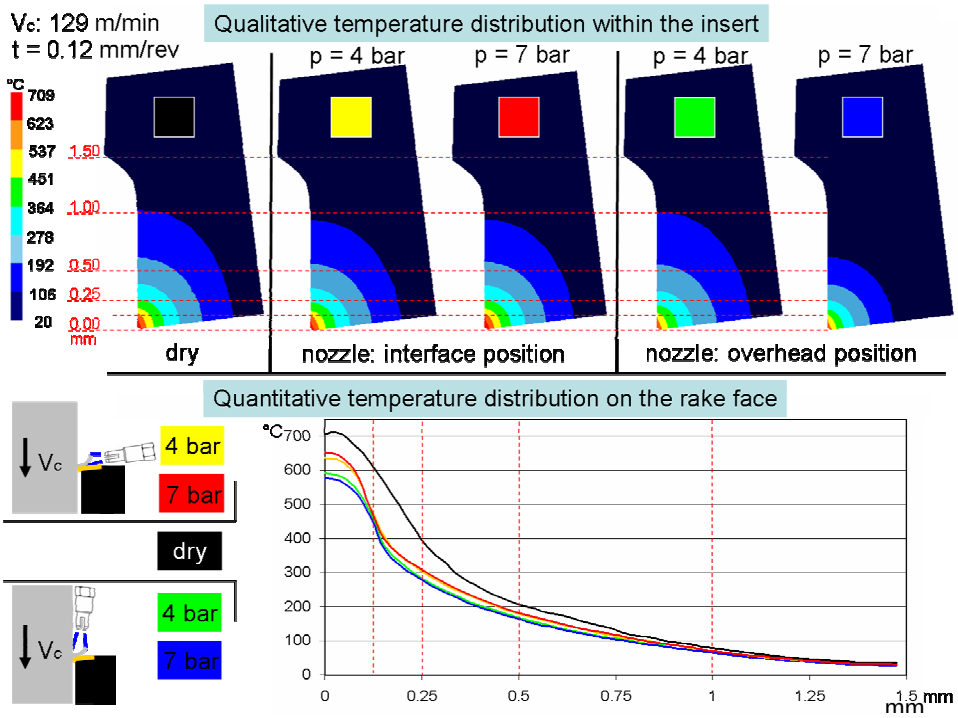

Figure 3.10d – The temperature distribution within the insert and along the rake face. The cutting speed is 129 m/min and the feed rate is 0.12 mm/rev.

The rating of cooling efficiency for the five cooling condition, from the more efficient to the less efficient is:

1) overhead position, 7 bar
1) overhead position, 4 bar
2) interface position, 4 bar
3) interface position, 7 bar
4) dry cutting

Since a difference in the temperature rise within the insert is achieved by changing the pressure and the direction of the air jet (i.e. the elements where the pressure is applied), a mechanical effect related to the changing of the interface temperature exists. The results of the incremental 2D thermo-mechanical simulations do not show significant changes in the cutting force as the pressure and the position of the air jet are changed. This fact suggests a change in the local stress on within the workpiece, and consequently within the insert, is promoted by changing the cooling conditions. The analysis of the state of stress within the insert shows that a low temperature is associated with a low state of stress. The use of the air jet in the overhead position reduces the stress within the insert, and the opposite effect is obtained with the air jet in the interface position. The insert stress analysis is the result of a 2D steady state simulation requiring the interpolation of the state of stress of the workpiece, used as boundary condition, onto the surface of the insert, modeled as an elastic material.

It can be observed that the stress distribution, at the same cooling condition, depends manly on the feed rate. For the same cutting speed and feed rate, the stress distribution depends on the position of the nozzle and the pressure of the air jet. The results show a consistent change in the stress distribution when the air jet is applied. In particular the effective stress within the insert has maximum with the air jet is in the interface position with a pressure of 7 bar. On the other hand, a minimum is observed for the air jet in overhead position with a pressure of 7 bar. The Figure 3.11a, b, c, d show the effective stress distribution within the insert, with the five different cooling conditions: dry cutting and air jet with two positions of the nozzle and two pressures.

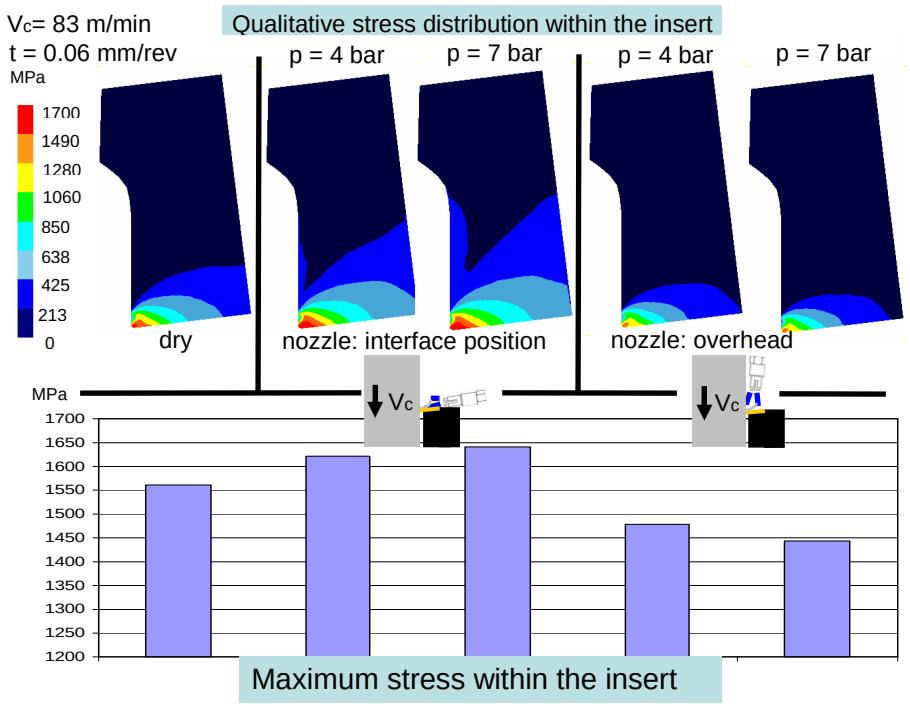

Figure 3.11a – The effective stress within the insert in the orthogonal cutting simulation with 83 m/min of cutting speed and 0.06 mm/rev of feed rate

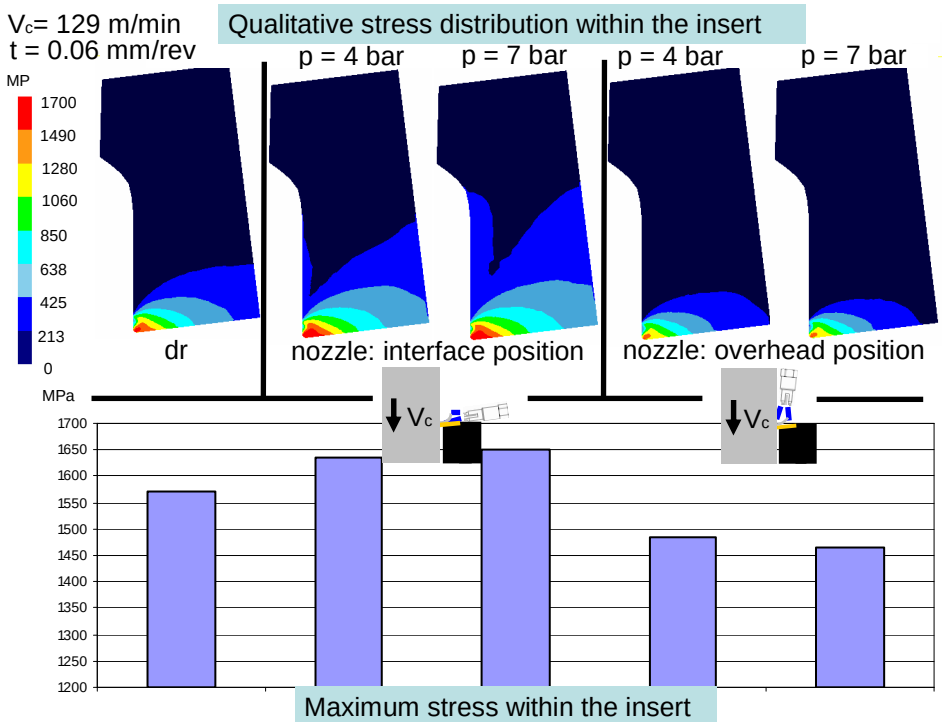

Figure 3.11b – The effective stress distribution within the insert in the orthogonal cutting simulation with 129 m/min of cutting speed and 0.06 mm/rev of feed rate

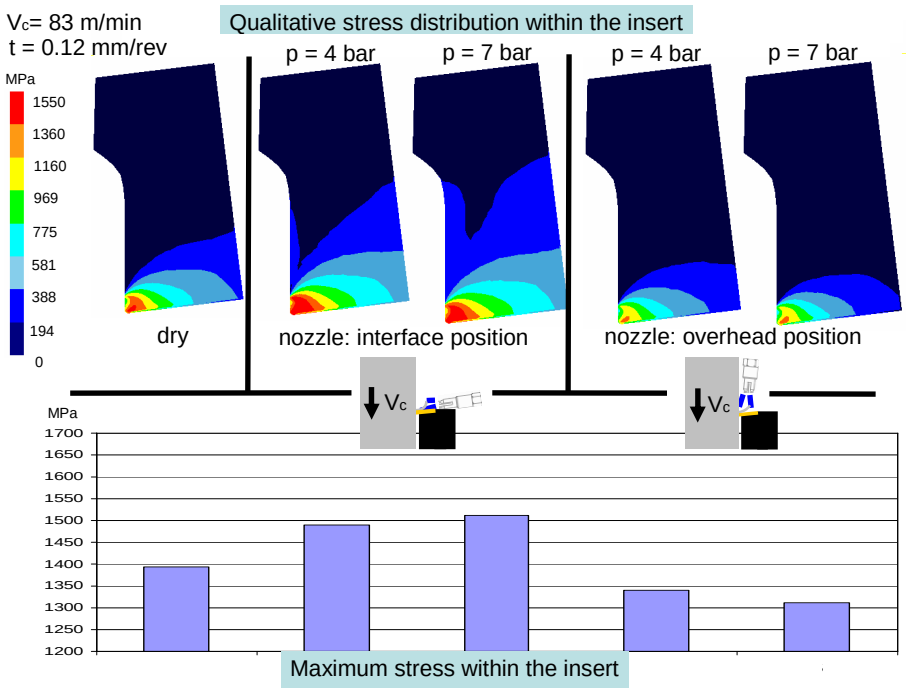

Figure 3.11c – The effective stress distribution within the insert in the orthogonal cutting simulation with 83 m/min of cutting speed and 0.12 mm/rev of feed rate

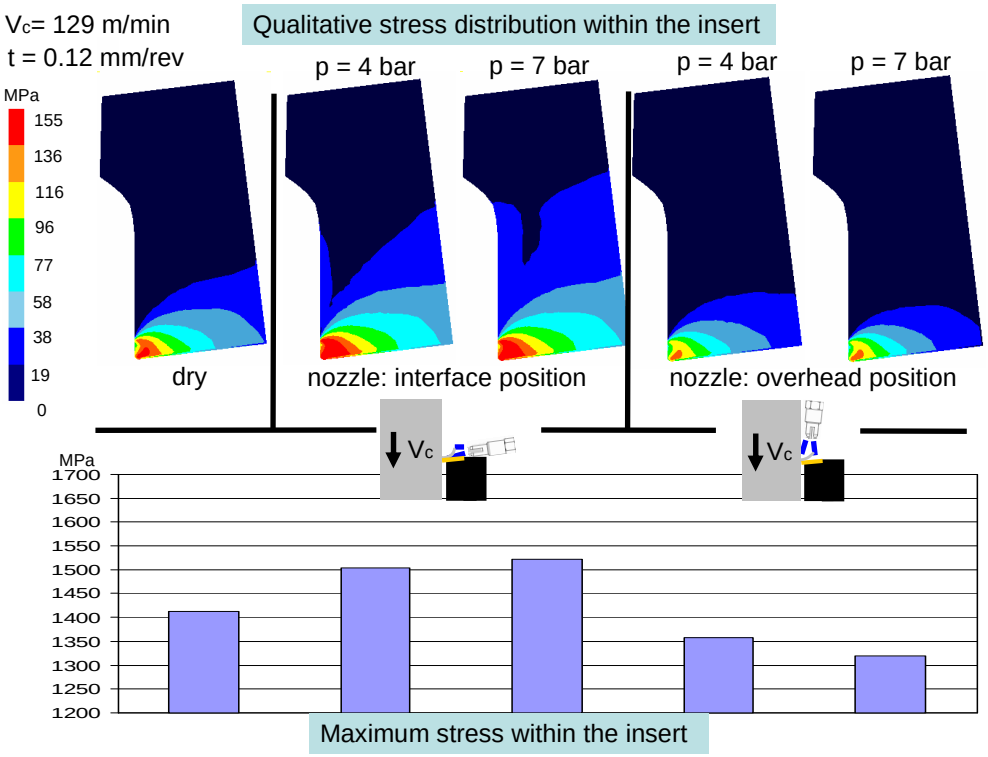

Figure 3.11d – The effective stress distribution within the insert in the orthogonal cutting simulation with 129 m/min of cutting speed and 0.12 mm/rev of feed rate

Once again, it can be observed that the condition that minimizes the effective stress is the use of the air jet in overhead position with 7 bar of pressure, while a maximum stress within the insert is shown when the pressure of 7 bar is applied in the interface. This behavior can be observed also in the workpiece. The Figure 3.12 shows the effective stress distribution within the workpiece in a 2D incremental simulation of orthogonal cutting with 129 m/min of cutting speed and 0.12 mm/rev of feed rate, when the pressure is applied in the interface (on the left) or on the top face of the chip, in overhead position (on the right).

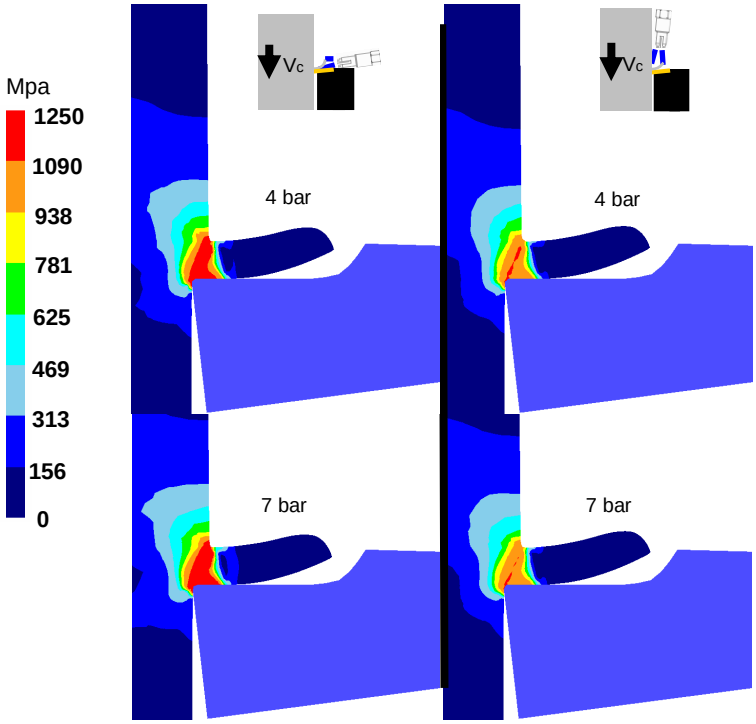

Figure 3.12 – The effective stress within the workpiece in a simulation with 129 m/min of cutting speed and 0.12 mm/rev of feed rate. The air jet is positioned in interface position (on the left) and in overhead position (on the right) with 4 and 7 bar of pressure

The results show an evident reduction of the effective stress when using the air jet in the overhead position, while a consistent increase of the effective stress is observed when the blowing force is applied into the interface. In particular when the nozzle is in the interface position, the Figure 3.12 shows a large area where the stress reaches values up

to 1250 MPa, while the maximum stress reaches 1103 MPa when the nozzle is positioned in the overhead position, with 7 bar of pressure.

3.9 Summary and conclusions

A wide set of finite element simulation was used for analyzing the effect of the air jet on the orthogonal cutting of AISI 1020. The main purpose of this investigation is proving the existence of a mechanical effect of the air jet and understanding its behavior by changing the three parameters representing the air jet: the elements of the workpiece and the insert affected by the air jet, the heat transfer coefficient and the pressure applied to the elements by the air jet. To achieve this goal, a fully coupled set of 2D and 3D simulations were set up. The material model of AISI 1020 steel is the model proposed by Hastings et al. [32] (equation of Oxley). The default material model for AISI 1020 in DEFORM uses the equation of Oxley; however, the material model is presented in a tabular form with few points, and for most of the cutting condition the flow stress has to be interpolated. The result is a stiffer material and higher cutting temperatures. By using the material model proposed by Hasting et al., the results of the finite element analysis get much closer to the experimental results in terms of cutting temperatures and cutting forces; therefore they provide reliable data on the information that can be analyzed by finite elements only, such as the effective stress within the workpiece and the insert. The boundary conditions applied include the thermal effect of the air jet, modeled with the heat transfer coefficient, and the mechanical effect of the air jet, modeled as a pressure applied to elements of the workpiece. The simulations reproduce the experimental tests presented in Chapter 6. A sensitivity analysis on the mesh and on the heat transfer coefficient between the air jet and the insert was carried out. The most important set of the finite element simulations is the 2D incremental thermo-mechanical simulation set. By modeling the insert with an elastic material it was possible to investigate the stresses within the insert. The results of these analyses were presented in the figures in the previous paragraph. From a holistic point of view, the finite element simulations confirm the existence of a mechanical effect of the air jet during orthogonal cutting, and provide fundamental guidelines for understanding the phenomena. By comparing the thermal

analysis with the effective stress analysis on the workpiece and the insert, it can be assumed that the air jet can be considered as an external source of energy that can be used, if correctly directed, for reducing the temperature rise in the chip-tool interface, as shown by Figures 3.13 and 3.14

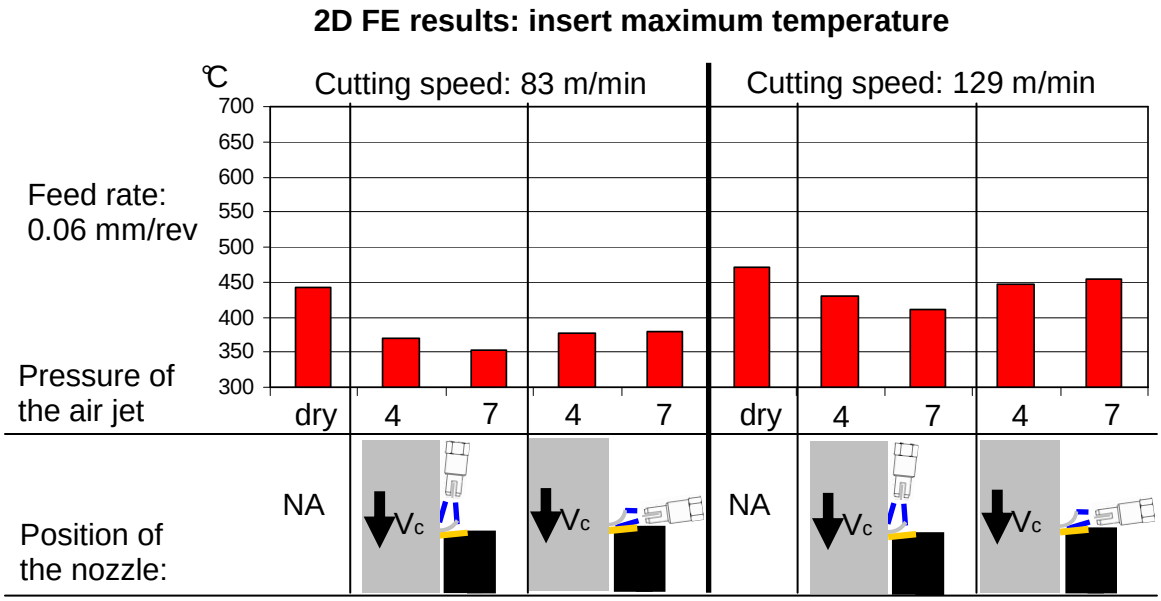

Figure 3.13 – Maximum insert temperature in 2D incremental simulations with a feed rate of 0.06 mm/rev

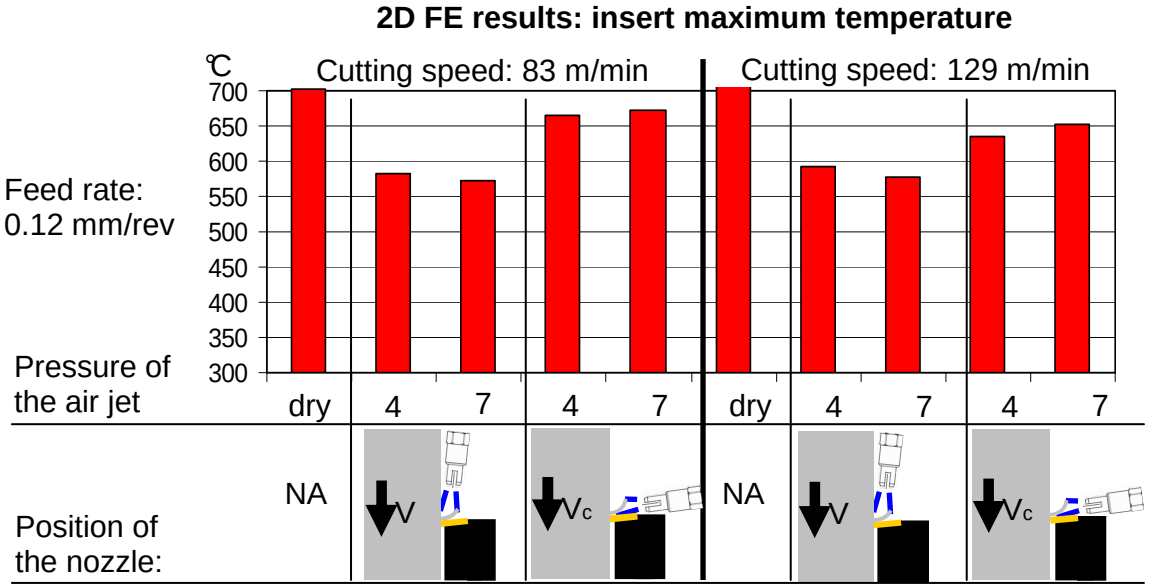

Figure 3.14 – Maximum insert temperature in 2D incremental simulations with a feed rate of 0.12 mm/rev

From a thermal point of view, the greatest reduction of temperature is obtained when the air jet is in the overhead position (the heat transfer and the pressure are applied on the top face of the chip), and temperature falls with increasing pressure. It can be concluded that when the air jet is directed into the chip-tool interface, a small reduction of temperature is obtained in the interface but the temperature rises as pressure is increased. Figures 3.13 and 3.14 show a summary of the maximum interface temperature at different cutting and cooling conditions. There is a consistent difference in the maximum interface temperature when the feed rate is maximal. The reduction of temperature due to the air jet shows similar trends for the two cutting speeds for the cooling conditions considered.

These observations show that the mechanical effect is just as important as the thermal effect. Umbrello et al. [20] suggest that the global heat transfer coefficient is influenced not only by the temperature of the contact area, but also by the stress applied by the workpiece to the rake face. Following the intuition of Umbrello, the distribution of the effective stress within the workpiece and the insert was investigated by finite element analysis. The results are consistent with the intuition of Umbrello and they explain the consistent reduction of temperature when the air jet is directed from the overhead position. The Figures 3.15 and 3.16 show the maximum effective stress in the insert, and Figures 3.17 and 3.18 show the maximum effective stress in the workpiece It can be observed that for the entire set of cutting parameters (cutting speed and feed rate), dry cutting excluded, the ranking of effective stress, from minimum to maximum, is:

1) overhead position, 7 bar
2) overhead position, 4 bar
3) interface position, 4 bar
4) interface position, 7 bar

The same ranking occurs for maximum temperature and maximum effective stress in the insert and workpiece.

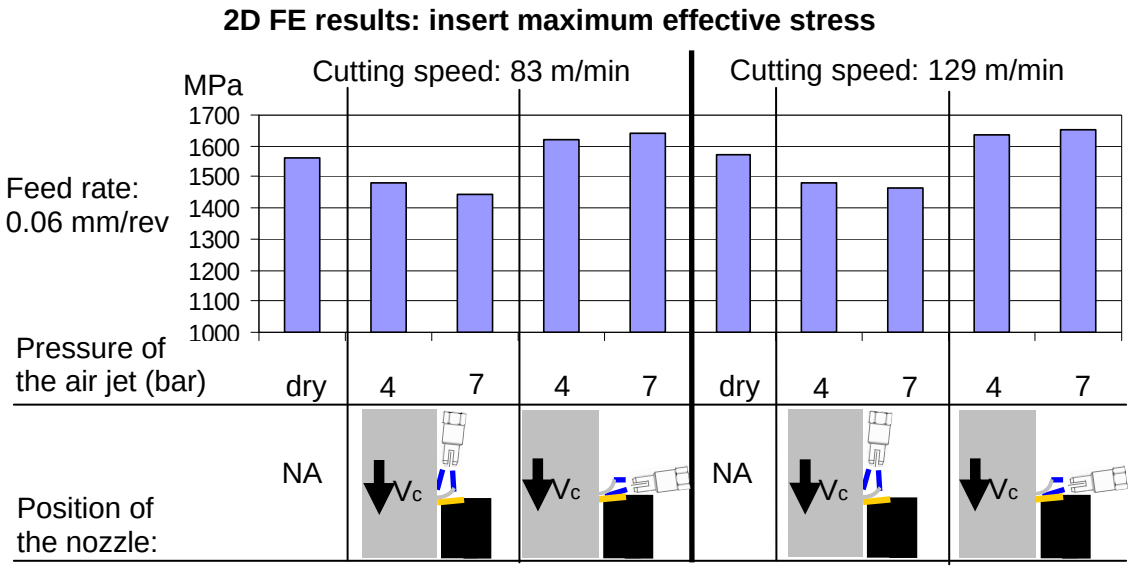

Figure 3.15 – Maximum effective stress in the insert in 2D incremental simulations with a feed rate of 0.06 mm/rev

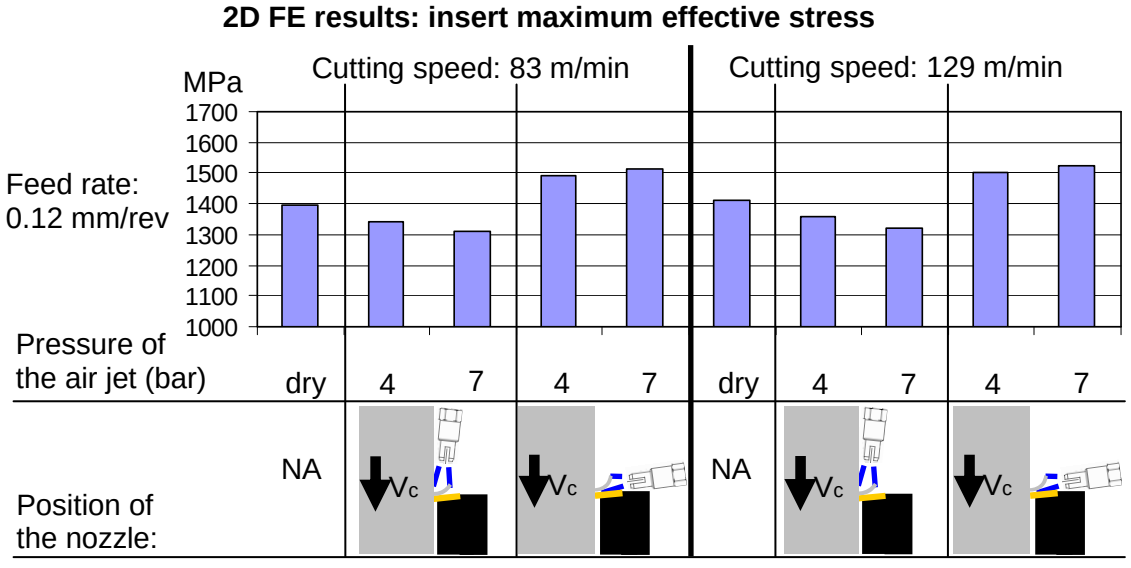

Figure 3.16 – Maximum effective stress in the insert in 2D incremental simulations with a feed rate of 0.12 mm/rev

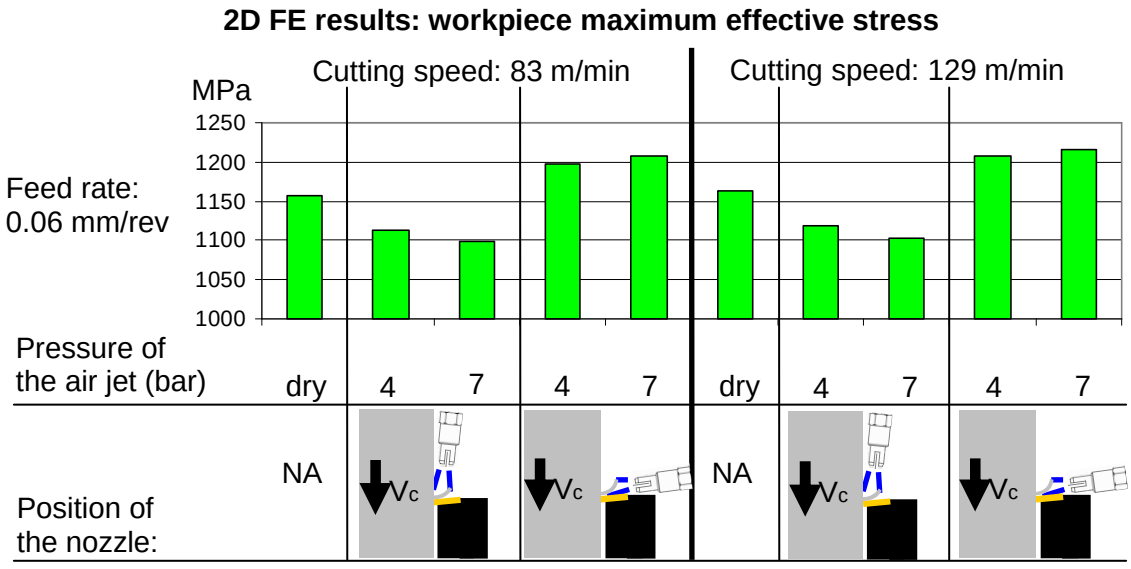

Figure 3.17 – Maximum effective stress in the workpiece in 2D incremental simulations with a feed rate of 0.06 mm/rev

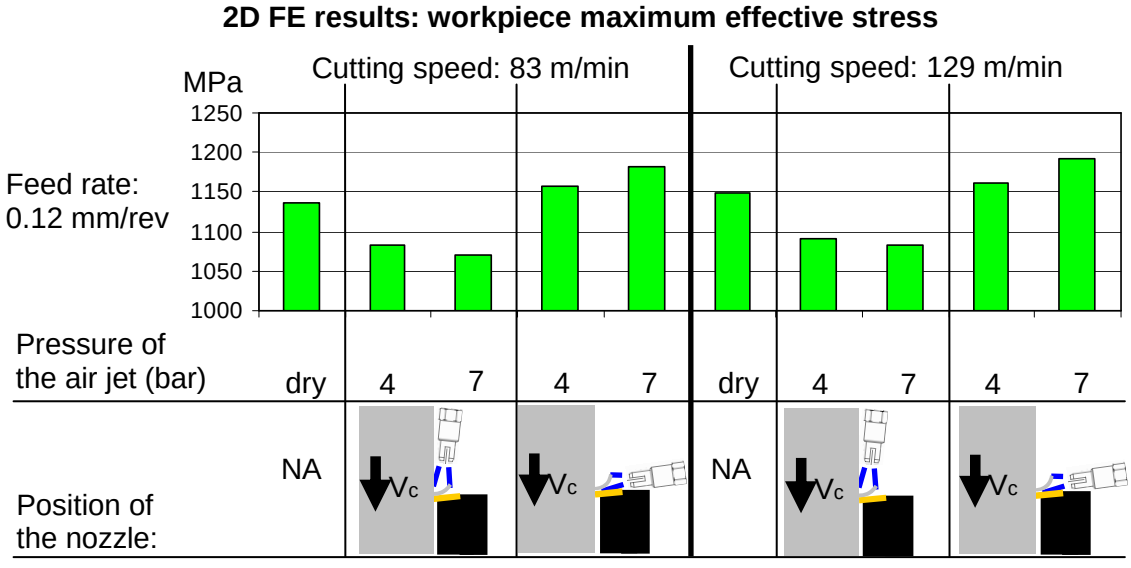

Figure 3.18 – Maximum effective stress in the workpiece in 2D incremental simulations with a feed rate of 0.12 mm/rev

The finite element analysis shows that a small external force, provided by the air jet, can consistently change the stress distribution in the cutting area, and the thermal analysis shows that an altered state of stress causes a consistent change in the temperature rise. The chip morphology was investigated by 2D and 3D incremental thermo-mechanical finite element simulations. The 2D simulations provide data on chip thickness and curvature radius and the 3D simulations provide data on the shape of the contact between the chip and the rake face. It was found that the use of an air jet has little effect on the steady state shape of the chip. Not surprisingly, the morphology is mostly influenced by the feed rate.

The contact length was found by 3D simulations. The mean value of the contact length is 0.13 mm when a feed rate of 0.06 mm/rev is used, and 0.28 when the feed rate is 0.12 mm/rev. This information was used to design a 3D simulation for reproducing the calibration process of the embedded thermocouple. In the experimental phase of the project, the maximum steady state temperature of the rake face was directly correlated to the signal provided by the thermocouple. Since a wall of tungsten carbide exists between the rake face and the tip of the thermocouple, the embedded thermocouple technique is an indirect measurement method that requires a deep insight into the way the temperature is transmitted to the thermocouple. The transmission was supposed to be affected by the shape of the contact (i.e. the temperature distribution in the contact area), by the convective heat transfer coefficient the maximum temperature value, and the heat flux due to the thermocouple. A set of 3D steady state thermal simulation of the calibration process was carried out for obtaining the information for designing the calibration process. It was found that the convective heat transfer coefficient affects the temperature distribution in the proximity of the rake face, but within the insert the transmission of heat to the thermocouple is due to conduction; therefore the transmission of heat from the contact between chip and rake face to the top face of the cylinder housing the thermocouple, has little sensitivity to the convective heat transfer coefficient. Also the shape of the contact has little effect on the temperature recorded by the thermocouple. This fact is also supported by the observations made by Shaw et al. [67, 35] and Jaeger [38]. The heat flux due to the thermocouple minimally influences the temperature on the tip of the thermocouple, but the heat flux is so small that the maximum error produced is

0.34%. The most realistic simulation of the set was chosen to simulate the calibration process. The result of this simulation is a correlation curve between the temperature imposed on the nodes of contact and the temperature on the top face of the cylinder drilled into the insert for embedding the thermocouple. In the concluding chapter of the thesis, a comparison between the results of the simulation of the calibration process and the data obtained by the calibration of the sensor show a good agreement between the FE prediction and the physical experience. In the same chapter, a comparison between the 2D incremental thermo-mechanical simulations and the cutting tests carried out in this research project show excellent agreements in terms of cutting forces and maximum cutting temperature, mainly due to an appropriate choice of the material model, that represents the main issue for a correct approach to machining simulations with finite element techniques [21].

4. Analytical modelling of air jet assisted orthogonal cutting

4.1 Introduction

Metal cutting is an extremely complex process that cannot be described by a single mechanism. While a single mechanism may be predominant over a limited range of operating conditions, experience teaches that no single mechanism holds in general. Shaw [67] suggests that is impossible to predict metal cutting performance, but it should not be inferred that detailed study of the cutting process is without value: each fundamental study carried out and properly interpreted helps our understanding of the process. Shaw addresses the understanding of the cutting process under the following headings

1) shear strain in cutting and slip line field theory
2) plastic behavior at large strain and flow stress modeling
3) energy considerations
4) cutting temperature
5) chip control

The purpose of the analytical model developed for this work is to provide a deeper insight in the mechanical and thermal effect of air jet assisted orthogonal cutting. The model is based on energy balance in the orthogonal cutting process with the contribution of the air jet, which was considered as an external source of energy (thermal and mechanical). The core of the analytical model is the energy balance. According to Shaw [35] and Leone [37] there are two major sources of thermal energy in metal cutting. Figure 4.1 shows the location of the major sources Q of thermal energy with the heat partition coefficients R in orthogonal cutting. The primary source of heat is located in the shear zone and the secondary source is located along the friction zone between the chip

and the tool. The tertiary source of heat indicated in Figure 4.1 is negligible if the cutting tool is sharp. This hypothesis is consistent with the experiments carried out in this research project because a relatively sharp tool was used. In the finite element model of orthogonal cutting a sharp tool was modeled.

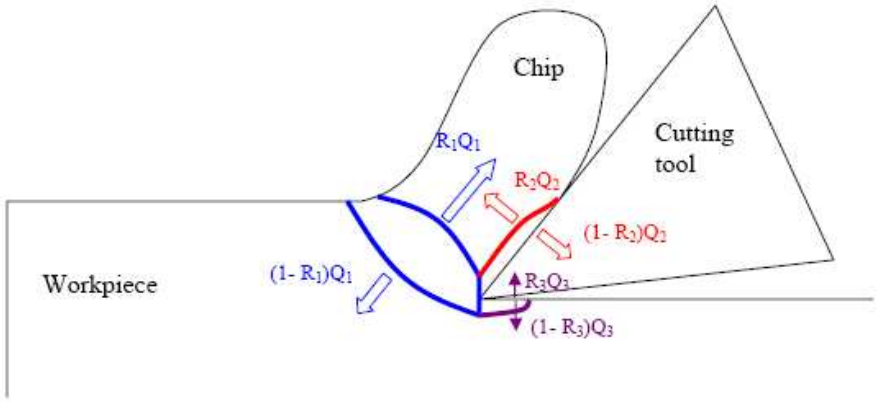

Figure 4.1 – energy partition diagram showing the areas where the heat is generated and relative heat flux with heat partitioning coefficient [126]

As a first approximation, it is assumed that all the energy Q_1 and Q_2 is converted to thermal energy, the energies in the shear zone and friction zone are distributed on two plane surfaces, and the heat flux along the two surfaces is constant, so that the energy is uniformly distributed along the planes. Even with these assumptions, the problem of estimating the mean temperature of the shear temperature (T_s) and the mean temperature of the chip-tool interface (T_t) is complex. This is because part of the energy at the shear plane will usually go to the chip and part will flow to the workpiece, and also part of the energy generated at the friction zone will go to the chip and part to the tool.

There are two partition coefficients, R_1 and R_2 (representing the fraction of energy flowing into the chip) to be evaluated. In this work the method for estimating the heat partitioning coefficients is the same as used by Shaw [67] with the assumption that all the heat flows into a stationary and extensive member. This last assumption involves the heat source solution for an insulated slider moving across a semi-infinite solid, calculated by Jaeger [38]. To introduce the partition coefficient it is necessary to estimate the specific

cutting energy in its main components (shear and friction energy). Once that all the components of the energy balance are known, and they are introduced in they subsystems (the primary or the secondary zone), it is possible to use the two heat partition coefficients for calculating the temperature rise. The estimation of the specific cutting energy requires an understanding of the shear strain in orthogonal cutting and the plastic behaviour of the workpiece at large strain.

Since the main purpose of the analytical model is to estimate the contribution of the shearing energy, the friction energy, and the mechanical and thermal effect of the air jet to the cutting process, the model do not use a sophisticated slip line field theory. In particular it was observed that the iterative method proposed by Hastings, Oxley and co-workers [31, 32] produced a very low flow stress value along the shear plane, compared to the results by finite elements. For this reason the flow stress from finite elements modelling was used as input for the orthogonal cutting model. The material model used in FE was the model proposed by Oxley [31] and coded in Matlab (see Appendix C). In the analytical model proposed in this chapter for predicting the cutting forces, the shear plane temperature and the interface temperature, several different approaches, each of them with a specific purpose, are combined: Leowen and Shaw [36] for the shear plane temperature, Jaeger [38] for the temperature rise due to friction, Merchant for the force estimation [28, 29], Hastings et al. [32] for the flow stress of AISI 1020 used for modeling the material, and Lee and Shaffer [127] slip line field theory. The Figure 4.2 shows the flow chart representing the contributions to the analytical model. The innovation is represented by the approach based on energy balance, that consider the contribution to the energy involved in the cutting process, including external source of energy such as the air jet. The energy contribution due to the air jet has a thermal and mechanical nature. The mechanical contribution is applied in the primary zone (shear area), while the subsystem where the thermal contribution is applied depends on the position of the jet (overhead or interface position). The convective heat transfer by an impinging jet has been modeled using the relations developed by Gau and Chung [130] for a jet impinging on a concave surface. The mechanical effect has been modeled as the deformation energy in the chip caused by the air jet. Slip line field theory treats the plastic zone as incompressible [55], so that the motion of each element of material is

conditioned by the motion of adjacent elements, as shown by the kinematic considerations of Nakayama [54]. Thus part of the shearing energy is responsible for chip curling and the characteristic ear-type chips, associated in the literature with ease of chip fracture, as mentioned by Spaans [131]. According to Shaw [67] chip control theory shows the influence of the chip shape and flow direction on the cutting force, the cutting temperature and the tool life.

A simplistic kinematic explanation of chip curl, introduced by the pioneers of metal cutting theory (Ernst and Merchant [132]) was developed; and as improved by later authors (Nakayama [54] and Spaans [131] among the others), is sufficient to explain chip shape and provide support for the analytical model proposed in this work. There have been some attempts at influencing the cutting force and the cutting temperature through chip control, so as to improve the material removal process. These range from clamped chip-breakers to the latest grooved tools, and from hot machining to the latest laser (Pfefferkorn et al. [25]) and plasma (Shin et al. [133]) heating techniques for controlling the plasticized zone. Also high pressure water jet were used for controlling the chip in orthogonal cutting [134, 11].

The complete investigation of the changes produced by the introduction of the air jet into the shear zone goes beyond the purpose of this project; however it is possible to include the deformation caused by the air jet into the energy balance, and to add it to the shear energy (the sign of the term depends on whether the blowing force reduces or promotes chip curl). The energy approach allow a holistic approach to the analytic modeling of the way an air jet assists the orthogonal cutting process, and allows an easy comparison with other approaches to controlling the shear zone (typically achieved by introducing an external source of energy). The hypotheses required for this simplification are introduced below when the new energy balance term is analytically evaluated. The analytical model is affected by the limitations of the approach used by Shaw and Jaeger and also by the limitations due to the simplification of the aerodynamic field. However, the interest of the analytical model here proposed is to provide a tool for understanding how an external source of energy constituted by an air jet impinging on the chip affects the cutting process. It is not an attempt to propose an analytical model that fits all the results of the finite element modeling and the experimental tests.

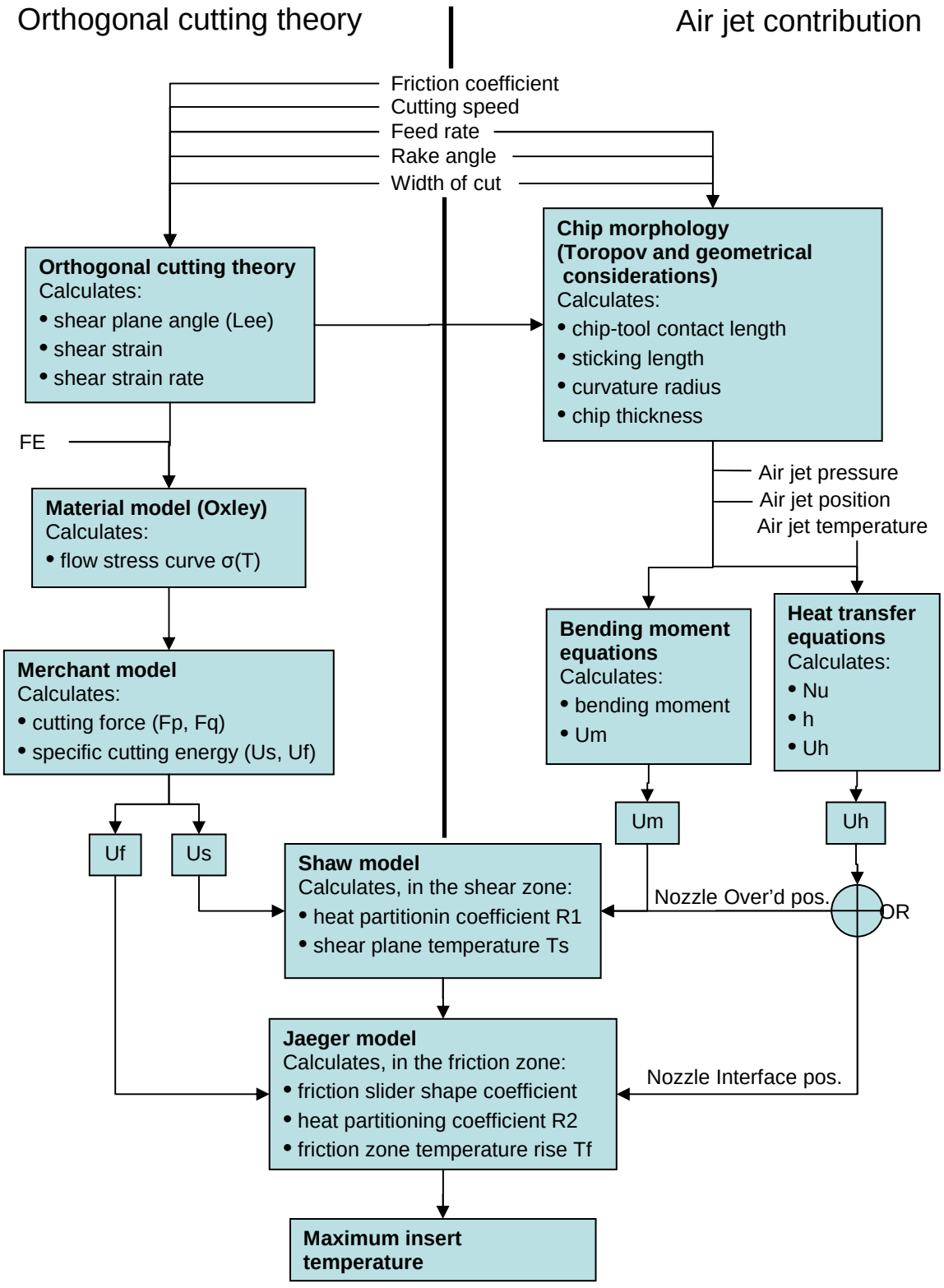

Figure 4.2 – The flow chart of the analytical model includes the contribution of pioneers of orthogonal cutting theory and an energy balance extended to the air jet contribution

Each part of the analytical model here proposed is taken from work already published. In most cases the relations developed by pioneers of metal cutting are used, which have been shown fit the extensive experimental database developed since the early ‘50s [139]. Whilst prediction of metal cutting performance can only be made with any accuracy with finite element methods, these are case-specific. To obtain an idea of the effects of changes in process parameters on performance, it would be necessary to run a whole series of finite element models, and to try to fit the results with some kind of function. This can be very time consuming, and in the absence of an analytical model of the process, the choice of fitting function becomes arbitrary [137].

A closed-form analytical solution can never be accurate. However, it may still be useful. Firstly, it can give a clearer insight into the underlying physics of the process, and may provide a good idea of the trends to be expected when different process variables are altered. Secondly, if it is successful, it can be used to choose the appropriate functions to fit the trends derived from a campaign of finite element modelling [138].

With these aims in mind, an attempt will be made in this chapter to develop such a model. Many approximations must be made to achieve this end, so it is clear that a perfect fit to experimental and finite element results is not to be expected. The intention is to predict the trends in performance – cutting forces and temperatures in particular – when process variables – feed rate, depth of cut, air jet characteristics and position – are altered.

4.2 Shear strain and slip line field theory

In Chapter 1 a literature review of the mechanics of orthogonal cutting has been presented. There we see that if all the shear deformation takes place on a plane, the shearing component of the specific cutting energy is the product of the shear stress and the shear strain on that plane, as shown by Equation 4.1:

$$u_s = \tau \, \gamma \qquad \text{Eq. 4.1}$$

A first step for predicting cutting performance involves estimating the shear stress τ on the shear plane and the shear strain γ associated with chip formation. Both of these

quantities are strongly influenced by the friction on the face of the tool which is expressed in terms of the friction angle β,

$$\beta = \tan^{-1}\frac{F_C}{N_C} \qquad \text{Eq. 4.2}$$

F_c and N_c are referred to Figure 4.2, that shows the balance of forces involved in the orthogonal cutting process with a sharp tool.

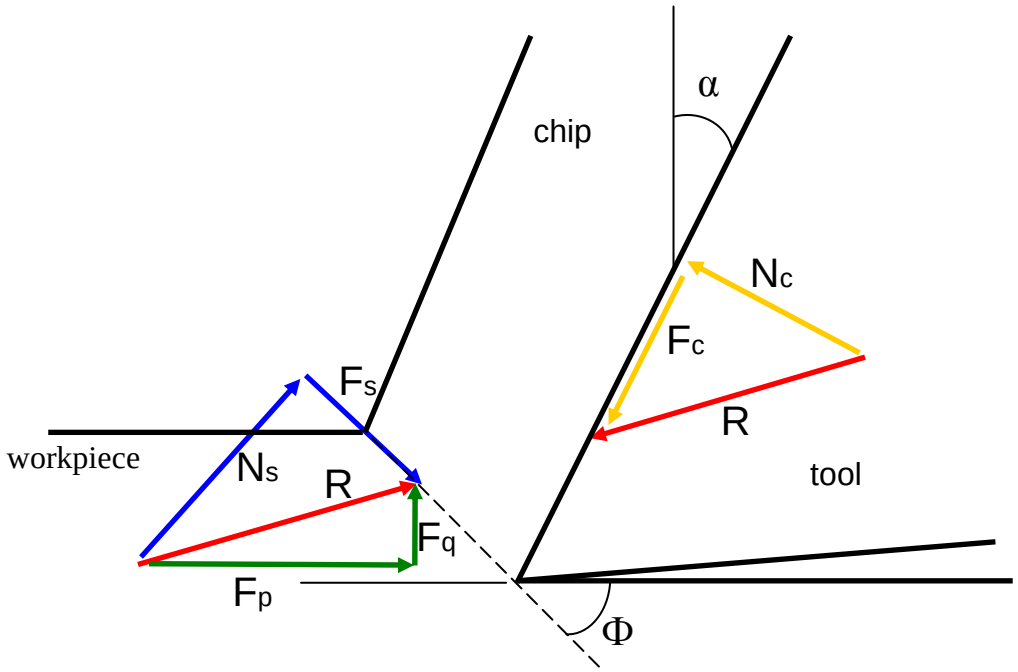

Figure 4.3 – The balance of forces involved in orthogonal cutting with a sharp tool in the reference system of the tool (F_c and N_c), in the reference system of the shear plane (F_s and N_s) and in the reference system aligned with the direction of cut (F_p and F_q)

The Figure 4.3 indicates the components of the cutting force R in the reference system of the tool, in the reference system of the shear plane and in the direction of cutting. The rake angle α and the shear plane angle Φ are also indicated in the figure. A relatively simple relation (Merchant [28, 29] exists between shear strain, rake angle and shear angle:

$$\gamma = \frac{\cos\alpha}{\sin\Phi\cos(\Phi-\alpha)} \qquad \text{Eq.4.3}$$

Since the rake angle will be known, the problem of predicting the shear strain reduces to the prediction of the shear plane angle Φ.

The estimation of the strain rate required that shearing takes place within a zone of finite thickness. This is the only part of the model where the hypothesis of a shear zone concentrated on a plane surface cannot be used. The shear zone is usually very thin, as shown by Kececioglu [30], and the strain rate can be estimated as follows:

$$\dot{\gamma} = \frac{\cos\alpha}{\cos(\Phi - \alpha)} \frac{V}{t_S} \qquad \text{Eq.4.4}$$

where V is the cutting speed and t_s is the thickness of the shear zone. As described in paragraph 3.8, the FE simulations show that the thickness of the shear zone is 25 μm. This value was observed to be constant for all the cutting condition examined in the simulations. Also, Shaw reports this value as a reasonable thickness for the shear "plane", on the basis of the work of Kececioglu [30].

Two distinct operations are involved in a metal cutting process: the shearing action along the shear zone (a shear plane in the model here proposed) and the sliding along the rake face of the tool [128]. According to Lee and Shaffer's [127] model, which appears to be the best simple model for orthogonal cutting, for a sharp tool and small rake angles, the friction angle β can be obtained by inverting the relation between the friction angle and the friction coefficient μ (Equation 4.5), which depends on the two materials in contact and the contact temperature. The coated insert used in this research gives excellent friction coefficients: between 0.5 and 0.6 according to Sandvik [124] (0.55 was chosen for the analytical model).

$$\mu = \tan\beta \qquad \text{Eq.4.5}$$

Lee and Shaffer [127] assumed that the material behaves as an ideal plastic material when cut and that the shear plane represents the direction of maximum shear stress. Their slip line field theory is one of the most frequently used as a starting point for more elaborated analysis [127]. Figure 4.4 shows the slip line field used for obtaining the shear plane angle.

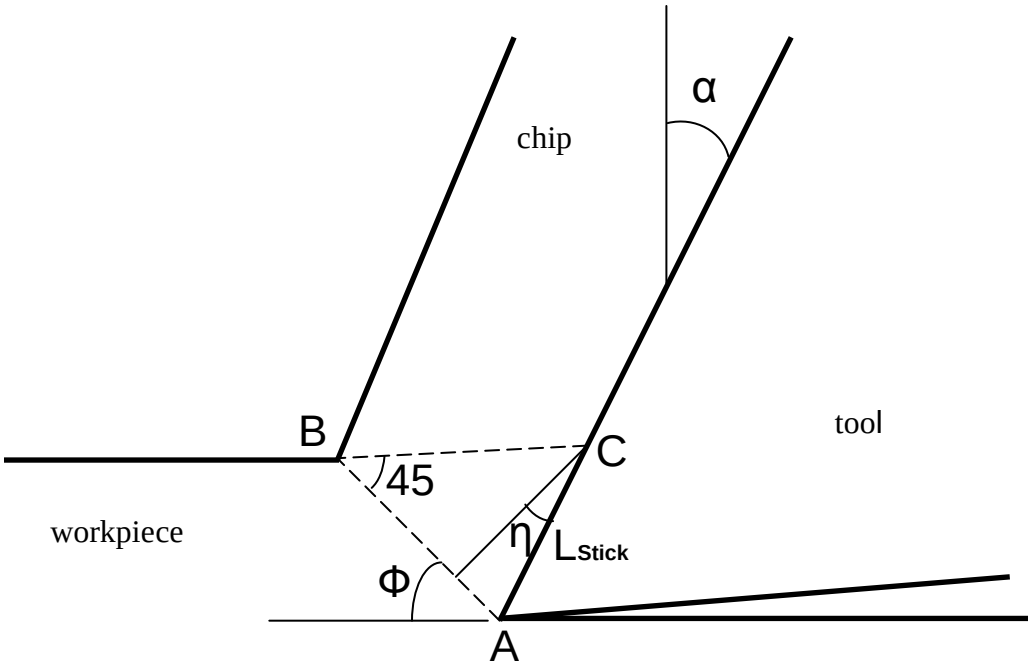

Figure 4.4 - The slip line field ABC used by Lee and Shaffer

Geometrical considerations allowed Lee and Shaffer to write the following relations for η:

$$\eta = 45° - \beta \quad \text{and} \quad \eta = \Phi - \alpha \qquad \text{Eq.4.6}$$

Hence

$$\Phi = 45° - \beta + \alpha \qquad \text{Eq.4.7}$$

The slip line field theory also provides a relation for the length of the sticking region, where the shear stress is maximal and the material is purely plastic (L_s), as shown in Equation 4.8:

$$L_S = \frac{t\sqrt{2}}{2\sin\Phi\sin(45° + \Phi - \alpha)} \qquad \text{Eq.4.8}$$

where t is the undeformed chip thickness. The analysis of Lee and Shaffer also include an additional hypothesis: no Built-Up edge (BUE) is formed in the cutting process. If a BUE is formed, an additional term should be added to the Equation 4.7:

$$\Phi = 45° - \beta + \alpha + \theta \qquad \text{Eq.4.9}$$

where the angle θ represents a small BUE, as shown in Figure 4.5. In more detailed models the task about shear angle solution for each slip-line in the triangle ABC can be solved if shear stress in corresponding line is known. However there has been no experimental data according to changes of this parameter in cutting conditions while many ways to determine shear stress in imaginary shear plane have been proposed, including the solution of Hastings, Oxley and Mathew [32], with the introduction of strain hardening effect. The solution provided by Oxley and co-workers use a flow stress that depends on temperature, strain and the strain rate can be provided by using an iterative model. In this work the solution of Oxley was not used, it was used instead the solution provided by FE simulation. It was observed that the material model developed by Oxley provided better results in the simulation, therefore the work of Oxley was included, in a tabular form, in the material library of DEFORM. The stress as a function of temperature, strain and strain rate developed by Oxley for low carbon steels are shown in the Appendix C. The results by FE were used for obtaining the correction angle θ (Figure 4.5).

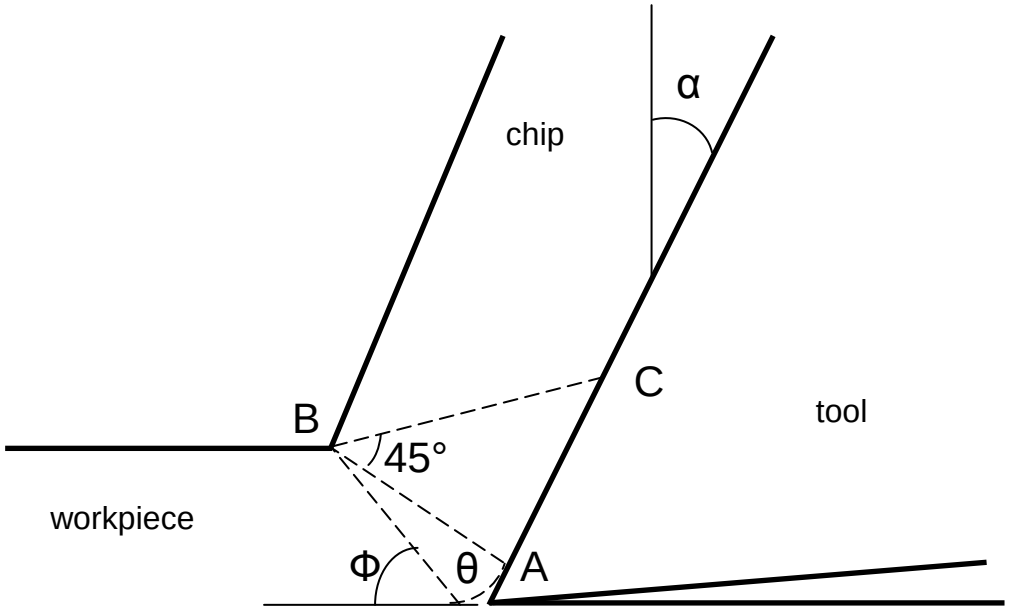

Figure 4.5 – The rotation θ promoted by the Built-Up edge

By estimating the shear plane angle it is possible also to estimate the chip thickness ratio (Equation 4.10) and the shear plane angle area (Equation 4.11):

$$r_t = \frac{\tan \Phi}{\cos \alpha + \sin \alpha \ \tan \Phi} \qquad \text{Eq.4.10}$$

$$A_S = \frac{b\ t}{\sin \Phi} \qquad \text{Eq.4.11}$$

4.3 Shear stress in metal cutting and estimation of cutting forces

According to Shaw [67] plastic flow on the shear plane in orthogonal cutting may be characterized as follows:

1) large values of strain rate and temperature
2) small values of normal stress (compared to the shear stress) on the shear plane
3) progressive deformation with a very small volume deformed at one time
4) proximity of the shear zone to the rigid cutting tool

The influence of strain, strain rate and temperature in cutting leads to the need for a reliable flow stress model. The theory of plastic flow stress can be considered as an extension of dislocation theory, and a few material models have been developed for low carbon steels. The material model for AISI 1020 used for the analytical and finite elements model proposed in this work was developed by Oxley and co-workers [31]. The model of Oxley was originally designed for AISI 1016, and subsequently extended to most of the low carbon steels, since the model depends on the content of carbon. The starting point of Oxley's model is the strain hardening curve:

$$\sigma = \sigma_1 \varepsilon^n \qquad \text{Eq.4.12}$$

where σ_1 is the stress at $\varepsilon = 1$ and n is the strain hardening coefficient. The strategy used by Oxley for developing his model consists in calculating a modified temperature T_{mod} according to Equation 4.13, expressing σ_1 and n for AISI 1016 (here called σ_{1C16} and

n_{C16}) as a function of T_{mod} then subsequently extending the model to other carbon contents:

$$T_{\text{mod}} = T\left(1 - 0.09 \log_{10} \dot{\gamma}\right) \qquad \text{Eq.4.13}$$

where T is the cutting temperature. The equations used by Oxley (reported in the Appendix) are derived by experimental test on AISI 1016, and subsequently verified for other low carbon steels. Figure 4.5 shows the flow stress for three low carbon steels at the strain rate of 10000 sec^{-1} and unitary strain. It can be observed that the flow stress of AISI 1020 is quite similar to the flow stress of AISI 1018. The curve shown in Figure 4.5 is consistent with the results achieved from Ozel et al. [21] for low carbon steels. The flow stress model obtained from the equations of Oxley were converted into tabular form and imported into DEFORM, since the use of the equation in the form expressed in Equation 4.12 caused problems of convergence. As reported in the Figure 4.5 few points of discontinuity have been reported for plain carbon steel of high carbon content. The curve for AISI 1045 shows a discontinuity at $T = 1089°C$ - a high temperature in AISI 1045 machining. This is a limit of the material model, which can be safely applied only for low carbon steels, with carbon contents from 0.12% to 0.45%. For AISI 1020 machined under the conditions modeled here, the flow stress seems to be independent of the cutting speed, but it changes with feed rate. Since the FE modeling used the flow stress model shown in this paragraph, the FE simulations were used for finding the stress on the shear plane and the shear plane angle for each cutting condition.

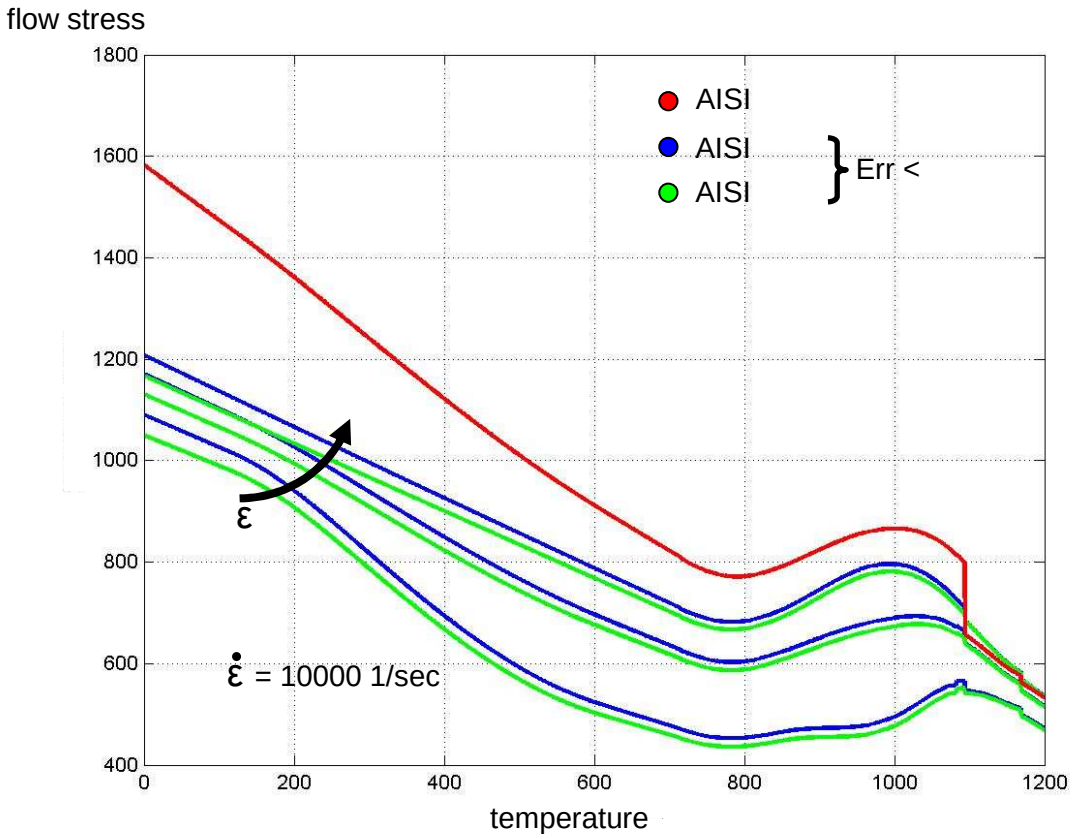

Figure 4.5 – A plot of the flow stress model developed by Oxley for three low carbon steels

ID	$\dot{\gamma}\,(s^{-1})$	γ	*Ts (℃)*	σ *(MPa)*	Φ *(Lee)*	θ
v83f06	28900	1	303	1074	16.18°	2.61°
v83f12	24600	1	320	1041	16.18°	3.38°
v129f06	45000	1	312	1087	16.18°	2.61°
v129f12	38200	1	334	1065	16.18°	3.38°

Table 4.1 – The results of the FE simulation obtained by using the material model developed by Oxley and the correction angle θ, obtained by comparing the shear plane angle of Lee to the results by FE simulations

By rotating the flow stress by using the Möhr's circle of associated with the slip line field (Shaw [67]), it is possible to calculate the shear stress τ as follows:

$$\tau = \frac{\sigma}{\tan(\Phi + \beta - \alpha + \theta)} \qquad \text{Eq.4.14}$$

By multiplying the shear stress and the flow stress over the area of the shear plane it is possible to estimate the cutting force in the reference system of the shear plane angle (F_s and N_s), and geometrical considerations allow the cutting force to be resolved into its component in the cutting direction F_p and in the perpendicular direction F_q, and also in the reference system of the tool (F_c and N_c)

$$F_s = \tau \ A_s \qquad N_s = \sigma \ A_s$$

$$R = \sqrt{F_s^{\ 2} + N_s^{\ 2}}$$

$$F_p = R \ \cos\left(\Phi - \tan^{-1}\frac{F_s}{N_s}\right) \qquad \text{Eq.4.15}$$

$$F_q = R \ \sin\left(\Phi - \tan^{-1}\frac{F_s}{N_s}\right)$$

$$F_c = F_p \sin\alpha + F_q \cos\alpha$$

$$N_c = F_p \cos\alpha - F_q \sin\alpha$$

The Table 4.1 illustrates the results for the cutting forces at the four cutting conditions considered in the experimental tests. These values show a good agreement with the results obtained by experimental tests and shown in Chapter 6 (F_p and F_q)

cutting condition	F_p	F_q
t=0.06 v=83	117	65
t=0.12 v=83	235	129
t=0.06 v=129	117	65
t=0.12 v=129	235	129

Table 4.1 – The cutting forces predicted by the analytical model. The units for the feed rate are mm/rev, for the cutting speed the units are m/min. The force are expressed in N

4.4 The effect of induced chip deformation on the energy balance

In the orthogonal cutting process, the total energy consumed per unit time per unit volume of metal removed is

$$u = \frac{F_p}{bt} \qquad \text{Eq.4.16}$$

The specific cutting energy u is dissipated in several ways, but according to Shaw [67] the two main source of energy are the shear energy per unit volume (u_s) on the shear plane and the friction energy per unit volume (u_f) on the rake face. The shear energy can be written as the product of shear stress and shear strain, and the friction energy can be obtained by subtraction:

$$u_s = \tau\ \gamma \qquad u_f = u - u_s \qquad \text{Eq.4.17}$$

The specific shear energy calculated by the analytical model is in good agreement with the examples proposed by Shaw [67] and Trent [140]. Since the flow stress is not affected by the cutting speed, two values of the specific shear energy have been found: 2059 MPa for *t=0.06 mm/rev* and 2108 MPa for *t=0.12 mm/rev*. This result is very close to the data given by Shaw for similar cutting conditions and low carbon steel, AISI 1018, which has a flow stress similar to AISI 1020: 2100 MPa. However, the data given by Shaw are representative data rather than precise figures.

Most of the analytical models for predicting cutting performance are based on the hypothesis of all the occurring on the shear plane; but in fact the shear zone, which can be approximated as a perfectly plastic zone, has a thickness. The strategies for improving cutting through an external source of energy, including the use of laser and plasma techniques [9, 25], work by inducing a state of stress which changes the size of the plastic zone.

According to slip line theory field [127], the material moves incompressibly, following the stress trajectory described by the slip line field. Figure 4.6 represents the state of

shear stress in the chip-tool interface according to Zorev 141. The shear stress in the sticking length is constant and equal to the plastic stress, and decreases to zero when the distance from the edge is approximately twice the sticking length.

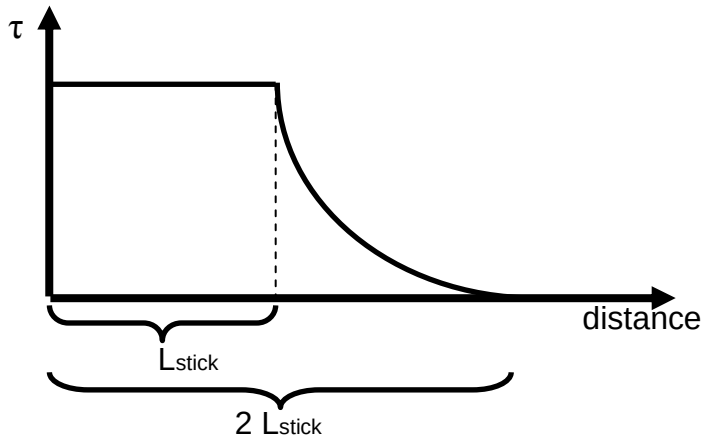

Figure 4.6 – Qualitative diagram of the shear stress distribution as a function of distance from the edge of a sharp tool.

Toropov et al. [142, 143] approximate the sticking length as

$$L_{stick} = \frac{t\sqrt{2}}{2\sin\Phi\sin\left(\frac{\pi}{4}+\Phi+\alpha\right)} \qquad \text{Eq.4.18}$$

The contact length and the sticking length between the chip and the rake face are used for estimating the chip shape by kinematic relations within the assumptions of the slip line field theory. The Figure 4.7 represents a simple kinematical model of chip formation. The triangle ABC represents the plastic zone of the chip and the line AA' is the contact length, which is approximately twice the sticking length L_{stick} [142]. The triangle ABC translates to the position A' ($AA'=2\ L_{stick}$), and since the chip is not constrained anymore to the rake face in A', it rotates according to the plasticization of the workpiece. If the workpiece material is a perfectly plastic material and the cutting process is approximated by a discrete process, then Figure 4.7 illustrates a fully developed chip just before the self-contact with the uncut surface.

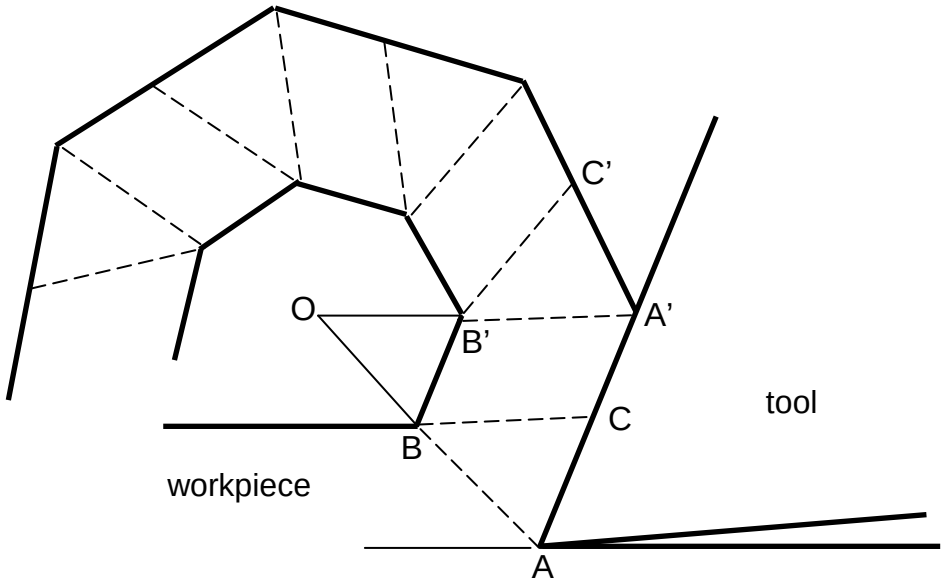

Figure 4.7 – Graphic interpretation of chip curling due to plastic zone ABC

By geometrical considerations

$$AC = AB\frac{\frac{\pi}{4}+\theta}{\Phi+\alpha}$$

$$B\hat{O}B' = \pi - \Phi - \alpha$$

$$BB' = 2L_{stick} - AC \qquad \text{Eq.4.19}$$

$$OB = OB' = \frac{BB'}{2\sin B\hat{O}B'}$$

By introducing into the Equations 4.18 (L_{stick}) the length AB of the shear plane angle and by adding to OB half the chip thickness, it is possible to obtain the curl radius R_c in orthogonal cutting for a continuous chip and perfectly plastic material:

$$R_c = \frac{2L_{stick} - \frac{t}{\sin\Phi}\frac{\frac{\pi}{4}+\theta}{\Phi+\alpha}}{2\sin(\pi-\Phi-\alpha)} + \frac{t}{2r} \qquad \text{Eq.4.20}$$

The Table 4.2 shows the predicted chip thickness t_1, the curvature radius R_c of the chip and the sticking length L_{stick}. The comparison between the chip morphology by the analytical model and the experimental tests is shown in Paragraph 6.2.

cutting conditions	t_1	R_c	L_c
t=0.06 v=83	0.1660	0.5532	0.1379
t=0.12 v=83	0.3320	1.1064	0.2757
t=0.06 v=129	0.1660	0.5532	0.1379
t=0.12 v=129	0.3320	1.1064	0.2757

Table 4.2 – The chip thickness, the curvature radius and the contact length, expressed in mm, predicted by the analytical model at different cutting conditions.

The perfectly plastic material in the slip line field zone is an idealization. Under this hypothesis the stress in the triangle ABC is constant, and decreases in the zone A'B'BC in the way illustrated by Figure 4.7. The simple kinematic analysis carried out in this paragraph suggests that a link between the chip curl and the shear energy exists. The assumption of a triangular fully plastic zone is a strong simplification. A more realistic distribution of the plastic zone is shown in Figure 4.8, and constitutes also a more efficient condition from the energetic point of view.

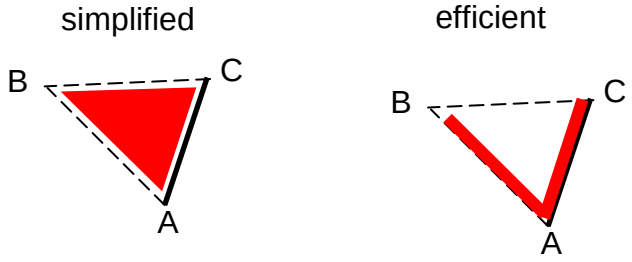

Figure 4.8 – The maximum stress zone (marked in red) idealized by the slip line field theory (simplified) and concentrated in the primary and secondary zone (efficient).

If the maximum stress is concentrated along the primary and secondary zone, we have an optimized situation. Minimizing the plastic zone also minimizes the shear energy, and the chip shape (curl radius in particular) is directly related to the minimization of the shear energy, as stated by Baker [26]. From a qualitative point of view, a small curl radius (i.e.

a small value of the ratio $\frac{BB'}{AA'}$) indicates a large plastic zone, and for particularly large plastic zones, the chip can segment in order to minimize the shear energy. By using a strategy for maximizing the ratio $\frac{BB'}{AA'}$ (by directing a laser or a plasma beam on *B*, by using a reduced contact grooved tool, or by bending the chip with an external source of energy) it is possible to minimize the shear energy and the temperature rise. Baker also observes that the shear plane does not adjust itself to minimize the energy, therefore it can be assumed that in the case of a deformation of the chip by an external source of energy, all of the deformation energy is used for minimizing the shear energy without affecting the cutting forces (the calculation of the cutting forces depends on the shear plane angle and the flow stress of the workpiece material). The Figure 4.9 shows the effect of changing the curvature radius of the chip by mechanical effect. When the curvature radius is forced to reduce, the fibers of the chip in contact with the tool are forced to stretch, and the upper fibers of the chip are force to crunch. In this condition the effect of curling the chip is traduced in an extra amount of energy, compatible to the enlarged plastic zone, according to the observation of Baker. The opposite effect is obtained if the mechanical effect is applied on the top face of the chip. In this case the chip curl radius is bigger, and the plastic zone became more similar to the situation described in Figure 4.8, in the most efficient solution. Since early experience with laser assisted cutting, laser beams (more recently plasma beams) were used for produce an instantaneous thermal treatment at the root of the incipient chip [50]. The reduction of the cutting force observed by Kou et al. [22] is mainly related to the austenitic transformation at the root of the chip. However Gratias et al. [23] show with micrographs that the transformation affects the material only at shallow depth. Therefore the thermal treatment is also promoting a stretching of the fibers interested by the beam. Dekumbis [86] observed the thermal treatment by high power laser beam also promote an increment of the curling radius of the chip and reduction of chip length.

The energy associated to the increment of the curling radius of the chip is not negligible, and may promote a difference in the energy balance of the system. According to Figure 4.9, a counter-clockwise rotation of the chip promote an increment of energy in the shear

zone, a clockwise rotation of the chip promote a decrement of energy in the shear zone. The ideal situation is the production of a straight chip, with no compression of the fibers at the root of the chip, corresponding to the early orthogonal cutting model of Piispanen [146, 147]. In this research project a high speed air jet was used as external source of energy to apply a pressure to the chip and to bend it. It has been observed that the maximum pressure applied by the air jet is not sufficient by itself to promote a plastic hinge in the chip, as illustrated by Yu et al. [148].

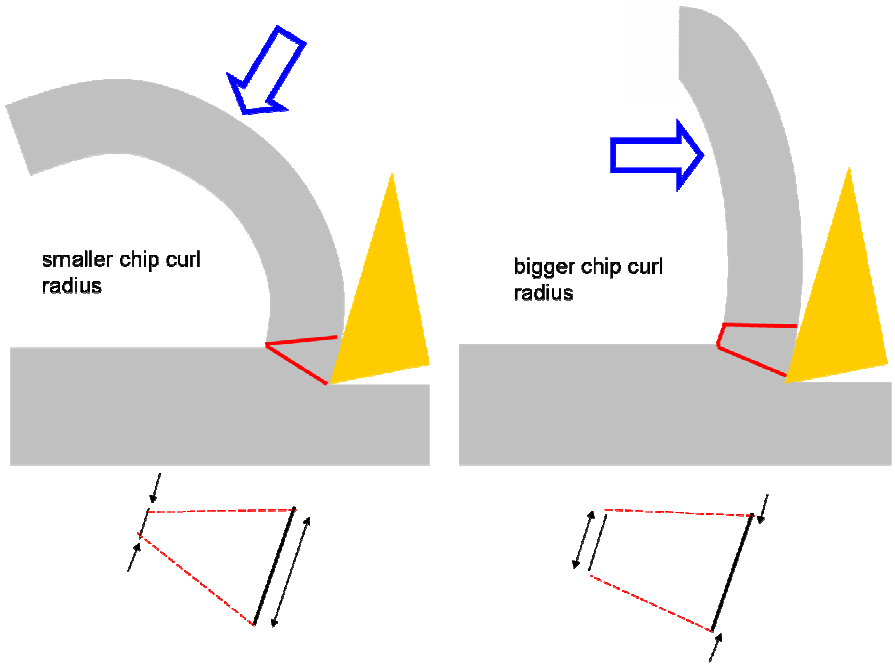

Figure 4.9 – The qualitative effect of mechanical chip curling. The effect on the fibers of the chip is shown in the diagram below the two sketch of the chip. On the right the fiber in contact with the tool are compressed. On the other hand, on the left the fiber in contact with the tool are stretched

Figure 4.10 shows the section of the chip, where *b* is the width of cut. This will be used to analyze the bending effect of the air jet under the hypothesis of small displacement and elastic behavior of the chip.

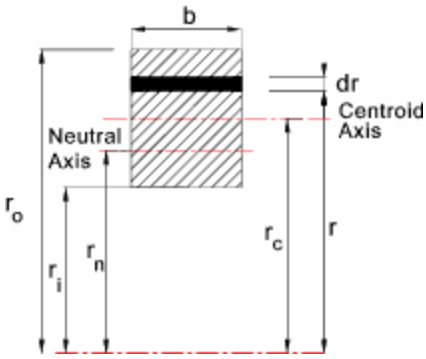

Figure 4.10 – The chip section with the radius used for the curved beam analysis

In the following analysis the position on the chip is identified by the polar coordinates $\bar{r}$ and the angle $B\hat{O}B' = \vartheta$, starting from the segment OB. (Fig. 4.7)

$$\sigma_{el} = E\varepsilon = E\bar{r}\frac{d\vartheta}{r\vartheta} \qquad where \qquad r_n = \frac{r_o - r_i}{\ln\frac{r_o}{r_i}} \quad , \quad \bar{r} = r - r_n \qquad \text{Eq.4.21}$$

By introducing the eccentricity e and the chip thickness t:

$$\begin{aligned} e &= r_c - r_n \\ t_1 &= r_o - r_i \end{aligned} \qquad \text{Eq.4.22}$$

it is possible to write the stress due to a bending moment M as follows:

$$\sigma_{el} = \frac{M(r - r_n)}{bt\ e\ r} \qquad \text{Eq.4.23}$$

The Figure 4.11 represents the chip with a constant distributed load *p*, applied to the top side of the chip (overhead) and in the interface between the chip and the rake face (interface).

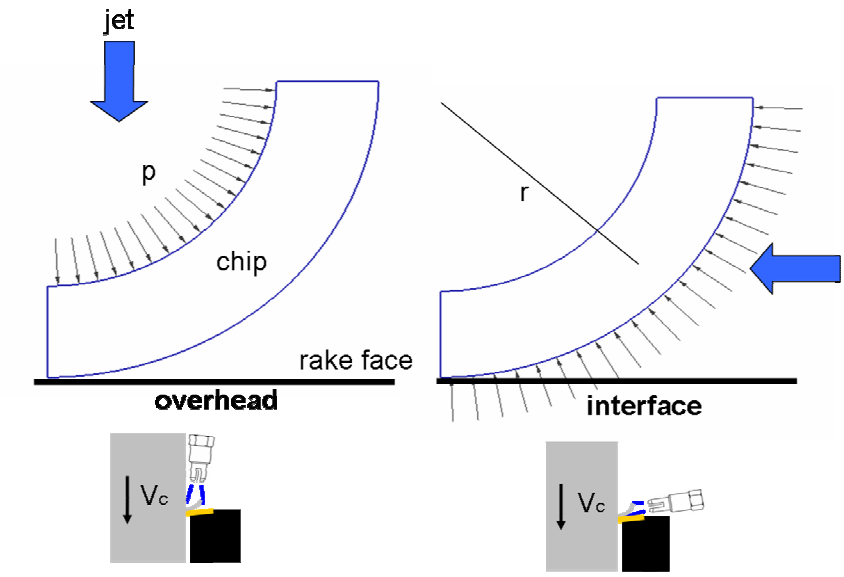

Figure 4.11 – The chip under constant distributed load on the top face (overhead) and in the chip-tool interface (interface). The blue arrow indicate the direction of the air jet

The analytical solution has to account the direction of the air jet and the projection of the component of the blowing force represented by the distributed load. It can be observed that when the jet is directed from the overhead position, the blowing force is applied only to a quarter of a circle. Equations 4.27 give the moment *M* due to the two loading condition as

$$M_{over} = \int_0^{\pi/2} p\ b\ \frac{\bar{r}}{2}\cos\vartheta\ \bar{r}\vartheta\ d\vartheta = p\ b\ \bar{r}^2\left(\cos\vartheta + \vartheta\ \sin\vartheta\Big|_0^{\pi/2}\right) \qquad \text{Eq.4.24}$$

$$M_{\text{int}} = \int_0^{\pi} p\ b\ \frac{\bar{r}}{2}\sin\vartheta\ \bar{r}\vartheta d\vartheta = p\ b\ \bar{r}^2\left(\sin\vartheta - \vartheta\ \cos\vartheta\Big|_0^{\pi}\right)$$

It can be observed that the solution for the moment applied in the overhead case with $\vartheta = 0$ (the chip is not curled) reduces to that of a cantilevered beam under distributed load. Also the moment applied in the interface at $\vartheta = 0$ is zero, since the air jet is aligned

with the chip. The convention used for the sign of the bending moment takes as positive the moment that promotes a rotation of the chip in the direction of the curl. By combining Equations 4.24 with 4.21 and 4.23, the energy associated with the deformed state for a rectangular chip section of area *bt* is expressed by the following equations:

$$U_{Mover} = \frac{M^2 \bar{r}}{2EI} = \frac{6\ p^2 b \left(r_c - \dfrac{r_o - r_i}{\ln \dfrac{r_o}{r_i}} \right)^6 \left(\cos\vartheta + \vartheta\ \sin\vartheta \Big|_0^{\pi/2} \right)}{E\ t^3 e}$$

Eq.4.25

$$U_{M\,\mathrm{int}} = \frac{M^2 \bar{r}}{2EI} = \frac{6\ p^2 b \left(r_c - \dfrac{r_o - r_i}{\ln \dfrac{r_o}{r_i}} \right)^6 \left(\sin\vartheta - \vartheta\ \cos\vartheta \Big|_0^{\pi} \right)}{E\ t^3 e}$$

By dividing the expressions of the energy associated with chip deformation due to the air jet by the undeformed chip section, the specific deformation energy is obtained. Table 4.3 illustrates the contribution of the specific energy associated with chip deformation. In the case of the nozzle in the overhead position, there are two values for the energy, because the contribution changes with the length of chip. The contribution has a minimum for $\vartheta = 0$, corresponding to the situation of a chip of length equal to *2L*$_{stick}$, and maximum for $\vartheta = \pi/2$, corresponding to the situation of the maximum impact length of the air jet on the chip. Both maximum and minimum values are referred to the absolute value of the specific deformation energy (the deformation energy divided by the product of the width of cut and the feed rate), expressed in MJ/m^3. The sign convention takes the incipient rotation in the direction of chip curling as positive. Eight cutting conditions are represented: two cutting speeds (83 and 129 m/min), two feed rates (0.06 and 0.12 mm/rev) and two air jet pressures (0.4 and 0.7 MPa).

cutting conditions	U_{Mover} (min)	U_{Mover} (max)	U_{Mint}
T=0.06 v=83 p=0.4	-18.8	-29.6	59.2
T=0.12 v=83 p=0.4	-37.7	-59.2	118.4
t=0.06 v=129 p=0.4	-18.8	-29.6	59.2
t=0.12 v=129 p=0.4	-37.7	-59.2	118.4
t=0.06 v=83 p=0.7	-57.7	-90.6	181.3
t=0.12 v=83 p=0.7	-133.7	-265.8	328.3
t=0.06 v=129 p=0.7	-57.7	-90.6	181.3
t=0.12 v=129 p=0.7	-133.7	-265.8	328.3

Table 4.3 – The contribution of the chip deformation energy (MJ/m^3) at different cutting conditions

4.5 Heat transfer to an impinging jet

The Figure 4.12 shows a sketch of the cutting area cooled by two high speed air jets in the overhead and the interface position. The figure also shows the positions of the two main sources of heat, the shear zone (blue) and the friction zone (red). In order to account the cooling action of the air jet, the heat dissipated by the air jet has to be evaluated for both positions of the jet. Newton's law of cooling is the essential ingredient of the evaluation of the effects of forced convection.

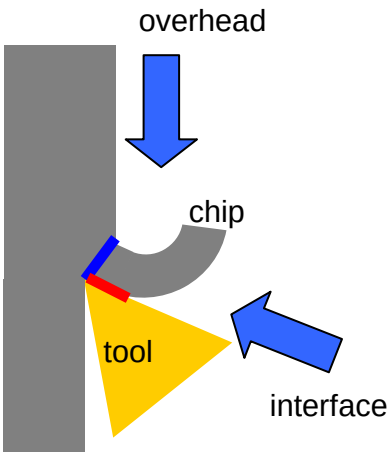

Figure 4.12 – Sketch of the cutting area cooled by high speed air jets in the overhead or in the interface position

Equation 4.26 represents the rate of heat u_h dissipated by forced convection for unit of removed material:

$$u_h = h \ \frac{Area}{bt} \ (T_w - T_\infty) \qquad \text{Eq.4.26}$$

where h is the heat transfer coefficient, *Area* is the cooled area where the heat is dissipated, T_w is the temperature of the cooled surface and T_∞ = 4°C is the free fluid stream temperature, measured by a thermocouple in the centre of the air stream, where the conditions are closest to an undisturbed stream. The section of the air cone pattern of the air jet is much wider then the *Area*, so the properties of the air stream can be considered uniform. In order to evaluate u_h the Nusselt number *Nu* has to be estimated by using correlations with the Reynolds number, *Re* and the Prandtl number, *Pr*.

$$Nu = \frac{h \ L}{k_{air}} \qquad Re = \frac{\rho \ V_{flow} diam}{\mu_{air}} \qquad Pr = \frac{c_p \mu_{air}}{k_{air}} \qquad \text{Eq.4.27}$$

where k_{air} , μ_{air} , c_p are respectively the thermal conductivity, the viscosity and the specific heat at constant pressure of the air. L is the length of the cooled surface (in a 2D case) and *diam* is the diameter of the nozzle. The mass flow rate ρV_{flow} as a function of pressure has been estimated by experimental correlation:

$$\rho V_{flow} = \frac{7.5(p-4)+30.5}{60 \ \frac{diam^2}{4}\pi} \qquad \text{Eq.4.28}$$

where p is the pressure of the air jet. The Reynolds number is determined as a function of pressure and the correlation can be used in the two pressure configuration used in this project: 0.4 MPa (*Re = 30000*) and 0.7 MPa (*Re = 51400*). The Prandtl number for the air at 4°C has been estimated as *Pr=0.714*. Different correlations for the Nusselt number in forced convection with turbulent flow, shown in the literature review have been compared. The correlation in the interface case is reported by Incropera and De Witt [149] and represents the Nusselt number for a turbulent flow parallel to the source of heat, evenly distributed in the chip-tool interface. Few correlations exist for impinging

turbulent flow on concave surface (the chip) and on flat surface at different angles (the rake face) [150, 151, 152]. However, the ideal 2D case is represented by a semi-infinite surface and therefore the jet has been experimentally produced by a slot nozzle (Gau and Chung [130]) or an array of round nozzles (Hrycak [153]). Gau and Chung reported on the effects of both concave and convex surfaces and included results from slots as well as orifices. The solution of Gau and Chung depends on the ratio between the distance from the concave surface and the exit section of the nozzle. If $\frac{dist}{diam} > 6$, the flow is fully developed and the relation also approximate the single round jet, if the heat source is in the core of the jet, and make the solution of Gau and Chung suitable for the case described in this work.

$$Nu_{over} = 0.394\,\mathrm{Re}^{0.68}\left(\frac{2R_c}{diam}\right)^{-0.15}\left(\frac{dist}{diam}\right)^{-0.38}$$

Eq.4.29

$$Nu_{int} = 0.0308\,\mathrm{Re}^{\frac{4}{5}}\,\mathrm{Pr}^{\frac{1}{3}}$$

The Table 4.4 shows the Nusselt number estimation for the two feed rates (0.06 and 0.12 mm/rev) and two pressures (0.4 and 0.7 MPa). When the nozzle is in the overhead position, the Nusselt number depends on the feed rate because the chip curl radius is involved in the calculation of the Nusselt number.

cutting conditions	Nuover	Nuint
t=0.06 p=0.4	149	104
t=0.12 p=0.4	135	104
t=0.06 p=0.7	218	161
t=0.12 p=0.7	190	161

Table 4.4 – The Nusselt number estimated by the analytical model as a function of air jet pressure and feed rate

The convective heat transfer coefficient calculated by the estimation of the Nusselt number ranges from *h=6000* to *h=9500* for the overhead case and from from *h=7300* to *h=9800* for the case interface. However, considering the low sensitivity predicted by finite elements modeling to the variation of *h*, the experimental tests carried out by Kops et al. [95] suggest that a suitable approximation of the local heat transfer coefficient is $h=2000\ {}^{W}\!/_{m^2 K}$, two order of magnitude greater than the natural convection with air.

4.6 Overall energy balance

Figure 4.12 shows how the specific energies estimated in the paragraphs 4.3 and 4.4 have been introduced into the system. According to Shaw [67], practically all of the energy associated with the shearing process and chip formation ends up as thermal energy. The mechanical energy provided to the chip by the air jet contributes to the energy in the primary zone (the shear plane). When the air jet is directed from the overhead position, the thermal energy associated with the heat transfer is contributing to the energy in the primary zone too. When the air jet is applied in the interface position, the thermal energy contributes to the energy in the secondary zone. The energy is considered as positive when entering the workpiece.

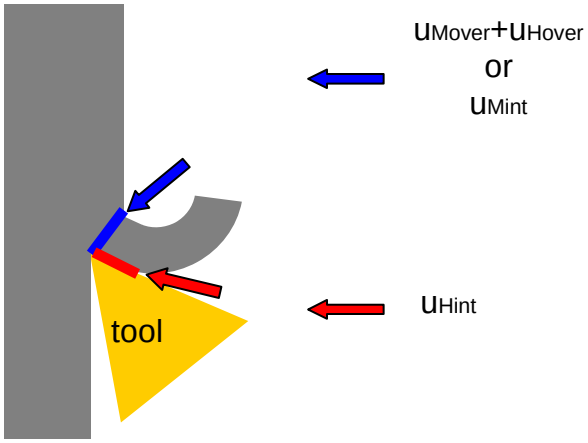

Figure 4.12 – Sketch of the energy balance with the contribution of the mechanical effect (u_M), and thermal effect (u_H)

According to Figure 4.12, the energy balance in the case of air jet applied from the overhead position is:

$$u_{primary} = u_S + u_{Mover} + u_{Hover}$$
$$u_{secondary} = u_f \qquad \text{Eq.4.30}$$

The energy balance in the case of air jet directed into the interface is:

$$u_{primary} = u_S + u_{M\,int}$$
$$u_{secondary} = u_f + u_{H\,int} \qquad \text{Eq.4.31}$$

The Table 4.5 shows the values of the specific energies (mechanical effect and thermal effect) of the air jet at the two pressures considered in the tests. It can be observed that the contribution of the air jet in terms of energy is small compared to the specific shear energy (approximately 2100 MJ/m^3).

cutting condition	u_{Mover} (min)	u_{Mover} (max)	u_{Mint}	u_{Hover}	u_{Hint}
t=0.06 p=0.4	-18.8	-29.6	59.1	-60.6	-53.8
t=0.12 p=0.4	-37.7	-59.2	375.3	-16.5	-13.1
t=0.06 p=0.7	-57.7	-90.6	181.3	-94.3	-78.3
t=0.12 p=0.7	-133.7	-265.8	328.3	-24.3	-20.5

Table 4.5 – The energetic contribution of the air jet at the two pressures considered in the tests: 0.4 and 0.7 MPa

4.7 Estimation of the shear plane temperature and interface temperature

The model developed by Loewen and Shaw [36] was used to estimate the heat partitioning coefficient R_1 in the primary zone and the friction slider developed by Jaeger [38] was used to estimate the heat partitioning coefficient R_2 in the secondary zone. The thermal diffusivity of the workpiece has been introduced in order to evaluate the two partitioning coefficients:

$$\chi = \frac{k}{\rho\, c} \qquad \text{Eq.4.32}$$

where k is the thermal conductivity, ρ is the density and c the specific heat.

$$R_1 = \frac{1}{1+1.328\sqrt{\frac{\chi\,\gamma}{V\,t}}} \qquad \text{Eq.4.33}$$

and the estimated shear temperature is

$$T_S = \frac{R_1 u_{primary}}{c_w \rho_w} \qquad \text{Eq.4.34}$$

where c_w is the heat capacity of the workpiece and ρ_w is the density. From an analytical point of view, the friction between chip and tool can be regarded as a heat source that is moving in relation to the tool. The heat-partitioning coefficient R_2 represents the heat fraction generated by friction at the tool-chip interface and evacuated by the chip. The coefficient is estimated by the analysis of Jaeger [38]. Jaeger derives the heat partitioning coefficient assuming a rectangular heat source of uniform strength acting as a friction slider and moving at a certain speed over a stationary semi-infinite body insulated everywhere except across the interface. According to Jaeger and Shaw the shape of the contact is not important for the calculation of mean temperature along the interface. Shaw introduced a shape coefficient

$$A = \frac{2}{\pi}\left[\sinh^{-1}\frac{b}{L_c} + \frac{b}{L_c}\sinh^{-1}\frac{L_c}{b} - \frac{1}{3}\left(\frac{b}{L_c}\right)^2 + \frac{1}{3}\frac{L_c}{b} - \frac{1}{3}\left(\frac{L_c}{b}+\frac{b}{L_c}\right)\sqrt{1+\left(\frac{b}{L_c}\right)^2}\right]$$

Eq.4.35

Using the friction slider model [38], the heat partitioning coefficient in the secondary zone is

$$R_2 = \frac{C - T_S}{C + B}$$

$$C = \frac{V\ A\ t}{k_t} u_{secondary} \qquad \text{Eq.4.36}$$

$$B = 0.754 \frac{u_{secondary}}{c_w \rho_w} \sqrt{\frac{t^2 V}{L_c \chi\ r}}$$

where k_t is the thermal conductivity of the insert and *r* is the cutting ratio. The estimate temperature of the interface is expressed by

$$T_t = T_s + (1 - R_2) u_{secondary} \qquad \text{Eq.4.37}$$

The Figures 4.13a,b,c,d illustrates the results of the analytical model in terms of average temperature of the shear zone (*Ts*) and average temperature of the interface zone (*Tt*). The histograms show the temperatures for two nozzle positions (overhead and interface) and two air jet pressures (4 and 7 bar). It can be observed that the temperature mainly depends on the feed rate. The results also reflect the contribution of the mechanical and thermal effect of the air jet to the energy balance. From a thermal point of view, the contribution of the air jet is a negative energy, according to the sign convention (positive when entering in the workpiece). The mechanical energy is negative when the air jet is applied from the overhead position, but it is positive when directed into the interface.

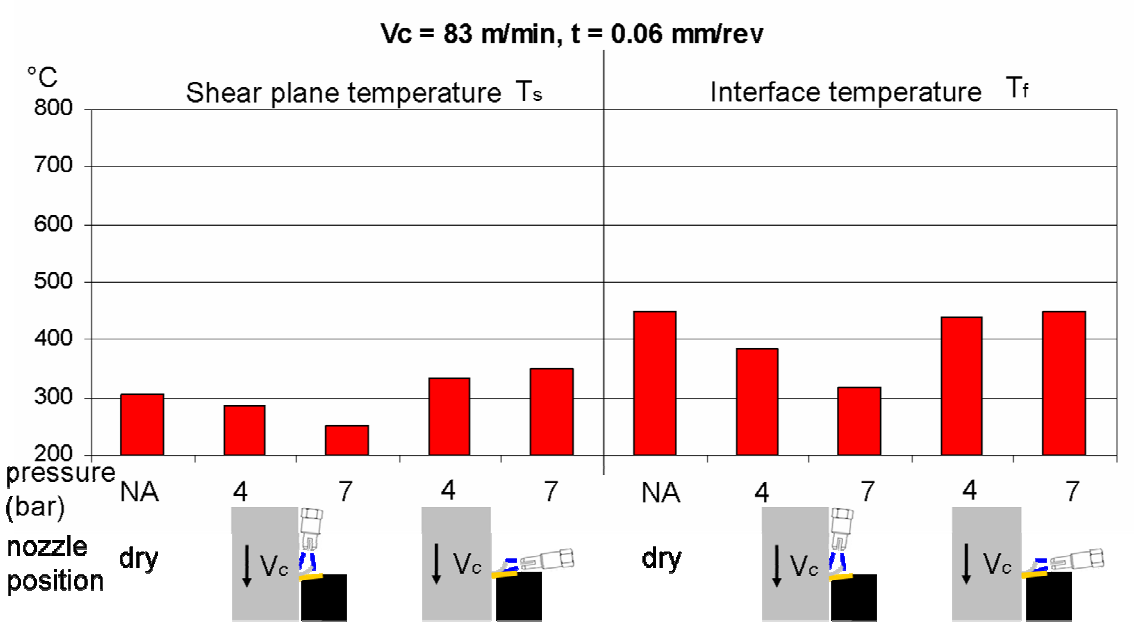

Figure 4.13a – The results of the analytical model in terms of average temperature of the shear zone (T_s) and the friction zone (T_t) for Vc = 83 m/min and t = 0.06 mm/rev

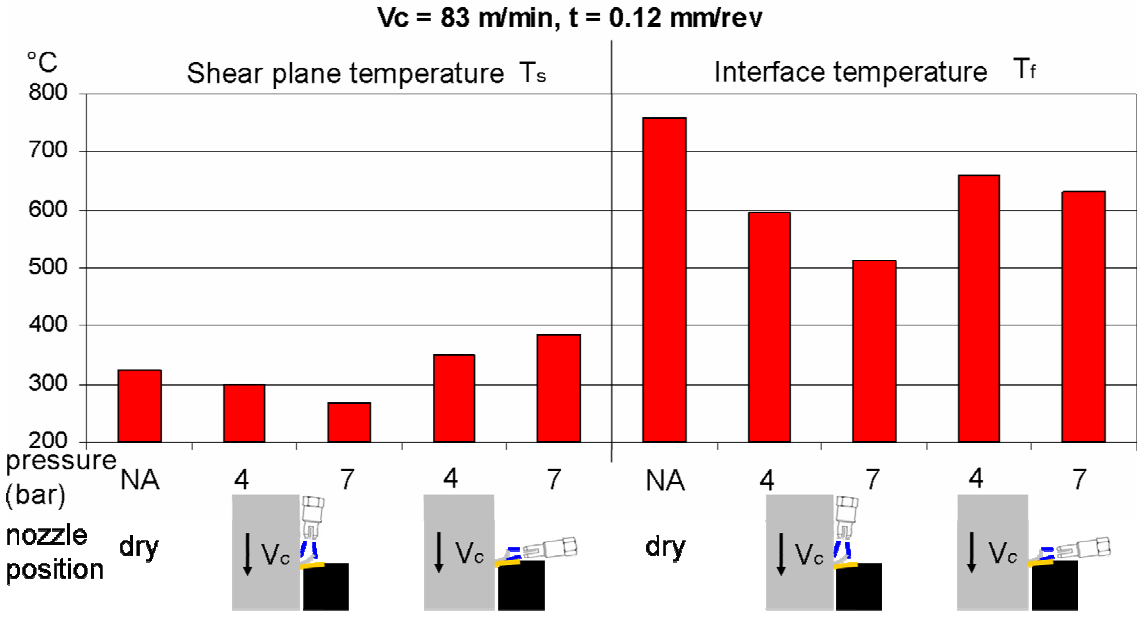

Figure 4.13b – The results of the analytical model in terms of average temperature of the shear zone (T_s) and the friction zone (T_t) for Vc = 83 m/min and t = 0.12 mm/rev

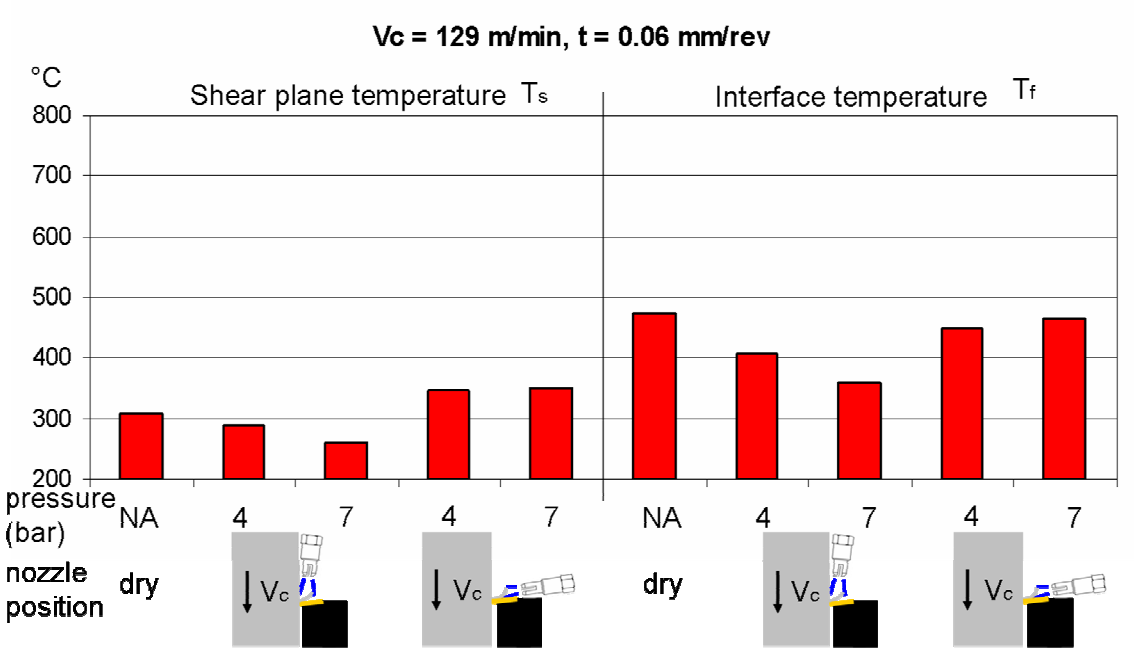

Figure 4.13c – The results of the analytical model in terms of average temperature of the shear zone (T_s) and the friction zone (T_t) for Vc = 129 m/min and t = 0.06 mm/rev

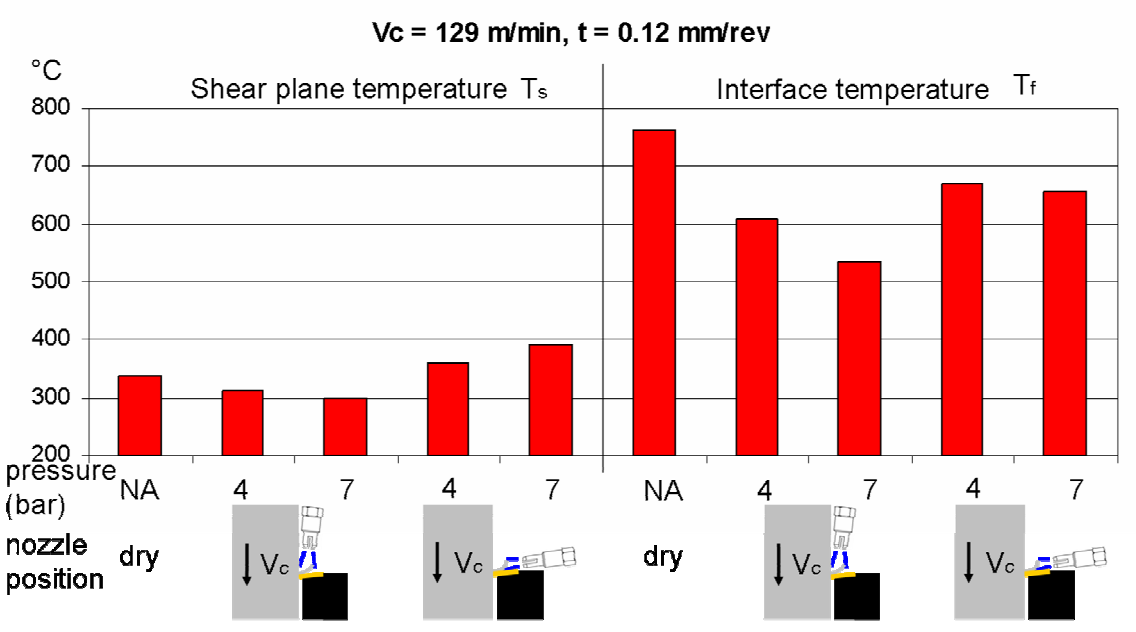

Figure 4.13d – The results of the analytical model in terms of average temperature of the shear zone (T_s) and the friction zone (T_t) for Vc = 129 m/min and t = 0.12 mm/rev

By analysing the Figures 4.13 in details, it can be observed that the jet in overhead position reduce the temperature of the shear zone, and the jet in interface position raise it. This is directly related with the energy balance in the shear zone and the sign of the mechanical contribution due to the air jet. The best achievements in terms of average interfacial temperature reduction are in the case of the air jet in overhead position.

4.8 Discussion and conclusions

An analytical model of orthogonal cutting has been developed in order to investigate the effect of a high speed air jet directed onto the top face of the chip (overhead position) and into the interface between the chip and the rake face of the insert (interface position). Shaw [67] believed it impossible to predict accurately cutting performance in this way; however he also appreciated the purpose of analytical models of metal cutting for understanding of the process. Since the mid 1950s different approaches based on the metal cutting theory of Merchant [29, 154], Oxley et al. [31], Lee et al. [12] have been used for predicting orthogonal cutting performance, including cutting forces, shear plane angle, strain and strain rate. Notable refinements have been developed by Adibi-Sedeh et al.[155], Smithey et al. [156], Trigger et al. [157], Usui et al. [158]. However, further refinements have generally been accompanied by increased complexity. The assumptions on which the orthogonal cutting model is based include:

1) the tool is rigid, perfectly sharp and there is no contact along the clearance face
2) the shear surface is a plane extending upward from the cutting edge
3) the cutting edge is a straight line extending perpendicular to the direction of cut
4) the chip flow in a plane with no lateral curl. Only the up curl is permitted
5) the depth of cut is constant
6) the workpiece moves relative to the tool with uniform velocity
7) a continuous chip is produced with no built-up edge (BUE)
8) the shear and normal stresses along shear plane and tool are uniform

These hypotheses are used in a simple approach to orthogonal cutting; however the assumptions are consistent with the case analyzed by finite element modeling and experimentally tested. The hypothesis of a simplified chip shape (no BUE, no segmentation, and no secondary shear plane) allows the analysis of the chip curl radius used in the estimation of the mechanical energy introduced by the air jet. One way of consider the influence of secondary shear is in terms of a decrease in rake angle by an amount corresponding to an equivalent rake face when cutting with sticking friction. This action on the rake angle tends to increase the shear plane angle, but since the decrease of the rake angle is usually very small in low carbon steels, the hypothesis of a continuous chip with no secondary shear plane represents a good approximation.

It is also possible to account the effect of the BUE by introducing the angle θ into Equations 4.9 and 4.17; however the presence of the BUE causes an alteration in the cutting force. Since the cutting force is in good agreement with the experimental data shown in Chapter 6, the modeling of BUE is not required. Slip line field (SLF) theory has been used for calculating the shear plane angle, as illustrated by Lee and Shaffer [12]. However, as remarked by Shaw [67], a simplistic SLF can never be accurate, and a correction angle θ is required. The FE simulations are used for estimating the correct shear plane angle, and obtain the angle θ to correct the solution of Lee and Shaffer, that is mainly used for kinematic considerations. According to the SLF theory, the material beneath a punch flows plastically in plain strain over a region consistent with the material displaced by the punch. At all other points, the specimen is considered rigid. The SLF is a network of curves along which the shear stress or shear strain rate is maximized. A suitable flow pattern need only be consistent from the point of view of velocities; therefore the SLF problem is a kinematic problem. However, Shaw attributes to the strain hardening the main source of error in the case of simple SLF theory. Here, strain hardening has been allowed for through a reliable flow stress model to be introduced in tabular form in the material library of DEFORM. Oxley et al. [31] developed this flow stress model for AISI 1016, based on experimental data. The model has been extended to generic low carbon steels. By using SLF theory of Lee and Shaffer, with the introduction of the correction angle, obtained by FE modeling that use a material model derived by

experimental data (Oxley [31]), it is possible to use a non iterative model for predicting the cutting forces and evaluate the shear energy and the friction energy.

The hypothesis that the air jet can interact in the cutting process from a mechanical and a thermal point of view was assumed. A model for chip curl radius, based on the geometrical considerations of the SLF theory, has been developed. The model shows good agreement with finite element modeling and experimental results and allows the introduction of the bending moment due to air jet. The comparative results of the three methods of investigations are shown and commented in Chapter 6 (Paragraph 6.4). The curl radius was estimated by kinematic considerations, after the estimation of the chip-tool contact length [142, 144].

The hypothesis that the chip configuration in terms of curl radius minimizes the energy dissipated by heat is supported by the work of Baker [26]. This concept has also been used in other projects based on the introduction of an external source of energy [25, 9]. The use of high pressure jets for bending the chip is not new, however current research are focused on chip flushing and rarely relate the bending effect to temperature reduction [27]. The use of the air jet for bending the chip and altering the state of stress in the cutting area represents an environmentally friendly and clean solution, compared to the use of laser and plasma guns. However, the mechanical energy provided by the air jet can have a negative effect, resulting in an undesired temperature rise, if the air jet is not properly positioned. The analysis shows that the energy is minimized when the air jet is directed from an overhead position. The effect is similar to that obtained by local pre-heating with laser and plasma guns of the intersection between the uncut surface and the top face of the chip, at the shear zone.

The equations for evaluating the strain energy are derived from the work of Mackenzie [34] for the 2D case. The thermal effect of the air jet was evaluated by estimating the Nusselt number and by calculating the heat transfer coefficient when the nozzle is placed in the overhead and interface positions. A heat transfer coefficient of 2000 W/m^2K is representative for calculating the thermal effect, and is consistent with the results obtained by Kops et al. [95]. However, the sensitivity of the cutting process to the heat transfer coefficient is limited, and only changes of an order of magnitude in the heat

transfer coefficient are significant from a global point of view. Umbrello and co-workers [20] evaluated the global heat transfer between the insert and the workpiece, and stated that the heat dissipation to the ambient requires a particularly high heat transfer coefficient, to be efficient.

The estimation of the energies involved in orthogonal cutting assisted by the air jet is followed by the Loewen and Shaw [36] analysis for the calculation of the heat partitioning coefficient R_1 for the primary zone and by the Jaeger analysis for the calculation of the heat partitioning coefficient R_2 for the secondary zone. The Shaw-Jaeger model has been chosen because the calculation of the cutting temperature has been done using an energy balance that made easier the inclusion of the deformation energy and thermal energy dissipation by the air jet. The use of the model of Oxley has been considered, but the problems of including the chip deformation energy and the heat dissipation were intractable, which made the Shaw-Jaeger model a more suitable choice. The results summarized in Figures 4.13a,b,c,d represent the average temperature of the shear zone (T_s) and the average temperature in the interface between the chip and the tool (T_t). The temperatures are lower than predicted by finite element analysis and lower than the results of experimental tests. However, the trends given by the predictions are consistent with the trends of the cutting tests. As the primary purpose of the analytical model is the understanding of the effect of the air jet in orthogonal cutting, the agreement between the analytical and finite elements prediction and experimental tests proves the concept of a consistent mechanical effect due to the air jet, and also proves that the mechanical effect operates in the modalities indicated by the analysis presented in this chapter.

5. Experimental investigation

5.1 Experimental procedure overview

The influence of air jet in orthogonal machining was experimentally investigated, with particular emphasis on the thermal effects in the chip-tool interface. The typical variable in the orthogonal machining process are cutting speed, feed rate, width of cut, rake angle, insert geometry, workpiece and insert material properties. In the experimental part of this work an AISI 1020 workpiece was machined with a commercial cutting tool. In order to approximate the orthogonal cutting with a turning machine, a thin walled tube was used. The mean diameter of the tube was 71 mm. and the thickness was 1 mm. The insert geometry and rake angle was selected as the best choice for the range of cutting speed and feed rake used for machining the AISI 1020 at the selected width of cut, according to the Sandvik Coromant technical guide [124] This choice reduces the variables to cutting speed, feed rate and width of cut. Experiments were carried out on an URSUS 225 centre lathe, cutting forces were detected by a three components Kistler dynamometer, chip-tool interface temperature was detected by a K-type thermocouple embedded in the insert and a supersonic air jet nozzle was positioned in the proximity of the cutting area. Optimal cutting speed and feed were chosen based on the technical guide and also in order to minimise vibrations in the lathe. Therefore the cutting speed (83 and 129 m/min) and feed rates (0.06 and 0.12 mm/rev) were chosen. The use of a supersonic air jet as a cooling method introduces new variables in the experimental tests, such as the air jet pressure, the relative distance from the exit section of the nozzle to the edge of the insert and the relative angle from the nozzle axis to the plane of the rake face. The tests carried out for this work aim to investigate the effect of the air jet in the orthogonal machining process, therefore a sensitivity analysis on air pressure and nozzle positioning was carried out. The choice of embedding a K-type thermocouple in the insert as a temperature measurement technique introduces an uncertainty that were investigated using multiple holes for embedding the sensor. Figure 5.1 show the overview of the experimental setup, with the dynamometer mounted on the lathe, the dedicated computer used for data

acquisition, the air supply for the supersonic air jet, an air pressure regulator and a mass flow meter.

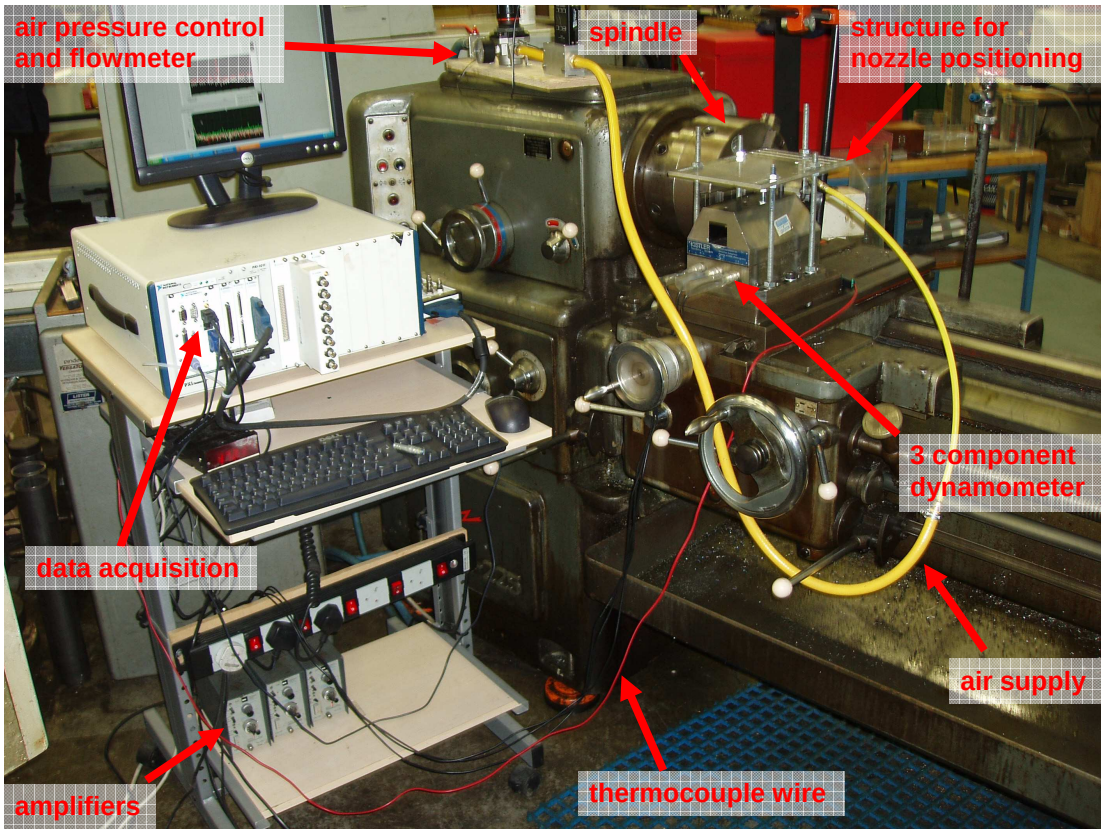

Figure 5.1 – Experimental setup overview: centre lathe and spindle, air pressure control and flow meter, dedicated data acquisition computer, amplifiers, three component dynamometer and the wire connected to the thermocouple

A supersonic nozzle was used to direct the jet onto the cutting area. The nozzle was mounted on a structural element with high stiffness and 5 degrees of freedom (3 by translation and 2 by rotation), without interfering with force and temperature measurement, providing essential support and flexibility in cutting test with the nozzle directing the jet in the chip-tool interface (interface position) or on the top face of the chip (overhead position). The 3D sketch in Figure 5.2 shows an overview of the insert and tool holder, mounted on the dynamometer, and the nozzle supported by the threaded the plate, with slots for precise positioning. The supports for the nozzle (the plate, the

threaded bar supporting the nozzle and the threaded ring) are securely fastened by tightly gripped bolts.

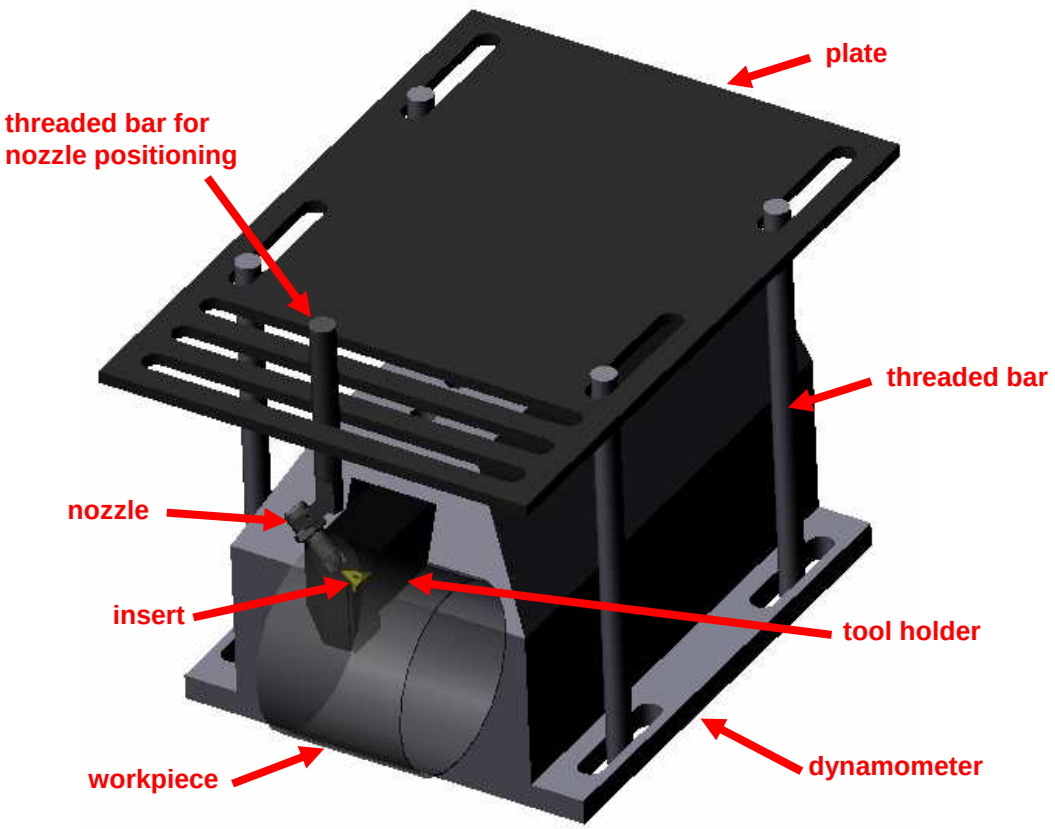

Figure 5.2 – 3D sketch showing the workpiece (transparent), the insert and the tool holder, the nozzle and the structure (plate and threaded bars) supporting the nozzle, top mounted on the dynamometer

The Figure 5.3 shows a 3D sketch of the cutting area. The tool holder and the insert with chipbreaker are recognisable in the figure. The plate with slots for nozzle's displacements in feed direction (x), the threaded bar bolted to the nozzle's connector for displacement in z direction and the nozzle's connector for rotation on y axis is recognisable as well. In the xy plane the nozzle was aligned with the y axis, perpendicular to the cutting edge, passing through the middle point of the cutting edge. Nozzle positioning was checked before and after each test with a distant camera. Quantitative information on nozzle positioning was extracted by analysing the images with the software ImageJ.

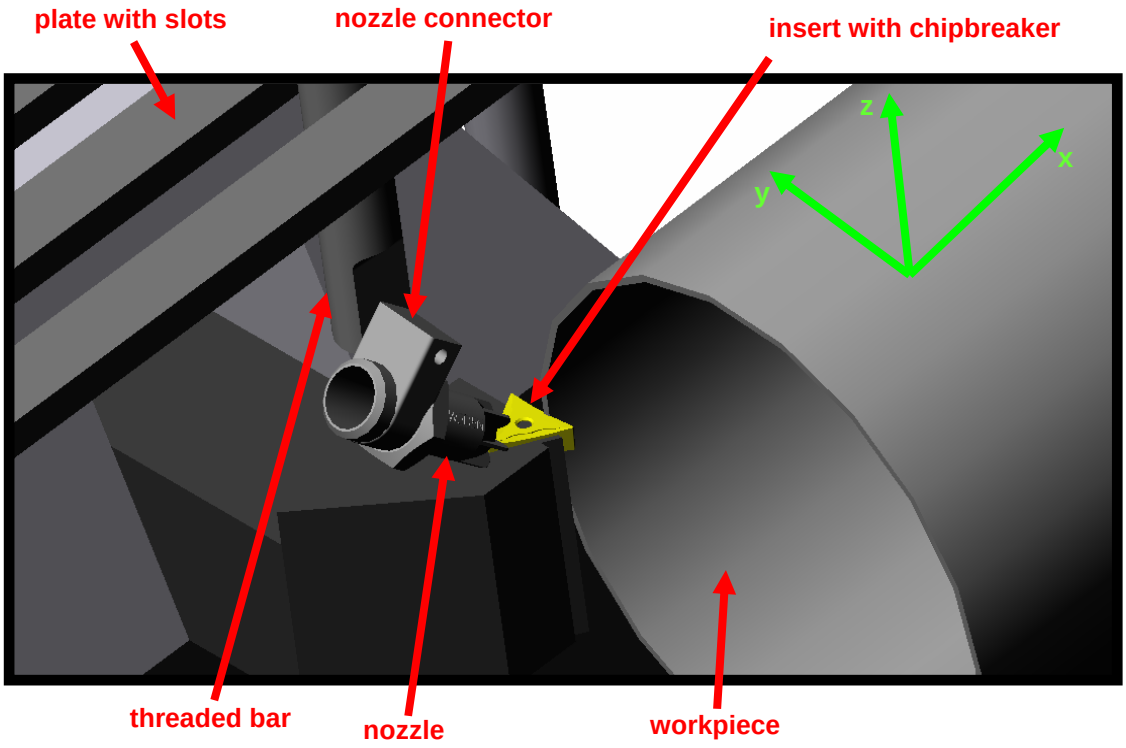

Figure 5.3 - 3D sketch of the cutting area: the insert with chipbreaker, nozzle and nozzle holder, workpiece and reference system aligned with cutting direction and feed

During the cutting tests the nozzle was positioned at a distance of 12 mm (6 times the throat section diameter) from the rake face. At this distance the air flow is fully developed. The Appendix B.3 gives full details about the pneumatic system (pressure regulator, mass flow-meter, supersonic nozzle) and the blowing force provided by the air jet and its variation with the distance of the nozzle from the rake face. It is possible to assume that between 11 and 13 mm of distance from the rake face the blowing force is approximately constant. The nozzle was placed in four different positions in order to investigate the effect of air jet direction in the orthogonal cutting process. The Figure 5.4 shows a sketch of the nozzle in interface position and overhead position. According to nozzle manufacturer, the air cone pattern has an angle of 21°. In order to estimate the sensitivity to small displacement of the nozzle, the angular position of the nozzle was

slightly changed, so that four nozzle positions were tested. They were labelled: *Interface A*, *Interface B*, *Overhead A*, *Overhead B*.

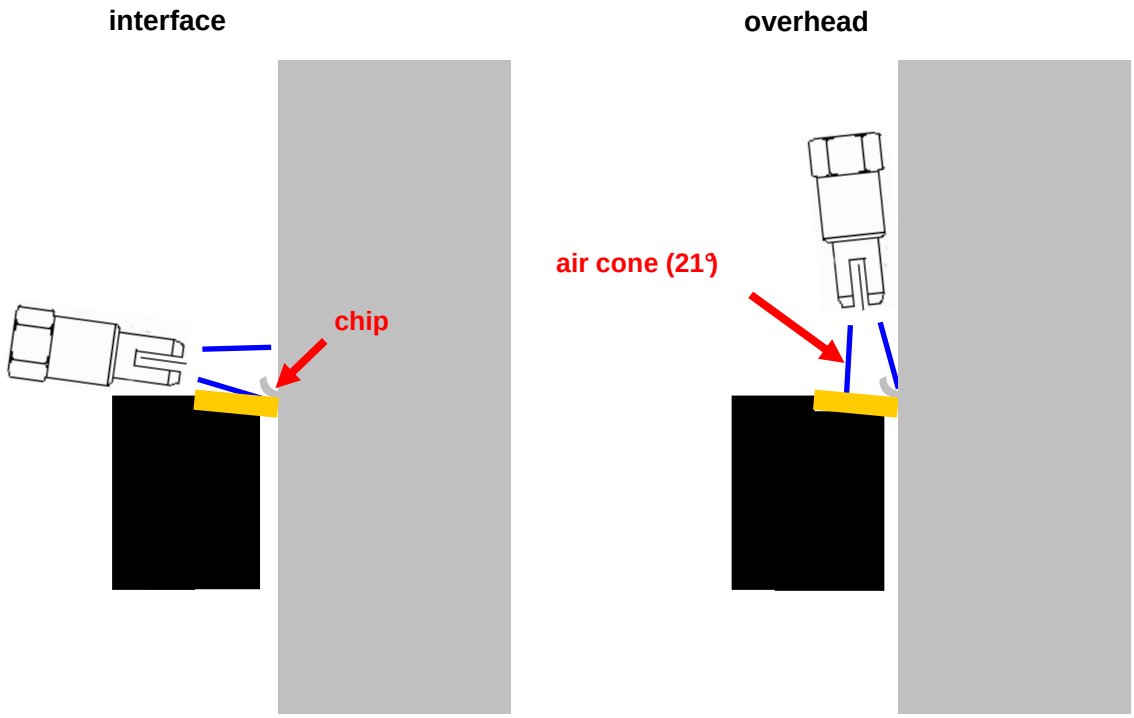

Figure 5.4 – Sketch of nozzle positioning: interface and overhead positioning. During the test it was ensured the expected position of the chip had been in the air cone pattern

A distant camera was used at the maximum resolution for obtaining precisely the position of the nozzle. The images was analysed with the software ImageJ and an algorithm for edge recognition in grey scale images was used in order to minimize source of error in measurement. Figure 5.5 shows a grey scale image and the correspondent binarised image. On a binarised image it is possible to apply a local gradient algorithm for extracting the orientation of a line, even if the point on the image for applying the local gradient algorithm is selected by the user. The information that can be extracted from a binarised image is the axis of the nozzle, referred to the z axis, the distance from the rake face and the distance from the cutting edge. In the binarised image in Figure 5.5 also shows the distance of the exit section of the nozzle from the rake face, the distance from the cutting edge and the angle between the feed direction (horizontally aligned) and the axis of the nozzle. With this data it is possible to obtain the exact position of the nozzle.

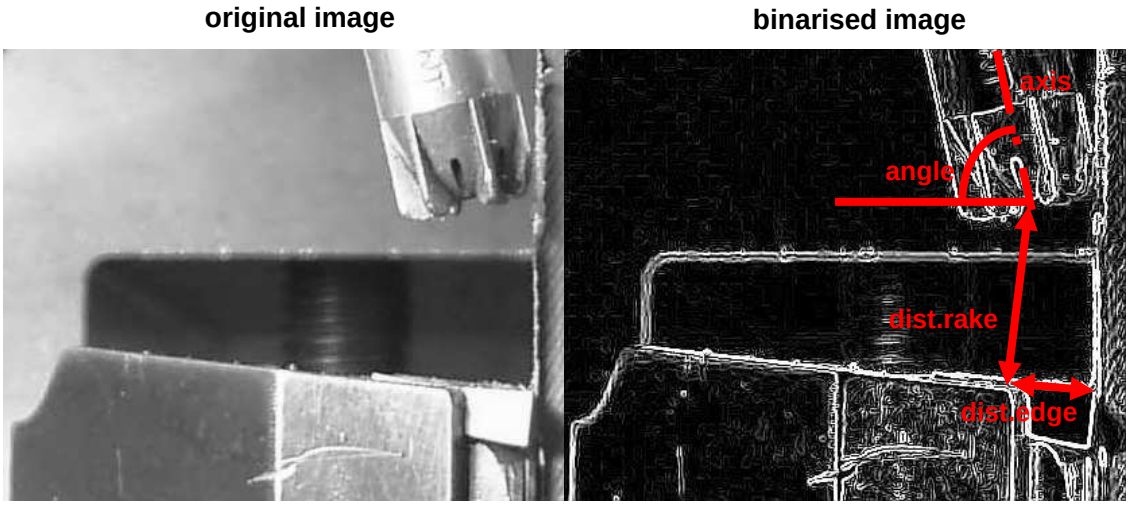

Figure 5.5 – The grey scale and binarised high resolution image of the nozzle in overhead A position, with focus on the nozzle. On the binarised image a sketch of the information extracted from the local gradient algorithm embedded in the latest release of ImageJ: the axis of the nozzle and its distance from rake face and cutting edge.

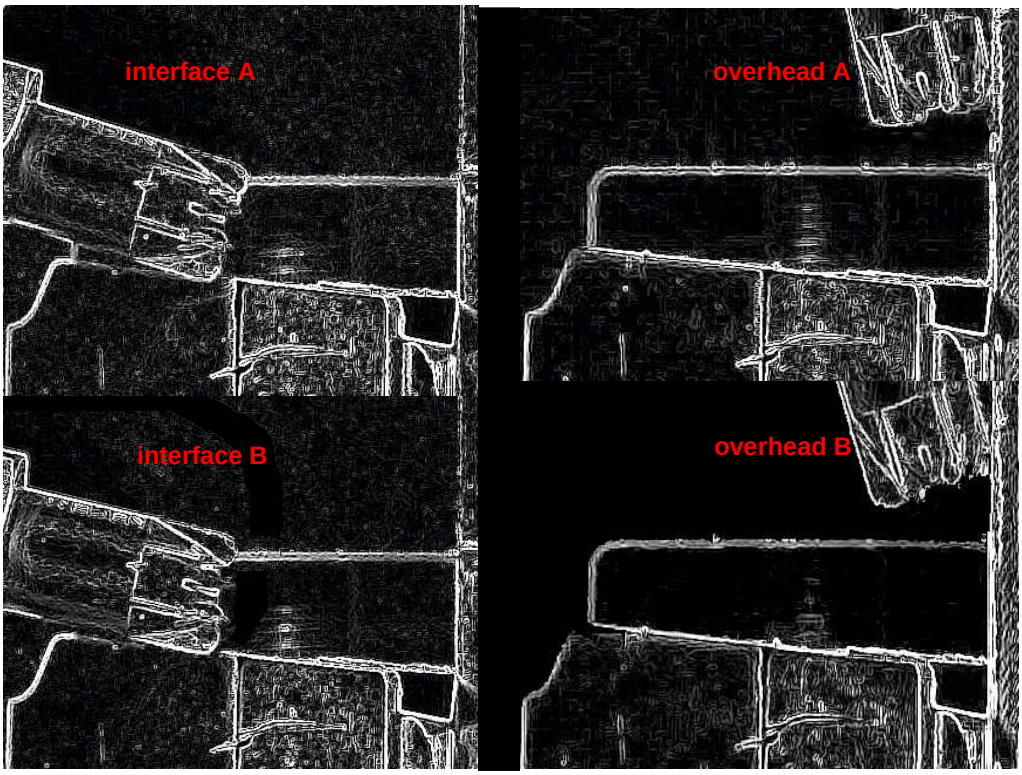

Figure 5.6 – The four positions of the nozzle in the filtered images from the distant camera

The Table 5.1 shows the results of the analysis of images. The two positions *A* and *B* had been used for a sensitivity analysis on angular position of the nozzle. The differences in the distances of position *A* and *B* are negligible.

position	dist.rake (mm)	dist.edge (mm)	angle
interface A	2.92	11.43	17°
interface B	3.06	11.46	13°
overhead A	10.15	4.42	78°
overhead B	9.96	4.13	73°

Table 5.1 – Measurement of nozzle positioning extracted by image analysis.

5.2 Temperature measurement: the embedded thermocouple

According to Davies, Ueda et al. [60] and Bacci Da Silva [94] different methods for measuring temperature in the chip-tool interface in general machining are currently available, but there is no general guideline for a measurement system setup, because of the many different situations occurring in machining. The most used families of methods include conductive methods (using thermocouples) or radiating methods (by IR imaging, radiometers or pyrometers). An indirect conductive method was chosen for measuring the chip tool-interface temperature: a K-type thermocouple was placed in a hole drilled in the insert, as shown in the following figure. Thermocouples are relatively cheap, reasonably stable and reproducible, subject to relatively low uncertainty when used as designed and fast responders, depending on size [60]. However, the advantages are tempered by the relative complexity of the thermocouple system and the possible associated sources of uncertainty, such as the case of embedded thermocouple. The method of embedded thermocouple was extensively used and studied by Attia and Kops [109, 110, 111, 112]. According to Attia and Kops, the main limitations of this technique are the weakening of the insert due to the insertion of the thermocouple, the reduced gain of the sensor and the

delay introduced by the distance between the thermocouple and the rake face. This technique was also used by Grzesik for investigating maximum cutting temperature of medium carbon steels with multilayer coated inserts [113]. The limitations of a direct measurement can be avoided if a relation between the maximum insert temperature and the temperature read by the thermocouple is found. Ren et al. [42] used finite elements to correlate the mean temperature of the bottom of the hole for the thermocouple and the maximum temperature in the rake face. By calibrating the system constituted by the thermocouple and the insert it is possible to find a relation between the signal by the thermocouple and the maximum temperature of the rake face. Full details on the calibration process can be found in the Appendix B.2.

A K-type uncoated thermocouple with the diameter of 0.5 mm was embedded in two different hole of the insert used for orthogonal cutting tests. Details on the thermocouple embedding and position of the holes can be found in the Appendix B.2. Since the thermocouple was uncoated, the electrical insulation on the toolholder and the clamping system of the lathe was achieved by thin insulating tape. The toolholder and the workpiece were tightly fastened in order to minimize the impact of the tape on force measurements and the electrical insulation was checked before and after each test. The lathe was cleaned before testing, in order to avoid any accidental contact, because if any accidental electrical contact is detected by the thermocouple cold-junction compensator, an out of scale signal is sent to the data acquisition board. The thermocouple wire has also been protected by a flexible and transparent tube. The Figure 5.7 shows an overview of the cutting zone, with the thermocouple connector attached to the carriage with the insulating tape, the flexible tube for protecting the thermocouple and part of the insulating tape on the chucks. An additional protection for the thermocouple was provided by a thin layer of aluminium, glued on the toolholder (Figure 5.8)

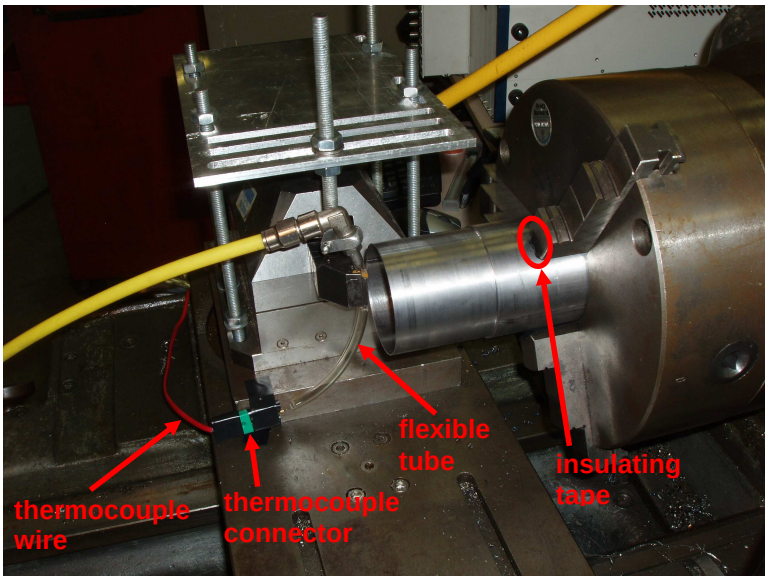

Figure 5.7 – The cutting area with the thermocouple embedded in the insert. The thermocouple was protected by the transparent and flexible tube and insulated from the lathe

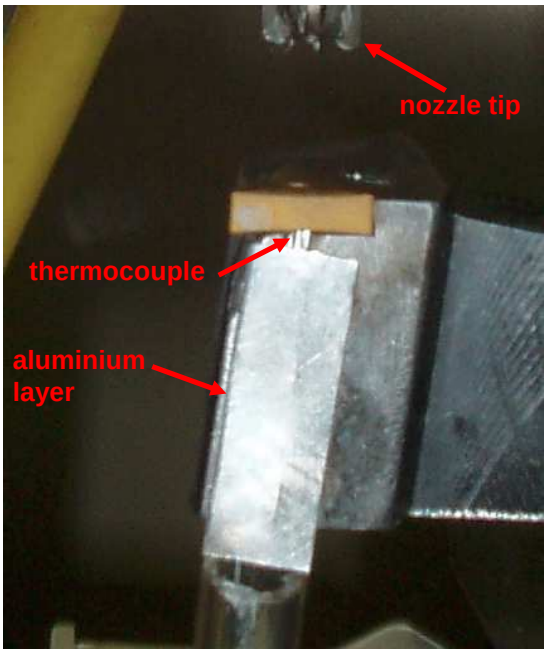

Figure 5.8 – An aluminium layer was glued on the tool holder in order to protect the thermocouple wire from accidental contact with the workpiece during machining

5.3 Data acquisition and test procedure

The three signals, two from the dynamometer, one from the thermocouple, were acquired by a USB National Instruments data acquisition board. A *VI* (virtual instrument) was designed with Labview for acquiring the three signals at a frequency of 2 kHz. A buffer for real-time storage of data was used. The data collected by the circular buffer were saved in a format exportable to Matlab and Excel was used. The use of a buffer is necessary for avoiding the delay due to the writing to disk process, however the buffer has a limited capacity, and therefore a circular buffer with a window of 3 seconds for each test was used. Unsaved data are visualised on the screen in real time. Once the temperature is steady state, the user triggers the circular buffer for data saving and at the end of the test 6001 acquisitions per channel were saved on the disk. The test procedure for each nozzle position is explained as following:

1) thermocouple positioning
2) insulation checking
3) workpiece-thermocouple alignment checking
4) cutting speed setting
5) feed rate setting
6) amplifiers resetting
7) air pressure setting and air jet on (if needed)
8) *VI* and lathe starting
9) buffer triggering at steady state
10) *VI*, lathe and air jet stopping

Two cutting speed (83 and 129 m/min), two feed rate (0.06 and 0.12 mm/rev), two air jet pressure (4 and 7 bar), two holes for the thermocouple and four nozzle position were tested. 80 different cutting tests was carried out, by considering any combination of cutting parameter, pressure, nozzle position, thermocouple position, dry cutting and a sensitivity analysis on pressure (carried out with a cutting speed of 129 m/min and

without changing the position of the thermocouple). Each test was labelled according to cutting parameters, pressure condition, nozzle position and thermocouple hole used for testing. The data in Table 4.3 are taken from Table 4.1 and 4.2. The Figure 5.9 shows the three signals of a cutting test, acquired for three seconds, carried out with $V_C = 129$ *m/min*, $t = 0.12$ *mm/rev*, nozzle in *interface A* position with 4 bar of pressure and thermocouple in the first cutting edge.

	thermocouple position				Nozzle position			
label	**depth**	**dist. rake face**	**dist. flank face**	**Diam**	**label**	**dist. rake face**	**dist. edge**	**angle**
1	2.288	0.268	0.647	0.58	*Interface A*	2.92	11.43	17°
2	2.313	0.243	0.671	0.58	*Interface B*	3.06	11.46	13°
					overhead A	10.15	4.42	78°
					overhead B	9.96	4.13	73°

Table 5.3 – Label used for indicating quantitative data about thermocouple position and nozzle position. All the distances are expressed in mm

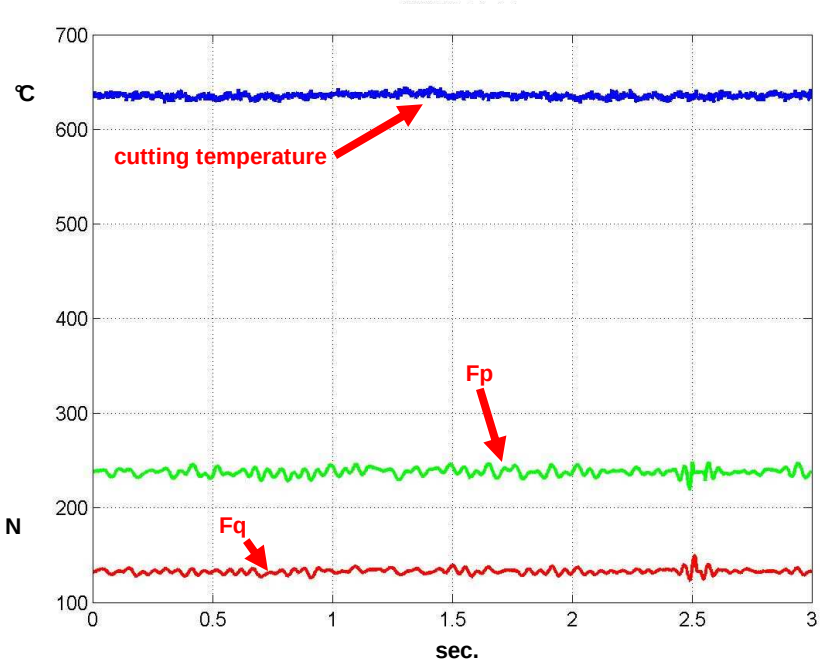

Figure 5.9 – The output on a single graph of the three signals, multiplied for calibrating constants

A closer look to the three signals shows the dynamics in the thermocouple signal is not coupled to the dynamics in the dynamometer signal. As expected, the tungsten carbide layer between the rake face and the tip of the thermocouple provides damping and delay in the signal, substantially decoupling the cutting force from temperature rise on the rake face. The Figure 5.10 shows the cutting temperature on the rake face for one cutting test. Similar signals were acquired for all the other cutting tests. The standard deviation of the temperature signal represented in the Figure 5.10 is 9.8°C, and this value is consistent with the standard deviation of entire set of cutting test with the thermocouple placed in the first hole. The mean standard deviation of the temperature signal when the thermocouple is placed in the second hole is 10.1°C. However, the error in the signal is small (9.8°C), if compared to the module (628°C), as shown in Figure 5.9.

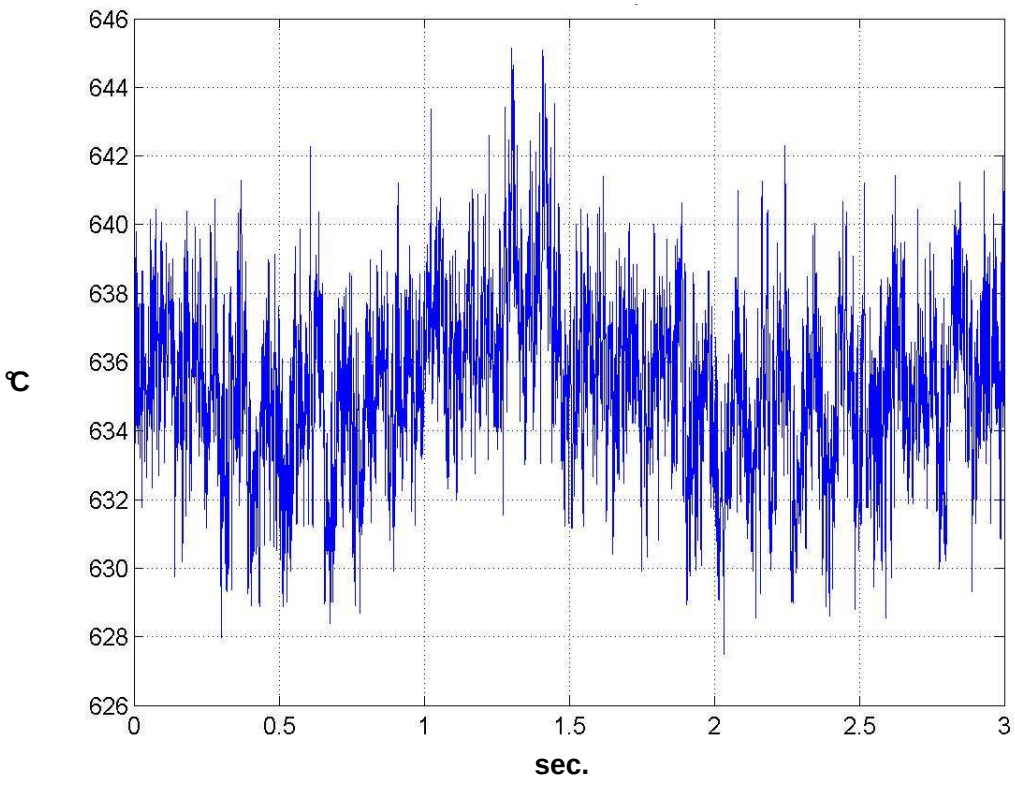

Figure 5.10 – The temperature measurement of test with V_C = *129 m/min*, *t = 0.12 mm/rev*, nozzle in *interface A* position with 4 bar of pressure and thermocouple in the

first cutting edge. The mean temperature is 628°C and the standard deviation for this signal is 9.8 °C

The acquisition frequency of 2 kHz was chosen for representing the dynamics of cutting force and feed force. The peaks in the cutting force are consistent with the cutting speed. The cutting speed of 129 m/min corresponds to 580 rev/min (9.667 Hz). The Figure 5.11 shows the cutting force for the test with V_C = *129 m/min*, *t = 0.12 mm/rev*, nozzle in *interface A* position with 4 bar of pressure and thermocouple in the first cutting edge. In 3 seconds of cutting the mean number of peaks observed in the measure of cutting force is 29 (9.666 Hz). The same result was found for the entire set of tests with V_C = *129 m/min*. The same result occurred for the set of test labeled V_C = *83 m/min* , where the rotation frequency was 6.199 Hz and the mean number of peaks in the cutting force was 19 (6.333 Hz).

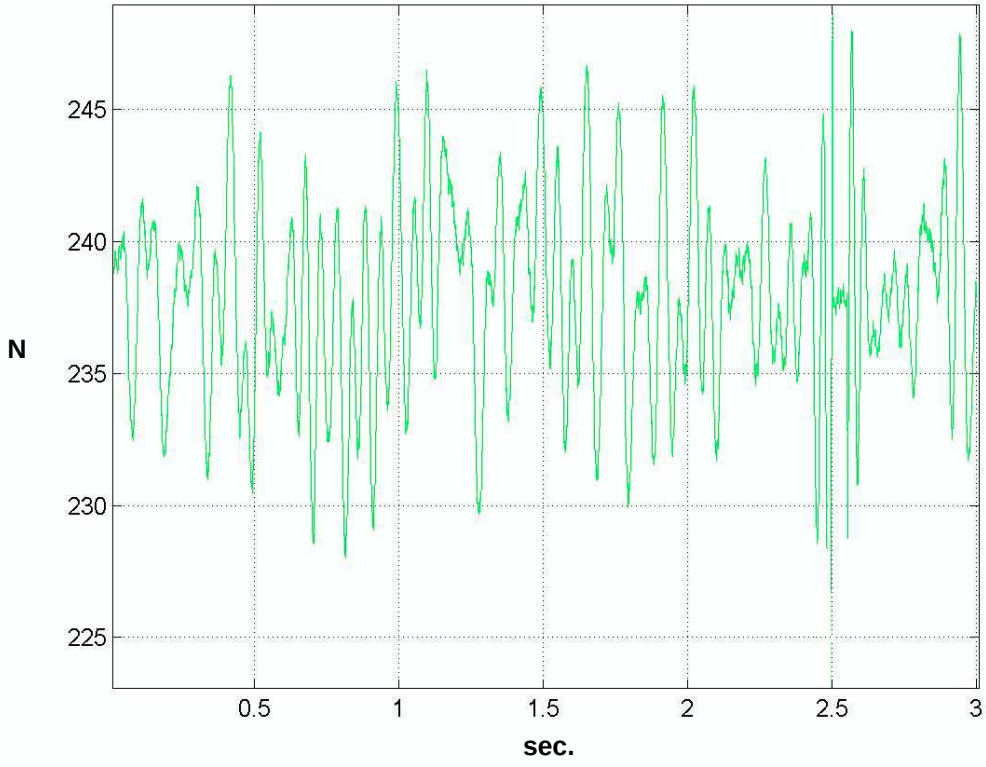

Figure 5.11 – The cutting force (*Fp*) measurement of test *v129f12int4-A1*. The mean value is 237 N and the standard deviation is 9.1 N

5.4 Summary of the experimental setup

The aim of the experimental test was investigating the effect of the air jet in the orthogonal cutting process. A coated WC insert with chipbreaker was selected for cutting a thin walled tube of AISI 1020 steel at the desired cutting speed and feed rate. A supersonic nozzle was used for directing the air jet in 4 different positions (two in the chip-tool interface, two overhead on the top face of the chip). The pressure of the nozzle was controlled by a pressure regulator and the flow rate was measured with a mass flowmeter and the blowing force of the nozzle as a function of distance from the target surface was measured at different pressure by a very sensitive balance. The exact position of the nozzle was measured by using a distant camera. The measurements taken in the cutting tests consist in force and cutting temperature measurement. The forces were measured by a three component dynamometer, and the cutting temperature was measured by using a thermocouple embedded in the insert. A spark eroder was used for drilling holes in the insert and two holes for the thermocouple were selected for the cutting tests, after providing precise geometry of the holes. The calibration of the sensors takes account of the amplifiers and also of the damping and delay due to the embedded thermocouple. The 80 tests and the results represent a solid experimental investigation about the effect of high speed air jet in terms of test repeatability, sensitivity on pressure and nozzle position, and represents a reliable proof of the different behaviour of air based cooling technique when the air jet is positioned in the chip-tool interface rather than on the top face of the chip (overhead).

The Figure 5.12 shows the methodology of the tests. The tests listed in the figure are designed to provide adequate insight into the problem of orthogonal cutting assisted by a high speed air jet, with different cutting speeds, different feed rates, different nozzle positions (including sensitivity analysis of the positions A and B), and different pressures (including sensitivity analysis).

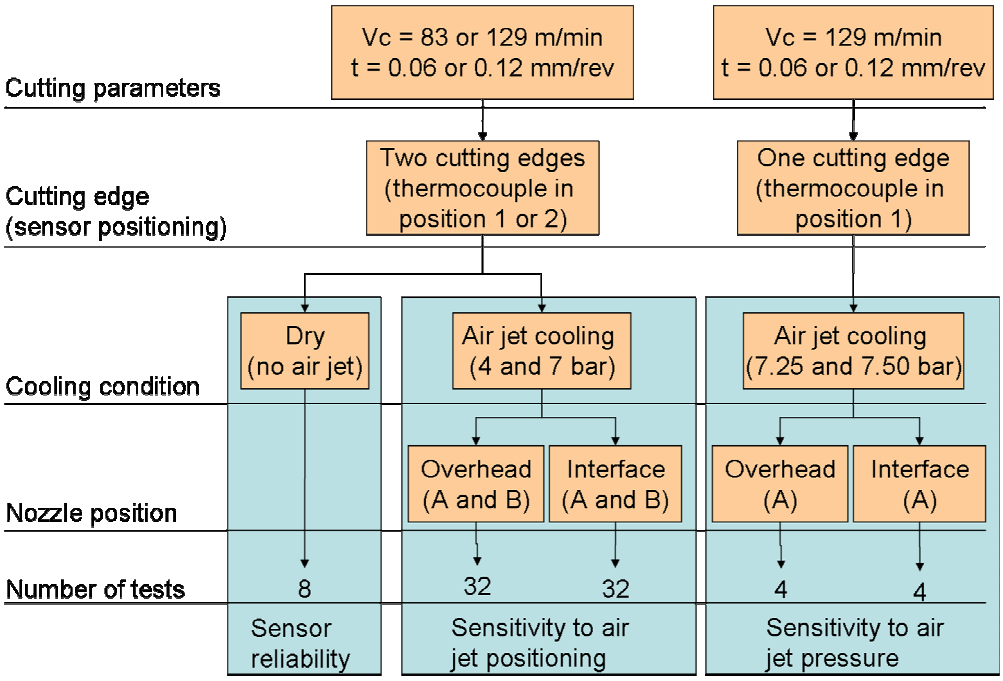

Figure 5.12 – The experimental tests are divided in terms of cooling conditions: dry cutting and the four positions of the nozzle with different air jet pressures.

5.5 Experimental tests results

The experimental tests results are presented in this section in terms of cutting force, force in the feed direction and maximum temperature of the chip-tool interface. Each figure represents the experimental results for one cutting speed and two feed rates. Each test was repeated twice by using two cutting edges equipped with embedded thermocouple, labeled *1* and *2* in the figures. Dry cutting results were compared to air jet cooled orthogonal cutting tests. Two pressure of the air jet were used: 4 and 7 bar, and two positions of the nozzle were used (*Overhead A* and *Interface A*).

For each set of tests, cutting forces vary little. However two trends can be observed in Figures 5.13a and 5.13b. Firstly, the cutting force measured when the second cutting edge is used is always greater than the cutting force measured when the first cutting edge is used. Secondly, when the nozzle is in the overhead position, a small increment of the cutting force is observed. This could be due to the blowing force of the air on the insert. The measurements reported in the Appendix B.3 show that the blowing force of the jet on

the rake face ranges from 1.1 N when the pressure is 4 bar up to 1.9 N when the pressure is 7 bar.

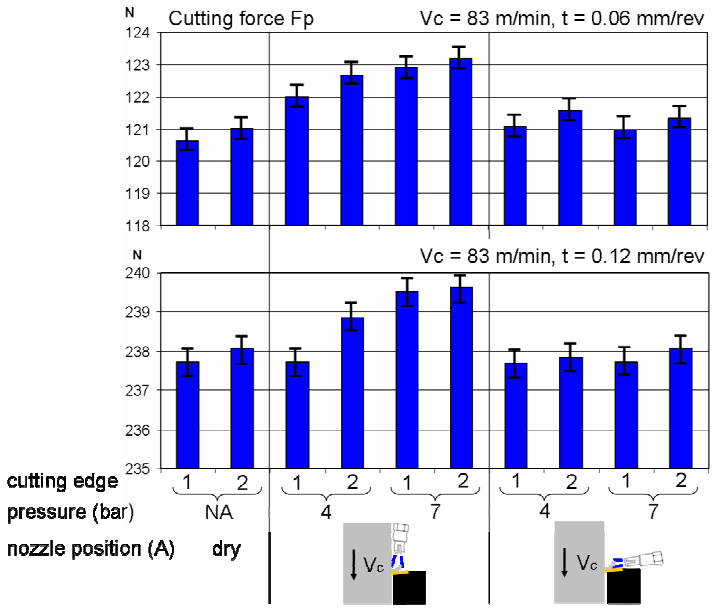

Figure 5.13a – The cutting force measurement for the tests at 83 m/min of cutting speed, a feed rate of 0.06 and 0.12 mm/rev and the nozzle in *overhead A* and *interface A* positions

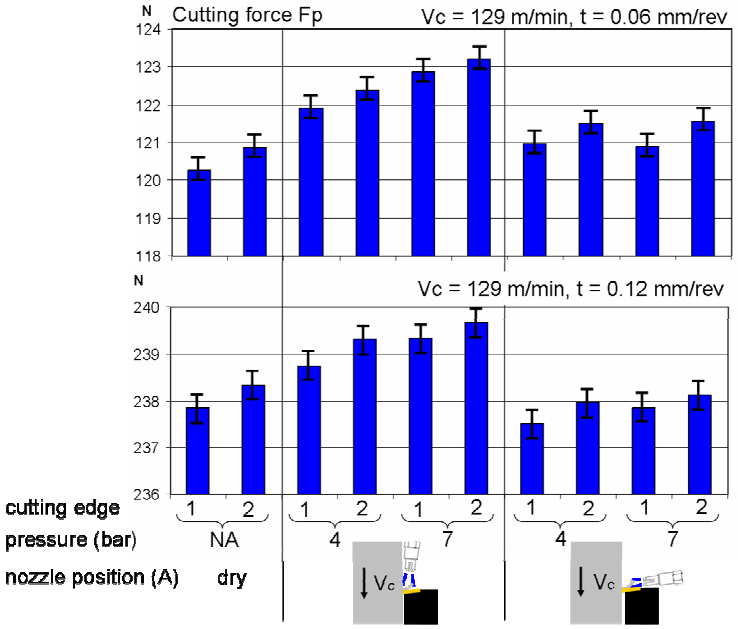

Figure 5.13b – The cutting force measurement for the tests at 129 m/min of cutting speed, a feed rate of 0.06 and 0.12 mm/rev and the nozzle in *overhead A* and *interface A* positions

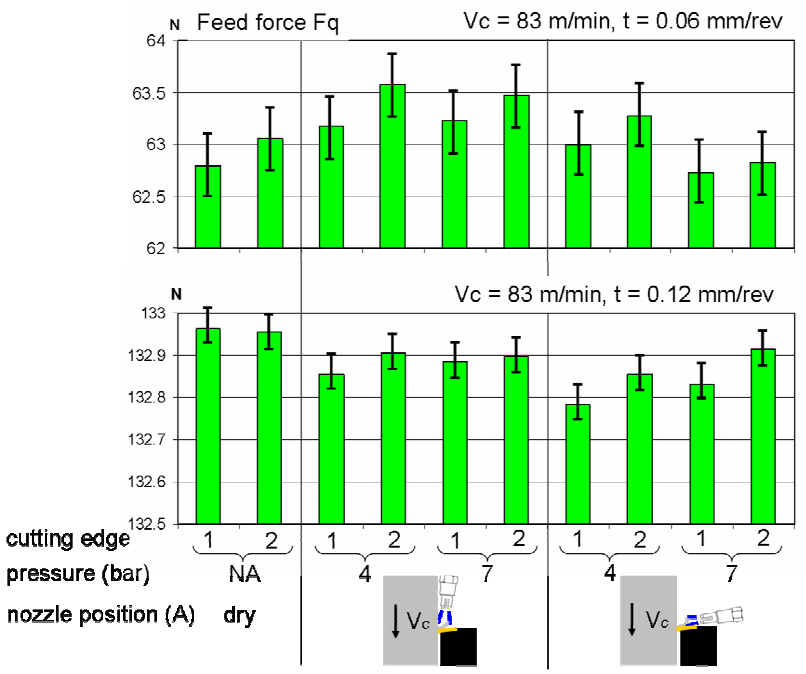

Figure 5.14a – The feed force measurement for the tests at 83 m/min of cutting speed, a feed rate of 0.06 and 0.12 mm/rev and the nozzle in *overhead A* and *interface A* positions

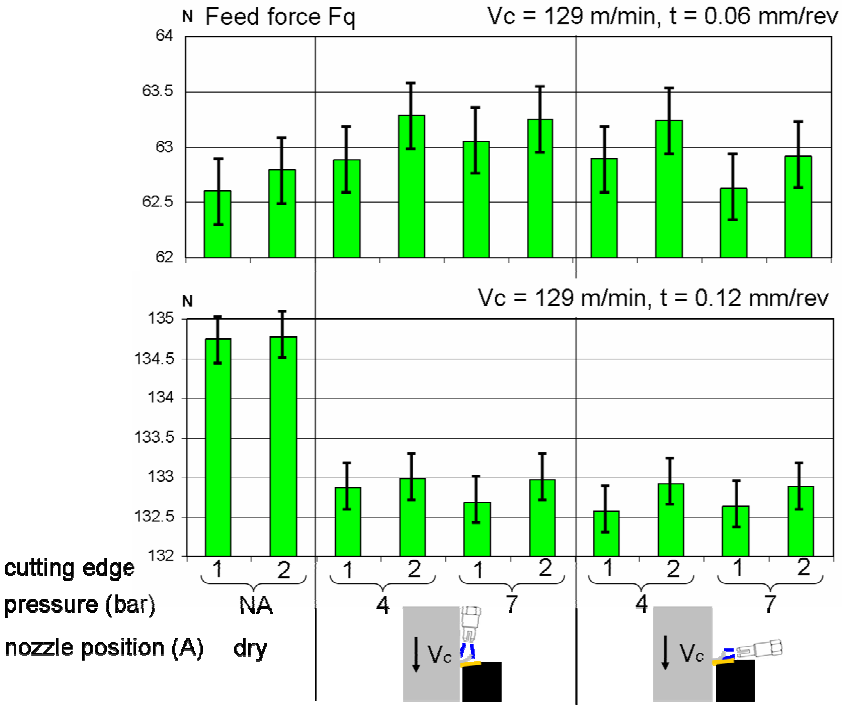

Figure 5.14b – The feed force measurement for the tests at 129 m/min of cutting speed, a feed rate of 0.06 and 0.12 mm/rev and the nozzle in *overhead A* and *interface A* positions

When the nozzle is directed into the interface, the flow is almost parallel to the rake face; so no extra force is applied to the insert. Figures 5.14a, 5.14b show the force in the direction of the feed. Once again when the second cutting edge is used, the force measured is slightly bigger. Since the insert was tightly secured to the tool holder, the rake face of the second edge used in the tests was observed in an optical microscope. Electro-discharge machining is a technique that can be aggressive to the coating of the insert.

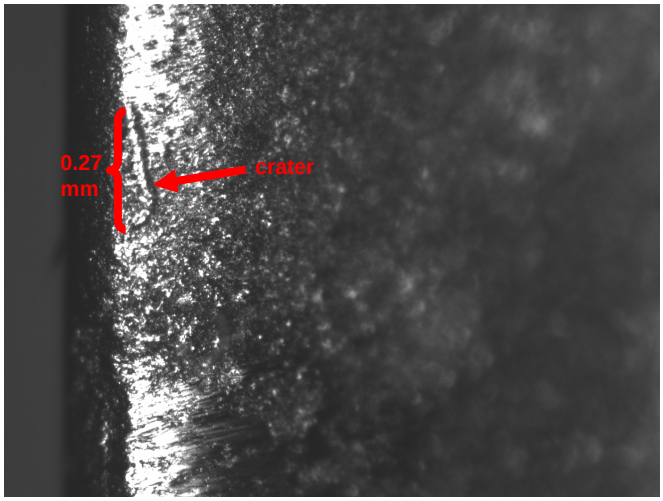

Figure 5.15a – The crater on the second edge used for the experimental test. The crater was not created by wear, but by electro-discharge machining

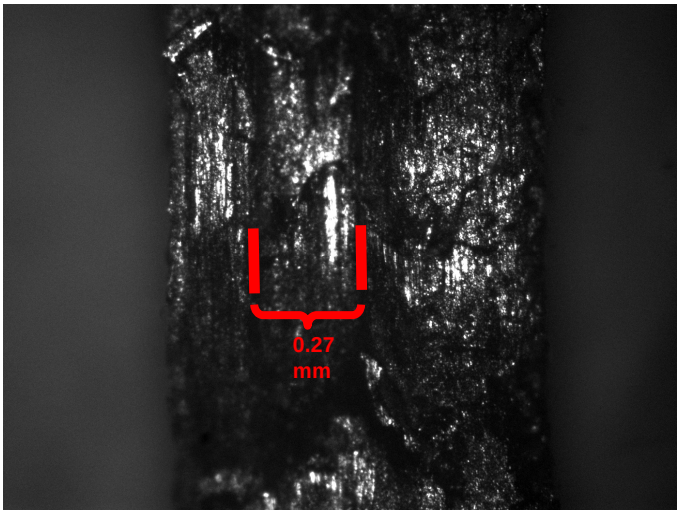

Figure 5.15b – The chip shows the trace left from the crater shown in Figure 5.15a

The chips collected during the tests with the second cutting edge show the trace of the crater on the face in contact with rake face, Figure 5.15b. The use of the air jet does not affect the measurement of the feed force. The quantity that is most affected by the use of the air jet is the average interface temperature. It can be observed that the highest temperature was measured in the case of dry cutting. Application of the air jet reduced the temperature, and the largest reduction was observed when the air jet was used in the overhead position. This trend was observed in all four cutting conditions considered. Figures 5.16a and 5.16b show the experimental results for one cutting speed and two feed rates. Tests were repeated using two cutting edges equipped with embedded thermocouple, labeled *1* and *2* in the figures. Dry cutting results were compared to air jet cooled orthogonal cutting tests. Two pressure of the air jet were used: 4 and 7 bar, and two positions of the nozzle were used (*Overhead A* and *Interface A*).

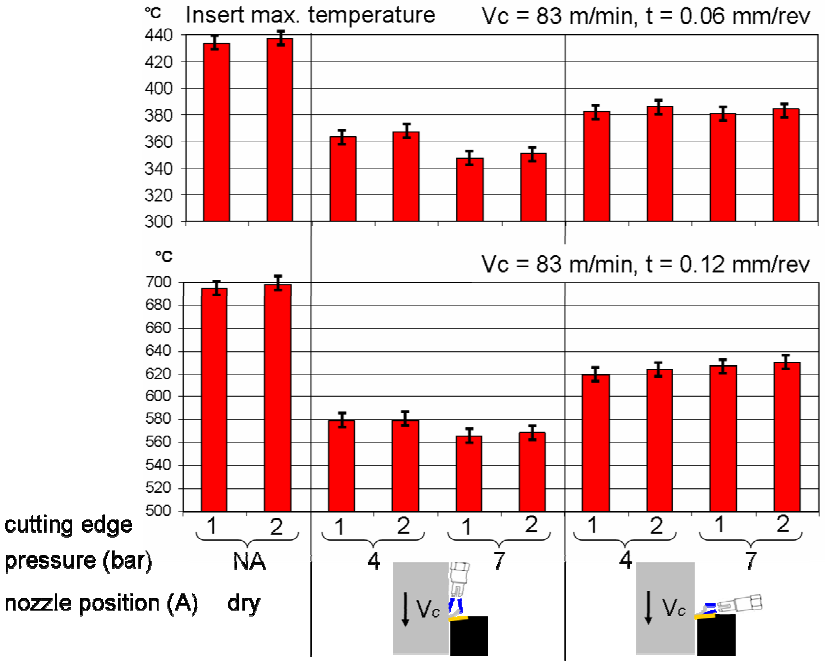

Figure 5.16a – The maximum insert temperature measured by the thermocouple for the tests at 83 m/min of cutting speed, a feed rate of 0.06 and 0.12 mm/rev and the nozzle in *overhead A* and *interface A* positions

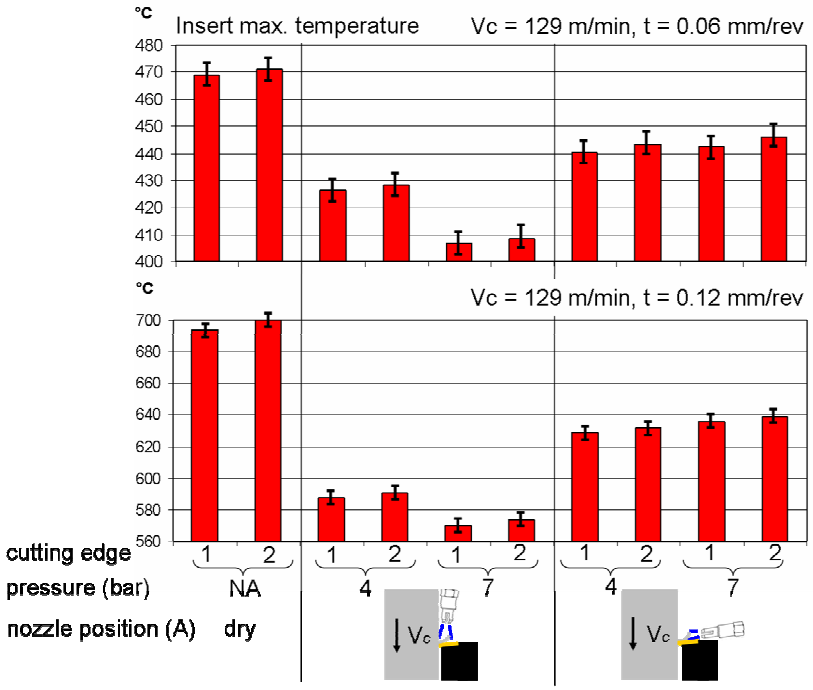

Figure 5.16b – The maximum insert temperature measured by the thermocouple for the tests at 129 m/min of cutting speed, a feed rate of 0.06 and 0.12 mm/rev and the nozzle in *overhead A* and *interface A* positions

A sensitivity analysis on cutting temperature was performed using small variations in the angle of the axis of the air jet and small variations of pressure. From a qualitative point of view the position *B*, compared to the position *A*, represents a counter clockwise rotation of the nozzle of approximately 5° (details of the precise positioning of the nozzle are reported in Table 5.3). In other terms, the angular distance between the axis perpendicular to the rake face and the axis of the nozzle is increased when passing from *overhead A* to *overhead B*; the angular distance between the rake face and the axis is reduced when passing from *interface A* to *interface B*. The difference of temperature when passing from the overhead to the interface position of the nozzle is evident. However it is interesting to remark that the air jet is more efficient in position *A*. This means that the air jet becomes more and more efficient, in terms of cooling by mechanical effect, as its axis approaches the perpendicular to the rake face.

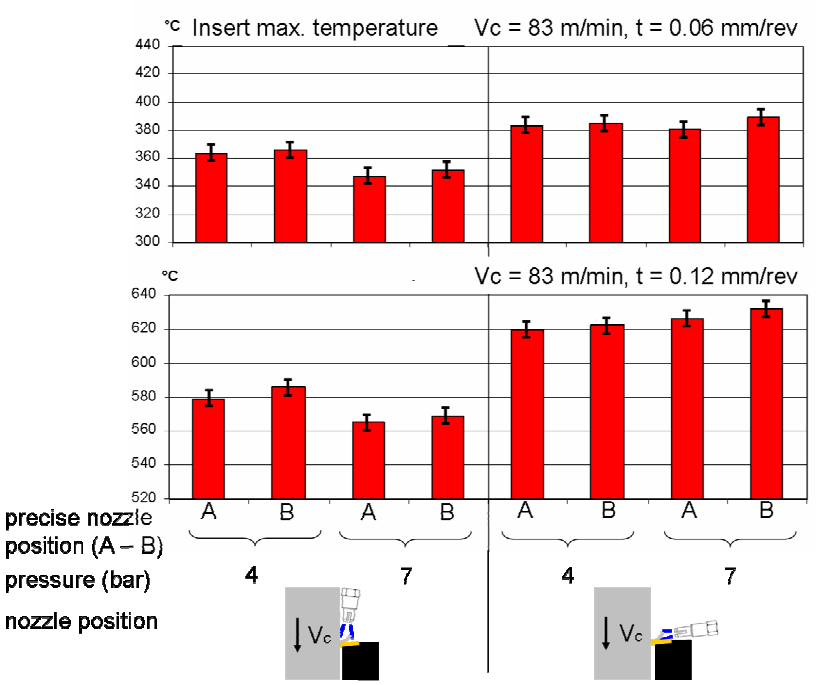

Figure 5.17a – The maximum insert temperature measured by the thermocouple for the tests at 83 m/min of cutting speed, a feed rate of 0.06 and 0.12 mm/rev and the nozzle in *overhead A* and *B, interface A* and *B* positions

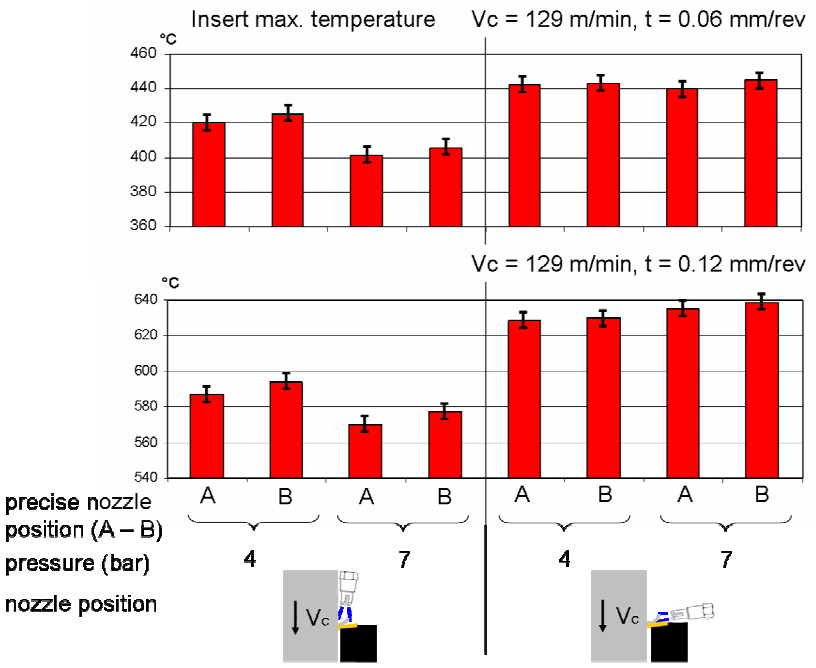

Figure 5.17b – The maximum insert temperature measured by the thermocouple for the tests at 129 m/min of cutting speed, a feed rate of 0.06 and 0.12 mm/rev and the nozzle in *overhead A* and *B, interface A* and *B* positions

The sensitivity analysis to the air jet pressure was performed with three values of pressure (7, 7.25 and 7.5 bar). The tests were carried out at a cutting speed of 129 m/min with the first cutting edge. Both of the feed rates, 0.06 mm/rev and 0.12 mm/rev, were used in the tests. It was observed that small changes in the pressure have no significant effect on the cutting force. This is consistent with the measurement shown in Appendix B.3, where the difference between the blowing force applied to the rake face when pressure was raised from 4 bar to 7 bar was shown to be 0.8 N. Once again, the sensitivity analysis of the pressure shows that the air jet has negligible influence on the feed force.

The most interesting results are those of maximum insert temperature, as shown in Figure 5.18. When the nozzle is in the overhead position, an increment of the air jet pressure causes a decrement of the temperature. When the nozzle is in the interface position, the same increment of the air jet pressure causes an increment of the temperature.

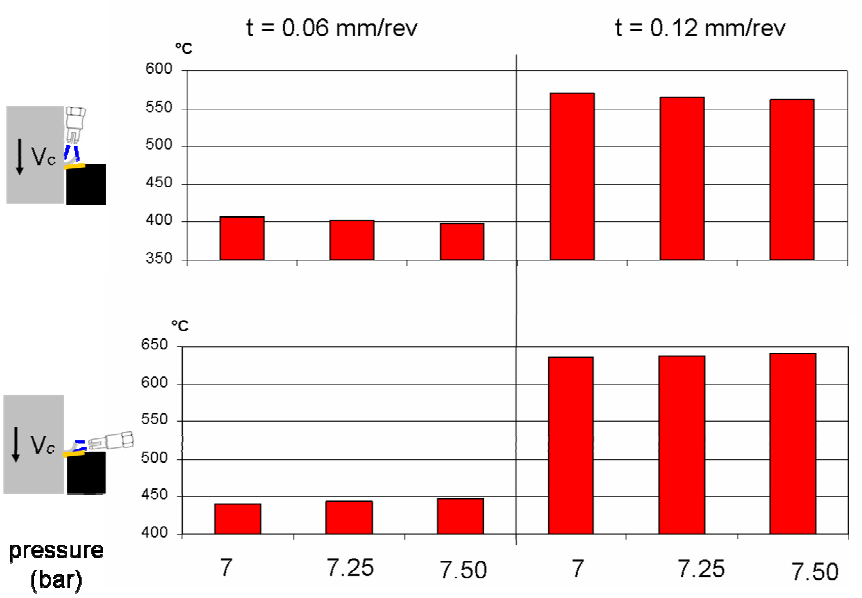

Figure 5.18 – Results for maximum interface temperature with small variation of temperature. V_C = 129 m/min

The result of this sensitivity analysis is quite important: combined with the measurement of the average cutting temperature in dry cutting, it not only proves that the air jet has a mechanical effect on the temperature, but also provides guidelines for applying it successfully to the case of orthogonal cutting. In fact, if the air jet is positioned in the

interface, the mechanical effect could cause an increment of the cutting temperature, compared to the effect obtained with the same air jet at a lower pressure. Both positions of the jet provide cooling by forced convection; however a temperature can be further reduced if the nozzle is appropriately positioned.

5.6 Summary and conclusions

The 80 tests carried out for investigating the effects of high speed air jets on orthogonal cutting have been designed to provide experimental data in terms of cutting forces and average interface temperature. The main purpose of the tests is proving that the blowing force of the air jet has a beneficial effect in terms of cutting temperatures when the jet is positioned in the overhead position. In order to achieve this goal, the nozzle has been positioned in 4 different positions: *overhead A, overhead B, interface A* and *interface B*. This positioning of the nozzle allowed a sensitivity analysis of the position of the jet. The tests were carried out in a particular order, so that the position of the nozzle was changed four times only, in order to reduce the error due to nozzle positioning. A remote camera, placed in the same position for each displacement of the nozzle, was used for measuring the exact position of the nozzle. The images from the camera were filtered in order to find the edges of the objects in the picture, and reduce the measurement error in the image. An embedded K-type thermocouple was used for measuring the maximum temperature at the chip-tool interface. The method of embedded thermocouple was extensively used by Attia et al. [109, 110, 111, 112] and it was a suitable method for the experimental investigation on air assisted orthogonal cutting. Two cutting edge was used for ensure repeatability. Tests for sensitivity analysis on pressure were also carried out. Full details on the experimental setup are presented in Appendix B. The main finding of the experimental test is the trend of the maximum temperature of the chip-tool interface as a function of the pressure of the air jet with different position of the nozzle. The experimental results show an increment of temperature when the pressure is increased with the nozzle in interface position, and a decrement of temperature when the pressure is increased with the nozzle in overhead position.

6. Results and discussion

6.1 Introduction

The investigation carried out in this research project aims to understand the effects of a high speed air jet in orthogonal cutting. In order to do this, three complementary methods of investigation have been used: analytical modelling, finite element modelling and experimental tests. This chapter compares the three approaches and the results obtained are critically examined.

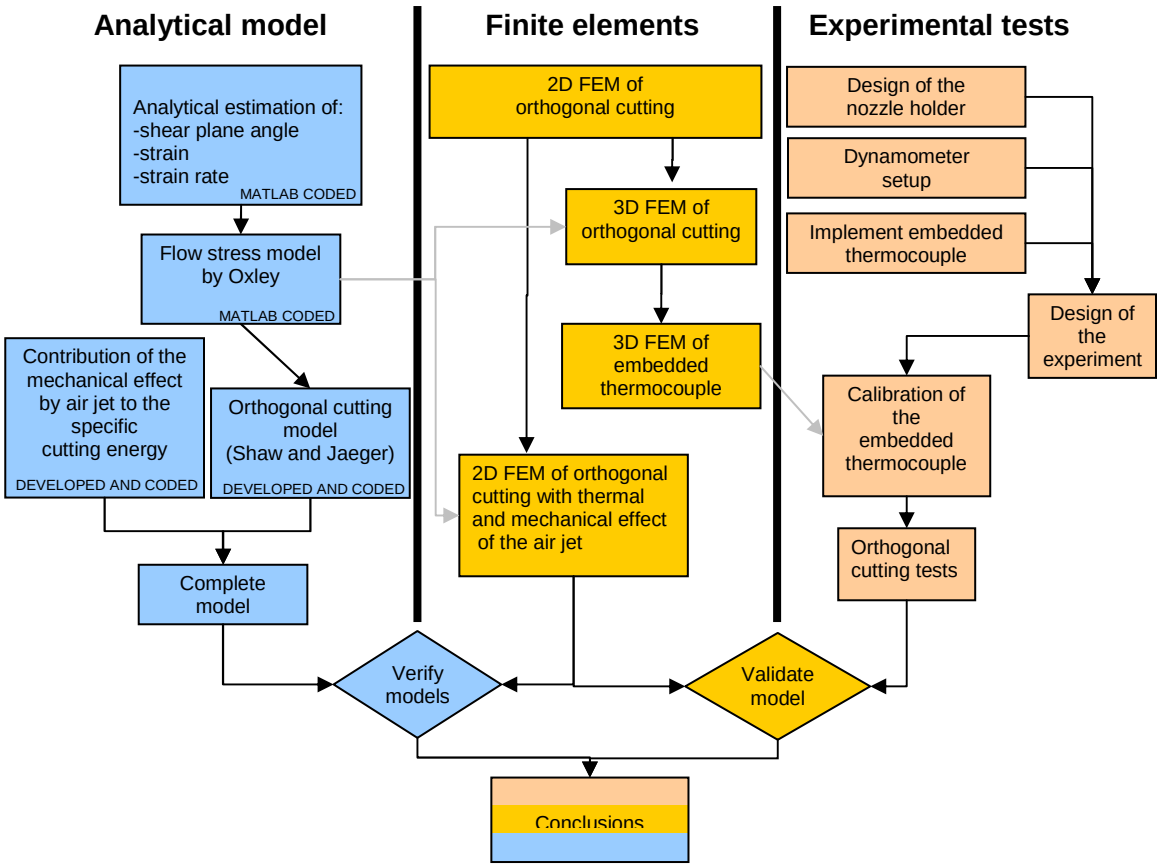

Figure 6.1 - The three approaches, analytical modeling, finite elements and experimental tests, contribute to the comprehension of the role of high speed air jet in orthogonal cutting

The scientific literature shows that the use of lubricant is not always positive in terms of cutting performance [3, 4]. The use of minimum quantity of lubricant (MQL) has been widely investigated and Li [83, 81] suggests that whilst flow rate of the coolant may be important in improving cutting performance, the force provided by the jet also plays a part. Intuition suggests that the mechanical effect provided by high flow rate cooling techniques might help to reduce cutting temperatures. The work carried out in this research project used three different approaches in order to test the hypothesis that the mechanical effect of the high speed air jet influences the machining processes, namely: theoretical analysis, finite element modelling and experimental tests, as illustrated by Figure 6.1. The discussion critically considers the approach and the methodology used for proving and understanding the role of the mechanical effect of a high speed air jet in orthogonal cutting. The cutting performance with high speed air jet is described in terms of:

1) chip formation and morphology
2) cutting forces
3) chip-tool interface temperature

6.2 Chip formation and morphology

Chip formation is a complicated process that is difficult to analyze theoretically even in the simplest cases so that simplifying assumptions have frequently been made to facilitate theoretical investigations [67]. In Chapter 4 it was assumed that the chip morphology is strongly dependent on the shear plane angle and chip-tool length. The following hypotheses have been assumed:

1) plane strain problem
2) perfectly plastic material
3) the shear stress is a maximum in the direction of the shear plane, and it is independent of the shear angle
4) the shear angle is such that the total power is a minimum

5) the coefficient of friction is independent of the shear angle (Coulomb friction with a constant friction coefficient)

The chip thickness and chip curvature radius were used in the analytical and finite element models for estimating the magnitude of the mechanical effect of the air jet, and the chips collected in preliminary cutting tests without an air jet, helped in the choice of a new material model for the finite element and analytical models. Also, the observation of chip shape was used for designing the experimental setup, as described in this section. The first step in modeling the chip shape is the calculation of the shear plane angle. The analysis presented in Chapter 4 gives a unique solution for the shear plane angle and the tool-chip contact. The shear plane angle provided by the simple slip line field (SLF) theory of Lee et al. [12] (described by Shaw as an appropriate starting point for estimating the shear plane angle) was used. The variables in the simple slip line field of Lee et al [12] are the rake angle and the friction angle. Therefore, assuming a constant friction coefficient ($\mu = 0.55$), a single shear plane angle results for all cutting conditions. The application of the Oxley model for variable flow stress is quite complicated and goes beyond the purpose of the analytical model developed for this project. Only part of the model of Oxley (the actual flow stress model for low carbon steel) has been implemented in order to provide a better material model than the default model provided within the finite element software DEFORM.

The Figure 6.2 shows the flow stress as a function of temperature with unitary strain and a strain rate of 28900 for s^{-1} for a feed rate of 0.06 mm/rev and 24600 for s^{-1} for a feed rate of 0.12 mm/rev. As reported by Shaw [67] and Toropov [142] the flow stress does not consistently change with the cutting speed.

T (mm/rev)	$\dot{\gamma}$ *(s^{-1})*	γ	T_s *(℃)*	σ *MPa*	Φ *(Lee)*	Φ *(FEM)*
0.06	28900	1	303℃	1074	16.18°	18.79°
0.12	24600	1	320℃	1031	16.18°	19.56°

Table 6.1 – The comparison of shear plane angles calculated by the simple slip line theory of Lee et al [12], and FE calculation for the same cutting condition (described in terms of feed rate, strain rate and strain) along the shear plane

After estimating the shear plane angle it is possible to calculate the chip thickness t_1, the curvature radius of the chip R_c and the contact length L_c. The results obtained by the analytical model are compared to the results by finite elements models, as shown by the Table 6.2.

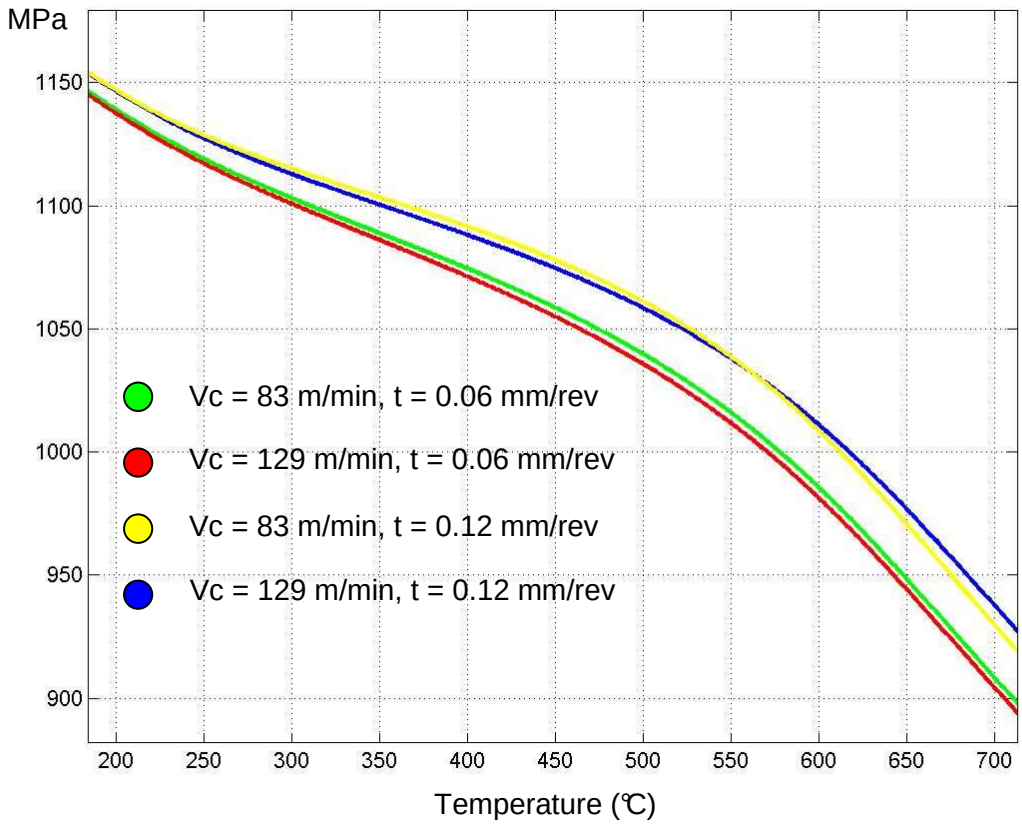

Figure 6.2 – The results of the flow stress model developed by Oxley (see Appendix C) as a function of temperature with unitary strain and a strain rate of 28900 for s^{-1} for a feed rate of 0.06 mm/rev and 24600 for s^{-1} for a feed rate of 0.12 mm/rev

cutting conditions	t_1 (mm)	R_c (mm)	L_c (mm)
t=0.06 mm/rev (analytical)	0.166	0.5532	0.1379
t=0.12 mm/rev (analytical)	0.332	1.1064	0.2757
t=0.06 mm/rev (FEM)	0.14	0.71	0.13
t=0.12 mm/rev (FEM)	0.28	1.71	0.28
V=83 m/min, t=0.06 mm/rev (test)	0.15	1.2	
V=83 m/min, t=0.12 mm/rev (test)	0.31	1.6	
V=129 m/min, t=0.06 mm/rev (test)	0.13	1.3	
V=129 m/min, t=0.12 mm/rev (test)	0.36	1.8	

Table 6.2 – The chip thickness t_1 (mm/rev), the curvature radius of the chip R_c (mm), and the contact length L_c (mm), analytically calculated are compared with the results obtained by finite elements modeling

The chip thickness and the curvature radius calculated by the analytical and finite element models are compared to the chip thickness and curvature radii of samples of chips collected during the cutting tests. Figure 6.3 shows a representative selection of the chips collected for the four cutting conditions. Two qualitative observations can be made from visual analysis:

1) all the chips machined at the feed rate of 0.12 mm/rev have a brown or blue color, whilst the chips machined at 0.06 mm/rev are shiny
2) the use of the air jet did not produced any difference in the chip shape, but all the chips machined with the use of the air jet are shiny

This second observation suggests that the air jet does not produce extra plastic strain in the chip. This supports the use of elastic linear relations in the analytical estimation of the stress due to the air jet in section 4.4. In Figure 6.4 it is possible to recognize two further characteristics of the chip: the breaking zone and the burr formed on chip sides. In a representative population of the chips collected for each cutting condition, the shape of the breaking zone, the curvature radius and the thickness were observed. While the shape of the breaking zone is random, the average curvature radius and the chip thickness are constant for the same cutting speed and feed rate.

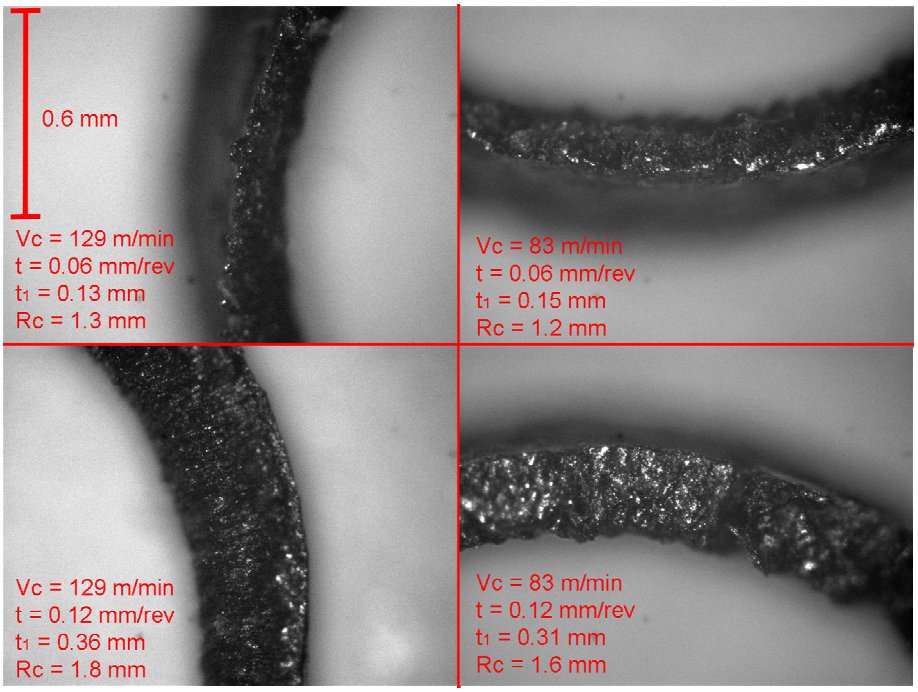

Figure 6.3 – Representative images of the collected chips analyzed at the optical microscope

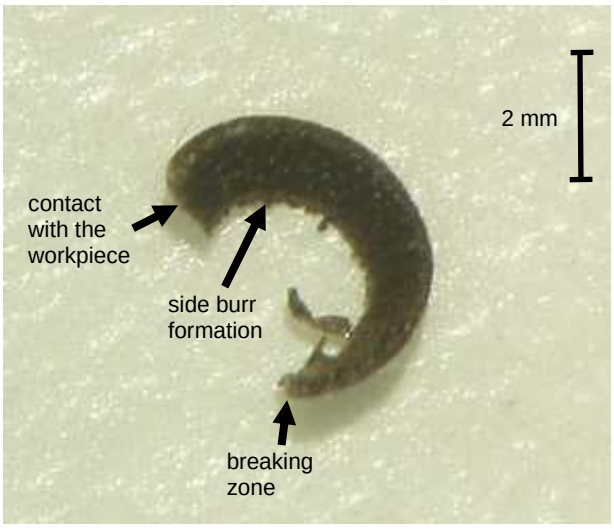

Figure 6.4 – The zones of interest in a chip: the zone of contact with the workpiece constitutes a constraint that lead to chip breaking in the breaking zone. The formation of burr has been confirmed in all the collected chips

The formation of burr can be explained also by finite element modeling. Figure 6.5 shows the formation of the chip in a 3D simulation. However, damage is not modeled, therefore a continuous chip is shown in Figure 6.5. The collected chips show segmentation in the side. This segmentation is confined to the side of the chip, and it is not due to a hypothetical formation of a secondary shear plane.

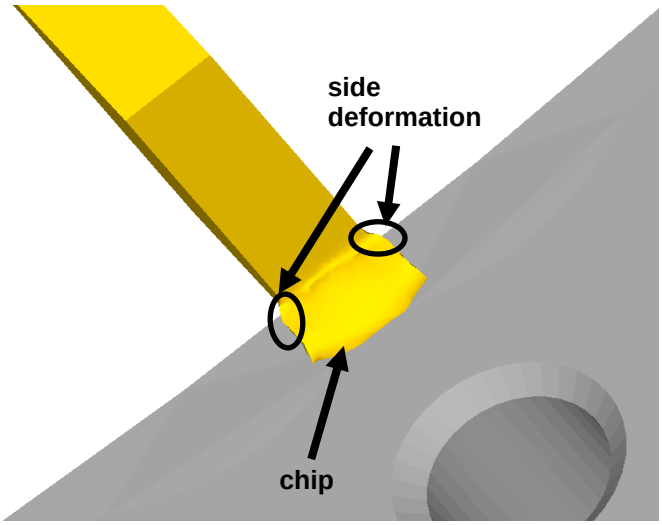

Figure 6.5 – The burr formation is represented by a side deformation of the chip, predicted by the 3D finite element model

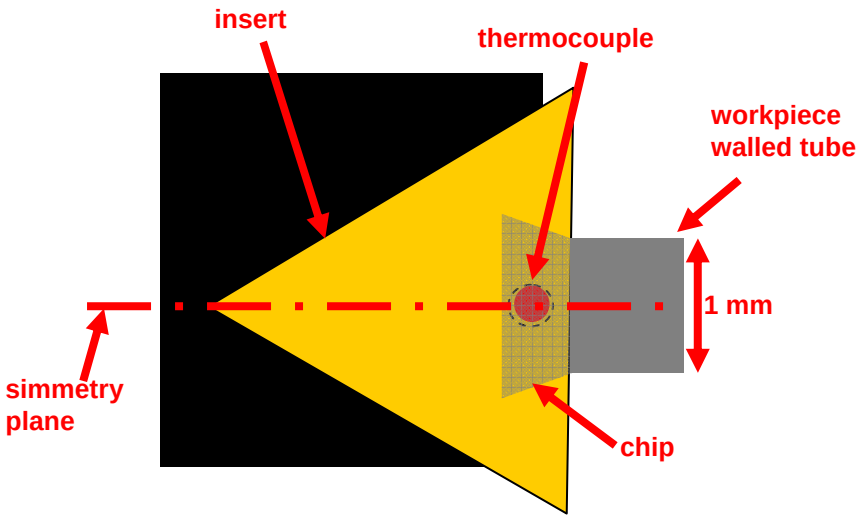

Figure 6.6 – The sketch represents the top view of the cutting zone. The transparent chip show the position of the thermocouple, placed 0.25 mm under the rake face

It can be observed that the width of the chip is bigger than the width of cut. In the model, the chip flows on the plane of the rake face in two directions as illustrated by the sketch in Figure 6.6. The side burr formation is a phenomenon that does not fit in the scenario of orthogonal cutting, but it is negligible in the symmetry plane shown in Figure 6.6, where the chip flows in the plane of the cutting direction.

Chip flow over insert-location of embedded thermocouple

Great care was taken in drilling the hole for the thermocouple in the insert. Precise drilling in the WC insert by spark erosion is a hard task and only two of the six holes drilled in the insert have the characteristics for a reliable temperature measurement by the K-type thermocouple. The Table 6.4 shows the exact position of the two holes that turned out to be aligned with the plane of symmetry of the insert and chip.

Label	Depth	dist.rake face	Dist.flank face	diam.
1	2.288	0.268	0.647	0.58
2	2.313	0.243	0.671	0.58

Table 6.4 – The depth, the diameter and the distance from the rake face and flank face of the holes drilled for embedding the thermocouple in the WC insert

The contact length between the tool and the chip is traditionally a difficult quantity to estimate, and quite often, observation of the rake face is the only direct measure that can reveal this quantity, even if this measurement is not always reliable [67]. The rake face was observed in the optical microscope, giving the image shown in Figure 6.7. The image intensity was adjusted in order to show the surface in contact with the chip, and therefore to allow an approximate measurement of the contact with the chip. The image in Figure 6.7 shows an altered width of cut (1.2 mm instead of 1 mm) confirming the side deformation of the chip indicated by finite elements in Figure 6.5. The length of contact indicated in the figure is consistent with the values calculated by analytical and finite element modeling. However, as remarked by Shaw [67], the analysis of the rake face provides a rough estimation of the contact length. In conclusion, a perfect fit of the

predictions of finite elements and analytical models with the chip shape was not expected. The intention of modeling is the prediction of the trends of chip thickness and curvature radius when the cutting conditions (feed rate and cutting speed) are altered. The predicted chip thickness itself is in good agreement with the experimental tests; however the curvature radius has been underestimated in the models. The consequence is an underestimation of the mechanical effect of the air jet.

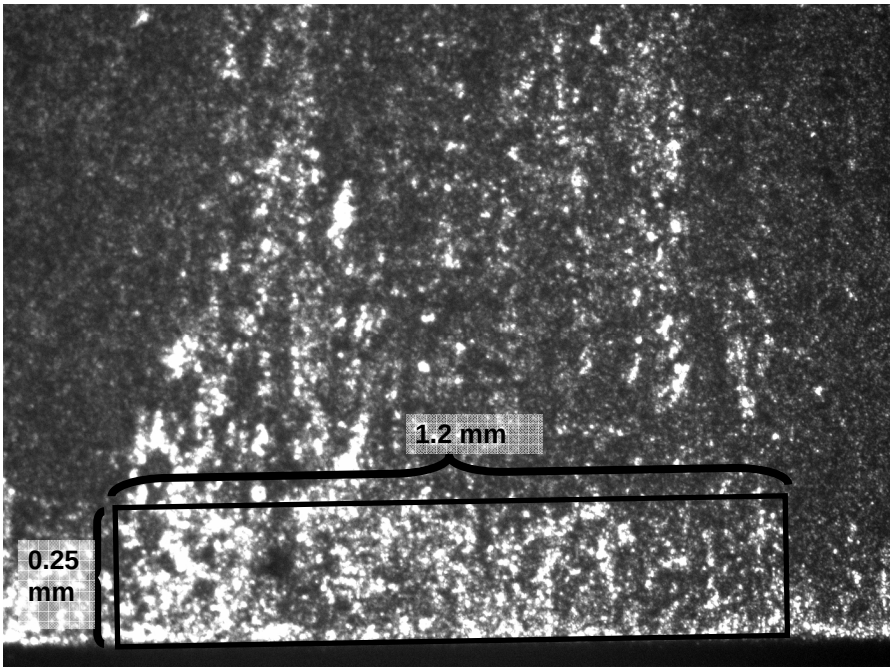

Figure 6.7 – The traces of the chip (white) on the rake face and the indicative measure of the chip contact area

Substituting the experimentally measured chip curl radius and thickness into the developed analytical model that estimates the energy contribution of the air jet gives an increment of approximately 7% with 0.06 mm/rev of feed rate and 9% with 0.12 mm/rev (see table 6.5). The predicted energy contribution was not dependent on cutting speed. Since the measured chip thickness and curl radius vary slightly with cutting speed, so also does the cutting energy.

The results for the estimated mechanical energy provided by the air jet are shown in Table 6.5. In the table the specific mechanical energy is given in MJ/m^3. The first three columns show the energy contribution for the predicted chip shape, the other three

columns show the energy contribution for the measured chip shape. The following table can also be considered as a sensitivity analysis for the mechanical energy provided by the air jet when the shape of the chip on which the air jet is applied changes.

		cutting conditions	U_{Mover} (min)	U_{Mover} (max)	U_{MInt}	U_{Mover2} (min)	U_{Mover2} (max)	U_{MInt2}
4 bar	Vc=83 m/min	t = 0.06 mm/rev	-18.8	-29.6	59.2	-20.1	-31.7	63.3
		t = 0.12 mm/rev	-37.7	-59.2	118.4	-41.0	-64.5	129.2
	Vc=129 m/min	t = 0.06 mm/rev	-18.8	-29.6	59.2	-20.8	-32.3	63.9
		t = 0.12 mm/rev	-37.7	-59.2	118.4	-41.4	-65.0	129.6
7 bar	Vc=83 m/min	t = 0.06 mm/rev	-57.7	-90.6	181.3	-61.7	-96.9	194.0
		t = 0.12 mm/rev	-132.7	-265.8	328.3	-144.6	-289.7	357.8
	Vc=129 m/min	t = 0.06 mm/rev	-57.7	-90.6	181.3	-62.0	-97.3	194.4
		t = 0.12 mm/rev	-132.7	-265.8	328.3	-144.9	-290.1	358.2

Table 6.5 – The specific mechanical energy by elastic deformation of the chip after the action of the air jet in overhead position (over) or in interface position (int), expressed in MJ/m³. The inputs for these results include the calculated chip curvature radius and chip thickness (first three columns) and the measured chip curvature radius and chip thickness (last three columns). In the column of cutting conditions the feed rate is expressed in mm/rev, the cutting speed in m/min and the pressure in MPa.

6.3 Discussion on the experimental tests - embedded thermocouple

It can be seen from the scientific literature on the various methods of temperature measurements, that the appropriate technique for a given thermal problem depends on the situation under consideration, such as the ease of accessibility of the sensor to the location of the subject, spot size, dynamics of the situation, accuracy needed, cost of instrumentation, advancements in sensor technology, and data collection and analysis [120]. According to Komanduri [121], embedded thermocouples were one of the earliest thermocouples used for the estimation of temperatures in various manufacturing and tribological applications. In order to use this technique in machining, a deep hole has to

be made in the cutting tool, and ideally, multiple holes for tracking the thermal field within the insert. Since multiple holes can alter the heat conduction into the tools as well as limit the strength of the tool, only a limited number of holes can be drilled in any given tool. Due to the small dimension of the insert and the reduced accessibility to the cutting zone, the average interface temperature was inferred from measurements made with a single K-type embedded thermocouple. Both Shaw [67] and Trent [140] report the problems of using such a temperature measurement technique. The thermocouple has to be positioned very precisely in order to provide reliable results and tungsten carbide is a difficult material to machine, even by electro-erosion. However, this method has been successfully used and was patented by Barlier [116, 117, 118].

In order to get reliable results, the thermocouple was placed in two different holes; therefore there are two tests for each cutting configuration (cutting speed, feed rate, position of the nozzle). One of the main problems associated with the embedded thermocouple is the correlation of the temperature recorded to the temperature at the chip-tool interface. Barlier use a simple conduction problem to obtain the average cutting temperature, but further improvements have been made by Lazard and Corvisier [119] using thermal quadrupoles.

In this research, rather than calibrating the thermocouple alone, the system constituted by the insert and the thermocouple was calibrated by using an external source of heat that provided a constant temperature on the rake face. This calibration, described in Appendix B.2, is valid only in the case of stationary heat transfer. The sensitivity of the calibration method to variation in the shape of the contact between the source of heat and the rake face was investigated by finite elements, as described in section 3.6. With the support of finite elements, the calibration of the system constituted by the insert and thermocouple allows a reliable correlation between the signal provided by the thermocouple and the average temperature in the chip tool interface.

6.4 Comparison of results: analytical model, finite element model and experimental tests

Examination of cutting forces

The comparison between the analytical model, the finite element model and the experimental tests shows that all agree on cutting force. The use of the material model proposed by Oxley [31] (details in Appendix C) is the key to obtaining reliable results with both the analytical model and the finite element model. The estimation of cutting temperature constitutes a more difficult problem, and an approach based on the specific cutting energy was found appropriate for introducing the influence of the mechanical effect of the air jet. The approach used in this research project follows the scheme of Leowen and Shaw [36] for the estimation of the heat partitioning coefficient and the friction slider analyzed by Jaeger [38]. The approach of Shaw was also convenient for introducing the mechanical effect of the air jet in terms of deformation energy. Figures 6.8a,b,c,d show the results for the cutting force F_p. Both the analytical and finite element models give the same results for these forces when the cooling conditions are changed, therefore the effect of cooling condition is reported only for the experimental tests; but even here the differences in the cutting force for different cooling conditions are so small that they might be considered negligible.

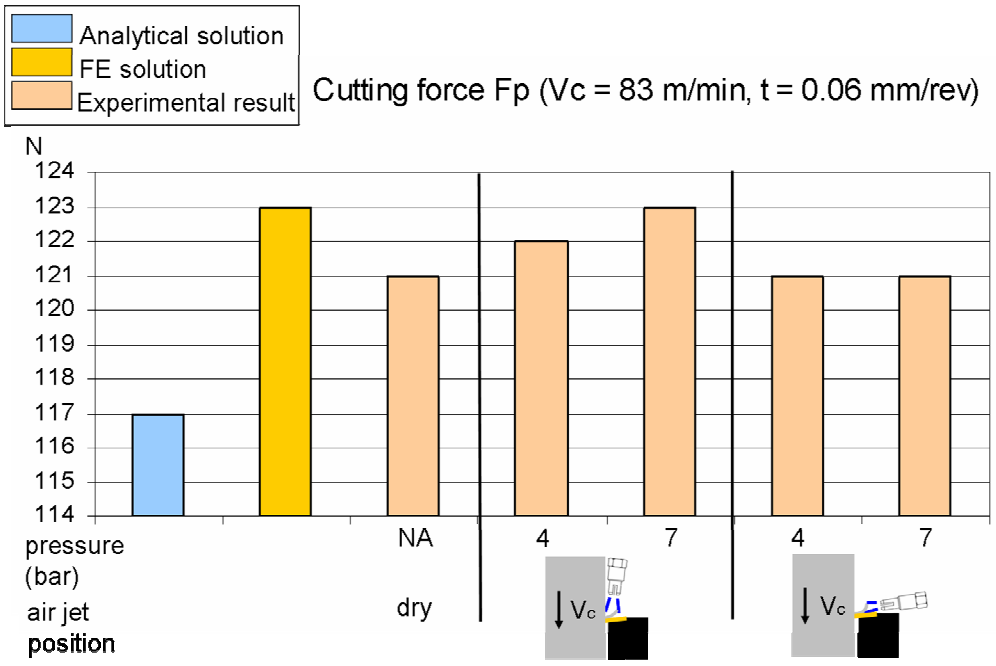

Figure 6.8a – Comparative results: the cutting force Fp for Vc = 83 m/min, t = 0.06 mm/rev

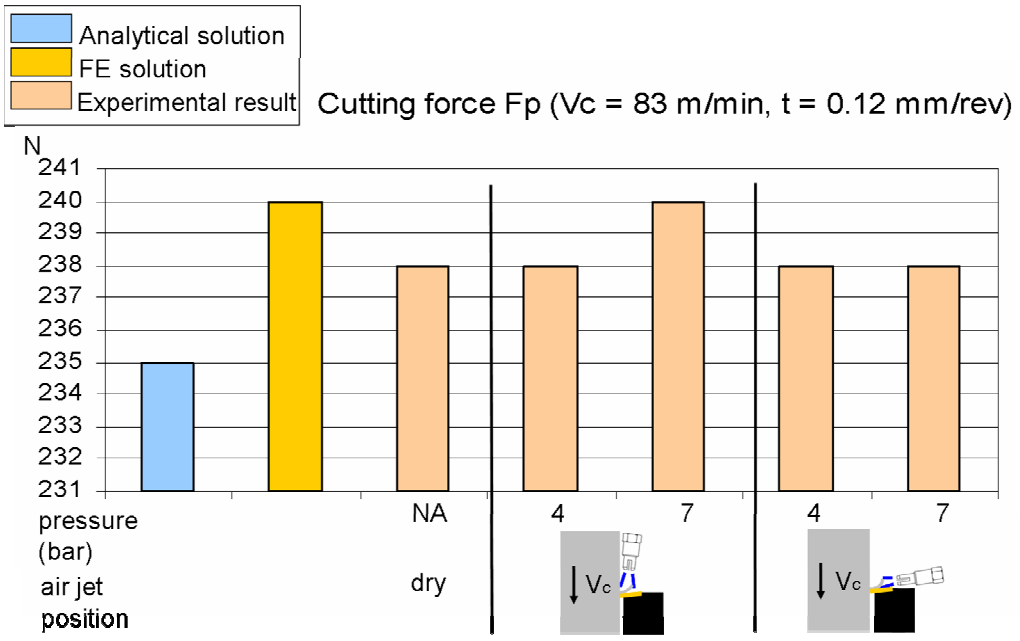

Figure 6.8b – Comparative results: the cutting force Fp for Vc = 83 m/min, t = 0.12 mm/rev

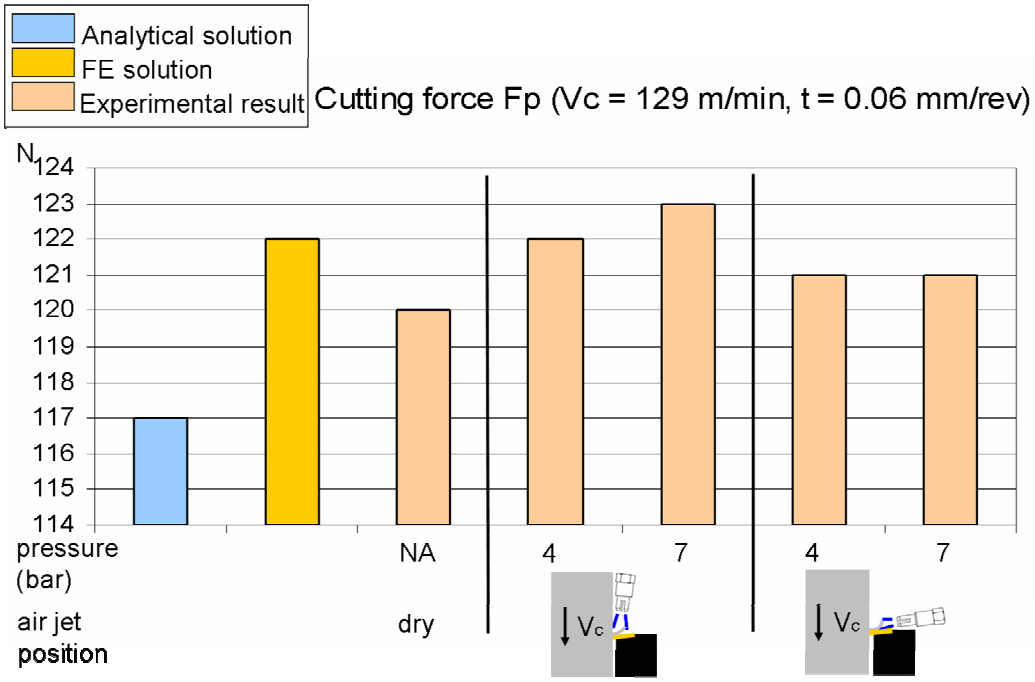

Figure 6.8c – Comparative results: the cutting force Fp for Vc = 129 m/min, t = 0.06 mm/rev

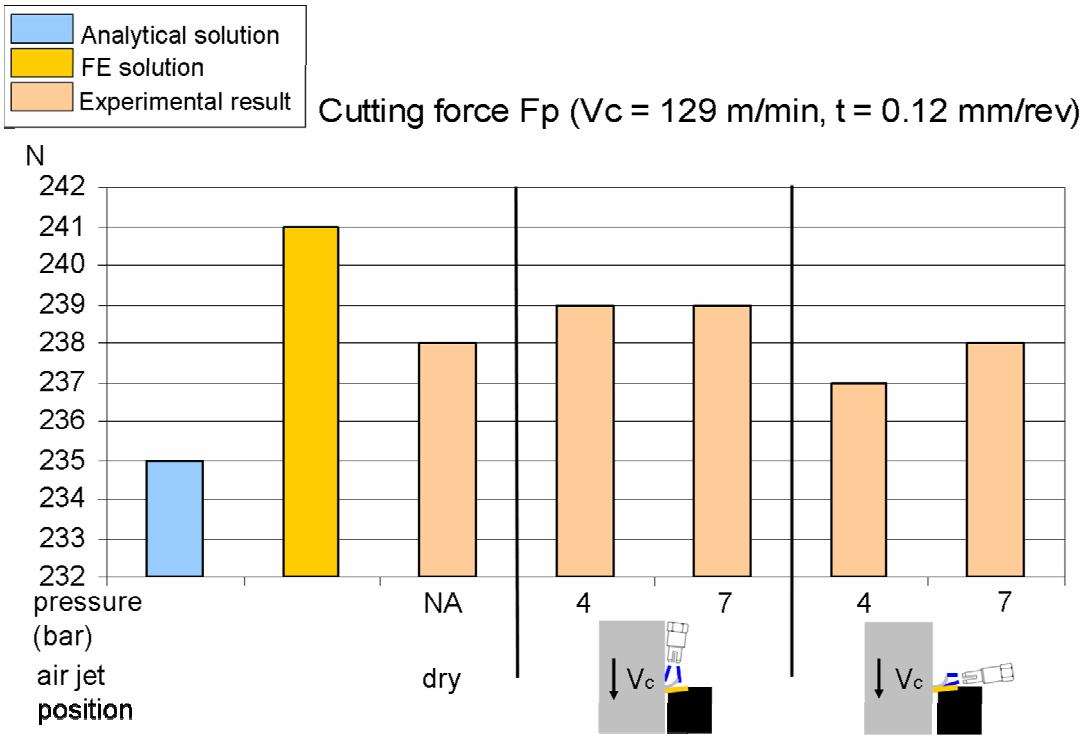

Figure 6.8d – Comparative results: the cutting force Fp for Vc = 129 m/min, t = 0.12 mm/rev

Examination of cutting temperature

The comparison of cutting temperature requires a more detailed analysis, since the cutting temperature changes as the cooling condition changes in the analytical model, in the finite element model and, of course, in the experimental tests. Figures 6.9a,b,c,d show the cutting temperature predicted by the analytical and finite element models compared to the test results. It can be observed that finite element modelling predicts a better correlation to the temperature measured by the thermocouple rather than the analytical model. However, the trend of the analytical model is consistent with the trends of the finite element model in the tests, as the cooling conditions are changed. Both of the models predict that the air jet is more efficient when the nozzle is in the overhead position.

It can be also observed that the analytical model over-estimates the mechanical effect at 7 bar. The reason for this is probably the approximation made of simplifying the fluid dynamics of the air jet into two variables; the pressure and the direction of the air jet.

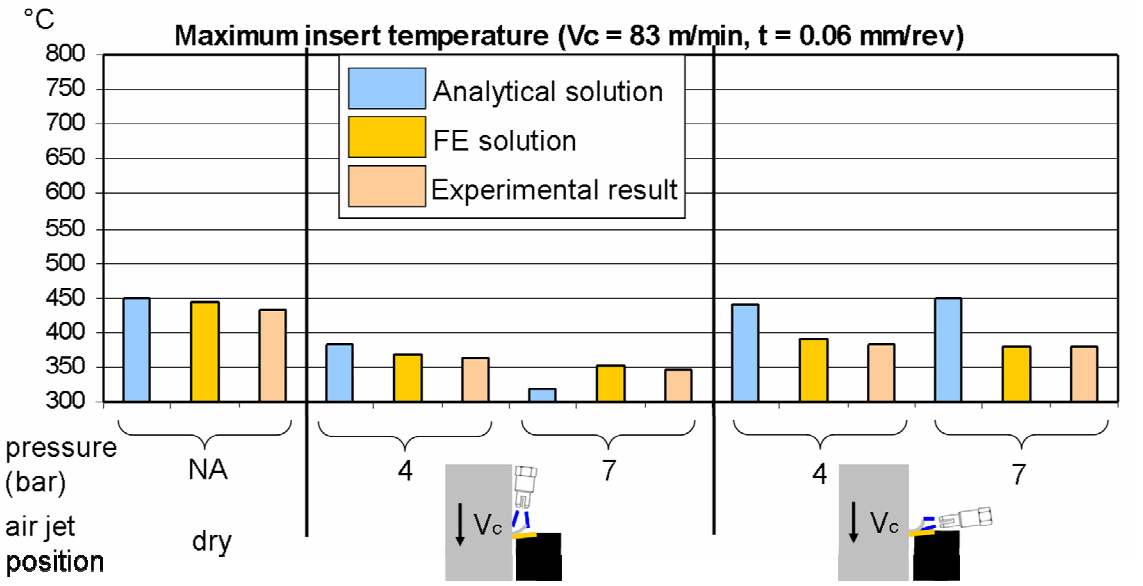

Figure 6.9a – The cutting temperature predicted by the analytical model and the finite elements model is compared to the experimental tests results for Vc = 83 m/min, t = 0.06 mm/rev with different cooling conditions

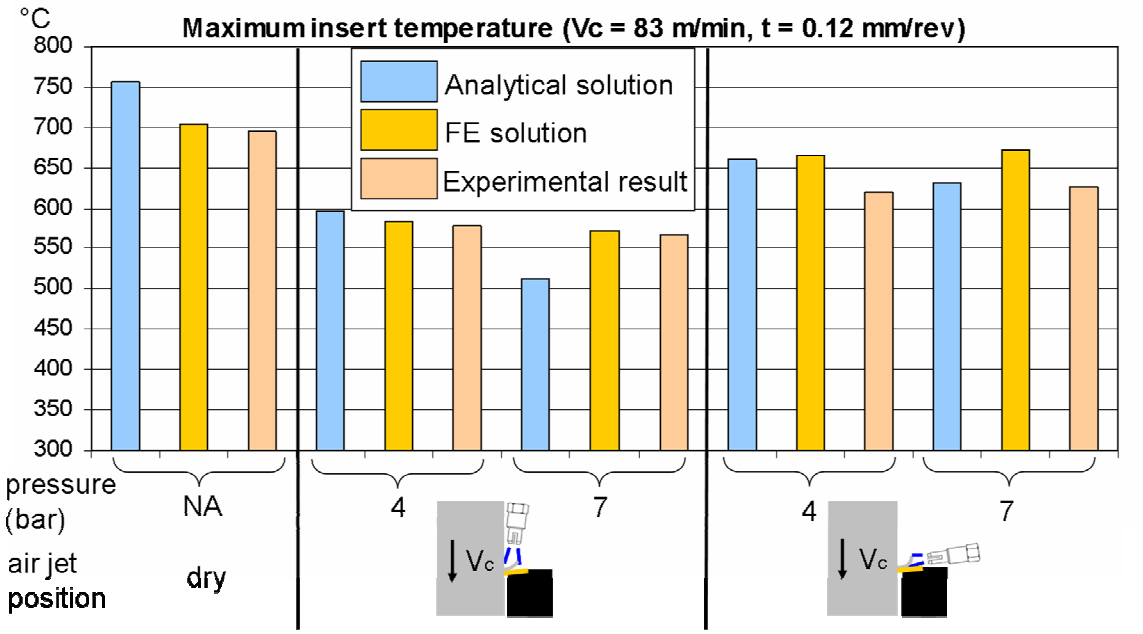

Figure 6.9b – The cutting temperature predicted by the analytical model and the finite elements model is compared to the experimental tests results for Vc = 83 m/min, t = 0.12 mm/rev with different cooling conditions

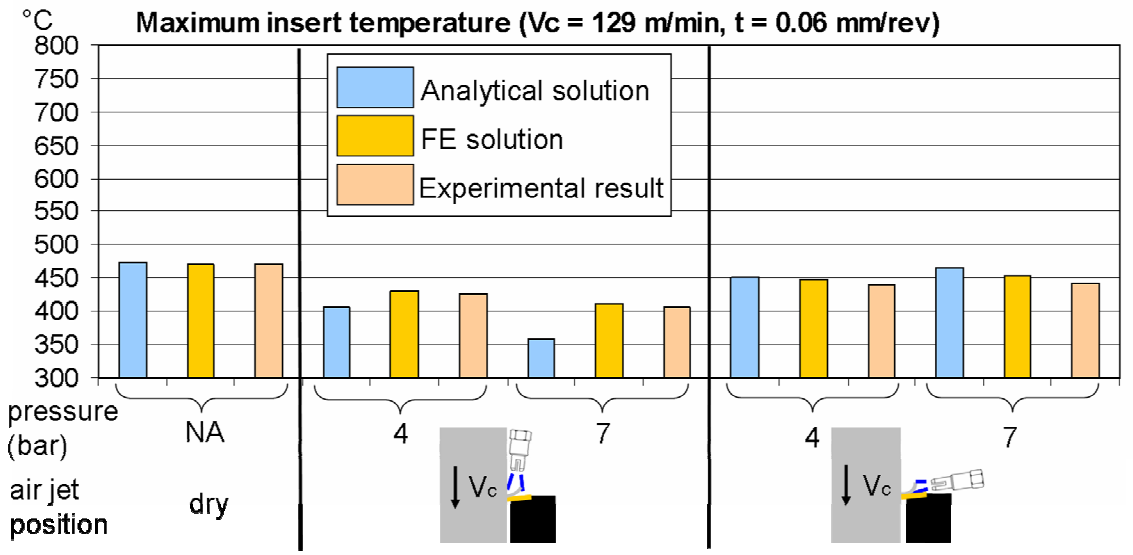

Figure 6.9c – The cutting temperature predicted by the analytical model and the finite elements model is compared to the experimental tests results for Vc = 129 m/min, t = 0.06 mm/rev with different cooling conditions

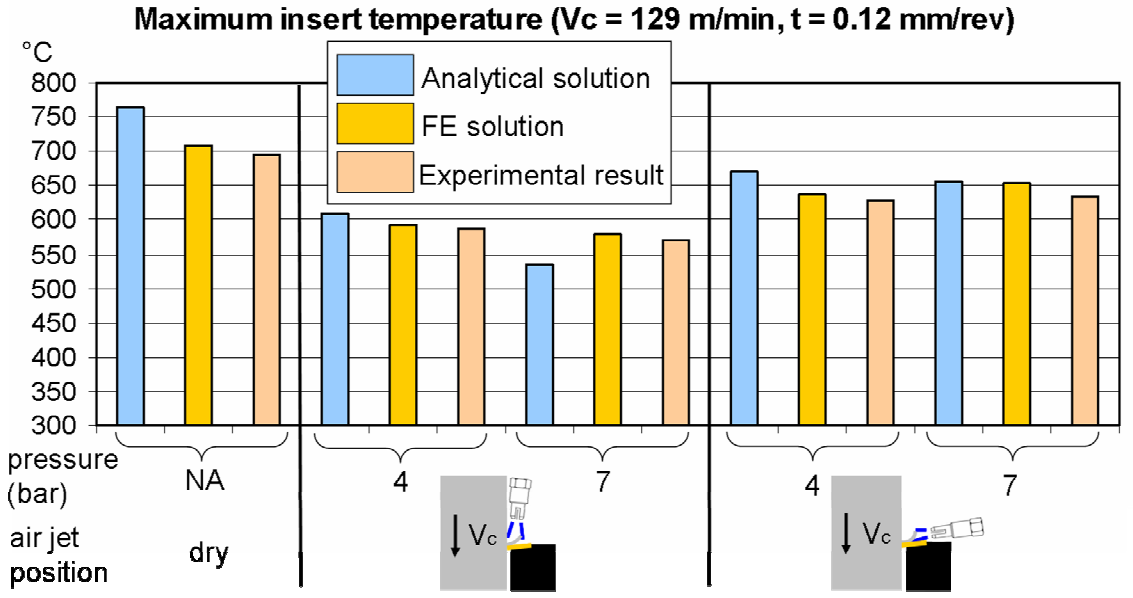

Figure 6.9d – The cutting temperature predicted by the analytical model and the finite elements model is compared to the experimental tests results for Vc = 129 m/min, t = 0.12 mm/rev with different cooling conditions

6.5 Summary and conclusions

Since the purpose of this work is not only to demonstrate the existence of a mechanical effect of high speed air jet cooling in orthogonal cutting, but also to understand the phenomenon, three methods of investigation have been used: analytical modeling, finite element modeling and experimental tests. Each of these methods of investigation gave a different level of understanding of the problem and together provided deep insight into the mechanism of the contribution of the air jet in terms of heat transfer and deformation of the chip.

Many approximations have been made to model the mechanics of orthogonal cutting and the air jet itself. In particular the air jet has been characterized by the pressure and the direction of the nozzle. As a stationary problem, the air jet can be modeled in terms of the two controllable variables (the pressure at the inlet of the nozzle and the position of the nozzle, directed over the top face of the chip or into the chip-tool interface). The consequences of this reduction to a stationary problem are important for the development of the analytical model, the finite element model and the design of the experimental campaign. In the analytical model and in the finite element model the effect of the air jet was decoupled into two static contributions, thermal and the mechanical. The force applied by the air jet was modeled as a constant and uniformly distributed pressure over the impinged surface. Without any other information on the fluid-dynamic variables in the 3D domain, this seems to be a reasonable approximation. Since the results from the finite element model show good agreement with the results of experimental tests, this simple representation of the air jet is close to the actual global behavior of the system, even if the dynamic behavior of the chip, excited by the detachment of the vortex generated by the air jet is unknown

According to Komanduri [121] the cumulative delay in techniques involving embedded thermocouples is can not be ignored. However in this research project the problem of estimating and measuring the cutting temperature has been reduced to a stationary problem, not affected by the delay. The technique of the embedded thermocouple, also used extensively by Barlier et al. [116, 117, 118] and Lazard et al. [119], proved to be effective in measuring the cutting temperature. The particular way of calibrating the

sensor, composed by the thermocouple and the insert, has been extensively studied by finite elements increasing the confidence in the measurement and sensitivity to errors.

In conclusion, the comparison of the results provided by the three methods of investigation (analytical model, finite element model and experimental tests) is quite consistent, especially between the finite element model and the tests. The use of the analytical model provided a solid explanation of the mechanical effect of the air jet, and provided fundamental guidelines for applying the air jet in a functional and efficient way. The finite element modeling included 2D and 3D modeling, workpiece and insert stress analysis. The results of finite elements indicate that the mechanical effect of the air jet generates a state of stress that could be beneficial, if the nozzle is correctly positioned. Finally the experimental campaign includes a sensitivity analysis of the position of the nozzle, of the air jet pressure and of the hole for embedding the thermocouple.

7. Conclusions and further research

7.1 Introduction

The focus of the thesis is the understanding of the effects of an air jet in the orthogonal cutting process, with emphasis on the mechanical effect of the jet. Most of the new cooling techniques in machining, including minimum quantity lubrication (MQL) and high pressure jet assisted machining (HPJAM), use an air jet for delivering oil based emulsion to the cutting area. The understanding of the behaviour of the air jet can be used to optimize the performance of these cooling techniques.

Besides the thermal effect of the air jet, a mechanical effect was found to have a role in reducing the cutting temperature. This role was critically considered and investigated by finite element modelling, analytical modelling and experimental tests. The preliminary experimental investigations show that high speed air jet assisted machining has a greater potential than previously suspected. In particular the mechanical effect of the air jet has previously been investigated only for extremely high pressures (up to 130 MPa) according to Pusavec [1] and Klocke [24]. Since systematic research on the effect of a low pressure air jet, considering variations in air pressure, nozzle positions and cutting conditions had not yet been carried out, the purpose of this research work is to investigate the use of an air jet as a function of these parameters in the orthogonal cutting process. The findings provided in this thesis can be applied to different cutting process, including oblique turning and milling, and can be used to optimize the performance of jet based cooling methods by using the guidelines, in terms of pressure and jet positioning, provided in this work

7.2 Materials and methods

The experimental tests

The effect of air jet cooling in orthogonal cutting was considered from a thermal and mechanical point of view. The low carbon steel AISI 1020 was chosen for the tests. AISI

1020 is used for a wide range of applications. Its widespread use requires an optimization of the manufacturing process, and since the low carbon steels are relatively well known materials, they are particularly suitable for experimenting new machining techniques.
Orthogonal cutting was preferred to the oblique cutting process because its two-dimensional nature makes it suitable for analysing the performance of new features in the air jet as coolants that were previously neglected.
A Sandvik TNMG 11 03 02-MF 4025 insert was selected to provide optimal cutting performance on low carbon steel at the cutting speeds (83 and 129 m/min) and feed rates (0.06 mm/rev and 0.12 mm/rev) selected for the orthogonal cutting tests. At the selected cutting speed and feed rate the lathe does not show any relevant vibration that could affect the force measurement.
A particularly silent De Laval round nozzle was used for directing the air jet into the cutting zone. Cutting forces were measured with a three components Kistler dynamometer, and chip-tool interface temperature with a K-type thermocouple embedded in the insert. Two holes having same depth, distance from rake face, distance from flank face and diameter were used for embedding the thermocouple. The nozzle was positioned in four positions, two “overhead” (the jet is directed on the top face of the chip) and two “interface” (the jet is directed in the chip-tool interface. The position of the nozzle was precisely identified by a distant camera. With this experimental setup 84 orthogonal cutting tests were carried out: 72 tests with two cutting speed, two feed rates, two air jet pressure (4 and 7 bar), two holes for the thermocouple and four positions of the nozzle; 12 tests for the pressure sensitivity analysis. The intent of the experimental campaign was to provide a set of test where one parameter only for each test was changed, compared to all the other tests, in order to understand the behaviour of air jet cooling. The set of tests was compared to the finite element model and to the analytical model

The finite element simulations

The commercial software DEFORM in its 2D and 3D version was used for the finite element modeling. Thermal and mechanical boundary conditions were used, in order to reproduce by 2D finite element simulations the tests carried out in the experimental analysis. The results of the 2D finite element simulations provide information that cannot

be obtained by experimental tests, such as the effective stress within the insert and the workpiece. From a mechanical point of view, the air jet causes an increment of the local stress in the workpiece when the pressure is applied in the interface position. In this way, the elastic deformation of the chip due to the air jet promotes a rotation in the chip, so that the curvature is slightly increased. On the other hand, when the pressure is applied in the overhead position on the top face of the chip, the curvature is reduced and the effective stress within the workpiece is reduced too, next to the shear zone.

Similar behavior is observed in the stresses within the tool. By increasing the pressure the mechanical effect of the air jet in terms of effective stress is increased. Also the mechanical effect of the air jet depends on the length of the chip, since the air jet can apply the pressure on an area that varies with the length of the chip. If only the mechanical effect is considered, the variation of effective stress is translated, in terms of cutting temperature, into a reduction of the temperature when the air jet is in the overhead position (increased radius of curvature, decreased effective stress), and an increase of temperature when the air jet is positioned in the interface (reduced radius of curvature, increased effective stress). The overall result of the finite element simulations is a combination of the mechanical and thermal contributions. The observations in terms of stress were useful for formulating an analytical model of the mechanical and thermal effects of the air jet.

The analytical model

The analytical model uses the strain, the strain rate and the stress in the shear zone calculated by FE modeling as an input. The purpose of the analytical model is the understanding of the physics of the mechanical effect of the air jet, an estimation of the thermal effect and the overall cooling effect of the air jet during machining. The model uses the approach of Shaw [37] and Jaeger [40] for calculating the specific shear energy and the specific friction energy, and subsequently the temperature rise by estimating the heat partitioning coefficients. The results from the finite element simulations are used in the analytical model to introduce the elastic deformation energy due to the air jet impinging on a curved surface (the chip), and the heat transfer coefficient is estimated by using correlations for the Nusselt number. However a better heat transfer coefficient is

provided by the experimental measurements of Goldstein et al. [109]. The analytical model reproduces the behavior shown by the finite element model, as explained in section 4.4. Since the effect of the air jet depends on the length of the chip, the maximum and the minimum length were both considered in the model.

7.3 Results

Chapter 6 shows the comparative results of the finite element simulations with the results from the analytical model and the experimental tests in terms of feed force, cutting force and mean temperature of the interface. The results show minimal changes in terms of feed force and cutting force. The interface temperature calculated by the analytical model (temperature rise), by finite elements (maximum interface temperature) and obtained by experimental tests (k-type thermocouple) are shown and summarised in the following figure.

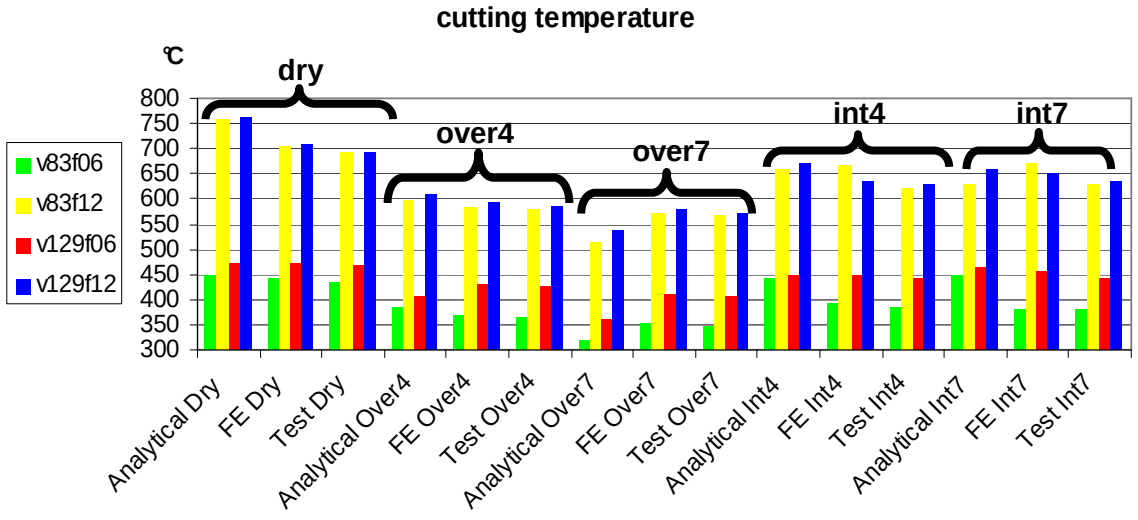

Figure 7.1 – The cutting temperature predicted by the analytical model and the finite elements model is compared to the experimental tests results for different cutting and cooling conditions. The results are grouped by colour (cutting condition) and by cooling condition

The Figure 7.1 shows the results in terms of interface temperature for different cooling conditions:

- dry cutting
- nozzle in overhead position, 4 bar
- nozzle in overhead position, 7 bar
- nozzle in interface position, 4 bar
- nozzle in interface position 7 bar

The figure shows four cutting conditions, grouped by colours:

- green : v = 83 m/min, t = 0.06 mm/rev
- yellow : v = 83 m/min, t = 0.12 mm/rev
- red : v = 129 m/min, t = 0.06 mm/rev
- blue : v =129 m/min, t = 0.l2 mm/rev

where *v* is the cutting speed and *t* is the feed rate. The results show good agreement between the finite element simulations and the experimental tests. Also, the analytical model follows the same trends as the results by FE and tests, which suggests that the phenomena are correctly modeled. The results show an increase of the cooling performance of the air jet when the nozzle is in the overhead position. When the air jet is directed into the interface, the mean decrease of temperature is 10.7% of the interface temperature in dry cutting. When the nozzle is in the overhead position, the mean decrease of the temperature is 16.2% for 4 bar, 18.9% for 7 bar .

The use of the nozzle in the overhead position improves the cooling performance of the air jet. The analysis carried out by finite elements supports the theoretical analysis and provides data for the development of an analytical model. Analytical investigations explain the advantage in terms of cutting temperature with a local reduction of stress in the shear zone. With these results in mind, the mechanical effect of the air jet can be considered as an external source of energy introduced in the cutting area. In the contect of introducing external sources of energy, the literature review presents alternatives such as high power laser assisted machining (LAM) as the practical way of heating the workpiece just before the cut is taken. The main effects of this technique are the change of phase of

the workpiece material in the shallow layers of the workpiece material and a beneficial alteration of the state of stress. In a broadly similar manner, the mechanical effect of the air jet is also locally altering the state of stress with a bending moment on the chip. While the effect of the air jet can not be directly compared to the effect of LAM, it can be considered as another approach in energy assisted machining.

The analytical model corresponds to the physics of the problem, and also the trends shown in the analytical modelling follow the trends of the experimental tests and finite element modelling. This provides confidence in the approach and opens the field for more in-depth investigations into particular aspects, for example in-depth focus on finite element correlation with experimental, or in-depth analysis on influence of impinging air jet on the chip all of which could form further research.

In conclusion:

- Low pressure air jets were shown to provide effective cooling of orthogonal turning
- An approximate theoretical model of the process shows how cooling can be optimised by correctly positioning the air jet
- The trends predicted by the theoretical model were confirmed by finite element simulations and experimental tests
- The results of the finite element model show the mechanical effect of the air jet produce local variation of the effective stress in the cutting zone
- The embedded thermocouple technique was found to be a reliable method of measuring cutting temperature if correctly calibrated

7.4 Further research

Considering that the research work undertaken and presented in this thesis provides a foundation for the approach of using air jets to assist cutting, future work should address a number of areas of interest, notably:

- Detailed finite element investigations and correlation of finite element with experimental data. This should include a detailed analysis of the sensitivity of the concept to parameter changes, tools and materials

- Detailed finite element, analytical and experimental investigation focussing on the embedded thermocouple as a temperature measurement technique. This work could also consider alternative temperature measurement techniques such as radiation for temperature measurement
- Detailed investigation into the fluid-dynamics of the air jet impinging on the chip and in the cutting zone.

Most of the simplifications introduced concerning the effects of the air jet on the overall process are to do with the difficulties of estimating the fluid-dynamic field in the cutting area when a compressible flow impinges upon the chip and the rake face during the cutting process. The problem of a fluid-structure interaction can be solved by direct numerical simulation (DNS) only for simple geometries and with many simplifications.

Finally future work should consider the technoeconomic considerations of this technique as well as the potential to apply this technique to other applications such as milling.

References

[1] Byrne, G., Dornfeld, David, Denkena, B., *Advancing cutting technology*, CIRP Annals - Manufacturing Technology, vol.52/2, 2003, pp.483-507

[2] Byrne, G., *Recent Developments in High Performance Cutting (Summary of CIRP Working Group Activities)*, CIRP Conference 2004 (electronic resource)

[3] Klocke, F., Eisenblätter, G.,1997, *Dry Cutting*, CIRP Annals – Manufacturing Technology, vol.46/2, 1997, pp.1-7

[4] Weinert, K, Inasaki I, Sutherland, J.W., Wakabayashi T., *Dry machining and minimum quantity lubrication*. CIRP Annals – Manufacturing Technology, vol.53/2, 2004, pp.511–537

[5] Klocke, F., Essel, I., *Basics of HPC and Mechanical and Thermal Characteristics*, Laboratory of Machine Tools and Production Engineering (WZL), RWTH Aachen, Germany, CIRP Conference 2004 (electronic resource)

[6] Pusavec, F, et al., *Transitioning to sustainable production – Part I: application on machining technologies*, Journal of Clean Production (2009), doi:10.1016/j.jclepro.2009.08.010 (article in press)

[7] Jegatheesan, V., Liow, J.L., Shu, L., Kim, S.H., Visvanathan, C., *The need for global coordination in sustainable development*, Journal of Cleaner Production, vol 17/7, 2009, pp.637–643

[8] Takeyama, H., Murata, T., *Basic investigations on tool wear*, Transaction of ASME J. Eng. Ind., vol.85, 1963, pp. 33-38

[9] O'Sullivan, D., Cotterell, M.G., *Temperature measurement in single point turning*, Journal of Materials Processing Technology, vol.118, 2001, pp.301-308

[10] Dawson, T.G., Kurfess, Thomas R., *Tool life, wear rates and surface quality in hard turning*, The George W. Woodruff School of Mechanical Engineering, Georgia Institute of Technology, eScholarship Repository, Copyright by the authors, 2006

[11] El-Hossainy, T.M., *Tool wear monitoring under dry and wet machining*, Materials and Manufacturing processes, vol.16/2, 2001, pp.165-176

[12] Wright, P.K., Horne, J.G., Tabor, D., *Boundary conditions at the chip-tool interface in machining: comparisons between seizure and sliding friction*, Wear, Vol. 54, 1979, pp. 371-90

[13] Childs, T.H.C. and Rowe, G.W., *Physics in metal cutting*, Reports on Progress in Physics, Vol. 36, 1973, pp.223-238

[14] Grzesik, W., *Friction behaviour of heat isolating coatings in machining: mechanical, thermal and energy-based considerations*, International Journal of Machine Tools and Manufacture, vol.43, 2003, pp.145-150

[15] Renevier, N.M., Oosterling, H., Konig, U., Dautzenberg, H., Kim, B.J., Geppert, L., Koopmans, F.G.M., Leopold, J., *Performance and limitations of MoS_2/Ti composite coated inserts*, Surface and Coatings Technology, vol.172/1, 2003, pp.13-23

[16] Da Silva, F.J., Franco, S.D., Machado, A.R., Ezugwu, E.O., Souza, Jr. A.M., *The performance of cryogenically treated HSS tools*, Wear, vol. 261, 2006, pp.674–685

[17] Paul, S., Dhar, N.R., Chattopadhyay, A.B., *Beneficial effects of cryogenic cooling over dry and wet machining on tool wear and surface finish in turning AISI 1060 steel*, Journal of Materials Processing Technology, vol.116, 2001, pp.44-48

[18] Atmadi, A., Stephenson, D.A., Liang, S.Y., *Cutting fluid aerosol from splash in turning: analysis for environmentally conscious machining*, International Journal of Advanced Manufacturing Technology, vol.17, 2001, pp.238-243

[19] Friedman, M.Y., Lenz, E., *Investigation of the tool-chip contact length in metal cutting*, International Journal of Machine Tool Design and Research, vol.10/4, 1970, pp.401-416

[20] Umbrello, D., Filice, L., Rizzuti, S., Micari, F., *On the evaluation of the global heat transfer coefficient in cutting*, International Journal of Machine Tools and Manufacture, vol.47, 2007, pp.1738–1743

[21] Özel, T., Altan, T., 2000, *Determination of workpiece flow stress and friction at the chip-tool contact for high-speed cutting*, International Journal of Machine Tools and Manufacture, vol.40/1, pp.133-152

[22] Kou, S., Sun, D.K., Le, Y.P., *A fundamental study of laser transformation hardening*. Metallurgical Transactions, Vol. 14A. April 1983, pp. 643-653

[23] Gratias, J.F., Fan, L.J., Marot, G., Cohen, P., Moisan, A., Chitenay-Malabry, E.C.P., *Proposition of a Method to Optimize the Machining of XC42 Steel with Laser Assistance*, E.N.S.A.M., Aix-en-Provence/France, January 1993, pp. 116-118

[24] Jau, B.M., *Laser assisted Machining of hard to machine materials*. Dissertation, Faculty of the graduate School. University of South California, 1981

[25] Pfefferkorn, F., Jeon, Y., *Effect of laser preheating the workpiece on micro end milling of metals*, Journal of manufacturing science and engineering, vol. 130, 2008

[26] Baker, M., *Does chip formation minimize the energy?*, Computational Materials Science, vol. 33/4, 2005, pp. 407-418

[27] Wertheim, R., Rotberg, J., Ber, A., *The influence of high-pressure flushing throughthe rake face of the cutting tool*, CIRP Annals – Manufacturing Technology, vol.41/1, 1992, pp.101–106

[28] Merchant, M.E, *Principles of metal cutting*, Die Casting, vol.4, 1946, pp.59-66

[29] Merchant, M.E., *Mechanics of the metal cutting process*, Journal of Applied Physics, vol.6, 1945, pp.267-318

[30] Kececioglu, D., *Shear-Strain Rate in Metal Cutting and Its Effects on Shear-Flow Stress*, Transactions of ASME, vol.80, 1958, pp. 158–168

[31] Oxley, P.L.B., Hastings, W.F., Proceedings of Royal Society of London, vol. 356 A, 1977, p.395

[32] Hastings, W.F., Mathew, P., Oxley, P.L.B., *A machining theory for predicting chip geometry, cutting forces etc. from work material properties and cutting conditions*, Proceedings of the Royal Society of London. Series A, Mathematical and Physical Sciences, vol. 371/1747, 1980, pp. 569-587

[33] Oxley, P.L.B., *International research in production engineering*, ASME, 1963, p.50

[34] Mackenzie, I., *Strain energy function for large deformations of curved beams*, PhD thesis, University of Waterloo, Canada, 2008

[35] Shaw, M.C., *Temperatures in Cutting*, ASME Winter Annual Meeting, vol. 30, 1988, pp.133-143

[36] Leowen, E.G., Shaw, M.C., *On the analysis of cutting tool temperatures*, Transactions of ASME, vol.71, 1954, pp.217-231

[37] Leone, W.C., *Distribution of shear zone heat in metal cutting*, Transactions of ASME, vol. 76, 1954, pp. 121-125

[38] Jaeger, J.C., *Moving sources of heat and the temperatures of sliding contacts*, Proceedings of Royal Society N.S.W., vol.76, 1942, pp.203-204

[39] Li, K.-M., Liang, S.Y., *Modeling of Cutting Temperature in Near Dry Machining*, Transactions of ASME, vol.128, 2006, pp.416-424

[40] Abdel-Aal, H.A., *A remark on the flash temperature theory*, Heat Mass Transfer, vol.24/2, 1997, pp.241-250

[41] Diniz, A.E., Micaroni, R., *Influence of the direction and flow rate of the cutting fluid on tool life in turning process of AISI 1045 steel*, International Journal of Machine Tools and Manufacture, vol.47/2, 2007, pp.247-254

[42] Ren, X. J., Yang, Q.X., James, R.D., Wang L., *Cutting temperatures in hard turning chromium hardfacings with PCBN tooling*, Journal of Materials Processing Technology, vol.147, 2004, pp.38-44

[43] Konig, W., Berktold, A., and Kock, K. F., *Turning versus Grinding-A comparison of Surface Integrity Aspects and Attainable Accuracies*, Annals of the CIRP, vol.42, 1993, pp.39-43

[44] Fifty Years of CIRP: "Its Origins, Its Objectives, Its Achievements", 51st CIRP General Assembly, Nancy, France, August 2001

[45] Jovane, F., Westkamper, E., Williams, D., *The manufacturing future road*. Berlin Heidelberg: Springer-Verlag; 2009

[46] Jawahir, I.S., Dillon, Jr. O.W., *Sustainable manufacturing processes: new challenges for developing predictive models and optimization techniques*, Proceedings of the first international conference on sustainable manufacturing, Montreal, Canada, 2007, pp. 1–15

[47] Gutowski, T., Murphy, C., Allen, D., Bauer, D., Bras, B., Piwonka, T., *Environmentally benign manufacturing: observations from Japan, Europe and the United States*, Journal of Cleaner Production vol.13/1, 2005, pp.1–17

[48] Jawahir, I.S., Dillon, Jr. O.W., *Sustainable manufacturing processes: new challenges for developing predictive models and optimization techniques*, Proceedings of the first international conference on sustainable manufacturing SM1. Montreal, Canada; 2007, pp. 1–15

[49] Ernst, H., *Fundamental Aspects of Metal Cutting and Cutting Fluid Action*, Annals of the New York Academy of Sciences, vol.53, 1951, pp.936-961

[50] Taylor, F.W., *On The Art of Cutting Metals*, Transactions, American Society of Mechanical Engineers, vol.28, 1906, pp.70-350

[51] Oraby, S.E., Hayhurst, D.R., *Tool life determination based on the measurement of wear and tool force ratio variation*, International Journal of Machine Tools and Manufacture, vol.44, 2004, pp.1261-1269

[52] Machado, A.R., Wallbank, J., *The effect of extremely low lubricant volumes in machining*, Wear, vol.210, 1997, pp.76-82

[53] Hoff, M.L., *Cutting Fluid Developments to Meet the Demands High Performance Machining Operations*, CIRP Conference on High Performance Cutting, Aachen, 2004

[54] Nakayama, K., *Chip Curl in Metal Cutting Process*, Bulletin of the Faculty of. Engineering, Yokohama National University, vol. 1, 1962, pp. 1 – 13

[55] Hill, R., *The Mathematical Theory of Plasticity*, Clarendon Press, Oxford, 1950

[56] Sales, W.F., Guimara, G., Machado, A.R., Ezugwu, E.O., *Cooling ability of cutting fluids and measurement of the chip-tool interface temperatures* - Industrial Lubrication and Tribology, vol. 54/2, 2002, pp. 57–68

[57] De Chiffre, L., *Testing the overall performance of cutting fluids*, Lubrication Engineering, vol.34/5, 1978, pp.244-51

[58] Da Silva, M.B., Wallbank, J., *Lubrication and application method in machining*, Industrial Lubrication and Tribology , vol.50/4, 1998, pp.149-152

[59] Quinn, L.J., *Metal working fluids - at the cutting edge of health and safety*, ASTM Standardisation News, May 1992, pp.40-43

[60] Davies, M. A., Ueda, T., M'Saoubi, R., Mullany, B., Cooke, A.L., *On The Measurement of Temperature in Material Removal Processes*, Annals of the CIRP Vol. 56, 2007, pp. 581-604

[61] Abukhshim, N.A., Mativenga, P.T., Sheikh, M.A., *Heat generation and temperature prediction in metal cutting: A review and implications for high speed machining*, International Journal of Machine Tools and Manufacture, vol.46, 2006, pp.782-800

[62] Liu, X.L., Wen, D.H., Li, Z.J., Xiao, L., Yan, F.G., *Cutting temperature and tool wear of hard turning hardened bearing steel*, Journal of Material Processing Technology, vol.129, 2002, pp.200-206

[63] Seah K.H.W., Li X., Lee K.S., *The effect of applying coolant on tool wear in metal machining*, Journal of Materials Processing Technology, vol.48/1, 1995, pp.495-501

[64] Al Huda, M., Yamada, K., Hosokawa, A., Ueda, T., *Investigation of temperature at tool-chip interface in turning using two-color pyrometer*, Transactions of ASME, vol.124, 2002, pp.200-207

[65] Dahlman P., *Comparing the temperature reduction in high-pressure jet assisted turning using high pressure versus high flow*, Journal of Engineering Manufacture, vol.216/4, 2002, pp. 467–473

[66] Dahlman, P., Escursell, M., *High-pressure jet-assisted cooling: a new possibility for near net shape turning of decarburized steel* - International Journal of Machine Tools & Manufacture, 2004, vol. 44, pp. 109–115

[67] Shaw, M.C., 1984, *Metal Cutting Principles*

[68] Diniz, A.E., Ferreira, J.R., Filho, F.T., *Influence of refrigeration/lubrication condition on SAE 52100 hardened steel turning at several cutting speeds* - International Journal of Machine Tools and Manufacture vol. 43, 2003, pp. 317–326

[69] Minekawa, H., Inasaki, I., Nakamura, M., Suzuki, S., Kamina, T., Yokota, H., *Cutting with Minimal Quantity Lubrication. Fundamental Research on the Milling Process*, Transactions of the Japan Society of Mechanical Engineers, vol.66/646, 2000, pp.2054-2059

[70] Rahman, M., Senthil Kumar, A., Salam, M.U., *Experimental evaluation on the effect of minimal quantities of lubricant in milling*, International Journal of Machine Tools and Manufacture, vol.42/5, 2002, pp.539-547

[71] Attanasio, A., Gelfi, M., Giardini C., Remino, C., *Minimal quantity lubrication in turning: Effect on tool wear*, Wear, vol.260/3, 2006, pp.333-338

[72] Varadarajan, A.S., Philip, P.K., Ramamoorthy, B., *Investigations on hard turning with minimal cutting fluid application (HTMF) and its comparison with dry and wet turning*, International Journal of Machine Tools and Manufacture, vol.42/2, 2002, pp.193-200

[73] Vikram Kumar, C.R., Ramamoorthy, B., *Performance of coated tools during hard turning under minimum fluid application*, Journal of Materials Processing Technology, vol.185, 2007, pp.210-216

[74] Han, R., Liu, J., Sun, Y., *Research on experimentation of green cutting with water vapor as coolant and lubricant* - Journal of Tribology. (Transactions of the ASME) [ISSN 0036-8792], 1999

[75] Rahman, M., Senthil Kumar, A., Manzoor-Ul-Salam, Ling, M. S., *Effect of Chilled Air on Machining Performance in End Milling*, International Journal of Advanced Manufactoring Technology, vol. 21, 2003, pp. 787–795

[76] Çakir, O., Kiyak M., Altan, E., *Comparison of gases applications to wet and dry cuttings in turning*, Journal of Materials Processing Technology, vol.153-154, 2004, pp.35-41

[77] Diniz, A.E., Micaroni, R., *Cutting conditions for finish turning process aiming: the use of dry cutting*, International Journal of Machine Tools and Manufacture, vol.42, 2002, pp.899–904

[78] Stevens, J., Webb, B.W., *The effect of inclination on local heat transfer under an axisymmetric, free liquid jet*, International Journal of Heat and Mass Transfer, vol.34/4-5, 1991, pp.1227-1236

[79] Elison, B., Webb, B.W., *Local heat transfer to impinging liquid jets in the initially laminar, transitional, and turbulent regimes*, International Journal of Heat and Mass Transfer, vol.37/8, 994, pp.1207-1216

[80] O'Donovan, T., *Fluid flow and heat transfer of an impinging air jet* – Mechanical and Manufactoring Engineering, Trinity College Dublin, 2005, PhD thesis

[81] Li, X.P.*Study of the jet-flow rate of cooling in machining*, Journal of Materials Processing Technology, vol. 62, 1996, pp. 149-156

[82] Su, Y., He, N., Li, L., Iqbal, A., Xiao, M.H., Xu, S., Qiu, B.G., *Refrigerated cooling air cutting of difficult-to-cut materials*, International Journal of Machine Tools and Manufacture, vol.47/6, 2007, Pages 927-933

[83] Li, X.P., Seah, K.H.W., *A pressured air jet approach to tool wear minimization in cutting of metal matrix composites*, Wear, vol.255, 2003, pp.1352–1358

[84] Davim, J.P., *Application of Merchant theory in machining particulate metal matrix composites*, Materials and Design, vol.28, 2007, pp.2684–2687

[85] Ezugwu, E.O., *High speed machining of aero-engine alloys*, Journal of the Brazilian Society of Mechanical Science and Engineering, vol. 26/1, 2004, pp. 1-11

[86] Dekumbis. R., *Traitement de surface par laser C02 de haute puissance*. La Technique Moderne. Janvier -Fevrier. 1987, p. 23-28

[87] El-Sheikh, H.A., Garimella, S.V., *Enhancement of air jet impingement heat transfer using pin-fin heat sinks*, IEEE Trans. Compon. Packag. Technol., vol.23, 2000, pp. 300–308

[88] Röger, M., Buck, R., Müller-Steinhagen, H., *Numerical and experimental investigation of a multiple air jet cooling system for application in a solar thermal receiver*, Int. Journal of Heat Transfer, vol.127, 2005, pp.863-876

[89] O'Donovan, T.S., Murray, D.B., Torrance, A.A., *Jet heat transfer in the vicinity of a rotating grinding wheel*, Proceedings of I.Mech.E. Part C – Journal of Mechanical Engineering Science, vol.220, 2006, pp.837-845

[90] Babic, D.M., Murray, D.B., Torrance, A.A., *Mist jet cooling of grinding processes*, International Journal of Machine Tools and Manufacture, vol.45, 2005, pp.1171-1177

[91] Gillespie D.R.H., Byerley A.R., Ireland P.T. and Kohler S.T., *Detailed measurement of local heat transfer coefficients in the entrance to normal and inclined film cooling holes*, ASME, 1994, paper no. 94-GT-1

[92] Ekkad, S.V., Ou, S., Rivir, R.B., *A transient infrared thermography method for simultaneous film cooling effectiveness and heat transfer coefficient measurements from a single test*, ASME, vol.126, 2004, pp.597-603

[93] Martinez-Botas, R.F., Lock, G.D., Jones, T.V., *Heat transfer measurements in an annular cascade of transonic gas turbine blades using the transient liquid crystal technique*, ASME, 1994, paper no. 94-GT-172

[94] Da Silva, M.B, Wallbank, J., *Cutting temperature: prediction and measurement methods—a review*, Journal of Materials Processing Technology, vol.88, 1999, pp.195–202

[95] Kops, L., Arenson, M., *Convective heat transfer coefficients in turning*, Proceedings of 15th Brazilian Congress of Mechanical Engineering, 1999

[96] Altan, T., Sartkulvanich, P., Al-Zkeri, I., *Status of FEM in Modeling of High Speed Cutting*, CIRP conference 2006 (electronic resource)

[97] Potdar, Y.K., Zehnder, A.T., *Measurements and Simulations of Temperature and Deformation Fields in Transient Metal Cutting*, Journal of Manufacturing Science and Engineering, vol.125, 2003, pp.645-655

[98] Fischer, C.E., Wu, W.T., *Industrial Applications of Finite Elements Analysis for Metal Cutting*, CIRP conference 2006 (electronic resource)

[99] Fischer, Christian E., Mylavaram, Nikhilesh K. R., *Design and Simulation of Cutting Tools*, CIRP Conference 2004 (electronic resource)

[100] Grzesik, W., Bartoszuk, M., Nieslony, P., *Finite element modelling of temperature distribution in the cutting zone in turning processes with differently coated tools*, Journal of Materials Processing Technology, vol.164, 2005, pp.1204-1211

[101] Özel, T., *Influence of friction models on finite element simulations of machining*, International Journal of Machine Tools and Manufacture, vol.46/5, 2006, pp.518-530

[102] Mackerle, J., *Finite element analysis and simulation of machining: an addendum a bibliography (1996-2002)*, Journal of Material Processing Technology, vol.43, 2003, pp.103-114

[103] Yen, Y.-C., Söhner, J., Lilly, B., Altan, T., *Estimation of tool wear in orthogonal cutting using the finite element analysis*, Journal of Materials Processing Technology, vol.146, 2004, pp. 82–91

[104] Shet, C., Deng, X., Bayoumi, A.E., *Finite element simulation of high-pressure water-jet assisted metal cutting*, International Journal of Mechanical Sciences, vol.45, 2003, pp.1201–1228

[105] Childs, P. R. N., *Practical temperature measurement*, Butterworth-Heinemann, Oxford, Woburn, 2001

[106] Stephenson, D. A., *Tool-work thermocouple temperature measurements - theory and implementation issues*, Journal of Engineering for Industry, vol.115, 1993, pp.432-437

[107] Davies, M.A., Yoon, H., Schmitz, T.L., Burns T.J., Kennedy, M.D., *Calibrated thermal microscopy of the tool-chip interface in machining*, Machining Science and Technology., vol.7/2, 2003, pp.167-190

[108] Chen, W.-C., Tsao, C.-C., Liang, P.-W., *Determination of temperature distributions on the rake face of cutting tools using a remote method*, Int. Comm. HeatMass Transfer, vol.24/2, 1997, pp.161-170

[109] Attia, M. H., Kops, L., *Distortion in thermal field around inserted thermocouples in experimental interfacial studies*, Journal of Engineering for Industry, vol.108, 1986, pp.241-246

[110] Attia, M. H., Kops, L., *Distortion in Thermal Field Around Inserted Thermocouples in Experimental Interfacial Studies - Part 2: Effect of the Heat Flow Through the Thermocouple*, Journal of Engineering for Industry, vol.110, 1988, pp.7-14

[111] Attia, M. H., Kops, L., *Distortion in the thermal field around inserted thermocouples in experimental interfacial studies - Part 3: Experimental and numerical verification*, Journal of Engineering for Industry, vol.115, 1993, pp.444-449

[112] Attia, M. H., Cameron, A., Kops, L., *Distortion in the thermal field around inserted thermocouples in experimental interfacial studies, Part 4: End effect*, Transactions of ASME, Journal of Manufacturing Science and Engineering, vol.124, 2002, pp.135-145

[113] Grzesik, W., *Experimental investigation of the cutting temperature when turning with coated indexable inserts*, International Journal of Machine Tools and Manufacture, vol.39, 1999, pp.355–369

[114] Ay, H., Yang, W.J., Yang, J.A., 1994, *Dynamics of cutting tool temperatures during cutting process*, Experimental Heat Transfer, vol.7/3, 1994, pp.203-216

[115] Ay, H., Yang, W.-J., *Heat transfer and life of metal cutting tools in Turning*, Int. J. Hear Mass Transfer, vol.41/3, 1998, pp.613-623, 1998

[116] Barlier, C. Lescalier, C., Moisan, A., *Continuous flank wear measurement of turning tools by integrated microthermocouple*, 47th Annal of CIRP, vol. 46/1, 1997, pp. 35–38

[117] Barlier, C. Lescalier, C., Muller, J.M., Delebecque, B., *Mesure en continu de l'usure des outils de coupe par microsondes incorporées—Acquisition par Capteur de Température Appliquée à la Recherche de l'Usure—Le système ACTARUS*, First International Conference on Integrated Design and Manufacturing in Mechanical Engineering, Nantes, April 1996.

[118] Barlier, C., Procédé pour la détection directe, en continu, de l'usure des outils de coupe par sonde électrique incorporee, Brevet BARLIER no. 87 07969 (France) and 88-470021-2 (Europe)

[119] Lazard, M., Corvisier, P., *Modelling of a tool during turning - Analytical prediction of the temperature and of the heat flux at the tool's tip*, Applied Thermal Engineering, vol, 24, 2004, pp.839–849

[120] Sutter, G.,Ranc, N.,*Temperature fields in a chip during high-speed orthogonal cutting-An experimental investigation*, International Journal of Machine Tools & Manufacture, vol.47, 2007, pp.1507-1517

[121] Komanduri, R., Hou, Z.B., *A review of the experimental techniques for the measurement of heat and temperatures generated in some manufacturing processes and tribology*, Tribology International, vol. 34, 2001, pp. 653–682

[122] Pelosi, G., The finite-element method, Part 1: R.L.Courant [Historical Corner], *Antennas and Propagation Magazine*, Vol 49/2, 2007, pp.180-182

[123] Gardner, J.D., Vijayaraghavan, A., Dornfeld, D.A., *Comparative Study of Finite Element Simulation Software*, eScholarship Repository, University of California, Copyright 2005 by the authors

[124] Sandvik Coromant machining manual, 2008

[125] DEFORM 3D v6.1 User Manual, *Scientific Forming Technologies Corporation*, Columbus, Ohio, Oct. 2007

[126] Dessoly V., *Modeling and verification of cutting tool temperatures in rotary tool turning of hardened steel*, 2004, master degree thesis in Mechanical Engineering, Georgia Institute of Technology

[127] Lee, E. H., and Shaffer, B. W, *The Theory of Plasticity Applied to a Problem of Machining*, Journal of Applied. Mechanics, vol. 18, 1951, pp. 405–413

[128] Das, N.S., Chawla, B.S., Biswas, C.K., *An analysis of strain in chip breaking using slip-line field theory with adhesion friction at chip/tool interface*, Journal of Materials Processing Technology, vol.170, 2005, pp.509–515

[129] Cooke, W.B.H., Rice, W.B., *Mechanics of deformation in the machining process*, Canadian Mining Journal, 1973, pp.145-158

[130] Gau, C. and Chung, C.M., *Surface Curvature Effect on Slot-Air-Jet Impingement Cooling Flow and Heat Transfer Process*, Transaction of the ASME, vol. 113, 1991, pp. 858–864

[131] Spaans, C., *The fundamental of three-dimensional chip curl, chip-breaking and chip control*, Dissertation, Delft Technical University, Netherlands, 1971

[132] Ernst, H., Merchant, M.E., *Chip formation, friction and high quality machined surfaces*, Transactions of American Society for Metals, vol.29, 1941, pp.299-378

[133] Shin, Y. C., Kim, J. N., *Plasma Enhanced Machining of Inconel 718,* ASME International Mechanical Engineering Congress and Exposition, Atlanta, Vol. MED-4, 1996, pp, 243–249

[134] Crafoord, R., Kaminski, J., Lagerberg, S., Ljungkrona, O.,Wretland, A., *Chip control in tube turning using a high-pressure water jet*, Proceedings of the institution of mechanical engineers, part B. Journal of Engineering Manufacture, vol.213/B8, 1999, pp.761–767

[135] Kaminski, J., Ljungkrona, O., Crafoord, R., Lagerberg, S., *Control of chip flow direction in high pressure water jet assisted orthogonal tube turning*, Proceedings of the Institution of Mechanical Engineers, Part B. Journal of Engineering Manufacture, vol.214/B7, 2000, pp.529–534

[136] Kalpakjian, S., *Manufacturing engineering and technology*, Fourth Ed.,

Addison-Wesley Publishing Company, 1995

[137] Tounsi, N., Vincenti, J., Otho, A., Elbestawi, M.A., *From the basic mechanics of orthogonal metal cutting toward the identification of the constitutive equation*, International Journal of Machine Tools and Manufacture, vol.42, 2002, pp.1373-1383

[138] Usui, E., Shirakashi, T., *Mechanics of machining -from descriptive to predictive theory. In on the art of cutting metals-75 years later*, ASME Publication PED 7, 1982, pp. 13-35

[139] Merchant, M.E., Moehring, S.M., *An interpretative review of 20th century US machining and grinding research*, e-Monograph on a Notable Chapter in the Lore of Machining Process Technology, TechSolve, Inc.Cincinnati, Ohio, USA, 2003

[140] Trent, E.M., *Metal Cutting*, London, Butterworths, 1977

[141] Zorev, N.N., *Metal Cutting Mechanics*, Pergamon Press, Oxford, 1966

[142] Toropov, A. and Ko S.L., *Prediction of tool-chip contact length using a new slip-line solution for orthogonal cutting*, International Journal of Machine Tools and Manufacture, vol.43/12, 2003, pp.1209-1215

[143] Toropov,A. and Ko, S.-L., *Prediction of shear angle for continuous orthogonal cutting using thermo-mechanical constants of work material and cutting conditions*, Journal of Materials Processing Technology, vol.182/1-3, 2007, pp.167-173

[144] Lin, Z.-C., Lo, S.-P., *A study of the tool-chip interface contact problem under low cutting velocity with an elastic cutting tool*, Journal of Materials Processing Technology, vol.70, 1997, pp.34-46

[145] Blok, H., *Theoretical Study of Temperature rise at surfaces of actual contact under oiliness conditions*, Proceedings of Institute of Mechanical Engineering General Discussion on Lubrication, Institute of Mechanical Engineering London, 1937, pp.222-223

[146] Piispanen, V., *Plastic deformation of metal: Theory of simulated sliding* Wear, vol.38/1, 1976, pp.43-72

[147] Piispanen, V., *Lastunmuodostumisen Teoriaa*, Teknillinen Aikakauslehti (On the Theory of Chip Formation), vol.287, 1937, pp.315-322

[148] Yu, T.X., Hua, Y.L., Johnson, W., *The plastic hinge position in a circular cantilever when struck normal to its plane by a constant jet at its tip,* International Journal of Impact Engineering, vol. 3, 1985, pp. 143-154

[149] Incropera, F.P., De Witt, D.P., *Introduction to Heat Transfer*, John Wiley & Sons, 1996

[150] Sparrow, E.M., Lovell, B.J., *Heat Transfer Characteristics of an Oblique Impinging Circular Jet*, Transaction of ASME, vol. 102, 1980, pp. 202–209

[151] Tawfek, A.A., *Heat Transfer Studies of the Oblique Impingement of Round Jets upon a Curved Surface*, Heat and Mass Trans., vol. 38, 2002, pp. 467–475

[152] Wu, J., Tang, L., Luke, E.A., and Tong, X., A Comprehensive Numerical Study of Jet Flow Impingement over Flat Plates at Varied Angles, AIAA, 2001, p.745

[153] Hrycak, P., *Heat Transfer From a Row of Impinging Jets to Concave Cylindrical Surfaces*, Intl. J. Heat and Mass Trans., vol. 24, 1981, pp. 407–419

[154] Merchant, M. E., *Basic Mechanics of the Metal Cutting Process*, Journal of Applied Mechanics, vol.11, 1944, pp.168-175

[155] Adibi-Sedeh, A.H., Madhavan, V., Bahr, B., *Extension of Oxley's analysis of machining to use different material models*, ASME Journal of Manufacturing Science and Engineering, vol.125, 2003, pp.656-666

[156] Smithey, D.W., Kapoor, S.G., DeVor, R.E., *A new mechanistic model for predicting worn tool cutting forces*, Machining Science and Technology, vol.5/1, 2001, pp.23-42

[157] Trigger, K.J., Chao, B.T., *An analytical evaluation of metal cutting temperatures*, Transactions of ASME, vol. 73, 1951, pp. 57-68

[158] Usui, E., Hirota, A., Masuko, M., *Analytical prediction of three dimensional cutting process. Part 3. Cutting temperature and crater wear of carbide tool*, Transactions of ASME, vol.100, 1978, pp.222-228

[159] Shigeru M., Toshiaki, S.G., Takemasa, K., Shen, Y., *Study on the characteristics of supersonic Coanda jet*, Journal of Thermal Science, Vol.7(3), 1998, pp.165-175

[160] Carpenter, P.W., Green, P.N., *The aeroacoustics and aerodynamics of high-speed Coanda devices, Part 1: conventional arrangement of exit nozzle and surface*, Journal of Sound and Vibration, vol.208/5, 1997, pp.777-801

[161] Carpenter, P.W., Smith, C., *The aeroacoustics and aerodynamics of high-speed Coanda devices, Part 2: effects of modifications for flow control and noise reduction*, Journal of Sound and Vibration, vol.208/5, 1997, pp.803-822

[162] Li,P., Halliwell, N.A., *Industrial jet noise: Coanda Nozzles*, Journal of Sound and Vibration, vol.99(4), 1985, pp.475-491

[152] Goldstein, R. J., Behbahani, A. I., Heppelmann, K., *Streamwise distribution of the recovery factor and the local heat transfer coefficient to an impinging circular air jet*, International Journal of Heat and Mass Transfer, vol.29, 1986, pp.1227-1235

[164] Baron, A., *Alcune note sul corso di fluidodinamica*, Politecnico di Milano, 2003

[165] Hoyt, S.L., *Tungsten Carbide - A New Tool Material*, Transactions of American Society for Steel Treating, vol.14, 1928, pp.695-718

[166] Ojmertz, K.M.C., Oskarson, H.B., *Wear on SiC-whiskers reinforced ceramic inserts when cutting Inconel with water jet assistance*, Tribology Transactions, vol.42/3, 1999, pp.471–488

Appendix A - Materials

A.1 Cutting tool

A Sanvick Coromant™ tungsten carbide cutting tool was chosen for best performance in machining low carbon steel at high cutting speed. Tungsten carbide (WC) is a chemical compound containing tungsten and carbon, similar to titanium carbide. Its extreme hardness makes it useful in the manufacture of cutting tools, abrasives and bearings, as a cheaper alternative to diamond [165]. Carbide cutting surfaces are often useful when machining tough materials, such as carbon steel or stainless steel, as well as in situations where other tools would wear away, such as in high-quantity production runs. Sometimes, carbide will leave a better finish on the part, and allow faster machining. Carbide tools can also withstand higher temperatures (melting point: 2870 °C) than standard high-speed steel tools. To increase the life of carbide tools, inserts are sometimes coated. Two such coatings are TiN (titanium nitride) and TiC (titanium carbide). Most coatings generally increase a tool's surface hardness and or lubricity, very useful in dry machining. A coating allows the cutting edge of a tool to cleanly pass through the material without having the material gall (stick) to it. The coating also helps to decrease the temperature associated with the cutting process and increase the life of the tool [166].

insert TNMG 11 03 02-MF 4025:

- *weight = 0.002kg*
- *l = 11 mm*
- *s =3.175 mm*
- *iC = 6.35 mm*
- r_e *= 0.2 mm*

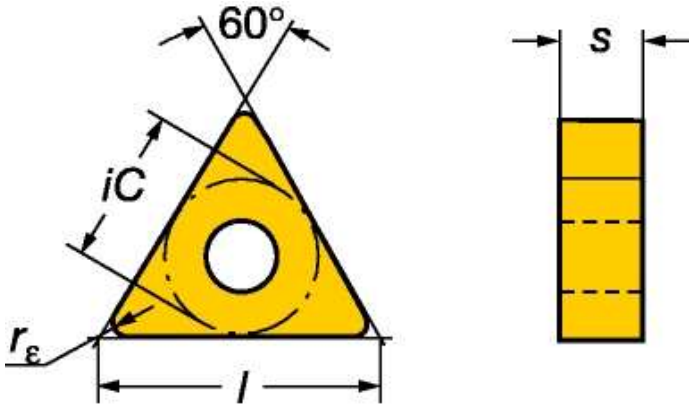

Figure 1 – Sketch of the insert (after Sandvik Coromant website)

holder PTGNR 2525M 11:

- *weight = 0.742 kg*
- *Insert Size = 11 mm*
- *b = 25 mm*
- *f_1 = 32 mm*
- *h =25 mm*
- *h_1 = 25 mm*
- *l_1 = 150 mm*
- *l_3 = 20 mm*

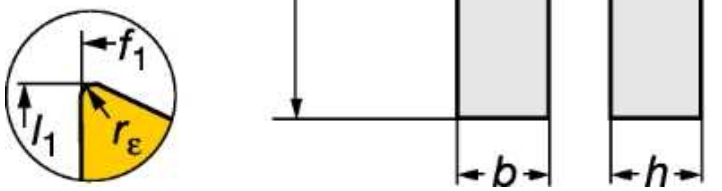

Figure 2 – Sketch of the tool holder (after Sandvik Coromant website)

A.2 Workpiece – AISI 1020 steel

Category	Steel
Class	Carbon steel
Type	Standard

Composition

Element	Weight %
C	0.18-0.23
Mn	0.30-0.60
P	0.04 (max)
S	0.05 (max)

Mechanical Properties at 25 °C

Density (x 1000 kg/m3)	7.7-8.03
Poisson's Ratio	0.27-0.30
Elastic Modulus (GPa)	190-210
Tensile Strength (Mpa)	394.7
Yield Strength (Mpa)	294.8
Elongation (%)	36.5
Reduction in Area (%)	66.0
Hardness (HB)	111

Appendix B – Data acquisition system

The three signal used for the experimental investigation have been amplified and the whole system, composed by the sensor and the amplifier, has been calibrated. The following three figures show the calibration data (dotted data) and the calibration curve (dashed line). In the figures are also represented the expressions of the interpolated curves, that have been estimated with a least square algorithm by Matlab. The maximum error of the interpolated curve is 0.08 mV for the dynamometer and 0.01 mV for the thermocouple.

B.1 Force measurement

The cutting force and the feed force was measured by a piezoelectric tool-force dynamometer. The following sketch show the dynamometer with the tool, the nozzle, the workpiece and the structure for supporting the nozzle mounted on the dynamometer

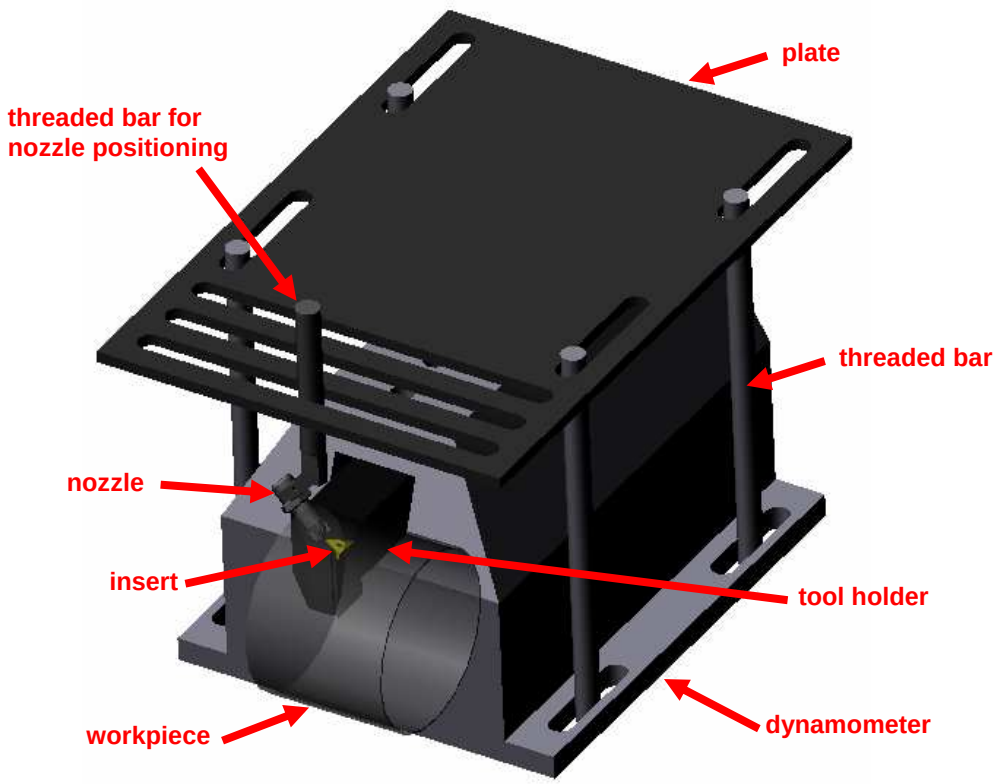

Figure 3 – The dynamometer with the tool, the nozzle the workpiece and the structure for supporting the nozzle

The technical details of the dynamometer are listed in the following table.

Kistler 9263A piezoelectric tool-force dynamometer	
Range [N]	Fx, Fy: from –500 to 500 Fz: from –1000 to 1000
Calibrated partial range [N]	Fx, Fy: from 0 to 5 Fz N 0/10
Overload [N]	Fx, Fy: from –600 to 600 Fz: from –1200 to1200
Threshold [N]	<0,01
Sensitivity [pC/N]	Fx, Fz: ≈–8,1 Fy: ≈–4,3
Linearity, all ranges %	FSO ≤±0,5
Hysteresis, all ranges %	FSO ≤±0,5
Rigidity [kN/μm]	cx, cz >1 cy >2
Natural frequency [kHz]	f(x) ≈2, f(y) ≈3, f(z) ≈1,8
Operating temperature [°C]	from 0 to 70
Capacitance (of channel) [pF]	≈170
Insulation resistance [TΩ]	>10
Ground isolation [MΩ]	>100
Weight [kg]	5,12

Table 1 - Technical details of the dynamometer

The calibration of the dynamometer has been carried out by loading the sensor in the z-direction (cutting force F_p) and in the x-direction (feed force F_q) with a set of weights of 2 kg each. The Figure 4 and Figure 5 show the calibration curves for the force in feed direction (F_x) and the cutting force (F_z). The force is expressed in N and the correspondent signal in mV. The temperature is expressed in °C and the correspondent signal in mV. The system composed of the thermocouple, the insert and the amplifier needed a source of heat in order to impose a temperature on the rake face.

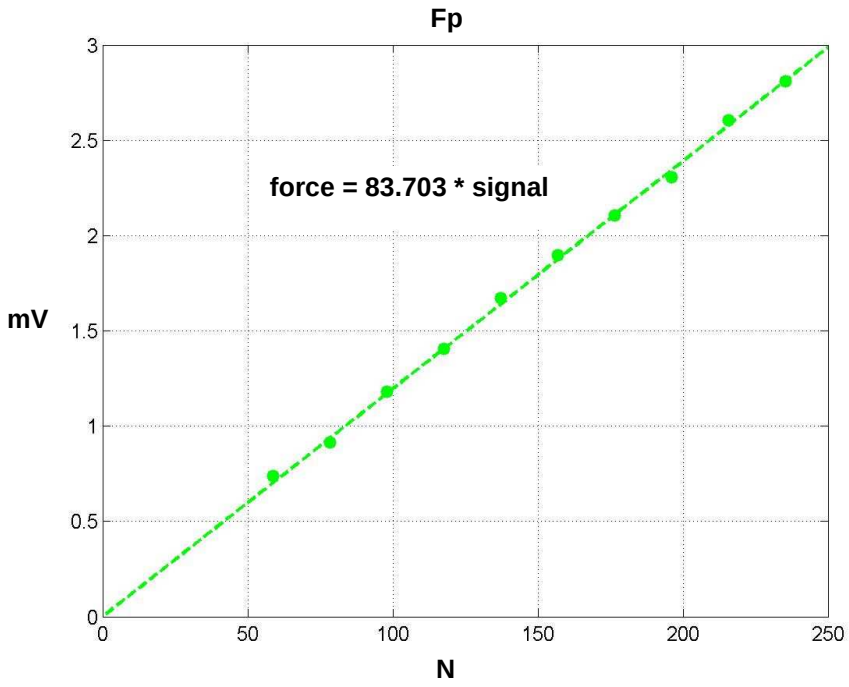

Figure 4 - Calibration data, interpolation curve and relation for the force in feed direction

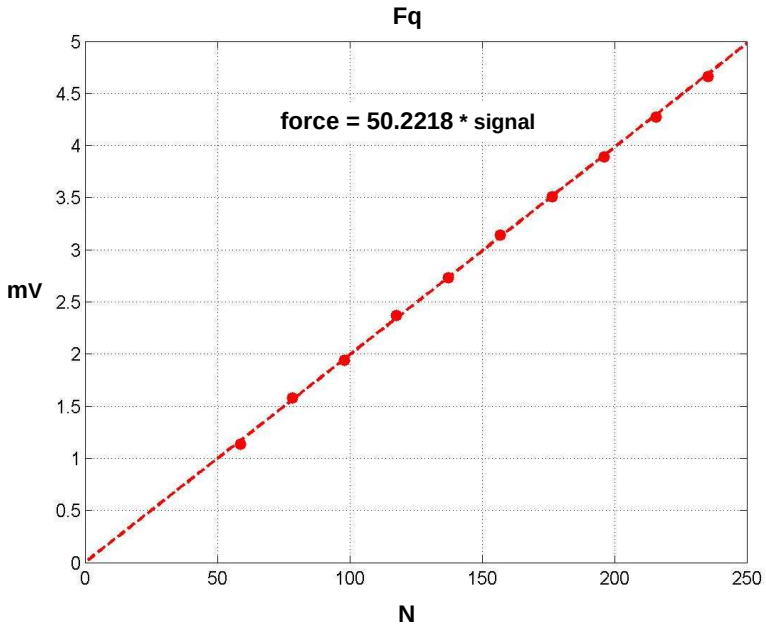

Figure 5 - Calibration data, interpolation curve and relation for the force in cutting direction

B.2 Temperature measurement

A uncoated K-type thermocouple has been used for temperature measurements. The diameter of the sensing head is 0.50 mm. This kind of thermocouple allows fast response at a wide range of temperature, compared to other type of thermocouple of the same diameter.

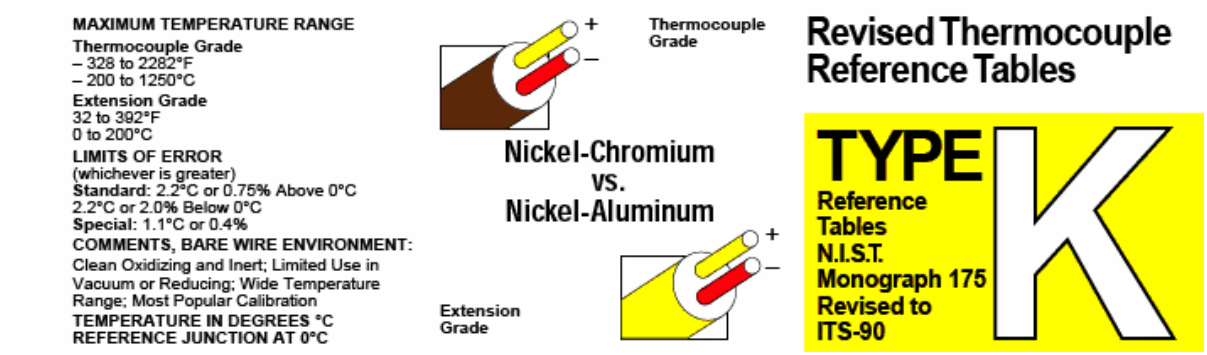

Figure 6 - Specification for K-type thermocouple and color code

Figure 7 - K-type thermocouple

During the tests the K-type thermocouple with the diameter of 0.5 mm was embedded in two different holes of the insert used for orthogonal cutting tests, as shown by Figure 8. Since the thermocouple was uncoated, the toolholder and the clamping system of the lathe were electrically by a thin insulating tape.

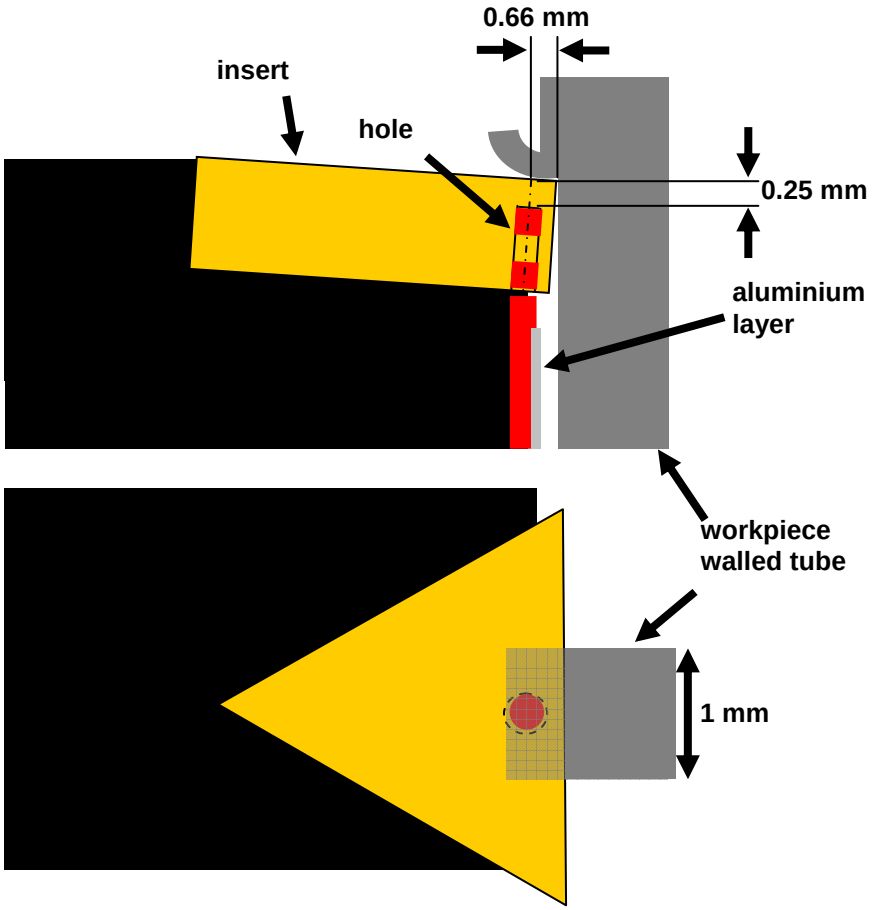

Figure 8 – quoted sketch of the embedded thermocouple, lateral view (top part of the sketch) and top view (bottom part of the sketch)

Traditional drilling at more than 2 mm of depth is not effective on coated tungsten carbide. A spark eroder ARD M50 has been used to drill the hole for the thermocouple in the insert. The flaws of this technique are mainly related to the precision of the machining process with a spark eroder and even for an experienced technician it is difficult to drill multiple holes with the same depth. In order to ensure the best conditions for temperature measurement (maximum signal and minimum delay and noise) the holes were drilled in

order to achieve minimum distance of the thermocouple from the rake face and cutting edge, without affecting the integrity of the insert. The Table 2 shows the technical specifications of the spark eroder (Figure 9)

ARD M50 spark eroder	
Ampere	50
Tank	850x500x300 mm
Table	600x360 mm
Max distance table-mandrel	550 mm
Z axis stroke	200 mm
X axis stroke	300 mm
Y axis stroke	200 mm
Max electrode weight	50 Kg
Max chargeable weight	500 Kg

Table 2 – Technical specifications of the spark eroder

Figure 9 - ARD M50 spark eroder

A set of six holes have been drilled on two inserts and two best holes in terms of depth and good finishing were selected for embedding the thermocouple, and hard finished with

a micro drill (0.58 mm of diameter) for minimizing asperities at depth and ensure a good contact between the tip of the thermocouple and the top face of the hole. The contact between the thermocouple and the insert was ensured by using the thermocouple wire as a spring. Figure 10 explain the concept: the red wire that represents the thermocouple wire in Figure 10a is not loaded. When the insert is in the correct position (Figure 10b) the thermocouple wire is loaded and elastic behaviour of the wire ensure the contact. Also a thermal compound with a thermal conductivity of 220 W/mK was used for a better thermal contact between the thermocouple and the insert.

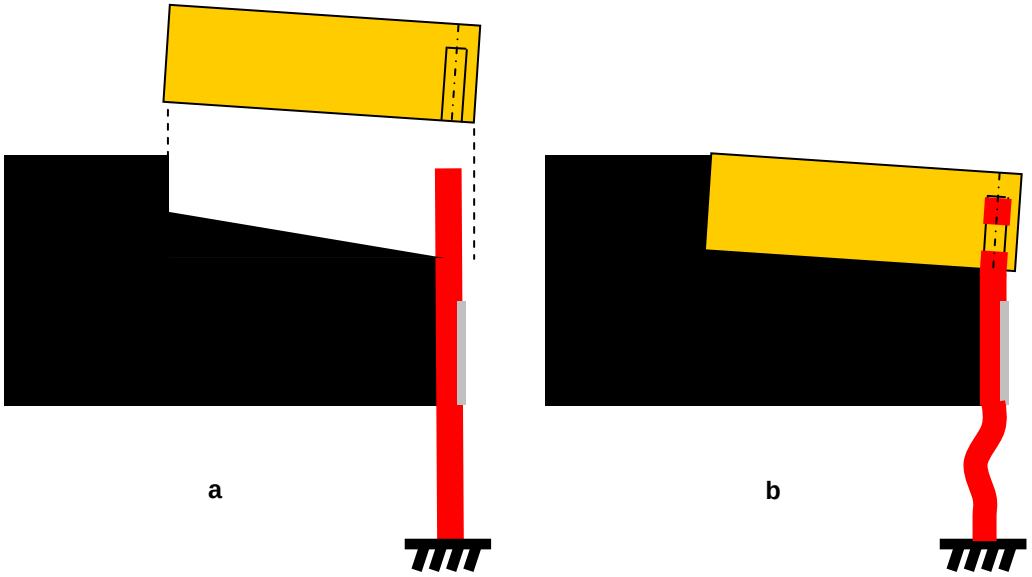

Figure 10 – The elastic behaviour of the thermocouple wire (in red) hold the tip of the thermocouple at the bottom of the hole drilled in the insert

Figure 11 shows a 3D shaded sketch with visible edges of the triangular insert with a hole drilled close at each flank face. On the sketch are shown the toolholder clamping, the holes for embedding the thermocouple and the filleted chipbreaker. Precise position of the holes was checked with an optical microscope equipped with xy-stage, as shown in Figure 12.

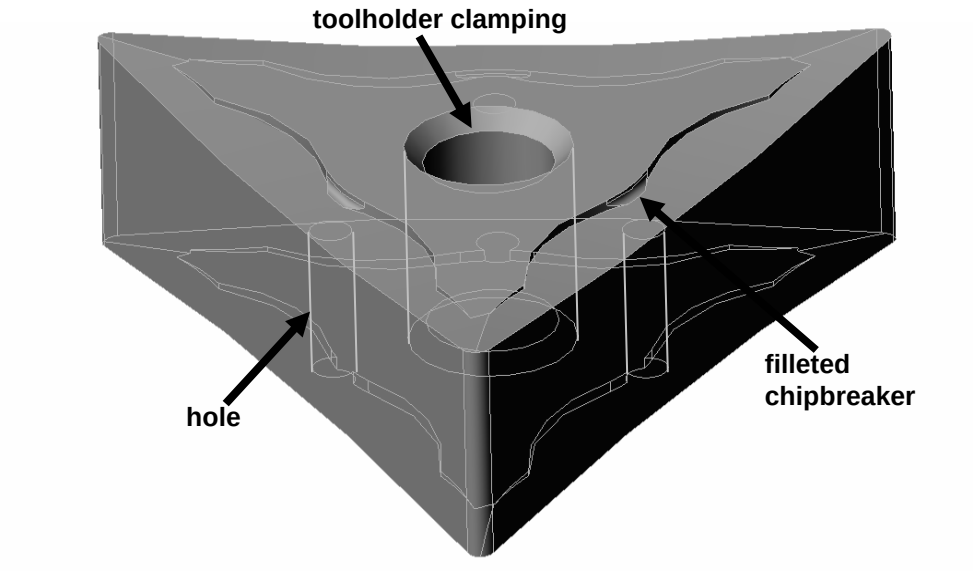

Figure 11 – 3D shaded sketch with visible edges. The holes for thermocouple, the hole for toolholder clamping and the chipbreaker

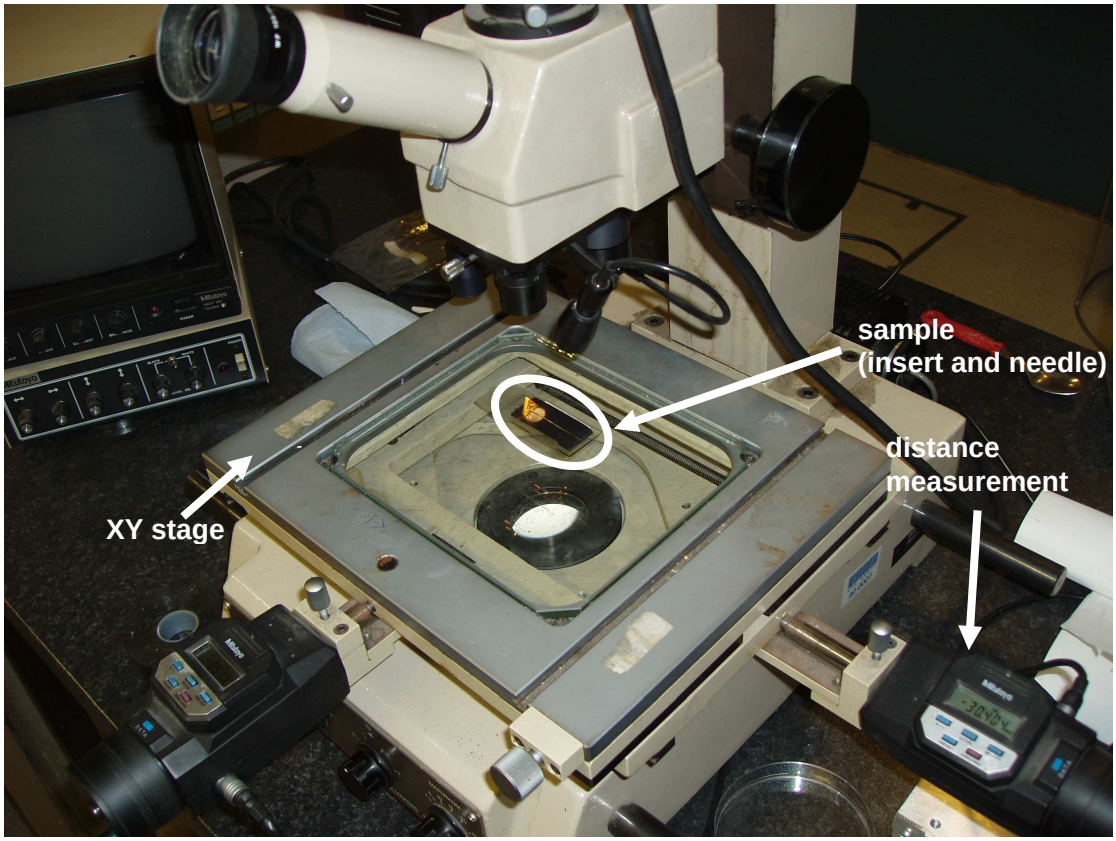

Figure 12 – The optical microscope used for precise measurement of the holes position and depth

A set of needles was fitted in the six holes drilled in the two inserts for measuring the internal diameter of each hole. The depth of the holes has been measured by subtracting the total length of the needle and visible part of the needle, when fitted in the hole. Figure 13 shows a quoted picture of the needle fitted in one of the holes in an insert. The measurements of the hole have been repeated three times for minimizing the measurement error.

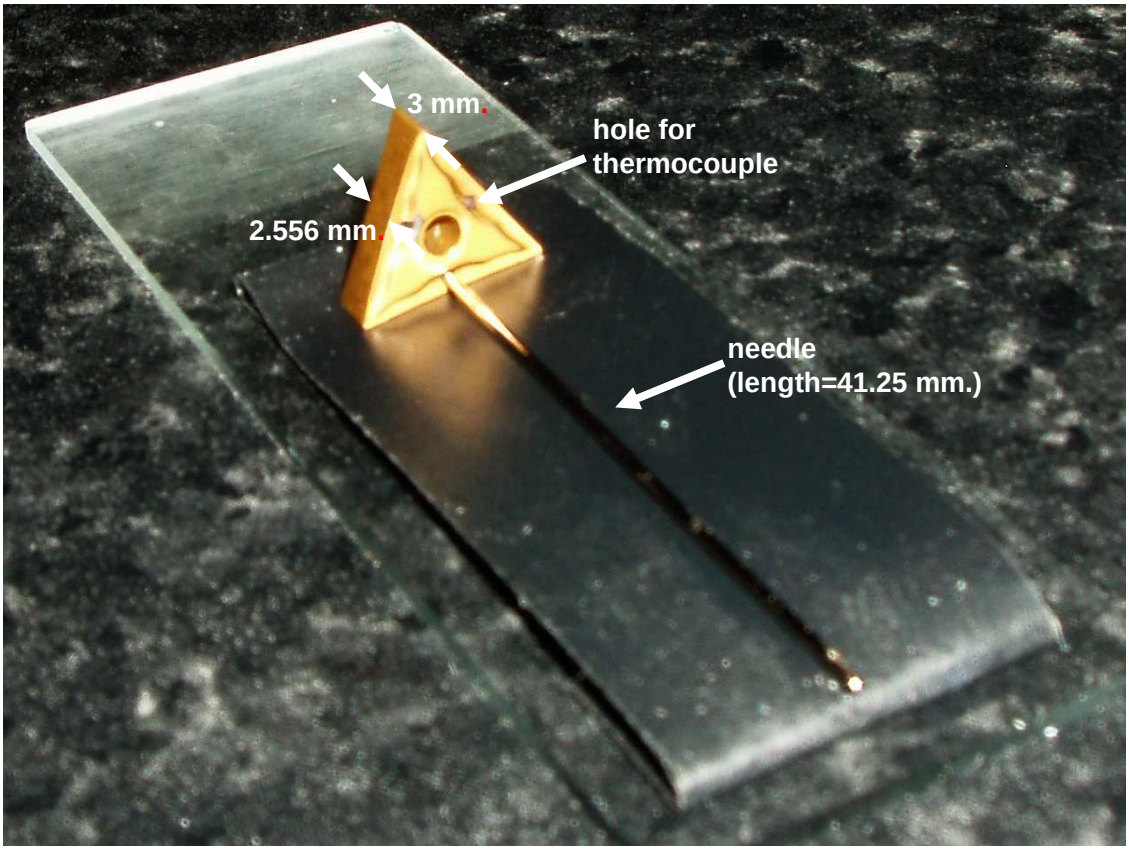

Figure 13 – The needle is fitted in the hole for the thermocouple. The xy-stage has been used for measuring the length of the needle, the depth of the hole (by subtraction) and the section of the insert

The Figure 14 shows the six holes drilled on the two inserts and provides visual information on the labels used in the Table 3. A couple of holes was chosen in order to ensure the repeatability and have an evaluation of the accuracy of the temperature measurement with embedded thermocouple. The holes labelled *A1* and *A2* were used in the cutting tests, since all the other holes presented defects that could affect the experiments. The two holes chosen for the tests have a similar distance from the rake face

and cutting edge, considering the precision of electro-discharge machining (EDM) techniques. If the tension used for machining is too high, EDM affect the TiN coating, causing a local detachment of the coating layer from the substrate. This flaw was evident in the hole labelled *B3*, where EDM was stopped because the high tension used for the erosion was damaging the coating on the rake face and around the hole (also visible in Figure 14). The holes labelled *B1* and *B2* are too distant from the cutting edge, compared to *A1* and *A2* and the diameter of *B1* is bigger than the others holes. The smallest distance from the rake face was achieved with the hole labelled *A3*, however the poor rake face quality and the slightly conic shape of the hole did not made the *A3* a suitable candidate for testing.

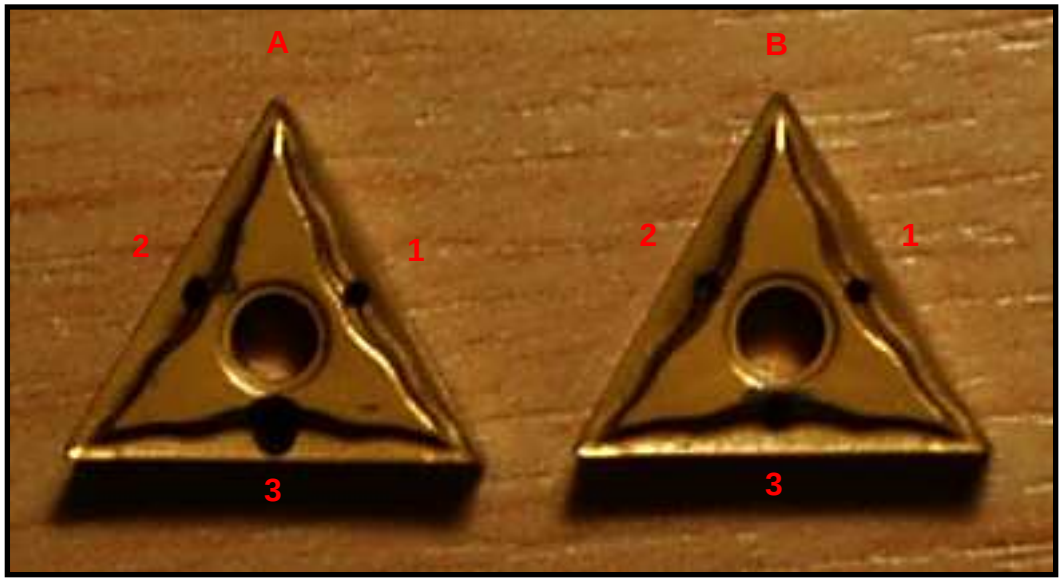

Figure 14 – The two inserts machined with the spark eroder. Two of the six holes (*A1* and *A2*) were selected for the cutting tests. The criteria for the choice were: proximity to rake face, proximity of cutting edge, shape and finishing of the hole, integrity of the coating on the rake face

	insert A				Insert B			
hole	**depth**	**dist.rake face**	**dist.flank face**	**diam.**	**depth**	**dist.rake face**	**dist.flank face**	**Diam.**
1	2.288	0.268	0.647	0.58	2.192	0.364	0.907	0.63
2	2.313	0.243	0.671	0.58	2.337	0.229	0.889	0.58
3	2.367	0.189	0.812	0.58	0.477	none	none	None

Table 3 – Measurements (mm) of the three holes drilled by EDM in each insert. The distance to the rake face and to the flank face has been measured by the xy-stage mounted on the optical microscope, the depth has been measured with a needle of known length and the diameter has been measured with a set of drills of different diameter

The source of heat was provided by a powerful solder. The contact between the solder and the insert was improved by using the high conductivity paste, and the solder tip was hardly pressed against the rake face. A calibrated K-type thermocouple, plugged to a multimeter, was used for reading the temperature on the cutting edge, as shown in Figure 15.

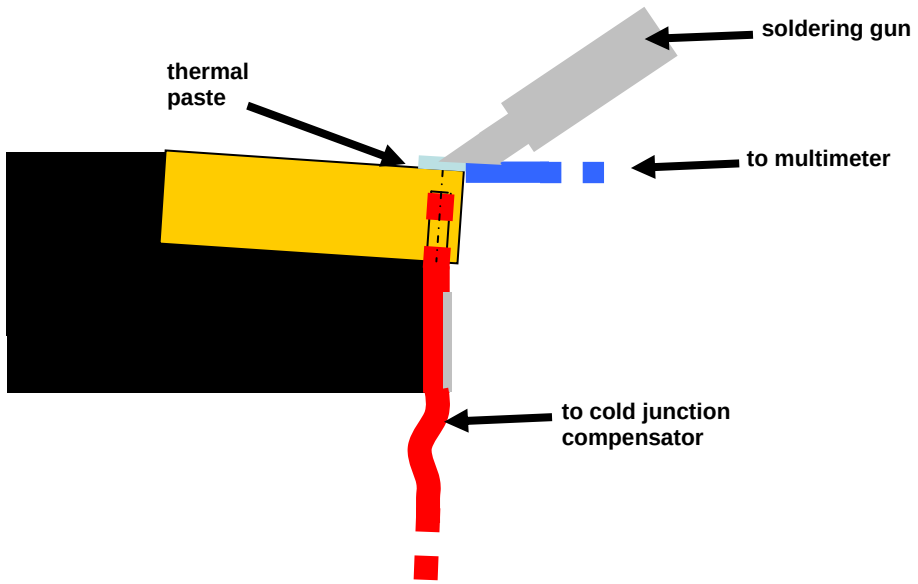

Figure 15 - Sketch of the thermocouple calibration setup. The layer of thermal paste allows optimal contact between the soldering gun and the insert

The soldering gun was used for heating the rake face up to 430°C. The calibration curve, shown in Figure 16 is linear in the considered range. Since the thermocouple is linear until 1200°C and the conduction equation is linear, the linearity of the system at higher temperature is a reasonable hypothesis. The calibrated thermocouple, marked in blue and connected to a high sensitivity multimeter, the thermocouple used in the test, marked in red, the layer of high conductivity paste and the soldering gun are shown in the following sketch.

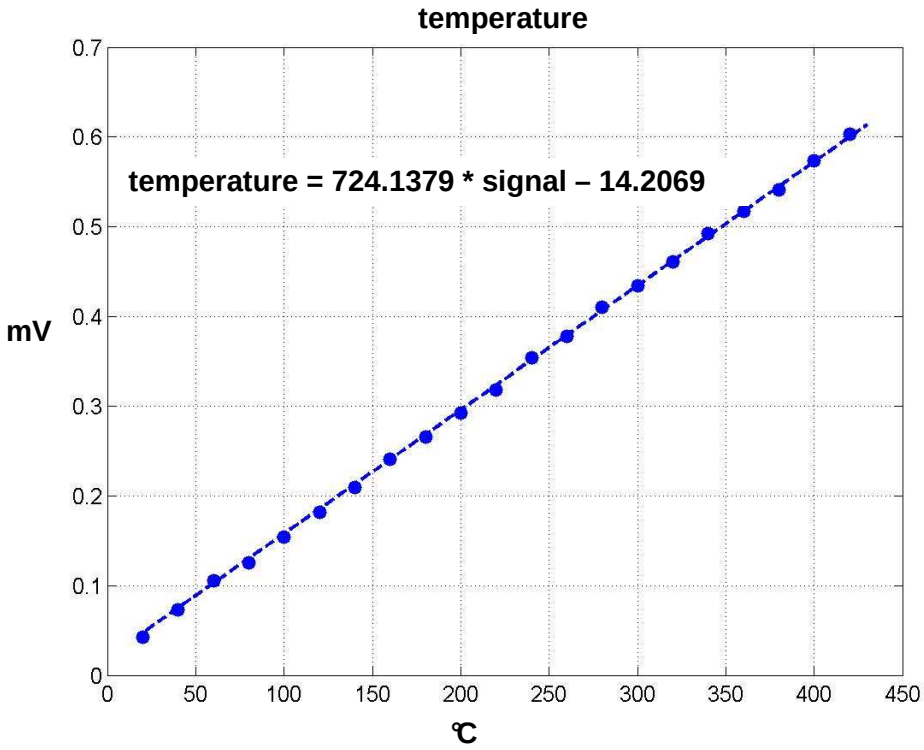

Figure 16 - Calibration data, interpolation curve and relation for the temperature on the rake face

B.3 Pneumatic system and air jet

Since a full fluid-dynamic investigation goes beyond the purposes of this project, only the fundamental fluid-dynamic parameters were considered for the experimental characterization of the air jet, such as nozzle geometry, air pressure and flow volume, jet flow direction and distance from the nozzle to the cutting edge. Current high speed jet applications use the air jet directed in the chip-tool interface. A description of coolant jet flow is given by Sandvik Coromant machining manual [124], that recommend aiming the jet in the middle of the chip-tool interface, with an angle of 10–20°, to form a wedge between the chip and the rake face. According to Sandvik Coromant, the jet should hit the insert surface 1 mm back from the cutting edge. Interfacial positioning is mainly due to intuition and there is no evidence this solution is optimized for air jet applications. Experimental observations show evidence of the different effect achieved in changing nozzle position from interface to overhead. A supersonic De Laval nozzle based on Coanda effect [159, 160, 161, 162] (with primary and secondary flow) was used. Figure 17 shows a 3D sketch of the nozzle, with the slots for external flow and internal flow exit section of 2 mm. of diameter.

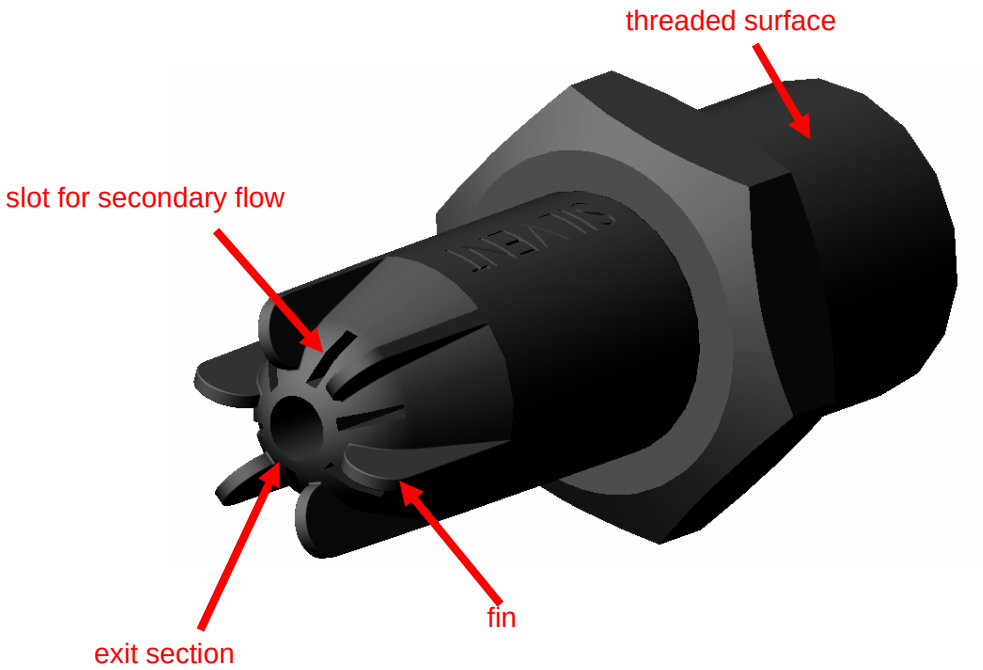

Figure 17 – 3D sketch of the supersonic nozzle used for directing the air jet

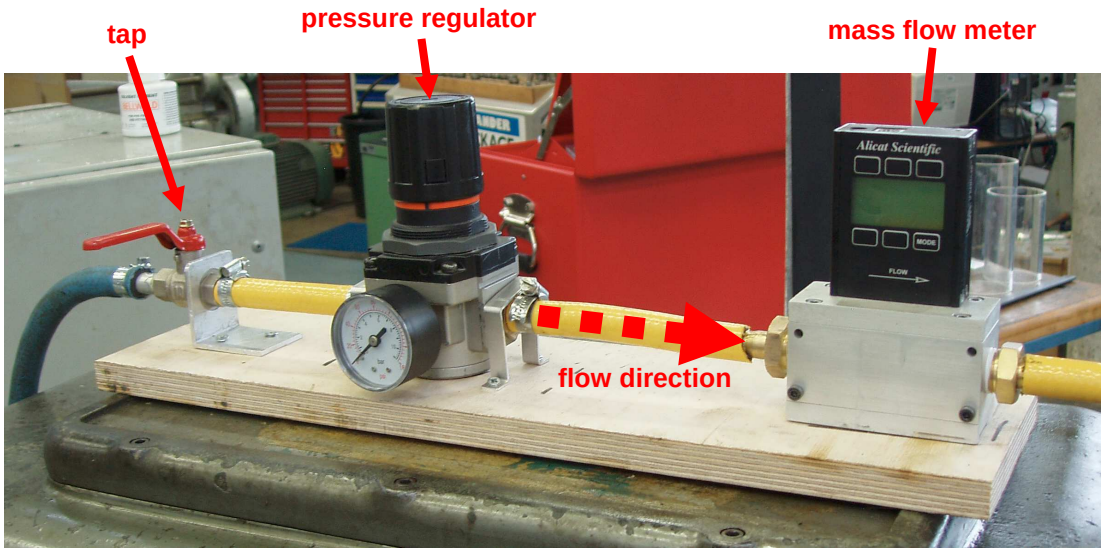

Figure 18 – Pressure control and flow rate measurement station: pressure regulator and mass flow meter

A pressure regulator was used for changing the pressure up to 7.5 bar, and a mass flow-meter FMA-1600A was placed in the air supply line before the nozzle. The Figure 18 shows the pressure control and flow rate measurement station. The Figure 19 shows the mass flow-meter, the Table 4 shows its technical details, and the Figure 20 shows the reading of the flow-meter as a function of the pressure controlled by the pressure regulator. The accuracy of the flow meter is 0.8% of the measured quantity.

Figure 19 - Mass flow-meter Omega FMA-1600A

Mass flow-meter Omega FMA-1600A			
Specification	*Mass meter*	*Volumetric meter*	*Description*
Accuracy	± (0.8% of Reading + 0.2% of Full Scale)		At calibration conditions after tare
High Accuracy Option	± (0.4% of Reading + 0.2% of Full Scale)		At calibration conditions after tare
Repeatability	± 0.2%		Full Scale
Operating Range	1% to 100% Full Scale		Measure
Typical Response Time	10		Milliseconds (Adjustable)
Standard Conditions (STP)	25ºC & 14.696PSIA	Not Applicable	Mass Reference Conditions
Operating Temperature	−10 to +50		ºCelsius
Zero Shift	0.02%		Full Scale / ºCelsius / Atm
Span Shift	0.02%		Full Scale / ºCelsius / Atm
Humidity Range	0 to 100%		Non–Condensing
Measurable Flow Rate	128%		Full Scale
Maximum Pressure	145	145[1]	PSIG
Output Signal Digital	Mass, Volume, Pressure & Temperature	Volumetric Flow	RS-232 Serial
Output Signal Analog	Mass Flow	Volumetric Flow	0-5Vdc
Optional Output Signal Secondary Analog	Mass, Volumetric Pressure or Temperature	Volumetric Flow	0-5 Vdc or 0-10Vdc or 4-20mA
Electrical Connections	8 Pin		Mini-DIN
Supply Voltage	7 to 30 Vdc (15-30Vdc for 4-20mA outputs)		
Supply Current	0.035Amp (+ output current on 4-20mA)		
Mounting Attitude Sensitivity	0%		Tare after installation
Warm-up Time	< 1		Second
Wetted Materials[2]	303 & 302 Stainless Steel, Viton®, Silicone RTV (Rubber), Glass Reinforced Nylon, Aluminum.		

Table 4 – Technical specifications of the mass flow-meter

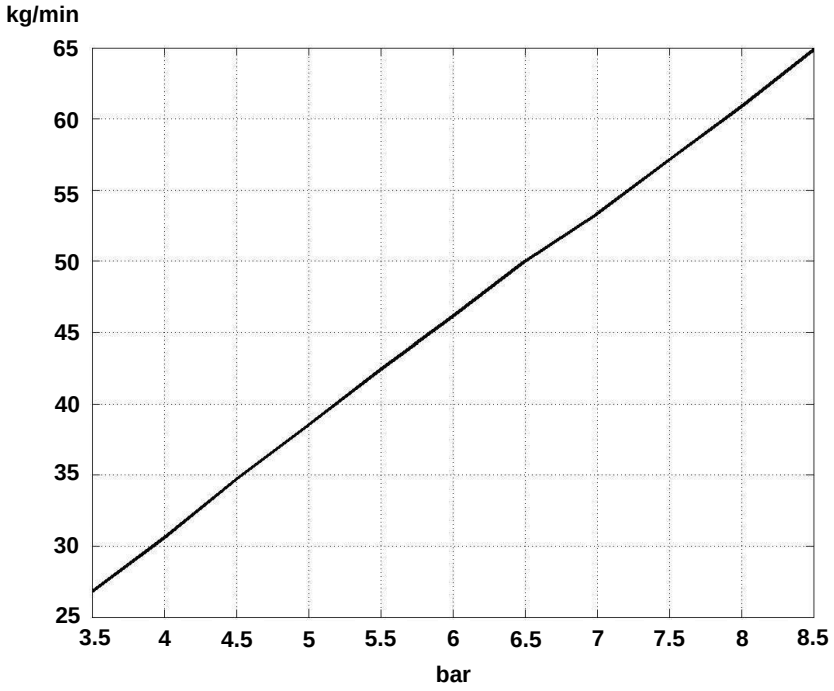

Figure 20 – The mass flow rate as a function of pressure, measured by the mass flow meter at the end of the flow control station

Nozzle manufacturer provided data about an air cone pattern of 21°. In order to test the force applied by the air jet, the nozzle was perpendicularly directed on a circular plate, lying on a high sensitivity balance. The distance between the surface and the nozzle was changed from 1.5 to 220 mm. The plate was large enough to get the entire air cone pattern at any distance considered for the test. The following graph shows the force applied by the air jet on the circular plate (Figure 21). The smoothness of each graph at different pressures shows the air jet has not significant pressure losses in its free air cone pattern. Since in this test the complete air cone is hitting the surface, the plate can be considered semi-infinite. Results at 7 bar are consistent with manufacturer data about blowing force (4.4 N). In order to estimate the pressure of air when the jet is impinging on the rake face, a test on a sample insert has been carried out.

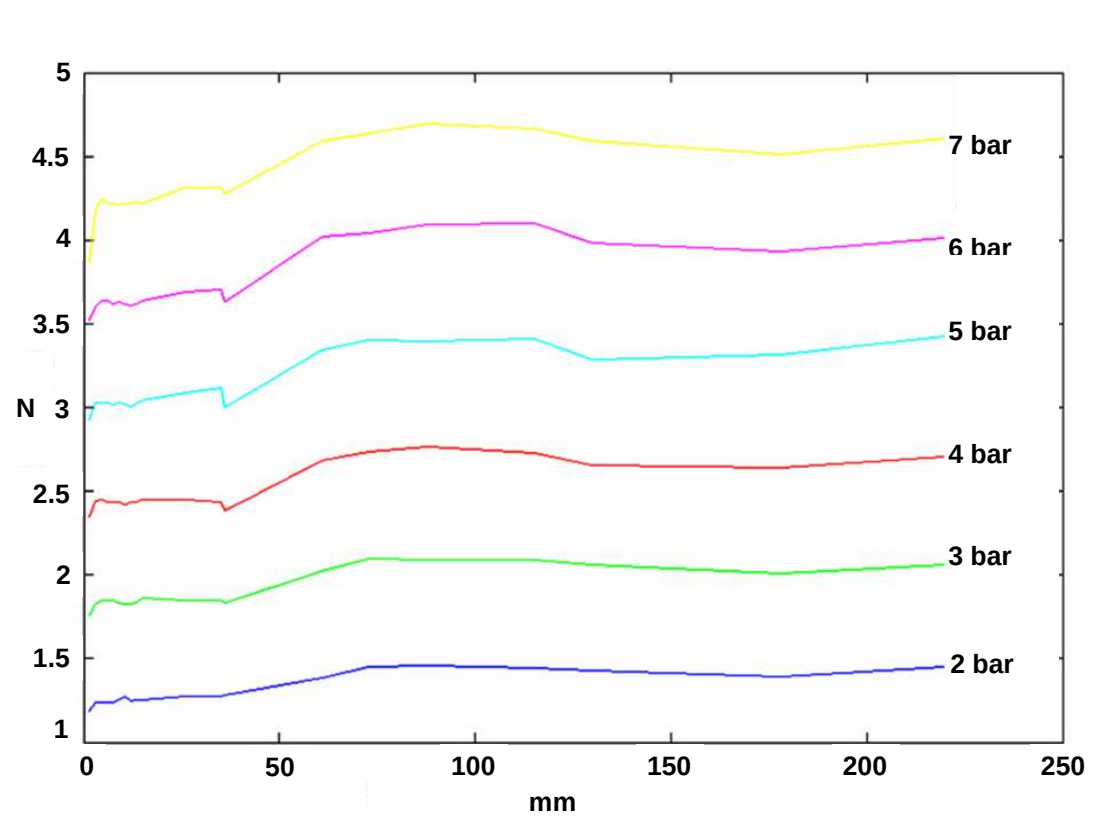

Figure 21 – Force applied by the air jet as a function of distance from a circular plate at different pressures

Since the balance has been protected by a box (see Figure 22) only the force applied on the rake face has been measured. The distance between the insert and the tip of the nozzle has been changed using a micrometer from 1.5 to 46 mm. The test shows the force is rapidly decreasing in the first 10 mm, and then it is slowly fading out with a smooth slope. This confirms the higher blowing force is achieved at short distance, on small surfaces. Before 1.5 mm the blowing force show a rapid decreasing with some scattered behaviour. The transition from subsonic to supersonic flow may be the cause of scattered behaviour of the blowing force around 1.5 mm of distance from the nozzle tip. Figure 23 show the force on the simulated rake face is not constant. In particular the force has a maximum when at the minimal distance. According to O'Donovan [30] the core of air jet is not completely developed until 5-6 times the diameter of the nozzle diameter.

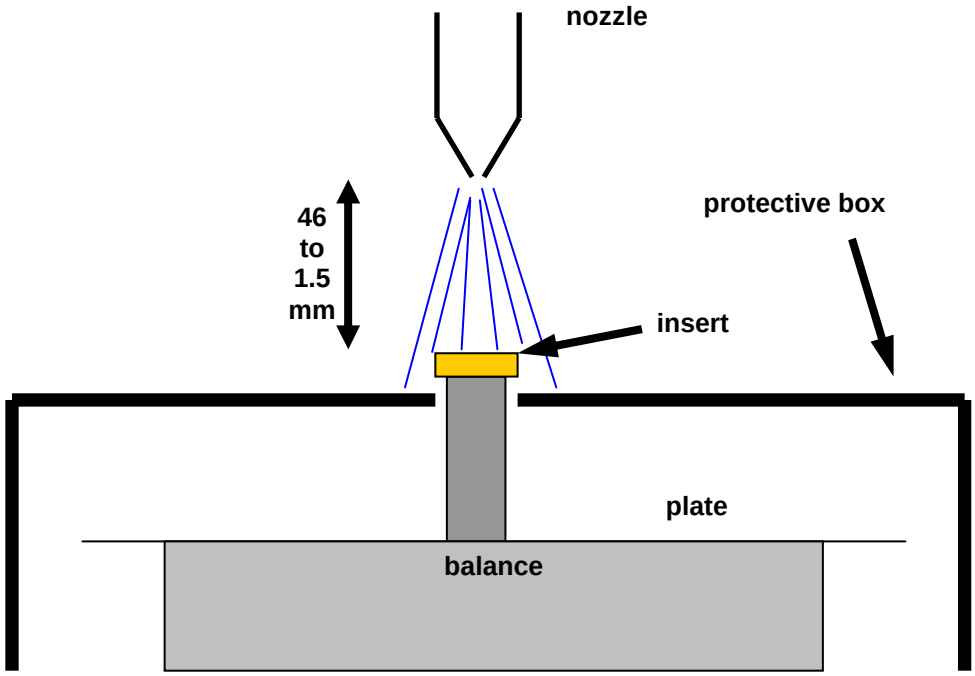

Figure 22 – sketch of force by air jet blowing on simulated insert measurement

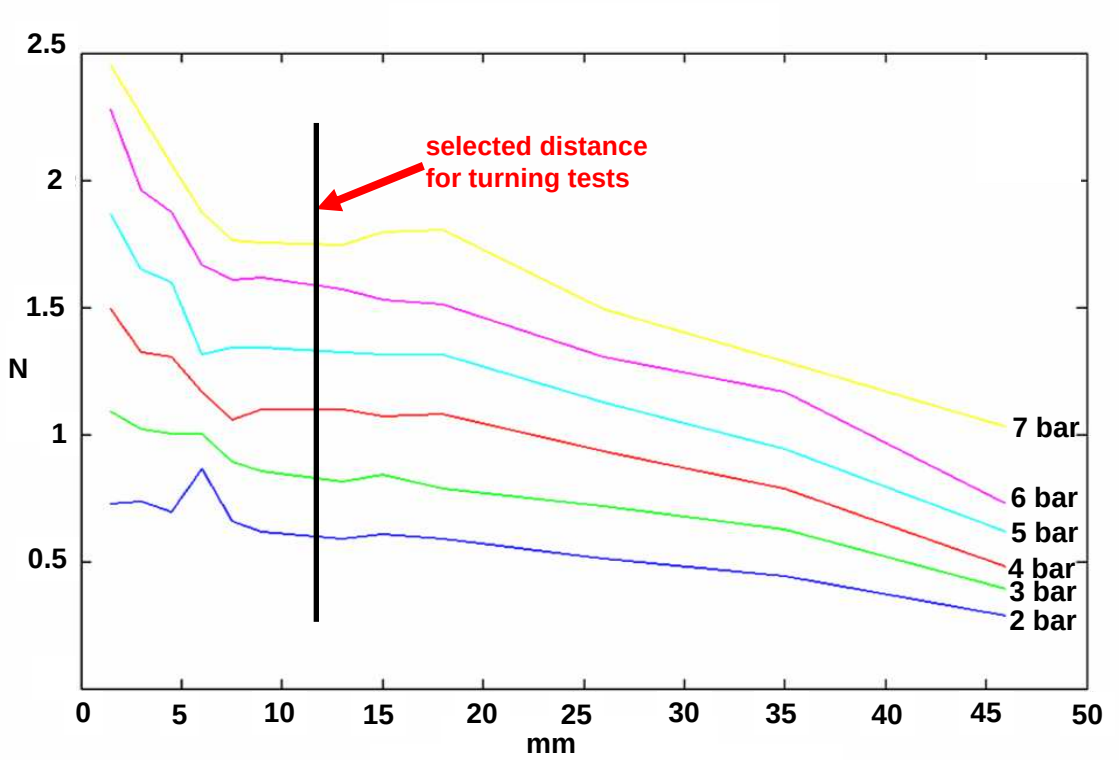

Figure 23 – Force as a function of distance plate at different pressure on the rake face

Due to high speed the development distance is consistently reduced, however during the cutting tests the nozzle has been positioned at a distance of 12 mm (6 times the throat section diameter) from the rake face also for allowing optimal chip flushing. From Figure 5.9 it is possible to assume that between 11 and 13 mm of distance from the rake face the blowing force is approximately constant. The nozzle has been placed in two different positions in order to investigate the effect of air jet direction in the orthogonal cutting process. The Figure 5.10 shows a sketch of the nozzle in interface position and overhead position. According to nozzle manufacturer, the air cone pattern has an angle of 21°.

Appendix C – Flow stress model for AISI 1020

C.1 Material model

The model of Oxley was originally designed for AISI 1016, and subsequently extended to most of the low carbon steels, since the model depends on the content of carbon. The starting point of Oxley's model is the strain hardening curve:

$$\sigma = \sigma_1 \varepsilon^n \qquad \text{Eq.C1}$$

where σ_1 is the stress at $\varepsilon = 1$ and n is the strain hardening coefficient. The strategy used by Oxley for developing his model consists in calculating a modified temperature T_{mod} according to Equation A2, expressing σ_1 and n for AISI 1016 (here called σ_{1C16} and n_{C16}) as a function of T_{mod} then subsequently extending the model to other carbon contents:

$$T_{\text{mod}} = T\left(1 - 0.09 \log_{10} \dot{\gamma}\right) \qquad \text{Eq.C2}$$

where T is the cutting temperature.

Oxley expresses the stress of AISI 1016 at $\varepsilon = 1$ in Equations A3 & A4. From the results of Equations A3 & A4, Oxley estimates a variable of stress, here called σ_C, as a function of the content of carbon $\%c$.

$$\sigma_{1C16} = 1126.62 - 0.98421\ T_{\text{mod}} \qquad for\ T_{\text{mod}} \le 458$$

$$\sigma_{1C16} = -19914.15 + 135.07\ T_{\text{mod}} - 0.20137\ T_{\text{mod}}{}^{2} - 3.1090e-4\ T_{\text{mod}}{}^{3} + 7.2551e-7\ T_{\text{mod}}{}^{4} + 7.3255e-10\ T_{\text{mod}}{}^{5} - 2.2977e-12\ T_{\text{mod}}{}^{6} + 1.2673e-15\ T_{\text{mod}}{}^{7} \qquad for\ 458 < T_{\text{mod}} \le 748$$

$$\sigma_{1C16} = 17756.97 - 97.198\ T_{\text{mod}} + 0.23022\ T_{\text{mod}}{}^{2} - 2.4637e-4\ T_{\text{mod}}{}^{3} + 2.8921e-8\ T_{\text{mod}}{}^{4} + 1.8495e-10\ T_{\text{mod}}{}^{5} - 1.6072e-13\ T_{\text{mod}}{}^{6} + 4.2722e-17\ T_{\text{mod}}{}^{7} \qquad for\ 748 < T_{\text{mod}} \le 1200$$

Eq.C3 – The stress as a function of the modified temperature for AISI 1016 at $\varepsilon = 1$

$$for\ T_{\text{mod}} \le 700$$

$$\sigma_C = \frac{531.31 + 753.17\ \%_C}{651.72}$$

$$\sigma_1 = \sigma_{1C16}\left(1 + \frac{\sigma_C - 1}{900}(1400 - T_{\text{mod}})\right)$$

Eq.C4

$$for\ T_{\text{mod}} > 700$$

$$\sigma_1 = \sigma_{1C16}\left(1 + \frac{\%_C}{T_{\text{mod}}}(T_{\text{mod}} - 700)\right)$$

After calculating the stress at $\varepsilon = 1$ for the generic low carbon steel, Oxley proceeded to calculate the strain hardening coefficient as a function of the modified temperature, as illustrated in Equations A5:

$$for\ T_{\mathrm{mod}} \le 73 \qquad n_{C16} = 0.04768$$

$$for\ 73 < T_{\mathrm{mod}} \le 396$$

$$n_{C16} = 0.04937 + 3.5861e-4\ T_{\mathrm{mod}} - 1.4026e-5\ T_{\mathrm{mod}}{}^{2} - 1.7680e-7\ T_{\mathrm{mod}}{}^{3} - 9.4992e-10\ T_{\mathrm{mod}}{}^{4} + 2.7341e-12\ T_{\mathrm{mod}}{}^{5} - 4.1361e-15\ T_{\mathrm{mod}}{}^{6} + 2.5569e-18\ T_{\mathrm{mod}}{}^{7}$$

$$for\ 396 < T_{\mathrm{mod}} \le 528 \qquad n_{C16} = 0.19109$$

$$for\ 528 < T_{\mathrm{mod}} \le 693$$

$$n_{C16} = -145.26 + 0.81927\ T_{\mathrm{mod}} - 0.88538e-3\ T_{\mathrm{mod}}{}^{2} - 2.5350e-6\ T_{\mathrm{mod}}{}^{3} + 5.0364e-9\ T_{\mathrm{mod}}{}^{4} + 2.4501e-12\ T_{\mathrm{mod}}{}^{5} - 1.04279e-14\ T_{\mathrm{mod}}{}^{6} + 5.8410e-18\ T_{\mathrm{mod}}{}^{7}$$

$$for\ 693 < T_{\mathrm{mod}} \le 827$$

$$n_{C16} = -21.227 + 0.08507\ T_{\mathrm{mod}} - 4.4837e-5\ T_{\mathrm{mod}}{}^{2} - 1.3310e-7\ T_{\mathrm{mod}}{}^{3} - 3.5910e-11\ T_{\mathrm{mod}}{}^{4} + 5.1253e-13\ T_{\mathrm{mod}}{}^{5} - 5.1724e-16\ T_{\mathrm{mod}}{}^{6} + 1.5471e-19\ T_{\mathrm{mod}}{}^{7}$$

$$for\ 827 < T_{\mathrm{mod}} \le 974$$

$$n_{C16} = -65.632 + 0.30193\ T_{\mathrm{mod}} - 0.49548e-3\ T_{\mathrm{mod}}{}^{2} + 2.7300e-7\ T_{\mathrm{mod}}{}^{3} + 9.1267e-11\ T_{\mathrm{mod}}{}^{4} - 1.0362e-13\ T_{\mathrm{mod}}{}^{5} - 3.1959e-17\ T_{\mathrm{mod}}{}^{6} + 3.0674e-20\ T_{\mathrm{mod}}{}^{7}$$

$$for\ T_{\mathrm{mod}} > 974 \qquad n_{C16} = 0.18388$$

Eq.C5 – Strain hardening coefficient as a function of the modified temperature for AISI 1016

Finally, the strain hardening coefficient is calculated for the generic low carbon steel:

$$n = \frac{n_{C16}}{0.189}\left(0.244 - 0.3396\ \%_{C}\right) \qquad \text{Eq.C6}$$

C.2 Matlab Version

```
clear;clc;
mu=0.55; %friction coefficient
theta=0; %shear plane correction angle (Shaw)
alpha=0; %rake angle
beta=atan(mu); %friction angle
fi=pi/4-beta-alpha+theta; %(Lee)

v=83*1000/60; %insert cutting speed (mm/s)
strnr=cos(alpha)*v/cos(fi-alpha)/0.25;

strn=1/(sin(fi)*cos(fi));
carbon=0.2;
maxT=800;
for temp=1:maxT
x=temp*(1-0.09*log10(strnr/1)); % x is modified temperature
   if x<=458
      sgma=1126.62-0.98421*x;
   elseif (x>458) & (x<=748)
      sgma=-19914.15+135.07*x-0.20137*x^2-3.1090e-4*x^3 ...
         +7.2551e-7*x^4+7.3255e-10*x^5-2.2977e-12*x^6 ...
         +1.2673e-15*x^7;
   elseif (x>748) & (x<=1200)
      sgma=17756.97-97.198*x+0.23022*x^2-2.4637e-4*x^3 ...
         +2.8921e-8*x^4+1.8495e-10*x^5-1.6072e-13*x^6 ...
         +4.2722e-17*x^7;
   else
      sgma=172.42;
   end
```

```
if carbon==0.16
   sig1=sgma;
elseif (x>=200) & (x<=700)
   sigfac=(531.31+753.17*carbon)/651.72;
   sig1=sgma*(1+(sigfac-1)*(1400-x)/900);
elseif (x>700) & (x<=1000)
   sig1=sgma*(1+carbon*(x-700)/x);
elseif x<200
   % disp('Modified temperature is below range')
   sigfac=(531.31+753.17*carbon)/651.72;
   sig1=sgma*(1+(sigfac-1)*(1400-x)/900);
elseif x>1000
   % disp('Modified temperature is over range')
   sig1=sgma*(1+carbon*(x-700)/x);
end

%              1.2) Calculation of strain hardening

if x<=73
   n=0.04768;
elseif (x>73) & (x<=396)
   n=0.04937+3.5861e-4*x-1.4026e-5*x^2+1.7680e-7*x^3 ...
      -9.4992e-10*x^4+2.7341e-12*x^5-4.1361e-15*x^6 ...
      +2.5569e-18*x^7;
elseif (x>396) & (x<=528)
   n=0.19109;
elseif (x>528) & (x<=693)
   n=-145.26+0.81927*x-0.88538e-3*x^2 ...
      -2.5350e-6*x^3+5.0364e-9*x^4+2.4501e-12*x^5 ...
```

```
        -1.04279e-14*x^6+5.8410e-18*x^7;
    elseif (x>693) & (x<=827)
        n=-21.227+0.08507*x-4.4837e-5*x^2 ...
            -1.3310e-7*x^3-3.5910e-11*x^4+5.1253e-13*x^5 ...
            -5.1724e-16*x^6+1.5471e-19*x^7;
    elseif (x>827) & (x<=974)
        n=-65.632+0.30193*x-0.49548e-3*x^2 ...
            +2.7300e-7*x^3+9.1267e-11*x^4-1.0362e-13*x^5 ...
            -3.1959e-17*x^6+3.0674e-20*x^7;
    elseif x>974
        n=0.18388;
    end

    if carbon==0.16
        nhard=n;
    else
        nfac=(0.244-0.3396*carbon)/0.189;
        nhard=nfac*n;
    end
    sig(temp)=sig1*(strn^nhard);  % Flow stress in MPa
end

t=1:maxT;
plot(t,sig)
grid
```

Appendix D – Analytical model

```
p=4; %air jet pressure (bar)
t=0.12; %feed rate (mm/rev)
v=83/60*1000; %cutting speed (mm/s)
sigma=1074; %flow stress (by Oxley)

mu=0.55; %friction coefficient
theta=0; %shear plane correction angle
alpha=0; %rake angle
beta=atan(mu); %friction angle

E=210000; %Young modulus (Mpa)
diam=1.5; %jet diameter
Tair=7; %air temperature (nozzle exit, °C)
b=1; %width of cut (mm)

fi=pi/4-beta-alpha+theta;
r=tan(fi)/(cos(alpha)+sin(alpha)*tan(fi));
t1=t/r; %deformed chip thickness
As=b*t/sin(fi); %Area shear plane
Ls=t/sin(fi); %length shear plane
Lstick=t*sqrt(2)/2/sin(fi)/sin(pi/4+fi-alpha); %Toropov
Lc=2*Lstick;
Rc=abs(2*(2*Lstick-Ls*(pi/4+theta)/(fi+alpha))/2/sin(pi-fi-alpha))+t1/2
tau=sigma/tan(fi+beta-alpha+theta);
strain=cos(alpha)/(sin(fi)*cos(fi-alpha));
strrate=cos(alpha)*v/cos(fi-alpha)/0.25;

Fs=tau*As; Ns=sigma*As;
```

```
R=sqrt(Fs^2+Ns^2);
%Fq=R*sin(abs(fi-atan(Fs/Ns)));
Fp=R*cos(abs(fi-atan(Fs/Ns)))/2;
Fq=mu*Fp
Fc=Fp*sin(alpha)+Fq*cos(alpha);
Nc=Fp*cos(alpha)-Fq*sin(alpha);
U=tau*strain;
Us=Fp/b/t;
Uf=U-Us;

Rext=Rc+t/r/2;
Rint=Rc-t/r/2;
ecc=(Rext-Rint)/2-(Rext-Rint)/log(Rext/Rint);
Cint=Rc-ecc-Rint;
Cext=Rext-Rc+ecc;
Area=b*t/r;

kw=51.9;%input('insert thermal conductivity of workpiece material (W/(m*K))\n');
cw=486;%input('insert specific heat of workpiece material (J/(kg*K))\n');
rhow=8000;%input('insert density of workpiece material (kg/m^3)\n');
alphaw=kw/(rhow*cw); %thermal diffusivity (workpiece)
kt=84;%input('insert thermal conductivity of tool material (W/(m*K))\n');
ct=180.7;%input('insert specific heat of tool material (J/(kg*K))\n');
rhot=15800;%input('insert density of tool material (kg/m^3)\n');
alphat=kt/(rhot*ct); %thermal diffusivity (tool)

%mean shear plane temperature calculation
R1=1/(1+1.328*((alphaw*strain/v/t*10e6)^0.5));
Ts=R1*Us*10^6/cw/rhow*2 %shear plane temperature
Aj=2/pi*(1/sinh(b/Lc)+b/Lc/sinh(Lc/b)-1/3*(b/Lc)^2+1/3*Lc/b-
1/3*(Lc/b+b/Lc)*(1+(b/Lc)^2)^0.5); %Area Jaeger
```

```
%determination of C and B coefficients
C=Uf*v*Aj*t/kt;
B=(0.754*Uf*10^6)/rhow/cw*(v*((t/1000)^2)/Lc/r/alphaw)^0.5;
R2=(C-Ts)/(C+B);
%Tt=Ts+R2*B
Tt=Ts+(1-R2)*Uf; %interface temperature

%mechanical energy
UMover1=6*p^2*b*(Rc-(Rext-Rint)/log(Rext/Rint))^6/E/ecc/t^4/b*10e12;
UMover2=6*p^2*b*(Rc-(Rext-Rint)/log(Rext/Rint))^6*pi/2/E/ecc/t^4/b*10e12;
UMint1=0;
UMint2=-6*p^2*b*(Rc-(Rext-Rint)/log(Rext/Rint))^6*pi/E/ecc/t^4/b*10e12;

Q=(7.5*(p-4)+30.5)/60/(diam/2)^2/pi; %kg/s jet mass flow
Re=Q*diam/1.46e-5;
Pr=0.714; %per aria a 10°C
Kair=0.025 %thermal conductivity air

%Nu semi-cylinder
%NuOver=1.85*Pr^(1/3)*Re^0.695*(1/2/Rc/1000)^1.05; %Hrycak, 14000<Re<67000
%NuOver2=0.763*Pr^0.39*Re^0.5*(10e-3/diam)*(1-AlphaImp^0.194) %corr. Tawfek
20°<alpha<90° [162]
NuOver=0.394*Re^0.68*(2*Rc/diam*2)^(-0.15)*(11.4/diam*2)^(-0.38);%Gau and
Chung [130]
NuInt=0.0308*Re^(4/5)*Pr^(1/3); %for small impingement angles 0.0308

%heat transfer coefficient
hInt=NuInt*Kair/Lc*100;
hOver=NuOver*Kair/Rc*100;
UHover=-hInt*Area*(Ts-Tair)/1000;
UHint=-hOver*Area*(Ts-Tair)/1000;
```

```
%thermal energy
UsOver1=Us+UMover1+UHover;
UsOver2=Us+UMover2+UHover;
UsInt1=Us+UMint1;
UsInt2=Us+UMint2;
UfInt=Uf+UHint/10;

%shear plane temperature
TsOver1=R1*UsOver1*10^6/cw/rhow;
TsOver2=R1*UsOver2*10^6/cw/rhow;
TsInt1=R1*UsInt1*10^6/cw/rhow;
TsInt2=R1*UsInt2*10^6/cw/rhow;

%R2 calculation
C=Uf*v*Aj*t/kt;
Cint=UfInt*v*Aj*t/kt;
B=(0.754*Uf*10^6)/rhow/cw*(v*((t/1000)^2)/Lc/r/alphaw)^0.5;
Bint=(0.754*UfInt*10^6)/rhow/cw*(v*((t/1000)^2)/Lc/r/alphaw)^0.5;
R2Over1=(C-TsOver1)/(C+B);
R2Over2=(C-TsOver2)/(C+B);
R2Int1=(Cint-TsInt1)/(Cint+Bint);
R2Int2=(Cint-TsInt2)/(Cint+Bint);

%
TtOver1=TsOver1+(1-R2Over1)*Uf;
TtOver2=TsOver2+(1-R2Over2)*Uf;
TtInt1=TsInt1+(1-R2Int1)*UfInt;
                    TtInt2=TsInt2+(1-R2Int2)*UfInt;
```